AFOSR-TR-97

0099

REPORT DOCUMENTATION PAGE

1. AGENCY USE ONLY (Leave blank)	2. REPORT DATE	3. REPORT TYPE AND DATES COVERED
	February 97	Final Report, Sept. 01/93-Aug. 31/97

4. TITLE AND SUBTITLE

Fundamental Investigation of Biomineralization

5. FUNDING NUMBERS

F49620-93-1-0539
3484/XS
61103D

6. AUTHOR(S)

Professor Mehmet Sarikaya

7. PERFORMING ORGANIZATION NAME(S) AND ADDRESS(ES)

Materials Science and Engineering, Box: 352120
University of Washington, Seattle, WA 98195-2120

(206) 543-0724; fx: (206) 543-6381
sarikaya@u.washington.edu

8. PERFORMING ORGANIZATION REPORT NUMBER

260 001 1000

9. SPONSORING/MONITORING AGENCY NAME(S) AND ADDRESS(ES)

Air Force Office of Scientific Research
Attn: Capt. Hugh DeLong
Chemical and Atmospheric Sciences, AFOSR/NL
110 Duncan Ave., bldg. 410-B115, Bolling AFB, DC 20322-8080

10. SPONSORING/MONITORING AGENCY REPORT NUMBER

11. SUPPLEMENTARY NOTES

12a. DISTRIBUTION/AVAILABILITY STATEMENT

Approved for public release;
distribution unlimited.

12b. DISTRIBUTION CODE

13. ABSTRACT *(Maximum 200 words)*

The research activities in this augmentation program on biomimetics focused on three areas: (a) understanding the formation of mollusk shell structures, with emphasis on abalone shell, studied by transmission electron microscopy imaging and diffraction; (b) biomineralization (and self-assembly) processes using the synthetic approaches (solution chemistry) with and without using the proteins extracted from the shell organic material and, in a parallel study, (c) understanding of the mechanical properties of the mollusk shell structures (biological composites). The results and major conclusions drawn from these studies are given in the accompanying report. The program supported on graduate student (Ph.D., Daniel Frech) and three undergraduate students (senior students: Demetriah Webster, Mary Katchur, and Gretchen Wahl) in their research in the development of human-resources in this interdisciplinary field.

14. SUBJECT TERMS

Biomimetics, Biomineralization, self-assembly, biological composites, biogenic materials

15. NUMBER OF PAGES

16. PRICE CODE

17. SECURITY CLASSIFICATION OF REPORT	18. SECURITY CLASSIFICATION OF THIS PAGE	19. SECURITY CLASSIFICATION OF ABSTRACT	20. LIMITATION OF ABSTRACT
U	U	U	U

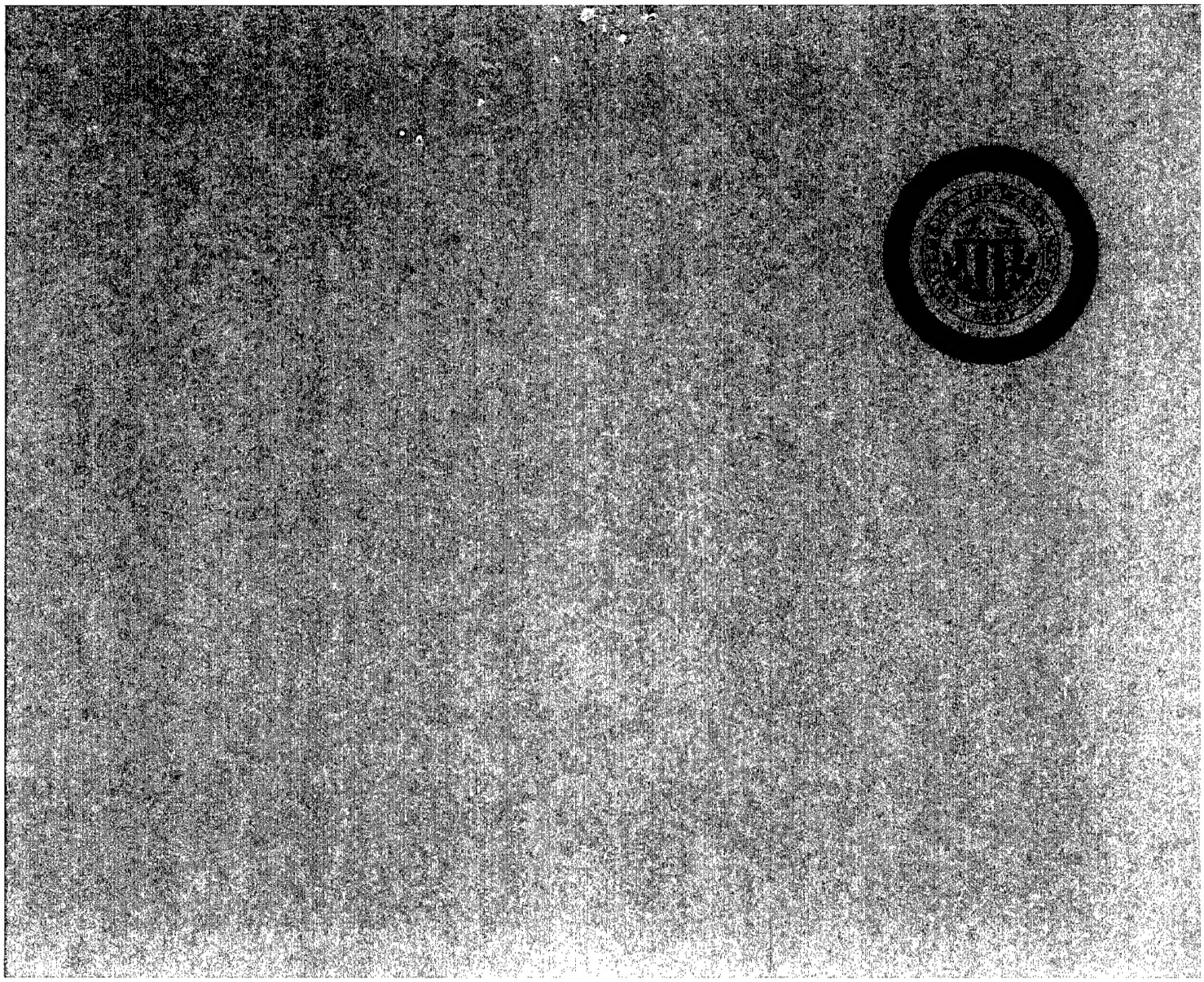

Final Report FUNDAMENTAL INVESTIGATION OF BIOMINERALIZATION Feb. 97

An AASERT - Project AFOSRF49620-93-1-0539

Submitted to: AFOSR
Attn: Capt. Hugh DeLong

Submitted by: Mehmet Sarikaya
University of Washington

UNIVERSITY OF WASHINGTON
SEATTLE, WASHINGTON 98195

DISCLAIMER NOTICE

THIS DOCUMENT IS BEST QUALITY AVAILABLE. THE COPY FURNISHED TO DTIC CONTAINED A SIGNIFICANT NUMBER OF PAGES WHICH DO NOT REPRODUCE LEGIBLY.

FINAL REPORT

(September 1, 1993, 1991-August 31, 1996)

on

Fundamental Investigation of Biomineralization

Augmentation Award
for Science and Engineering Research Training

by

Mehmet Sarikaya

Materials Science and Engineering
University of Washington
Seattle, WA 98195

Submitted to
Air Force Office of Scientific Research
Bolling Air Force Base
Washington, DC.

Attn. Capt. Hugh DeLong
(Dr. Frederick Hedberg)

February 1997

1. Summary

This is the Final Report for the 3-year grant entitled "Fundamental Investigation of Biomineralization," covering the period September 1, 1993 through August 31, 1996. The project has augmented the mother project entitled "Design and Processing of Materials by Biomimicking," monitored under the Grant # AFOSR-91-0281 covering the period June 1, 1991 through May 30, 1994. The report contains the accomplishments in various areas proposed for the final period of the project.

The objectives of the research in this augmentation proposal were three-fold: (i) fundamental understanding of the biomineralization process using 3-D organic network structure or a 2-D substrate; (ii) augment the major AFOSR project on the materials processing by biomimicking; and (iii) support a graduate student and an undergraduate student in training in this newly emerging multidisciplinary field.

In area (i) the research activities focused on (a) understanding the formation of mollusk shell structures, with emphasis on abalone shell; (b) biomineralization using the synthetic approaches (solution chemistry); (c) biomineralization using the proteins extracted from the shell organic material. In all these three areas, the investigation augmented the mother program, as area (ii). In this respect, in a parallel study, understanding of the mechanical properties of the mollusk shell structures have also been studied. In area (iii) the program supported on graduate student (Ph.D.) and partially or fully supported three undergraduate students (senior students) in their research as human-resources in this interdisciplinary field.

2.0 Background

Biomimetics is an area of research in which the analysis of structures and functions of natural materials provide source of inspiration for design and processing concepts for novel synthetic materials.[1-5] By biomimetics, structural control in synthetic materials may be established through a continuos length scale, resulting in superior structures able to withstand the requirements placed upon advanced materials.[6-7] It is well recognized that biological systems efficiently produce complex and hierarchical structures on the molecular, micrometer, and macro scales with unique properties, and with greater structural control than is possible with synthetic

materials.[1-12] The dynamism of these systems allows the collection and transport of constituents; the nucleation, configuration, and growth of new structures by self-assembly; and the repair and replacement of old and damaged components effectively. These materials include[1] all organic components, such as spiders' webs[11] and insect cuticles[12]; inorganic-organic composites, such as seashells[13-15] and bones;[16] all ceramic composites, such as sea urchin teeth[17] and spines;[18] and inorganic ultrafine magnetic[19] and semiconducting particles[20] produced by bacteria and algae, respectively. In addition, in certain cases, byproducts, such as enzymes, proteins, and other macromolecules, have chemical or physical properties superior to their synthetic counterparts.[21]

An approach based on biological systems is divided into two categories.[22] First, by studying the structures of biocrystals using various microscopy techniques at all scales of spatial resolution, the fundamentals of their unique structural designs can be acquired and then mimicked by techniques that are currently available to materials scientists, *biomimicking*. Second, by learning the molecular synthesis and processing mechanisms of biomaterials and using these hitherto unknown methodologies, new technological materials superior to those presently available can be produced, *bioduplication*. The bioduplication is much more involved and requires a long-term commitment to learn not only the intricacies of bioprocessing used by organisms but also to develop new strategies to synthetically process materials at the molecular level with the same size, shape, multifunctional and hierarchical complexity as the biomaterials. Biomimicking approach can be relatively short term, although by no means simple, and involves exploring the structures of biomaterials, which are often hierarchical with each level having a different functionality, and correlating these functionalities with the unique microstructural design and multifunctional properties of the biomaterials.

It is obvious that biomimetics is a wide area of research involving both the biological and physical sciences. Any research effort in biomimetics, therefore, in either biomimicking or bioduplication requires the collaboration of scientists from both of these fields. With this in mind, we formed a collaborative multidisciplinary group involving members from Materials Science and Engineering, Chemical Engineering, and Microbiology to start a major effort through the mother AFOSR program, entitled: Design and Processing of Materials by Biomimetics. This program was concluded in 1994. Before its conclusion, however, the present augmentation project was started involving several UG and one graduate students who performed research in this multidisciplinary environment at the cross-roads of biology and materials sciences. The following sections summarize the research results, and the appendixes provide copies of the manuscripts that have been published, or in preparation.

3.0 Major Research Accomplishments:

Our effort in the mother AFOSR project (that started in July of 1991) has focused both biomimicking and bioduplication approaches in parallel. Our major aim has been three-folds: (i) optimization of the conditions for the formation of biopolymers in an in-situ process with ceramic particles (ceramic processing with the aid of biopolymers); (ii) mechanism of ultrafine (<100 nm) inorganic particles formation in biological systems (in the bacterial species *Aquaspirrilum magnetotacticum*), and (iii) microstructure-property correlation in biocomposites (in a hard tissue, nacre, which is laminated ceramic-macromolecular composite).

As part of the major effort of the AFOSR program, this augmentation portion of the project focuses on item (iii), understanding of biomineralization processes, in addition to structure-property correlation. In this portion, determining mechanical properties, such as fracture toughness and strength, of biocomposites; developing understanding of the toughening and strengthening mechanisms in these nanolaminated composite structures; and correlating these to the micro- and nano-structural features have been areas of research in the AFOSR project (please refer to the publication list). The nacre section of the abalone and pinctada shells have been the specific hard-tissue used in this investigation. It is well-known now that nacre is a laminated composite of $CaCO_3$, in the form of aragonite platelets (orthorhombic) surrounded by a 10-40 nm thick film of organic matrix. The hexagonal-shaped platelets are 0.25 to 0.5 μm thick having a dimension of 5 - 10 μm edge size. The organic matrix is assumed to be a composite nanolaminate of three layers; polysaccharides (i.e., chitin, in the middle) surrounded by β-pleated sheets of proteins and acidic proteins. The fundamental understanding of biocomposites microstructures and their behavior under an applied load form the basis of mimicking these composites. However, from engineering and technological points of view, the real progress in biomimicking is largely dependent upon our ability to successfully produce these materials by synthetic means. Model microstructures, which are those composed of component phases which are not necessarily of immediate engineering importance but are easily processed and allow better control of microstructures, can serve as "pathways" for biomimicking more sophisticated microstructures with better properties. It is therefore, the purpose of the augmentation proposal was to obtain a better insight into the details of biomineralization processes in order to eventually mimick biocomposites and to achieve determination of the conditions and the structural development that would lead to "true" biomimicking of the process.

Major research accomplishments in the AASERT include the following with short descriptions (details of the results are in the copies of the manuscripts submitted or published as given in the appendices).

3.1 Mechanism of Biomineralization in Red Abalone

An understanding of the biomineralization mechanism in nacre structure of mollusk shells that involve macromolecular templating and assemblies: In the mother program of this research, the first major finding was that the nacreous section of red abalone (*Haliotis rufescens*) has an excellent combination of mechanical properties, i.e., fracture toughness and fracture strength, better than high technology ceramic materials(Appendix VII).[22] It was found out later on that these properties originate from the microarchitectural structure of the nacre, which is composed of aragonite platelets organized in a submicrometer-lamination separated to an organic matrix. These classic results are now widely known and form the basis of many biomimetic studies throughout this and other countries.[23] Better insight into the detailed processes that operate during the formation of the shell structure have formed the basis of the present augmentation program. Based on our investigation using transmission electron microscopy (TEM), scanning electron microscopy (SEM), and atomic force microscopy (AFM), it was revealed that the aragonite platelets nucleate on the last layer of organic as separate islands which then grow sideways, i.e., in the plane of the shell between the organic layers (i.e., transverse, fast, growth, 200 Å / min.) and in the normal direction, normal to the plane of the shell (i.e., longitudinal, slow direction; 20Å / min.).

We believe now that the nucleation starts on a macromolecular structure, possibly proteinaceous, in the middle of each of the aragonite platelet. This macromolecule, rather than being formed in the last organic layer as a flat substance, is present throughout the thickness of the nacreous section, extending down to the very first aragonite layer near the nacre/prismatic interface. As such, the protein probably acts as an anchoring site onto which the aragonite nucleate at each successive layer. We call this macromolecule the *anchoring protein.*

This finding radically changes the common belief that each layer of aragonite in the nacre structure forms freely and orients itself epitaxially onto a proteinaceous organic interlayer between the aragonite layers in the nacre, which acts as a template and directs the nucleation and crystallographic orientation (see Addadi and Weiner et. al 1980's, and Morse et. al, 1990s).

This finding also suggests that the organic layer in the nacre is dynamic, rather than it being static, as was suggested in earlier studies. The organic layer probably contains polysaccharides (that are the scaffolds), proteins (including transport proteins, that allow the nutrient and inorganic ion transfer from the extrapallial fluid, and acidic proteins, that fill in the space in between) in addition to the nucleator proteins, and lipids, that increase stability of the biological layer. We now believe that the organic layer as such constitutes nothing other than a *pseudo-membrane,* a dynamic structural entity that forms during the formation of the 2D structure of each of the aragonite layers and the aragonite platelets within each layer, as well as the 3D structure of the nacre, which all continue to grow simultaneously throughout the life of the organism.

Our most recent TEM results from the samples that were prepared in edge-on configuration of the nacre/prismatic interface suggest that the above hypothesis is correct, that the first-formed aragonite at the interface actually triggers the successive nucleation and eventual growth of the platelets resulting in the formation of nacreous structure (see Appendix V).

3.2 Morphology and Crystallography of the Mollusk Shell Nacreous Structures

We have investigated the ultrastructure in biological hard tissue, nacre, in terms of its morphology, crystallography, and composition in three different species of mollusks: cephalopods (*Nautilus pompelius*), bivalves (pearls oyster: *Pinctada margaritafera*) and in gastropods (*Haliotis rufescens*) (Appendix-I). The objective was to bring about the similarities among these widely different species that all practically have the same nacre in terms of their microstructure, irrespective of the fact that, in addition to being taxonomically they being different, the organisms have widely different habitats (depths of ocean they live in and hence the water pressure) and different predators (hence the need to have different defense mechanisms). In all cases, the aragonite appears in the TEM as being brick and mortar microarchitectured laminated structure. In all cases, again, the bricks are about 0.25 to 0.5 μm thick, multiedged (3, 4, 5, or 6-sided), side length being 2 to 5 μm. These were compared with geological aragonite formation.

We found that the aragonite platelets in a given layer are all oriented with their c axis (i.e., [001] axis of the orthorhombic lattice) perpendicular to the layer (shell) plane. Furthermore, all of the successive layers are in the same orientation. This is consistent with the finding above that each aragonite platelet is "anchored to a macromolecule that runs through the middle of the platelet,

and hence this anchoring proteins affects the nucleation of each the same way by orienting them in the same direction.

Rather than being oriented in any other crystallographic direction, the finding that [001] direction being common to each aragonite platelets is significant. Geological aragonite also nucleate at the center and grow spirally similar to the growth assisted by a screw dislocation, as commonly seen in the growth of the single crystal in many mineral systems. The growth is fast in the **c**-direction, and slow in the directions on the **a-b** plane, resulting in an aspect ratio (l_c/l_{a-b}) of ~100/1. During the growth, however, twins form to conform each platelet into 4-edged or 6-edged crystals, with twin plane being {110} parallel to [001] direction. Similar growth also takes place in biogenic aragonite, but in this case the growth in the **c**-direction is limited by the presence of the organic layer; this results in fractional aspect ratio; i.e., $l_c/l_{a-b} \sim 0.1$! As, it will be discussed in a later section, this results in the desirable layered architecture of the nacre structure constituting the inner section of the mollusk shell. this gives a tough section of the two-ply structure providing the energy absorption that is essential in any armor system (See Appendix-II).

One aspect of biogenic aragonitic structures being different than geological aragonite was thought to possibly be due to the elemental compositional differences in the former phase(s). We have performed both electron energy loss spectroscopy (EELS) in the TEM, energy dispersive x-ray spectroscopy (EDXS) in the SEM, and wavelength dispersive X-ray spectroscopy (WDS) in the microprobe. In particular, aragonite forming and stabilizing elements such as Mg, Sr, and K, were sought for. The results indicated no detectable levels of these elements throughout the nacreous structure in none of the mollusk species examined. *This lead us to conclude that the mineralogy (i.e., aragonite versus calcite), the crystallography, morphology, and shape of the aragonite as well as the calcite particles that make up the mollusk shell structures come about by the control of the organism, perhaps using macromolecules, such as proteins and enzymes, during the nucleation and subsequent growth of the hard tissue.*

3.3 Comparison of Nacreous Structures to Geological Aragonite

Morphological features within the structure, such as antiphase boundaries, twin boundary structures, dislocations, domain boundaries (including low angle-tilt boundaries), and their presence (and absence) in geological and biogenic aragonite are further discussed in detail in the copies of the publications given at the last section of this report (Appendix-I). One of the most

significant finding is the large difference in the aspect ratios in two systems as indicated above. The similarity, surprisingly, is in the hierarchical twin structure within the aragonite. While twins form between the platelets, among the domains within a given platelet, and the nanotwins within a given domain in an aragonite platelet in nacre, a similar twin relation is present between the columnar grains of the geological aragonite. Again, each columnar grain is divided into twinned domains, and which in turn also have nanoscale stress-accommodating twins, all having {110} as the twin plane, similar to those of the aragonite in nacre.

The differences were also found in other structural features such as the water-filled spherical pores present in the biogenic aragonite, while no such feature present within the geological aragonite. The function of these structural features has not been firmly established yet. However, we think that it may be possible during the growth of the shell, the water present between the pseudo-membrane (carrying the organic macromolecules that make up the organic layers and the inorganic ions) is trapped by the grown aragonite platelet at later stages of the growth process. The presence of these water-pockets might be significant in terms of providing means to soften the otherwise "brittle" aragonitic ceramic material, by a process similar to precipitation softening system(e.g., in Al_2O_3 (sapphire, hard) -TiO_2 (soft) in which precipitates of a second phase with a low elastic modulus within a matrix of high elastic modulus are distributed homogeneously resulting in a two-phase structure with substantially increased toughness. *This is certainly important from the fact that nacre provides the soft (tough) component of the mollusk which is an armor while calcite in the outer prismatic section of the shell provides the hard component (in which no water pockets have been found to be present)* (Appendix-I).

3.4 Calcite in the Prismatic Region versus the Single Crystal Geological Calcite

In addition to the inner nacreous section, the outer prismatic section of mollusk shells have been examined, especially with emphasis in the red abalone (Appendix-I). The most prominent structural feature is the fact that all calcite crystals are grown in a columnar fashion with their long axes normal to the shell-surface plane. Frequently, the calcite crystals confirm into a common crystallographic orientation, extending up to 10 or more grains. These crystals do not have the monoclinic shape that the single crystalline geological calcites have. As known, calcite can have over 600 different morphological forms, that are influenced by the conditions that include the temperature and pressure of formation, the presence of growth modifiers (or habit

modifiers, i.e., secondary elements within calcite), and the other solution conditions (acid and salt concentrations and the pH value). However, the calcite in the mollusk shells form at ambient temperature and pressure. The exterior oceanic water is basic with pH value about 7.5. Both the salt concentration and the pH value are most likely controlled by the organism within the confines of the shell (extrapallial fluid) (local concentrations have not yet been determined near the growth edge of the mollusk). *Our spectroscopic and elemental compositional analysis show no additional element other than the major components of the calcite (and aragonite), Ca, O, and C.*

3.5 Mollusk Shell as an "Ideal Armor": Structural Design as a Material System

The two-ply structure of the shell, calcite as the exterior section, and nacre as the interior section, in the abalone and other mollusk have evolved in order to provide protection of the organism against external predators. The unique morphologies of each of the sections of the mollusk shell described above and their crystallography, growth behavior, and strength/toughness properties have been optimized to make this biological composite to be used as a device by the organisms, i.e., cephalopods, gastropods, and bivalves (Appendix-II). For example, both the exterior prismatic section and the interior nacreous section are biological composites composed of both the organic and inorganic phases, with organic phase constituting only 2% of it by volume. One would then expect both of these sections to have similar properties. Neither of these sections is monolithic; in fact both are made up of small inorganic particles (calcite and aragonite, respectively) embedded within an organic matrix, albeit very small volume. It is the morphology of the individual filler, i.e., aragonite in the nacre and calcite particles in the prismatic sections that are different. As we discussed, aragonite crystallites are in the form of pseudohexagonal platelets, stacked parallel to the shell plane in submicron layers, rather than hexagonal columns, the morphology they usually grow to form. On the other hand, it is the calcite crystallites that are in the form of columnar grains, all arranged perpendicular to the shell surface. These morphologies are unusual among all the known (600 or so) morphologies of these two mineralogy types of calcium carbonate. Therefore, the questions are how such mineralogical forms develop in the mollusk shells and what purpose do they serve?

The major purpose of the shell as a device in mollusks is to shield the soft body of the organism against the predators. Therefore, the shell acts as the armor. The traditional armors have hard surfaces to stop the projectile, and soft interior section to absorb the energy of impact. Therefore, the surfaces are usually hard ceramics (such as B_4C or Al_2O_3, but usually in the form

of single block of material) (Appendix-II). In the interior, there is either a metal (e.g., Ti or alloy system) or a ceramic-metal composite. Neither of the sections however is highly structured, i.e., the grain orientation, size of individual grains, morphology, and thickness are not tailored. As we have seen above, the calcite on the exterior section is columnar and aragonite is hexagonal platelike crystals forming laminated structure. Both sections basically are ceramic-polymer composites (cerpoly), but with the polymer (organic) portion constituting a very small volume (2%). Presumably, outside portion is hard, and as we have seen in the first section, the nacre (inside) portion is tough (twice tougher compared to advanced ceramic materials, e.g., Si_3N_4).

The organization, however is odd in the sense that geological aragonite is harder than geological calcite! Hence one would expect aragonite to form on the exterior section and calcite on the interior. To solve this dilemma, we performed microhardness measurements from isolated sections of the red abalone, anticipating that the microscopic hardness would not be the same as the macroscopic hardness. In fact, the measurements made using a diamond-tip microhardness machine revealed that the microhardness as well as the elastic modulus of the prismatic exterior section displayed 30% more values than that of the interior nacreous section (Appendix-II). This reveals a drastic change of hardness properties between geological and biogenic materials. In the geological single crystals, the microhardness of calcite is 150 MPa and that of aragonite is 470 kg/mm^2, compared to the values of 210 versus 175 kg/mm^2, in biogenic calcite and aragonite respectively, a reversal or properties! These results clarify the affect of the organism in controlling the formation of different minerals of calcium carbonate, including their orientation, morphology, and size. *It appears, therefore, that through these manipulation of the microstructural parameters, the organism designs and constructs the structure to make it a useful device (a device, i.e., an ideal armor, so successful that it has been used by many mollusks species for 500 millions of years).*

3.6 Synthetic Biomineralization Studies: Biomineralization with and without Extracted Mollusk Proteins

The overall objective of the research in all these areas is to learn lessons from biological systems to develop new strategies in the design and processing of novel synthetic materials. In addition to ultimate design and processing objective of specifically manufacturing submicron-laminated ceramic-polymer (or ceramic-metal) composite materials for high-toughness/high-strength combination of applications, the desire in the current and future research has been also to produce particles with controlled size, mineralogy, and morphology. We still do not know what the

conditions are under which calcite or aragonite crystallites form. We know, however, how they grow to make the overall 3D-microstructure. Unusual structural parameters encountered in these calcium carbonate structures in sea-shells suggest that the organism must have influence over them. For example, the morphology may come as a result of the influence of the macromolecular habit (growth) modifiers. Similarly, the mineral types may be related to the nature of the nucleating proteins. 3D organization of the inorganic particulates may be controlled by the 2D or 3D macromolecular scaffolding (including polysaccharides in addition to proteins).

To test these hypotheses, we have prepared $CaCO_3$ in various different mineralogical forms in aqueous solutions at ambient conditions. For these tests, biomineralization studies, control samples were compared with those conditions but with the addition of either foreign inorganic ions and/or with the addition of acid-soluble proteins that were extracted from the shell sections in a parallel investigation (Appendix-II).

The experiment performed by using impurity inorganic ions included Mg, K, and Ba in various proportions, in addition to Ca^{+2} in the presence of CO_2 in solution, and the particles formed were sampled at different time intervals to study their structure and composition by XRD and TEM techniques. In the second set of mineralization experiments, mineralization was performed in the presence of organic extract of the shell nacre structure, which were mostly soluble proteins. Two of these proteins, one at 12,000 and the other at 14,000 were highly purified. The first set of experiments performed in the presence of foreign inorganic ions did not produce any significant change in the morphology of the calcium carbonate crystals formed, although they influenced the type of mineralogy (see Appendix-I). In the presence of proteins, however, two distinct structures formed, both producing aragonite form of $CaCO_3$. When a minute amount of Mg was added, the particles formed were in the shape of hexagonal platelets, a unique result which has never been achieved before (a manuscript is in preparation to report this result). Submicron-level thin (about 0.5 μm) and platelet-like (hexagonal) particles, are desirable for many applications, such as fillers in paints, paper and polymer composites. In these industrial applications, the major ceramic particles used are either titania (which is expensive), kaolinite (an alumina-silicate mineral) (which is highly brittle), and other ceramics. (Pfizer uses 1 M tons of $CaCO_3$ just as fillers in paper, with a desire t produce hexagonal $CaCO_3$ platelets).[24]

In the second set of experiments, when the protein was added in the absence of Mg, but under various pH values, then particles formed were tens or hundreds of micrometer sizes and in the form of spheres or semi-spheres (Appendix-VI). The cross-sectional structures of these particles revealed that they are actually composed of laminated layers, with the inorganic particles being

aragonite. Although the individual particles were not of platelike (they were extremely small, needle-like particles), they were configured in the form of layers, and gave the particles a pearly-appearance. We called this research, formation of *synthetic pearls*. We have also determined physical property of these particles by using microhardness measurements; as expected from the orientation of the aragonite crystallites and the laminated nature of the particle, the hardness values were as high as those of the nacre. These particles may be called *biomimetic ball bearings*.

4.0 Students involved in Research

4.1 The Undergraduate Students: Although we have originally requested funds for the support of one UG student, there were three students who worked on various aspects of this research during the course of the grant (sometimes as hourly paid students, and sometimes as junior and senior research students). These are:

i. Mary Katchur (completed Summer 1996) (now works at Intel, Oregon),
ii. Demetriah Webster (completed in Spring 1966) (now works in a private Company),
iii. Gretchen Wahl (completed in Spring 1994): This is another UG student, who has completed her research at the beginning of this AASERT Program and changed her department and is now a graduate student (Ph.D.) in Bioengineering with an NSF Fellowship.

(See Appendices III and IV for the their research reports)

4.2 Graduate Student: Daniel Weber Frech (expected to finish Summer 1997).

Appendices I and V give a report and a paper-in-preparation of Frech's research results (several additional papers are also in-preparation from Frech's results).

5.0 Conference, Workshop, and Symposia Presentations and Summer Schools Attended by the Students:

1. *Nanodesigning in Biological Composites*, M. Sarikaya, D. W. Frech, C. Furlong, and J. T. Staley, in: Nanofabrication and Biosystems: Frontiers and Challenges, Keauhou Beach Hotel, Kona, Hawaii, May 8-12, 1994.
2. *Formation, Crystallography, and Morphology of Biogenic and geological Aragonite*, Daniel Frech and Mehmet Sarikaya, Symp. S, *Biomolecular and Biomimetic Materials*, Fall Meeting of Materials Research Society, Boston, November 28-December 2, 1994.
3. *Biomineralization from Biology to Technology*, M. Sarikaya, Symp. S, Biomolecular and Biomimetic Materials, Fall Meeting of Materials Research Society, Boston, November 28-December 1994.
4. *The Growth Control in $CaCO_3$ Biomineralization*, Daniel Frech, Mary Katchur, Richard Humbert, Mehmet Sarikaya, Symp. U, *Materials Inspired by Biology*, Fall Meeting of Materials Research Society, Boston, November 27-December 1, 1995.
5. *Strategies of Biomineralization in Synthetic and Biological Systems*, M. Sarikaya, Symp. U, Materials Inspired by Biology, Fall Meeting of Materials Research Society, Boston, November 27-December 1, 1995.
6. *Design of Ceramic Microstructures by Biomimetics*, M. Sarikaya, in: Symposium on Biological and Biotechnological Materials, Annual Meeting of American Ceramic Society, Indianapolis, IN, May 1995.
7. *Biomimetic Strategies for Materials Processing*, D. W. Frech and M. Sarikaya, in: International Conference of the Pacific Basin Chemical Societies, Honolulu, Hawaii, December 1995.
8. *Controlled Growth and Texture in Biomimetic Materials*, M. Sarikaya, Symp. U, *Enabling Biomaterials Technologies - Molecular Structure-Properties Relationships,* Fall Meeting of Materials Research Society, Boston, December 2-6, 1996.

References

1. Biomimetics: Design and Processing of Materials, M. Sarikaya and I. A. Aksay (eds.) American Institute of Physics, New York, 1995).
2. (i) *Materials Synthesis Utilizing Biological Processes*, P. C. Rieke, P. D. Calvert, and M. Alper (eds.), MRS Symp., Vol. **174** (Materials Research Society, Pittsburgh, 1990) pp. 125-131, (ii) *Materials Synthesis Based on Biological Process*, M. Alper, P. C. Rieke, R. Frankel, P. D. Calvert, and D. A. Tirrell (eds.), MRS Symp., Vol. **218** (Materials Research Society, Pittsburgh, 1991); (iii) *Hierarchically Structured Materials*, I. A. Aksay, E. Baer, M. Sarikaya, and D. Tirrell (eds.) MRS Symp. Vol. **255** (Materials Research Society, Pittsburgh, 1992).
3. (i) L. Addadi. and S. Weiner, "Interaction between acidic proteins and crystals: stereochemical requirement in biomineralization," ***Proc. Natl. Acad. Sci.*, 82**, 4110-4114 (1985); (ii) L. Addadi and S. Weiner, "Interaction between acidic macromolecules and structured crystal surfaces, stereochemistry and biomineralization," *Mol. Cryst. Liq. Cryst.* **13**, 305-322 (1990).
4. I. A. Aksay and M. Sarikaya, "Bioinspired processing of composite materials" in ***Ceramics: Toward the 21st Century, Centennial International Symposium***, S. Soga and A. Kato (eds.), (Japanese Ceramic Society, Tokyo, 1991) pp. 136-149.
5. J. D. Currey, "The mechanical properties of some molluscan hard tissues," *J. Zool. London* **173**, 39-406 (1974).
6. J. D. Currey, "Biological composites," *J. Mater. Edu.* **9** [1-2] 118-296 (1987).
7. T. Degens, "Molecular mechanisms on carbonate, phosphate, and silica deposition in the living cell," *Top. Curr. Chem.* **64**, 1-112 (1976).
8. B. Frankel and R. P. Blakemore, ***Iron Biominerals*** (Plenum, New York, 1991).
9. Y. Bouligand, "Sur une architecture torsadee repandue dans de nombreuses cuticules d'arthropodes," *C R Hebd. Sceances Acad. Sci.* **261** [12] 3665-3668 (1965).
10. H. Fendler, "Atomic and molecular clusters in membrane mimetic chemistry," *Chem. Rev.* **87** 887-899 (1987).
11. J. Glimcher, "On the form and function of bone: from molecules to organs" in ***The Chemistry and Biology of Mineralized Biological Tissues: Wolff's Law Revisited***, A. Veis, (ed.) (Elsevier, New York and Amsterdam, 1981) pp. 617-673.
12. M. Gosline, M. E. DuMont, and M. W. Denny, "Structure and properties of spider silk," *Endeavor* **10** [1] 37-43 (1986).
13. M. Greenfield, D. C. Wilson, and M. A. Crenshaw, "Ionotropic nucleation of calcium carbonate by molluscan matrix," *Amer. Zool.* **24**, 925-932 (1984).
14. P. Jackson, J. F. V. Vincent, and R. M. Turner, "The mechanical design of nacre," ***Proc. Roy. Soc. London B234***, 415-440 (1988).
15. A. Lowenstam and S. Weiner, ***On Biomineralization*** (Oxford University Press, New York, 1989).
16. S. Mann, "Molecular recognition in biomineralization," *Nature* **33**, 119-123 (1988).
17. S. Mann, B. R. Heywood, S. Rajam, and D. Birchall, "Controlled crystallization of $CaCO_3$ under stearic acid monolayer," *Science* **334,** 692-695 (1988).
18. S. Mann, J. Webb, and R. J. Williams (eds.), ***Biomineralization: Chemical and Biochemical Perspectives*** (VCH Publishers, Weinheim, 1989).
19. M. Sarikaya, K. E. Gunnison, M. Yasrebi, and I. A. Aksay, "Mechanical property-microstructural relationships in abalone shell" in ***Materials Synthesis Utilizing Biological Processes***, proceedings of a symposium series, P. C. Reieke, P. D. Calvert, and M. Alper (eds.) Vol. 174 (Materials Research Society, Pittsburgh, 1990a) pp. 109-116.
20. K. Simkiss and K. M. Wilbur, ***Biomineralization: Cell Biology and Mineral Deposition***, (Academic Press, New York, 1989).
21. S. Weiner, "Organization of extracellularly mineralized tissues: a comparative study of biological crystal growth," CRC Crit. Rev. in *Biochem* **20** [4] 365-380 (1986).

22. M. Sarikaya and I. A. Aksay, "Nacre of Abalone Shell: A Natural Multifunctional Nanolaminated Ceramic-Polymer Composite Material," in: *Structure, Cellular Synthesis, and Assembly of Biopolymers*, S. Case (ed.) (Springer-Verlag, Berlin, 1992) pp. 1-25; M. Sarikaya, J. Liu, and I. A. Aksay, "Nacre: Properties, Crystallography, Morphology, and Formation," in: *Biomimetics: Design and processing of Materials*, (AIP, New York, 1995) pp. 34-89.
23. Some of the recent National and International Conferences, Symposia, and Conferences in Biomimetics:
    i. Workshop: *Molecular Design and Processing of Materials*, Friday Harbor, San Juan Island, WA; Sept. 4-6, 1996 (supported by ARO).
    ii. Workshop: *Biomimetics, Tissue Engineering, and Biomaterials*, Rockville, MD, September 23-26, 1996, organized by National Institutes of Health.
    iii. Seminar Series: *Form, Function, and Texture: Interrelationship between the Animate and Inanimate Worlds*," Tokyo September 15 - December 15, 1996, organized by Japanese Research and Engineering Center, Japan.
    iv. Annual Symposium on Biomimetics at the Fall MRS Meetings.
24. Dr. Kenneth Wise, Pfizer Co., Bethlehem, PA; private communication.

APPENDICES

Daniel W. Frech,

Ph.D. - GENERAL EXAMINATION

Formation, Structure, Properties of Nacre, and Bioinspired Processing

Paper on Research Project
For General Examination Committee
For PhD in Materials Science, at
University of Washington

Daniel Frech, February 1996

Preface: Purpose of the Research

The experimental work involved in this PhD project is designed to develop an understanding of how, in molluscan nacre, the formation and growth of $CaCO_3$ particles and the material system known as nacre is controlled by marine organisms using biomineralization. In this study, the approach applied to obtaining such an understanding has two phases. First, samples of natural biogenic shell material will be examined thoroughly using techniques of electron microscopy. The key microstructural features of this material system will be thereby established, and constituents critical to the process of biomineralization in nacre will be determined. Then, by synthetic means which simulate different aspects of growth conditions found in the environment of growing molusc shell, we will investigate the mechanisms of growth of $CaCO_3$ solids from aqueous solutions. In this portion of experimental work, we will try to answer specific questions about the regulatory effect of organic molecules and inorganic ions over the growth of precipitate of $CaCO_3$, as seen in biomineralization. More complete description of the investigation is provided in the Experimental Approach section.

I. Introduction

1.1 Justification: Study of Biomineralized Tissues

Hard tissues consisting of organic and inorganic phases are seen widely in the structural framework of natural living organisms. Certain microstructural characteristics which these materials display currently can not be produced by synthetic techniques. Composite structure at ultrafine length scales (a few nm) contributes to extraordinary mechanical, optical, and magnetic properties shown by these materials. In the area of metallic alloys, an analogy to the role and significance of microstructural inhomogeneities can be found in the use of small inclusions (precipitates) produced through controlled tempering of metallic alloys, and the advantages these precipitates offer to the metal in terms of greater toughness and strength. Other examples include artificially layered nanocomposites, alloys for anomalous increases in mechanical properties, and heterostructural semiconductors for electronic and optical properties.

The manipulation of crystal texture by organisms bearing biomineralized tissues provides another incentive for detailed study of such materials. Crystal textures in some tissues seem highly adapted to function. Better understanding of this apparently widespread biological phenomenon could result in new insights for the improvement of microstructure-controlled materials produced by synthetic processes.

Understanding of biological solid-state interactions between constituent phases (organic matrix and inorganic crystal) of biomineralized materials would be of substantial value in structural biology and medicine. It would, for example, possibly give insight into pathological mineralization in bones and teeth, and formation of kidney stones. In crystal growth and colloidal science, principles gained from the study of biomineralized tissues could be applied in prevention of industrial scaling and the controlled synthesis of ultrafine-structured electronic, magnetic, and catalytic devices.

The great variety of highly specialized shapes and forms displayed by biomineralized tissues inspire materials scientists as well, who would like to mimic biomineralization in the laboratory in order to produce structured ceramics, or single crystals of controlled shapes, for use in, for example, electronic devices and as magnetic storage medium.

Finally, study of biomaterials holds the possibility of uncovering a new method for the production of particles (submicron sized) of very regular, controlled morphology, by the regulatory mechanism/interaction of active organic molecules with growing inorganic crystalline material. High-purity, uniform powders (often equiaxed) are required raw materials for the production of high-quality ceramic materials (narrow and specific size distribution is needed, as well, to prepare proper colloidal or dry powders for use as constituents of structural ceramics, for reinforcements in paints, paper, and plastics). Many methods are available to produce controlled powders at high temperatures. But, high temperatures in processing can be equated to less controlled microstructures, due to high reactivities, and to high costs, due to expenses of required equipment and energy to conduct such processing. Research is underway to find synthesis techniques to produce high-purity, uniform powders at low temperatures. One area of study which has inspired this search is biological tissues exhibiting fine control of particle morphology, crystallography, and architectural buildup, such as is seen in mollusc shell structures.

1.2 Background on Biomimetics

1.2.1 Types of Organic/Inorganic Materials Systems

The biological composite materials systems which have recently aroused the interest of materials scientists, and which comprise the focus of this research, contain phases consisting of crystalline ceramic and biological macromolecular components. These biomineralized materials systems function as structural components for the living organism they are part of, often either forming a load-bearing member of the skeleton or a protective (e.g., shell) covering for the organism. Natural examples of these types of materials include (1) bone, in vertebrate organisms, (2) mammalian teeth, and (3) nacre in shells of molluscan organisms.

There are other systems composed of two-phase microstructure that can be termed biological organic/inorganic composite systems, such as insect cuticles and skeletal units of some echinoderm species, but a brief overview of each of these three examples will provide adequate illustration of the organization, structure, and properties of biological composites. A description of the compositions, microarchitecture, and properties of these three systems follows.

Bone

Bone consists of a mineral phase, which is mainly hydroxyapatite ($Ca_{10}(PO_4)_6(OH)_2$) and some amorphous calcium phosphate. The second component of bone is the protein collagen, which occupies approximately an equal volume as the mineral phase in bone. By weight, the mineral accounts for about 60% of the weight of bone; the mineral, 28%[1]. The remainder of the mass of bone is water. The structure of bone has been quite difficult to analyze because there are many hierarchical levels of organization present. Some details of the conformation (molecular structure) of the organic components

[1] J.D. Currey, "Biological Composites," *Handbook of Composites*, **4**, Chap. 9, 120-196.

have been determined, as well as information about the distribution and organization of the mineral phase in the collageneous matrix. Significant factors concerning the structure of bone include:

(i) The organic molecular constituents are mainly collagen; the primary sequence of the protein is:

glycine-proline-hydroxyproline-glycine-proline-X-glycine,

where X can be any of a variety of amino acids. Conformation of the collagen molecules can be related to weak bonds between the amino acid groups[2].

(ii) The collagen molecules adopt a triple-helical conformation of already helically arranged polypeptides. This conformation can be described as a coiled coil, and is called a tropocollagen molecule. Such tropocollagen molecules are arranged into fibrils, which are thought to be aligned in a head-to-tail fashion. Between the head and tail of adjacent fibrils are gaps, equal in length to the distance between homologous points on molecules that are adjacent in side-by-side fashion. The tropocollagen molecules have length of approx. 260 nm., with a 64 nm. head-to-toe gap between them[3]. From this description of structural organization of the protein phase, one can recognize that the structure is hierarchically organized.

(iii) The mineral phase interpenetrates the network of collagen molecules. It is thought that the mineral is deposited first in the gap between head and tail of collagen molecules, and later impregnates the spaces between fibrils. At present, there is limited information on the cause of nucleation, control of growth, and crystallography of the final composite, and on the relation between the organic and inorganic components of bone.

The illustration given on the following page shows the hierarchical nature of the structure of collagen as found in bone.

---

[2] J. Woodhead-Galloway, *Collagen: The Anatomy of a Protein*, (London: Edward Arnold, 1980).
[3] C. Berthet-Colomias, A. Miller, and S.W. White, *J. Mol. Biol.*, **134**, 431-445 (1979).

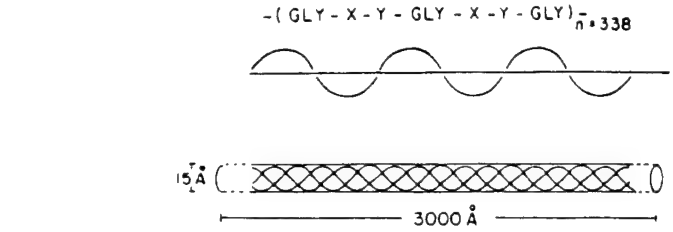

Schematic illustration of a collagen polypeptide chain with the (Gly-X-Y)$_n$ repeats (top) and the three polypeptide chains folded into the triple helical structure (bottom).

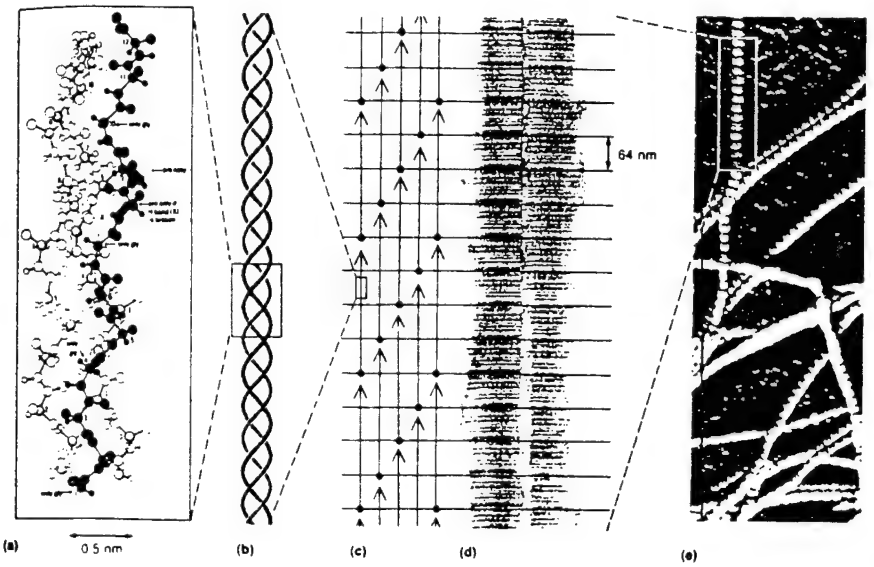

Figure 1: Schematic Illustration. Collagen Molecular Structure in Bone. Top Figure[4] depicts repeating (Gly-X-Y) Amino Acid Sequence, and the twisting of three such polypeptide chains, to form a "tropocollagen" molecule. Bottom figure[5] shows how collagen fibers are comprised of tropocollagen molecules aligned in a side-by-side, staggered fashion. Actual physical evidence for this model is seen in periodic pattern found in electron micrographs of collagen fibers, to right.

Mammalian Teeth

Mammalian teeth exhibit highly optimized structure and mechanical properties which render them capable of bearing heavy compressive loads during mastication of food. Teeth consist of two distinct regions, dentin, the underlying body of the tooth, and enamel, its hard covering. Dentin at the molecular level appears to be similar to bone. Collagen "Type I" framework molecules are first secreted

[4] H.A. Lowenstam and S. Weiner, *On Biomineralization*, (New York: Oxford University Press, 1989), 153 (for top illustration).
[5] C.K. Matthews and K.E. Van Holde, *Biochemistry*, (Redwood City, CA: Benjamin/Cummings Publishing Company, 1990), p. 183.

in the growth of teeth (dentin portion); these molecules self-assemble into an organic matrix framework in which mineral growth proceeds[6]. It is conjectured that the organic matrix is semipermeable; ions are thought to diffuse through the framework to mineralization sites.

Enamel, capping the dentin portion of teeth, consists of elongated crystals of dahllite ($Ca_5(PO_4, CO_3)_3(OH)$), also known as carbonate-apatite, which show an exceptional ultrastructure suggestive of a high degree of control in the process of biomineralization responsible for their formation. At the microscopic level, the crystals are arrranged in parallel arrays, which are in turn arranged in stacked sheets, which are oriented at 60-70° with respect to one another[7]. A microphotograph of this structure[8] is shown below.

Figure 2: SEM Photograph, Microarchitecture of Enamel in Teeth. Stacked sheets of Parallel Dahllite Crystals are evident.

Collagen fibrils are present among these dahllite crystals in some enamel. Remarkable in this system are the shapes of the dahllite crystals. Synthetic dahllite (grown at room temperature and 1 atm. pressure) never shows crystals with such an extreme aspect ratio - the biogenic crystals may reach tens of microns in length and are 0.05 to 0.10 micron thick - like spaghetti. Precise mechanisms of the growth processes are not known, neither is known the structural correlation between particles and collagen components of the composite.

---

[6] Collagen "Type I" framework molecules, dentin, teeth, etc. (Simkiss and Wilbur, Biomineralization?).
[7] A. Jodaikin, S. Weiner, and W. Traub, "Enamel Rod Relations in the Developing Rat Incisor," *Journal of Ultrastructure Research*, **89**, 324-332..
[8] H.A. Lowenstam and S. Weiner, *On Biomineralization*, (New York: Oxford University Press, 1989), 177.

Mollusc Shell Nacre

Nacre is a pearlescent, smooth lining found at the innermost layer of a number of shells of marine organisms. This material, under mechanical testing, has demonstrated exceptional fracture toughness and strength, surpassing the comparable mechanical properties of synthetic $CaCO_3$ by 30 times[9]. The microstructure of nacre is unique and represents a microcomposite, layered material of alternating hard and soft phases. The hard phase is $CaCO_3$, one polymorphic form aragonite, in single-crystalline, polygonal platelets of approximately 0.5 μm thickness and 5-10 μm in edge length; the ductile phase, termed the "organic matrix," is comprised of several layers; its precise composition and organization has not been fully determined but includes proteins and polysaccharides. The schematic diagram below provides an illustration to clarify this description of the nacreous microarchitecture.

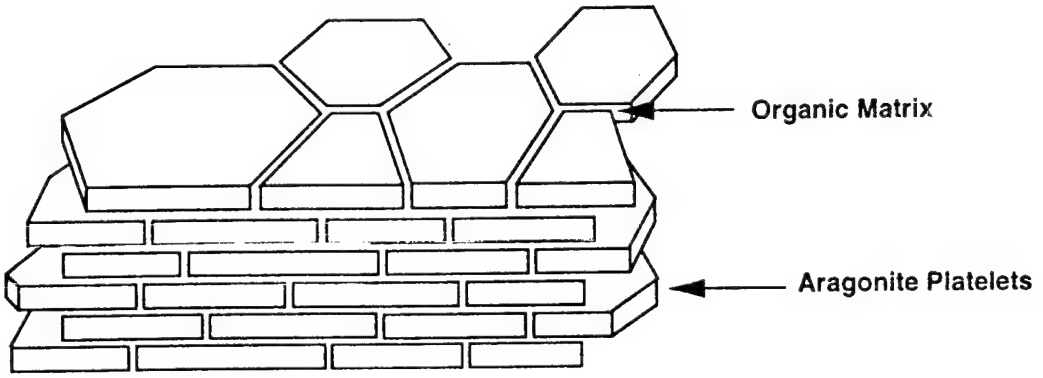

Figure 3: Schematic Illustration of Microarchitecture of Nacre

[9] M. Sarikaya, J.Liu, and I.A. Aksay, "Nacre: Properties, Crystallography, Morphology, and Formation," Unpublished research.

This material system offers for study a structural organization that is both hierarchical and comparatively simple, making it highly suitable for study to investigate principles of biomineralization, and a model system whose structure it may be possible to mimick by synthetic means. The crystalline phase of nacre, especially, can be studied in depth through application of TEM. The nacre structure also represents a unique product of natural processing. With current technology for the production of synthetic hard/soft phase composite systems, such as cermets, it is not possible to achieve laminated structures at the submicron dimensional level as exhibited by nacre. The ultrafine scale layering of the two-phase nacreous composite system, in conjunction with the mechanical characteristics of the constituent phases and strong interfacial bonding, are believed to confer upon nacre its exceptional mechanical properties. These features and the desire to synthetically produce high-performance ceramics for structural and high-stress application provide impetus for detailed study of nacre, aimed at developing understanding of the biogenic processes (biomineralization) involved in the formation of this material.

1.3 Principles of Biomineralization

From the preceding examples of biogenic organic/inorganic materials systems, some of the exemplary characteristics and features of biomineralized systems should be apparent. The key attributes of these types of systems include:

(i) Intimate mixing of inorganic, crystalline-phase material with organic macromolecular components. The relative proportions of inorganic and organic matter in a biomineralized material system can vary widely; usually the majority of the material is of the inorganic (crystalline) phase.

(ii) Highly specific shape (morphology) for components of the mineral phase. The inorganic crystalline components are typically sub-micron to several hundred microns in dimension; they show crystal habit which is regular but which differs strongly from habit of crystals of the same type formed by nonbiogenic

processes. In all cases (although this has not been investigated for all biomineralized tissues), there exists some ordering of the crystallographic disposition of platelets or particles in the mineral phase.

(iii) Functional organization of the organic phase. For example, in nacre the "organic matrix" forms thin sheets which are suspected to function as a compartmentalized framework on which, or within which, mineralization can take place. In bone, the fibrils of tropocollagen bundles are organized in a way that offers sites for mineralization to occur, i.e., in the gaps getween the ends of the matrix molecules. Calcium binding by active groups within organic matrix constituents has been hypothesized by several scientists seeking to explain the chemical processes involved in control of mineral nucleation and growth by components of the organic matrix[10]; analysis of its macromolecular constituents (i.e., amino acid compositional determination for proteins) has indicated the possibility that negatively charged sidegroups actively participate in biomineralization by binding calcium ions from solution.

(iv) Hierarchy in microarchitecture of biomineralized tissues.

Theories on Mechanisms of Biomineralization

From the traits of organic/inorganic composite biomineralized tissues, one can see that the structure and organization of these materials is highly specialized, regular, and specific. The state of knowledge of the chemical processes occurring *in vivo* that produce such materials is, at this time, incomplete. From compositional and structural analysis of these materials, however, a scientific concensus has been reached regarding the formation of specialized crystalline particles in the presence of an organic matrix. It is generally agreed that the nucleation and growth of the mineral phase is regulated

[10]A.P. Wheeler, J.W. George, and C.A. Evans, "Control of Calcium Carbonate Nucleation and Crystal Growth by Soluble Matrix of Oyster Shell," *Science*, **212**, 1397-1398, (1981); Stephen Weiner, "Aspartic Acid-Rich Proteins: Major Components of the Soluble Organic Matrix of Mollusk Shells," *Science*, **190**, 987-988; A.P. Wheeler, K.W. Rusenko, J.W. George, and C.S. Sikes, "Evaluation of Calcium Binding by Molluscan Shell Organic Matrix and its Relevance to Biomineralization," *Comp. Biochem. Physiol.*, **87B**, [4], 953-960 (1987); and M.A. Crenshaw, *Skeletal Growth of Aquatic Organisms*, (eds. D.C. Rhoads and R.A. Lutz), (NY and London: Plenum Press, 1980), 115-132.

by the organic matrix. Furthermore, some specific fundamental mechanisms of chemical interaction, which are responsible for the regulatory effect of organic molecules on biomineralized mineral growth (alternatively referred to as growth of *biogenic* crystalline material), have been proposed and partially substantiated. Several of the prominent views on the fundamental processes involved in mineral growth regulated by organic components will be briefly summarized below:

(i) Epitaxial role of the organic matrix

From electron diffraction patterns of organic matrices and mineral crystals in mollusc shells, alignment between structural components of the organic matrix (chitin fibrils and protein polypeptide chains) and crystallographic **a** and **b** axes in aragonite, which is adjacent to these proteins, has been detected. This suggests that the mineral has formed epitaxially on the matrix surface. The site of the nucleation of the mineral phase is postulated to be a well-oriented set of acidic macromolecules which form a surface layer on the structural core of the organic matrix[11].

(ii) Ionotropic role.

The sulfated fraction of the organic matrix from molluscan shell nacre appears to be involved in crystal nucleation. Pores in the organic matrix, thought to be nucleation sites, show high concentration of sulfur and muccopolysaccharides, which bind calcium. This calcium binding induces local anion binding, which then induces secondary calcium binding. The resultant local high concentration of ions is thought to bring about nucleation[12].

(iii) Organic macromolecules function as crystal poisons.

In the previous two views, the organic macromolecules found in biomineralized tissues are thought to function in a manner that would reduce the activation energy of formation of new mineral

---

[11] S. Weiner, Y. Talmon, and W. Traub, "Electron Diffraction of Mollusc Shell Organic Matrices and their Relationships to the Mineral Phase," *Int. J. Biol. Macromol.*, **5**, 325-328 (1983).
[12] E.D. Greenfield, D.C. Wilson, and M.A. Crenshaw, "Ionotropic Nucleation of Calcium Carbonate by Molluscan Matrix," *Amer. Zool.*, **24**, 717-729 (1984).

from ions in solution. A contrasting point of view posits that the organic matrix may effectively *inhibit* the growth of certain facets of the mineral phase. Proteins are thought to adsorb to specific faces of a growing mineral, forming a barrier layer which limits diffusion of ionic species from solution to these faces and thereby limits their growth. Specificity of regulation, leading to unique and unusual morphological features shown by biogenic mineral particles, can be attributed in this scheme to attachment of proteins and other functional macromolecules to faces with appropriate surface arrangement of atoms, or, in other words, to specific planar faces on minerals. Wheeler, Sikes, and George[13] found that a calcium-binding, soluble protein extracted from oyster shell suppresses nucleation of $CaCO_3$ and decreases the rate of crystal growth *in vitro*. Hence, it is thought that the soluble matrix of mollusc shells may acually inhibit mineral growth.

It may be that the organic matrix framework found in biomineralized tissues actually functions as both an initiator of crystal nucleation and later as an inhibitor of crystal growth. The view that the organic matrix has such a bifunctional role has been proposed by researchers in this field, as well. Through examination of features of biomineralized systems, analysis of the components present in these systems, and evaluation of the distribution of organic and inorganic phases found in biomineralized tissue, scientists have concluded that there exist specific modes of chemical (steric, geometric, stereochemical, and electrostatic) interaction between the organic and mineral phases which result in regulation and control of mineral growth from aqueous solution. As mentioned previously, at this time full understanding of the fundamental mechanisms involved in this controlled mineral growth has not been developed.

[13] A.P. Wheeler, J.W. George, and C.A. Evans, "Control of Calcium Carbonate Nucleation and Crystal Growth by Soluble Matrix of Oyster Shell," *Science*, **212**, 1397-1398 (1981).

1.4 Purpose of the Research, Objectives, and Task Areas

Purpose of the Research

The most significant overall goal of this research project is to elucidate the effects that organisms have on the formation, organization, microstructure, and properties of inorganic crystalline material. In this study, the system examined (in an attempt to uncover these effects) is nacre found in mollusc shells.

Objectives

The objectives involved in exploring the question of how the organism influences this biogenic material system are threefold. *The first objective* is to complete an in-depth analysis of microstructure and crystallography of nacre and primarily its inorganic constituent (aragonite); this analysis will be conducted using the techniques of transmission electron microscopy to explore this material at the finest scale possible. As part of this analysis, the microstructure of biogenic aragonite will be compared to that of aragonite of geologic origin, to determine how the biogenic growth process may influence fine structural features of the inorganic phase of nacre. *The second objective* is to develop insight into formation mechanisms for aragonite in nacre; the growth of the mineral phase in nacre is thought to be regulated by organic macromolecules present at the site of its nucleation and growth. Through study of crystallographic relationships, ordering, and microstructural features within the microarchitecture of nacre we will attempt to develop an explanation of crystal formation mechanisms in nacreous aragonite. *The third objective* is to investigate the influence of organic material on growing aragonitic particles through experimental biomimicking, where organic molecules are deployed in an aqueous solution from which aragonitic particles are caused to precipitate.

Specific Experiments and Tasks in this Research

Specific task areas which I will undertake in accomplishing these three objectives include the following experimental activities:

1) Characterization of microarchitecture of nacre through use of transmission electron microscopy. More specific goals in the microscopic analysis of nacre are:

a) To develop full, detailed knowledge of the microarchitecture, distribution, and dimension of the crystalline and organic phases found in the structure of nacre. From previous studies, it is known that molluscan nacre consists of platelets of aragonite less than 1.0 μm thick and several microns across, which are stacked, having an intermediate layer of "organic matrix" between their flat faces and edges (this structure has been described earlier). Additional details will be explored through TEM examination, including:

- Average shape (number of sides) of each platelet, and thickness
- Evidence of sites of nucleation for individual platelets
- Variation in nacre from different species of molluscan organism. Shells from different species will contain a different mixture of organic macromolecules. From microscopic examination of nacre from the respective shells, we will be able to determine if the difference in organic content has distinct effect on the microarchitecture of nacre.

b) To determine or investigate the possible existence of crystallographic relationships between the neighboring aragonite platelets (ordering, preferred alignment, etc.). This order may be correlated with the functional organization of the organic matrix.

c) To investigate or recognize features in biogenic aragonite which were not foreseen by teh researchers prior to making the TEM study, and which may contribute to the superior mechanical properties of nacre.

2) Comparison of the inorganic phase (aragonite) from nacre with aragonite of geologic origin. Comparison will be made between:

a) Macroscopic morphology of aragonite crystals of biogenic and geologic origin.

b) Defects and ultrafine-scale features of aragonite platelets in nacre. These features will be compared to the crystalline substructure found in geologic aragonite. The principal means to perform such a characterization of defect structures from the two respective materials is TEM. Examples of defects, and their abundances, which will be surveyed, include domains within individual platelets (twinned regions, for example), dislocations, pores, and stacking faults.

c) Comparative compositional analysis of biogenic and geologic aragonite, through use of energy-dispersive X-Ray analysis and through electron energy loss spectroscopy. In this phase of research, it may be possible to determine if occluded proteins are present in the structure of biogenic aragonite.

3) Attempt to grow controlled-shape precipitates of $CaCO_3$ from aqueous solutions. Here, an effort will be made to understand the relationship between composition of an ionic solution and the characteristics of precipitate one can produce from this solution. Specific goals in the investigation of crystal growth from solutions include:

a) Determination of the composition range (for a solution which is supersaturated in Ca^{2+} and CO_3^{2-}) that will yield particles of aragonite, rather than of calcite.

b) Developing a knowledge of the effect of individual inorganic ionic constituents of seawater on characteristics of precipitates deposited from solution containing these ions. For example, we would characterize the morphology of precipitate which formed from a solution containing Ca^{2+}, CO_3^{2-}, and one other primary ionic constituent of seawater, such as Sr^{2+}. Distinct morphological

features found in precipitate generated under such solution conditions could then be ascribed to the influence of strontium in this solution.

c) Growing and characterizing mineral precipitate under the influence of organic macromolecular additives. The organic molecules, which would be either extracted from nacre of molluscs or which would bear close resemblance to organic molecules from nacre, would be incorporated in a supersaturated $CaCO_3$ solution in a number of ways, including:

i) Adding proteins to the parent mineralizing fluid, in solution.

ii) Placing substrates, with organized arrays of macromolecules on them, in solutions supersaturated with respect to Ca^{2+} and CO_3^{2-}, and observing growth of mineral precipitate particles on these prepared substrates.

iii) Producing organized assemblies of active organic molecules at the surface of the supersaturated mineralizing solution, (2-D "self-assembled" films), and characterizing precipitate which forms on these molecular films.

Macromolecular additives to the solution chemistry experiments will include:

(i) extracted organic matrix molecules from mollusc shells,

(ii) derivatized rigid substrates (having active molecules affixed to their surfaces), and

(iii) Langmuir two-dimensional films of organized molecular arrays at the air/water interface.

II. EXPERIMENTAL APPROACH

2.1 Structural and Property Evaluation in Nacre

2.1.1 Mechanical Properties

Mechanical properties of a number of biological materials systems, for example, bone, teeth, and shell, have been shown to be superior in comparison to the same properties of the monolithic form of

mineral found in these materials. Nacre of the red abalone (*haliotis rufescens*) has been tested by other members of the Sarikaya research group to determine toughness, strength, and hardness.

The testing applied to this material (nacre, from red abalone) evaluated fracture toughness, through use of a straight-notched, three-point bend test, and fracture strength, by four-point bend testing. Tests were made in the transverse direction, that is, properties were evaluated for the material direction perpendicular to the shell plane. (The material (nacre) is not isotropic owing to the microarchitectural organization of its flat platelets and organic ductile phase). Typical values gathered through these testing methods indicate that σ_f is approximately 185 ± 20 MPa and K_{IC} is approximately 8 ± 3 MPa - $m^{1/2}$. Scatter in the testing data has been attributed to: (1) defects/variations in the nacre and (2) the curved shape of shells. The significance of the measured mechanical properties lies in the recognition that they are more than 20 times higher than values of properties for monolithic $CaCO_3$ and that these values place the material system nacre in the domain of high-performance composite ceramic materials such as B_4C-Al and WC-Co (both, cermets).

Fractography by SEM has been used to understand further the microstructure-mechanical property relationships demonstrated by nacre.

2.1.2 Morphological and Crystallographic Studies by TEM

Characterization of nacre at the ultrafine scale will be performed using transmission electron microscopy. The goals of microscopic analysis of nacre have been described in the "Task Areas" section. Experimental procedure involved in making the TEM studies is detailed below.

Part 1: Sample Preparation

The principal requirement for producing a sample suitable for examination by transmission electron microscopy is making a specimen of the material which is thin enough to permit transmission of

electrons accelerated in a collimated beam by the instrument (TEM). To produce such samples, we started with bulk samples of mollusc shell (from either abalone, pinctada, or nautilus).

Initial Thinning

Sections (rectangular beams or pieces of size and shape that can be handled by the wafering saw) were cut from the shells using a water-cooled, hi-speed diamond saw, first, to produce manageable pieces for further sectioning. Next, these sample blocks were sliced into thin (approx. .025 in. thick) wafers using a low-speed, water-cooled saw, equipped with a diamond-coated wafering blade. Pieces from these thin sections were thinned further by sanding them, starting with 600-grit SiC abrasive paper, and finishing with 1200-grit abrasive paper. Mechanical thinning in this fashion was carried out until the sample was as thin as it could be made while still capable of withstanding the strain of the abrasive process without breaking into smaller fragments. This portion of the sample preparation process demands patience and careful judgement to avoid destroying the specimen altogether. Typical final sanded thickness was .002 or .001 in. (or less).

Ion Beam Milling and Final Thinning

The final step in thinning the specimen was ion beam milling. A thin piece of the specimen was mounted onto a 3 mm copper disk (which would later serve as the specimen holder in the TEM sample stage) which had an oval hole in its center. The sample was bonded to the edge of the oval hole in the copper disk with silver paint, so that a portion of the sample projected over the edge of the oval hole. The sample, mounted on the copper disk in this manner, was then placed into an ion-beam mill. Focused ion beams of argon atoms accelerated to 6 KV struck the sample surface at a glancing angle of between 10 and 20 degrees. Their impact at the sample surface removed material from the sample at a controlled rate by the transfer of kinetic energy from argon (beam) ions to sample atoms, which ejected sample atoms from the crystal. Through frequent observation, it was possible to obtain a very thin region on the

sample which would be useful for TEM examination. Final preparation of the sample for TEM involved application of carbon coating to the sample; this was performed in a carbon evaporator. The thin layer of (conductive) carbon deposited on the sample surface in a layer approximately 1000 Å thick prevented charge from building up on an otherwise insulative specimen.

Part 2: TEM Imaging

A brief summary of modes of operation applied in examination of the sample by TEM, and the specific use of each mode, is provided below.

(i) Bright Field Imaging

Used extensively for inspection and overview of areas of the sample. In this mode, contrast is generated between regions of the sample which diffract more or less strongly. The central transmitted beam is allowed to continue after passing through the sample, to form the image of the region examined, whereas diffracted electrons from the incident beam are blocked by an aperture (objective aperture) which interacts with the electron beam after it has passed through the sample. Differences in crystallographic orientation between neighboring platelets, and domains within individual crystals, will be examined using bright-field imaging.

(ii) Two-Beam Condition

Here, the sample is oriented so that a particular diffraction condition is achieved, namely, that one diffracted beam from a specific crystalline plane is made to appear in the diffraction pattern for the sample. The relationship between the index of the diffracted beam, the visibility of certain defects within the sample, and the direction of Burgers vectors for allows one to estabish the geometry of atomic arrrangement for such defects in an otherwise regular and periodic crystalline lattice. The same two-

beam technique can be used to characterize atomic displacement for other types of crystalline imperfections (e.g., stacking faults) which involve specific displacement of atoms from their (perfect) lattice positions. Once appropriate specimen orientation has been established by selection of a two-beam condition in diffraction mode, a bright-field image of the region and features (defects) of interest is obtained, and the visibility of certain defect features is checked. By positioning the sample (via tilt capabilities of the microscope) in several distinct two-beam conditions, and examining the image at each orientation and looking for the appearance or absence of defects, it may be possible determine the local atomic rearrangement (departure from regular crystal lattice ordering) which characterizes the particular defect. Two-beam analysis will be used to conduct defect analysis of biogenic and geologic aragonite.

(iii) Electron Diffraction

Diffraction patterns from crystalline solids provide information about local crystalline orientation, lattice constants, and geometry of atomic arrangement in crystals. Diffraction (particularly selected area diffraction) will be used to establish orientation relationships between different regions within the nacreous solid. The significance in detecting such orientation relationships has been discussed earlier, with relevance to nucleation of mineral on an organic matrix template.

(iv) Electron Spectroscopy

Electron-energy loss spectroscopy (EELS) provides information concerning the local chemical and physical environment of selected atomic species within the lattice of a crystalline solid material. The mechanism by which EELS works is as follows. As electrons (from a nearly monoenergetic incident beam in TEM) pass through a sample, some electrons suffer losses of energy as they interact with sample atoms. Interaction may include ionization of sample atoms by ejection of their inner-shell electrons, which become energized when accelerated electrons collide with them. Such collisions "cost" incident electrons quantized amounts of energy, and through use of spectrometers positioned beyond the sample in TEM, it is possible to determine the relative abundances of electrons which have lost various amounts of energy (from their initial incident energy) in passing through the sample. This is the basis of the EELS

technique, as applied in TEM. The output of an EELS experiment is a plot of the number (intensity) of electrons emergent from the sample (after passing through it) at distinct energies below the incident beam energy. The variation in energy-loss peak positions from the expected ionization energies of inner-shell electrons for isolated atoms can be related to the local chemical environment and ligand field of the atoms in a solid. Thereby, EELS yields information about chemical bonding in solids. EELS can also be used in a more simplified approach to give elemental/compositional information for a solid. In our experimentation, we will employ EELS to make compositional analysis of biogenic and of geologic aragonite, and to compare their compositions.

2.2 Biomineralization (Experiments in Nucleation and Growth of Precipitates in Solution)

2.2.1 Synthetic Systems: $CaCO_3$ Precipitation in Solutions

Several methods have been applied to grow the mineral aragonite (the crystalline polymorph of $CaCO_3$ found in nacre) from supersaturated $CaCO_3$ solutions. Because the solubility product for the reaction:

$$CaCO_{3(s)} \rightarrow Ca^{2+}_{(aq.)} + CO_3^{2-}{}_{(aq.)}$$

has different value depending on whether the crystal form ($CaCO_{3\,(s)}$) is calcite or aragonite, calcite, with lower solubility, will precipitate first, at room temperature, as concentration of Ca^{2+} and CO_3^{2-} are gradually increased. (The solubility product of aragonite is 6.9×10^{-9} $kmol^2m^{-6}$, whereas that of calcite is 4.7×10^{-9} $kmol^2m^{-6}$) [14]. However, in the biomineral system nacre, the crystal form of $CaCO_3$ is aragonite. Hence, in our experiments in biomineralization, a challenge we face is to synthesize aragonite (as opposed to calcite) as precipitate from aqueous solution.

[14] K. Simkiss and K.M. Wilbur, *Biomineralization*, (San Diego: Academic Press, 1989).

A. Experimental Methods Examined

First Objective: Establish Conditions for Precipitation of Aragonite (rather than calcite) from Aqueous Solution

Several methods were attempted to cause precipitation of aragonite from an aqueous solution supersaturated in CaCO3. As a result, we were able to choose a preferred method with which we would subsequently investigate mineral growth influenced by specific ions and by proteins. The methods evaluated are described below.

Method 1: Elevated Temperature Conditions, Addition of Na_2CO_3 to $CaCl_2$ in Solution to Cause Precipitation

There are several methods by which one can precipitate aragonite from an aqueous solution. First, one can raise the temperature of the solution from which the precipitate is generated. From a supersaturated solution of $CaCO_3$ in distilled water at elevated temperatures (near the boiling point of the solution) and at atmospheric pressure, aragonite will precipitate first[15] (whereas, in a supersaturated solution (containing Ca^{2+} and CO_3^{2-}) at room temperature, calcite would precipitate). In our first attempt to grow aragonitic precipitate from aqueous solutions, we applied such an elevated temperature approach. The particular method of crystal growth was described in literature in a paper by Wray and Daniels[16]. Briefly, it involves mixing into a 200 ml., heated (60°C), 0.1 M solution of $CaCl_2$ 20 ml. of 1.0 M solution of Na_2CO_3. Instantaneous white precipitate is generated as a product, since upon addition of the precipitating agent, the product of ionic concentrations: $[Ca^{2+}][CO_3^{2-}]$ reaches nearly 0.01, which is far above the equilibrium value (discussed earlier) for either calcite or aragonite.

[15] W.S. Fyfe and J.L. Bischoff, "The Calcite-Aragonite Problem," DON'T KNOW JOURNAL, p. 8.
[16] J.L. Wray and F. Daniels, "Precipitation of Calcite and Aragonite," *Journal of the American Chemical Society*, **79**, [9], 2031-2034 (1957).

Method 2: Slow Addition of Precipitating Agent (Na_2CO_3), Inclusion of Magnesium Ions in Parent Solution, Room Temperature Conditions

It has been widely recognized[17] that precipitate generated from solutions with Mg:Ca ratio of 5:1 or greater, at low temperatures, will be predominantly aragonite (this same ionic ratio is, approximately, found in seawater). Taking these facts into account, a method for producing aragonitic precipitate, which relied on influence of included magnesium on precipitate, was investigated. This method was previously utilized by authors Kinsman and Holland[18] to examine the effect of auxiliary inorganic ions on precipitation product from solution. It consists, briefly, of:

(i) Starting solution of artificial seawater, a solution containing the principal ions, at their respective strengths, that are found in ocean water.[19]

(ii) Slow addition of a dilute solution of precipitating agent Na_2CO_3, due to which the concentration of CO_3^{2-} ions in solution will increase, thereby causing $[Ca^{2+}][CO_3^{2-}]$ to exceed $K_{sp(aragonite)}$ and result in the precipitation of mineral phase.

(iii) Room temperature conditions.

---

[17] Y. Kitano, A. Tokuyama, and T. Arakaki, "Magnesian Calcite Synthesis from Calcium Bicarbonate Solution Containing Magnesium and Barium Ions," *Geochemical Journal*, **13**, 181-185 (1979); S. J. Carpenter and K.C. Lohmann, "Sr/Mg Ratios of Modern Marine Calcite: Empirical Indicators of Ocean Chemistry and Precipitation Rate," *Geochimica et Cosmochimica Acta*, **56**, 1837-1849 (1992); Y. Kitano, "A Study of the Polymorphic Formation of Calcium Carbonate in Thermal Springs with an Emphasis on the Effect of Temperature," NOT SURE OF JOURNAL, **35**, [12], 1980-1985 (1962); W.S. Fyfe and J.L. Bischoff, "The Calcite-Aragonite Problem," NOT SURE OF JOURNAL, Pp. 3-13; and K. Sawada, T. Ogino, and T. Suzuki, "The Distribution Coefficients of Mg^{2+} Ion Between $CaCO_3$ Polymorphs and Solution and the Effects on the Formation and Transformation of $CaCO_3$ in Water," *Journal of Crystal Growth*, **106**, 393-399 (1990).

[18] D.J.J. Kinsman and H.D. Holland, "The Co-Precipitation of Cations of Sr^{2+} with $CaCO_3$ - IV. The Co-Precipitation of Sr^{2+} with Aragonite Between 16 and 96 C," *Geochimica et Cosmochimica Acta*, **33**, 1-17, (1969).

[19] Artificial seawater was produced from a chemical formulation provided in:

J. Lyman and R.H. Fleming, "Composition of Sea Water," *Journal of Marine Research*, **III**, [2], (1940).

The addition of Na_2CO_3 was made by using a slow, motor-driven syringe, delivering a dilute (concentration = 0.01 M or less) solution of Na_2CO_3 into the parent solution of artificial seawater. As precipitating agent accumulated in the parent solution,a white, fine precipitate appeared at the bottom of the solution, after it first became turbid.

Method 3: Supersaturation of Mother Solution by Dissolution of CO_2 Gas in Parent Solution

A final method has been assessed which appears to be appropriate for and consistent with simulation of growth of $CaCO_3$ mineral under biogenic conditions. This method was first described by Kitano[20], a Japanese researcher in aqueous solution chemistry who has extensively investigated the formation of $CaCO_3$ minerals in pearls and shells. This method involves dissolution of CO_2 gas in a calcium-containing solution to create a temporary increase in the solubility of $CaCO_3$. The procedure is conducted, briefly, as follows:

(i) $CaCO_3$ is mixed and suspended in DI water to produce a concentration well above its solubility limit in water of pH equal to 7. Powdered $CaCO_3$ is added to DI water in an amount which would produce a solution of strength 10 mM if all were dissolved.

(ii) The solution is carbonated with CO_2 for approximately 24 hours, and simultaneously stirred using a magnetic stirrer. No temperature control is employed; the experiment is run at room temperature. CO_2 is supplied to the solution through a sparging tube (producing a fine stream of CO_2 bubbles from an input gas tube which is submerged in the solution) which is connected to a tank of pressurized CO_2. As CO_2 is gradually dissolved in the solution through the process of sparging, the pH drops to a steady-state value of between 4 and 5. Concomitantly, the solubility of $CaCO_3$ in this solution goes up.

---

[20] Y. Kitano and N. Kanamori, "Synthesis of Magnesian Calcite at Low Temperatures and Pressures," *Geochemical Journal*, **I**, 1-10 (1966).

(iii) During this extended period of carbonation, the solution has reached steady calcium ion concentration levels. At this point, the carbonation is stopped for approximately 1 hour, during which the solubility of Ca^{2+} ions drops slightly, and pH rises slightly. Hence, in this interval, some small amount of $CaCO_3$ that has been dissolved (from its initial suspension) will reprecipitate. After resting (without carbonation) for approximately 1 hour, the solution is filtered using a vacuum filtration unit (pore size, 0.2 μm) to eliminate any residual solid material remaining in the reaction vessel, as such material could act as unwanted seed crystal in experiments which are designed to investigate homogeneous nucleation.

(iv) Mg, from $MgCl_2$, is added into the initial mixture of chemicals included in the solution. Mg is added in quantity that will result in parent solution ion concentrations $[Mg^{2+}]:[Ca^{2+}]$ = (approx.) 5:1.

(v) At this point, other inorganic ionic additives and, in the future, organic macromolecular components (such as proteins from mollusc shells) are introduced to the (parent) solution medium, which is be saturated with respect to $CaCO_3$.

(vi) The solution is then carbonated for 1 additional hour to assure the dissolution of any (possible) remaining solid crystalline material, and to establish a maximum dissolved $CaCO_3$ concentration in the parent solution.

(vii) The "prepared" parent solution is set aside, and carbonation by CO_2 stopped. With the evasion of dissolved CO_2 from the uncarbonated solution, the solubility of $CaCO_3$ in this solution decreases. As a consequence, precipitation of solid $CaCO_3$ occurs.

B. Discussion of Techniques for Synthesis of Aragonite Precipitate

Background: Growth of the Mineral Phase (CaO_3) in Mollusc Shells - The Model for Biomimicking Experiments

In mollusc shells, the process of growth of the shell occurs when calcium and carbonate ions from the fluid adjacent to the shell surface are deposited onto and bond to existing shell mineral crystallites or when these ions contribute to nucleation of new crystalline particles. The calcium carbonate solid material in mollusc shells is either polycrystalline (as seen in the calcitic region of the shells) or is an aggregate of a number of single-crystalline tablets. Particles (individual single crystalline regions) frequently display preferred orientation. Several distinct polymorphic forms of calcium carbonate have been shown to comprise mollusc shell [i.e., calcite (crystal type: rhombohedral), aragonite (crystal type: orthorhombic), and vaterite (amorphous)].

There are many factors which influence the formation of the various types of calcium carbonate in biological systems. Within the shelled molluscan organism, the growing shell inner surface is adjacent to the extrapallial fluid (or, E.P.F.). This term refers to the liquid found in the cavity between the external covering of the soft mollusc organism (this portion of the organism is known as the "mantle"), and the inner surface of the shell. The composition and ionic concentration of this E.P.F. may be controlled by release of ions (through the mantle) and other means, and by the allowed influx of new seawater into the cavity. In addition, the mantle is responsible for the release of organic components into the extrapallial space. While the inorganic ionic components of the E.P.F. are clearly necessary for the formation of new mineral from the solution, the role played by the organic components *is not known*. Some investigation has been made to determine the influence of other inorganic ionic species, such as Sr^{2+} and Mg^{2+} ions, on the crystal type of mineral precipitated[21]. Presence of Mg^{2+} at concentrations five

[21] D.J.J. Kinsman and H.D. Holland, "The Co-Precipitation of Cations with CaCO3 - IV. The Co-Precipitation of Sr^{2+} with Aragonite Between 16 C and 96 C," *Geochimica et Cosmochimica Acta*, **33**, 1-17 (1969); and Y. Kitano, A. Tokuyama, and T. Arakaki, "Magnesian Calcite Synthesis from Calcium

times or more than that of Ca^{2+} will act, apparently, to favor precipitation of aragonite over calcite. Though the specific chemical processes leading to control of crystal formation, orientation, and particle size in nacre have not been demonstrated or mimicked *in vitro*, it is suspected that periodic deposition of sheets of organic matrix over the aragonite crystals of the nacreous layer may retard growth of basal planes of aragonite, resulting in formation of tablets of nearly uniform thickness and consistent breadth.

In our attempt to develop an understanding of how, in nacre, calcium carbonate solids form in specialized shape and display unusual microarchitecture, *we would like to imitate as closely as possible the process of mineralization described above as using laboratory techniques of aqueous solution chemistry.*

Discussion of Precipitation Techniques Attempted So Far

Discussion of Wray and Daniels Technique (Method 1)

This method of aragonite production features several disadvantages which make it not suitable for use in simulation of biogenic production of aragonite in nacre. First, the temperature applied is unlike that found in biological systems where nacre grows. In the case of red abalone, for example, the organism resides at shallow ocean depths along the coastal waters of the Pacific Coast from Washington State to Baja, California, where temperatures fall in the range 10-15° C. The high-temperature regime of this synthetic process seems quite different. In addition, rapid supersaturation of the parent solution using this method will not produce near-perfect, faceted, single-crystalline particles. The resultant precipitate from this process tends to be rough, agglomerated, and irregular in morphology. The relative surface energies of distinct crystalline faces are unable to manifest themselves through the adaptation of distinct morphology when the degree of supersaturation is high, as in the case of this experimental technique. Hence, this technique is not well suited to explore the effects of ionic and organic molecular additives on

---

Bicarbonate Solution Containing Magnesium and Barium Ions," *Geochemical Journal*, **13**, 181-185 (1979).

particle morphology. Growth of relatively defect-free crystalline material requires a solution concentration just above saturation, in the region where conditions are "labile".[22] Examples of aragonite particles grown using this approach are presented in Figure 4 (in *Appendix: Figures*); the irregular morphology is apparent in these photos. A diffraction pattern for this precipitate is shown (in Figure 4) as well. By comparing of this X-Ray diffraction pattern with that from a sample of powdered geological aragonite crystal (diffraction pattern for powdered geologic aragonite is also presented in Figure 4, following the diffraction pattern for the synthetic precipitate), one can confirm that this precipitate is aragonite.

Discussion of Kinsman and Holland Precipitation Technique (Method 2)

Using the second technique described in the experimental procedure section, production of aragonite from solutions saturated in Ca^{2+} and CO_3^{2-} ions was feasible at low (room) temperature. Precipitation of aragonite under these conditions depends on the influence of (other) inorganic ions in saturated $CaCO_3$ solutions to determine the crystal form of precipitate. Numerous studies[23] have been made which explore the effect of composition of the mother solution and the auxiliary inorganic ion species in saturated $CaCO_3$ solutions on the crystal form of the precipitate. A reference point to examine in determination of the proper composition for the "mother liquor," to use in generating precipitate, is the ionic strength of seawater. Mineralized calcium carbonates which solidify from seawater compositions are typically aragonite[24]. The composition of seawater has been examined in several oceanographic surveys, but relatively recently, it was comprehensively detailed by Lyman and Fleming (1940). In their work[25], they indicated the following composition for marine seawater:

---

[22] H.E. Buckley, *Crystal Growth*, (New York: Wiley, 1951).
[23] References which explore the effect of auxiliary inorganic ions on mineralogy of precipitate from aqueous solution.
[24] J.W. Morse, "The Kinetics of Calcium Carbonate Dissolution and Precipitation," Chap. 7 in "Carbonates: Mineralogy and Chemistry," (ed. R.H. Reeder) *Reviews in Mineralogy*, **11** (1983).
[25] J. Lyman and R.H. Fleming, "Composition of Sea Water," *Journal of Marine Research*, **III**, [2] (1940).

Table of Hypothetical Composition of Ions in Sea Water
(Recipe to Prepare 1.0 liter Artificial Seawater, from Compounds)

Salt	NaCl	$MgCl_2$	Na_2SO_4	$CaCl_2$	KCl	$NaHCO_3$	KBr	H_2BO_3	$SrCl_2$	NaF	Sum	H_2O to:
Gms.	23.477	4.981	3.917	1.102	.664	.192	.096	.026	.024	.003	34.482	1000

Though it was confirmed that the precipitate formed via application of this technique was aragonite (by X-ray powder diffraction, where powdered precipitate sample was collected from the bottom of the reaction vessel, isolated by filtration, and dried), the morphology of crystalline samples produced in this fashion was, still, highly irregular, rough, and nonfaceted. It seemed difficult or impossible to overcome local high supersaturation and establish "labile" required for satisfactory near-perfect crystal growth, when the precipitating agent was added in this manner. Even use of very dilute solutions Na_2CO_3 and very slow addition of these solutions produced uneven, rough precipitate particles. Examples of the morphology generated in this way are shown in SEM micrograph in Figure 5 (in *Appendix: Figures*). An X-ray diffraction scan for this precipitate is shown below the SEM microphotograph (in Fig. 5), confirming that this material is aragonite.

Discussion of Kitano Technique (Method 3)

From the description of the "Kitano Technique" for production of a supersaturated solution and associated precipitation of $CaCO_3$, it can be gathered that this method approaches the conditions of biological mineralization that are seen in living organisms. Moreover, the change in supersaturation of the solution depends on the relatively gradual process of escape of CO_2 from the solution, which results in a gentle driving force for nucleation, crystal growth, and precipitation. The imitation of the biological event by this *in-vitro* process seems more accurate than by the two methods mentioned earlier;

precipitation seems controlled by pH, occurs at low temperature, and can be made to occur from solutions close in composition to seawater, or to that of the extrapallial fluid in molluscs[26].

2.2.2 Biomineralization Strategies: A Review of Literature

(i) In solution

Crystal growth from aqueous solution has been pursued in two primary directions pertinent to the study of mineral growth in living organisms. These are:

- Selection of polymorphic form and analysis of crystal growth kinetics as related to composition of the parent solution from which the solid material is nucleated, and
- Influence of proteins mixed into the initial parent solution over the resultant precipitate produced.

Kitano has explored the influence of additions of magnesium and barium to solutions supersaturated in $CaCO_3$ by bubbling of CO_2 gas.[27] He found that the addition of magnesium favored formation of aragonite, whereas addition of barium favored calcite formation. Examples of experimentation into the influence of organic molecules on crystal form include investigation of the interaction of macromolecules from sea-urchin spine and from mollusc *Mytilus Californianus* with solutions of growing calcium maleate and calcite. Morphology of crystals grown in presence of these macromolecules was compared to that of crystals grown in absence of any macromolecular additives.[28] In another study[29], soluble organic extracts from red abalone (*H. Rufescens*), Nautilus (*Nautilus Sp.*), and Atlantic Razor Clam (*Siliqua Costata*) were added to solutions supersaturated in $CaCO_3$, and growth of

---

[26] M.A. Crenshaw, "The Inorganic Composition of Molluscan Extrapallial Fluid," *Biol. Bull.*, **143**, 506-512.
[27] Y. Kitano, A. Tokuyama, and T. Arakaki, "Magnesian Calcite Synthesis from Calcium Bicarbonate Solution containing Magnesium and Barium Ions," *Geochemical Journal*, **13**, 181-185 (1979).
[28] A. Berner, L. Addadi, and S. Weiner, "Interactions of Sea-Urchin Skeleton Macromolecules with Growing Calcite Crystals - a Study of Intracrystalline Proteins," *Nature*, **331**, [6156], 546-548 (1988).
[29] R. Humbert, M. Sarikaya, and C. Furlong, "Layered Aragonitic Particles from Mollusc Shell Extracts," Unpublished research (1994).

layered pearl-like structures was observed in some cases. Other examples of studies (crystal growth in presence of organics) of this type exist. However, it should be noted that the charateristic brick-and-mortar, inorganic-organic microcomposite structure in nacre has not been produced synthetically *in vitro* through such an experimental approach.

(ii) On Rigid Substrates

Experimentation in growth of calcium carbonate on solid substrates has explored the use and influence of a variety of seed crystals and their effect on crystal form produced from supersaturated solution. Sabbides *et. al*[30] investigated growth of mineral atop seed crystals of calcite, aragonite, and vaterite from supersaturated artificial seawater solutions. Irrespective of which seed crystal was employed, the resulting precipitate was found to be aragonite. This result, in turn, was attributed to the high magnesium content in seawater. A study has also been performed investigating the growth of mineral phase atop a class cover slip inserted in the extrapallial space of a live mollusc.[31] Finally, through use of the atomic force microscope, growth of mineral atop molluscan nacre, from supersaturated solution, has been characterized.[32]

III. Experimental Results

3.1 Structure of a Biological Composite: Nacre of Mollusc Shells

3.1.1 Morphology, Substructure, and Composite Structure of Nacre

[30] T. Sabbides and P. Koutsoukos, "The Crystallization of Calcium Carbonate in Artificial Seawater, the Role of the Substrate," *Journal of Crystal Growth*, **133**, 13-22 (1993).
[31] S. Mann? D. Morse? Abalone? LOOK UP THE REFERENCE ON GROWTH OF MINERAL ON GLASS SLIDE IN EPF.
[32] R. Giles, S. Manne, S. Mann, D.E. Morse, G.D. Stucky, and P.K. Hansma, "Inorganic Overgrowth of Aragonite on Molluscan Nacre Examined by Atomic Force Microscopy," *Biological Bulletin*, **188**, 8-15 (1995).

There have been numerous scientific studies made concerning the structure of sea shells, the specific structure of nacreous hard material found in shells, and investigations of specific components of nacre, such as the soluble and insoluble fractions of the organic matrix[33], and crystalline tablets of aragonite found in nacre[34]. Boggild[35] produced a significant contribution to the early understanding of the various distinct structural regions of nacreous shells in his paper, published in 1930. K. Wada, over the years 1960-1985, has published substantial amounts on various studies performed which concern nucleation and crystal growth in molluscan shells[36], and on research into chemical mechanisms involved in shell growth. Sarikaya[37] has written several papers which provide greater insight into the heirarchical structure and microarchitecture found in the microcomposite nacre, with emphasis on crystallography and microstructure of aragonite tablets in nacre. Currey[38] has considered the structure of nacre in terms of the advantages and performance exhibited by this material system, and the superiority of its mechanical properties. Stephen Weiner and Steven Mann have published extensively[39] on their views on the

---

[33] K.M. Wilbur and K. Simkiss, "Calcified Shells," *Compr. Biochem.*, **26A**, 229-295 (1968). and S. Mann, "Mineralization in Biological Systems," *Struct. Bonding* (Berlin), **54**, 125-174 (1983).

[34] N. Watabe, "Shell Structure," in *The Mollusca* (E.R. Trueman and M.R. Clarke, Eds.), **111**, (San Diego: Academic Press, 1988), 69-104. and J.G. Carter and G.R. Clark, "Classification and Phylogenetic Significance of Molluscan Shell Microstructure," in "Molluscs: Notes for a Short Course," (T.W. Broadleaf, Ed.), Dep't of Geol. Sci. Stud. Geol. 13, (Knoxville, Tenn: Univ. of Tennessee, 1985), 50-71.

[35] O.B. Boggild, "The Shell Structure of Molluscs," *K. Dan. Vidensk. Selsk. Skr. Naturvidensk. Math. Afd.*, **9**, 233-326 (1930).

[36] K. Wada, "Studies on the Mineralization of the Calcified Tissue in Molluscs - V. Radioautographic Investigations on the Patterns of Layer Formation," *Bulletin of the Japanese Society of Scientific Fisheries*, **30**, [6], 467-471 (1964), 465-471; K. Wada, "Studies on the Mineralization of the Calcified Tissue in Molluscs - III. Localization and Distribution OF 45Ca in the Mantle Tissue and on the Growing Shell Surface in Several Marine Bivalves by Radioautography," *Bulletin of the Japanese Society of Scientific Fisheries*, **30**, [5], 385-392 (1964); K. Wada, "Studies on the Mineralization of the Calcified Tissue in Molluscs - II. Experiments by the Administration of Tetracycline on the Mineralization of the Shell," *Bulletin of the Japanese Society of Scientific Fisheries*, **30**, [4], 326-330, (1964); K. Wada, "Studies on the Mineralization of the Calcified Tissue in Molluscs - XII. Specific Patterns of Mon-Mineralized Layer Conchiolin in Amino Acid Composition," *Bulletin of the Japanese Society of Scientific Fisheries*, **32**, [4], 304-311 (1966); and K. Wada, "Studies on the Mineralization of the Calcified Tissue in Molluscs - XI. Comparative Biochemical Study on the Amino Acid Composition of Conchiolin from Calcitic and Aragonitic Layers," *Bulletin of the Japanese Society of Scientific Fisheries*, **32**, [4], 295-303 (1966).

[37] M. Sarikaya, J. Liu, and I.A. Aksay, "Nacre: Properties. Crystallography, Morphology, and Formation," Unpublished research, and M. Sarikaya, J. Liu, and I.A. Aksay, "Hierarchical twin Structures in the Nacre of Red Abalone Shell," _____, 948-949.

[38] J.D. Currey, "Biological Composites," in *Handbook of Composites*, **4**, Ch. 9, 120-196.

[39] S. Mann, "Molecular Recognition in Biomineralization," *Nature*, **332**, 119-124 (1988). and S. Weiner and W. Traub, "Macromolecules in Mollusc Shells and their Functions in Biomineralization," *Phil. Trans. R. Soc. London B*, **304**, 425-434 (1984).

interrelationship of the organic and inorganic phases in nacre; in these papers extensive description of the structure of these materials systems is included.

Distinct Goals, Microscopic Study of Nacre

Goal 1: Determination of Preferred Orientation of Neighboring Platelets

The first aspect of nacre investigated involves examination of crystallographic orientation and disposition for individual platelets of aragonite found in nacre. By investigating this issue, we aimed to uncover a pattern or ordering among neighboring crystalline platelets that could be interpreted as evidence of higher organizational control and regulation by the organic matrix or process of biomineralization over the crystalline fabric of nacre. Weiner and Traub[40] in 1980 published results of a study in which electron diffraction patterns generated simultaneously by the organic matrix and by the mineral (aragonitic) phase in nacre were recorded. This work claimed to demonstrate a distinct and direct relationship between periodically spaced groups in the conformational structure of the organic matrix and specific crystal directions in the mineral phase. This spatial relationship could be viewed as evidence for an epitaxial relation/interaction between the matrix and the crystal. If a stereochemical correspondence between matrix and mineral did, in fact, exist, one should be able to detect a manifestation of this effect from patterns of crystallization among neighboring aragonitic platelets in nacre. The study I have performed used electron diffraction, carried out in a transmission electron microscope, to determine crystallographic information. To study the individual nacre tablets, microdiffraction was employed, using selected area apertures to kpermit diffraction from one aragonitic platelet at one time. This study has yielded two primary conclusions:

[40] S. Weiner and W. Traub, "X-Ray Diffraction of the Insoluble Organic Matrix of Mollusc Shells," *FEBS Letters*, **111**, [2], 311-316 (1980), and S. Weiner, Y. Talmon, and W. Traub, "Electron Diffraction of Mollusc Shell Organic Matrices and Their Relationship to the Mineral Phase," *Int. J. Biol. Macromol.*, **5**, 325-328 (1983).

(i) Neighboring platelets are not strongly aligned in **a** and **b** axial directions. Samples of nacre were surveyed from an edge-on perspective, and the relationship between the [110] directions in adjacent platelets was compared. In photo (a), in Figure 6, a TEM bright-field micrograph from such a surveyed region is shown. A polar plot of the relative orientation of [110] in the neighboring platelets is presented in Graph(a), below the TEM micrographs. The respective platelets from which the diffraction was taken are numbered in the microphotograph; the orientation of [110] in each is correspondingly numbered in the polar plot.

(ii) The **c**-axial direction of neighboring aragonite platelets is strongly coincident. Microdiffraction was applied to adjacent individual platelets of several nacre samples which were prepared with the foil surface parallel to the flat surface of the aragonite platelets. From these diffraction experiments, it was clear that the [001] direction in the platelets, normal to their flat surface, varied only a few degrees from platelet to platelet. In Photo (b), in Figure 6, an example (TEM bright-field micrograph) of a region examined in this way is shown. In the corresponding polar plot for the relative orientation of [100] in this region, shown in Graph(b), the corresponding orientation for [110] in each platelet is indicated.

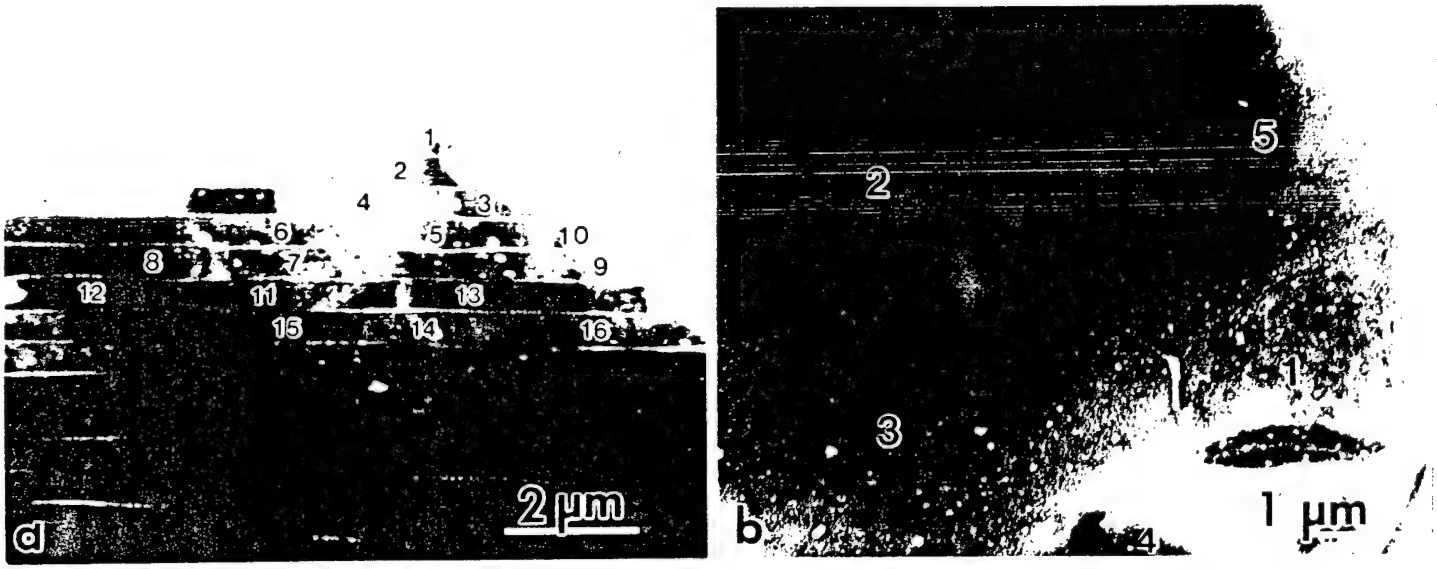

Figure 6: **(a) TEM BF Image, Neighboring Platelets, Edge-On Direction**
(b) TEM BF Image, Neighboring Platelets, Face-On Direction

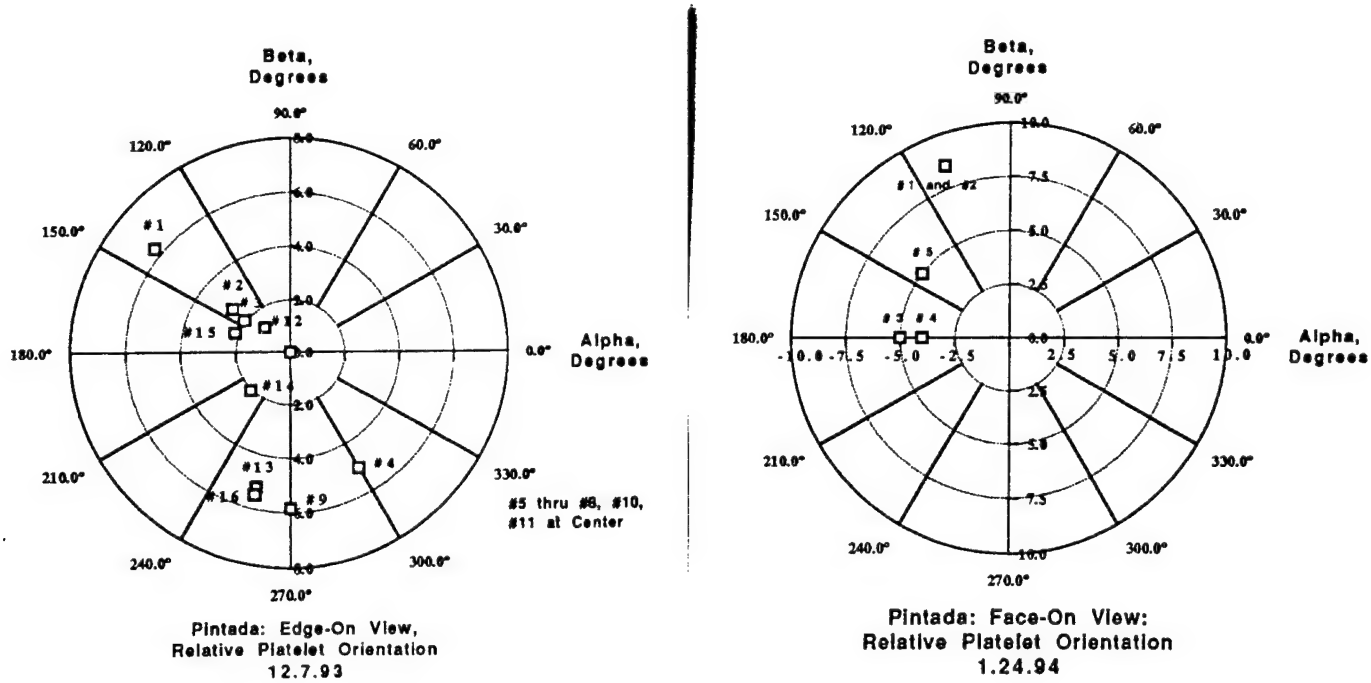

Graph(a): Polar Plot, [110] Direction for Neighboring Platelets, Viewed from Edge-on Direction
Graph(b): Polar Plot, [001] Direction for Neighboring Platelets, Viewed from Face-On Direction

Goal 2: Comparison of Microstructure of Nacre from Different Organisms

A second TEM-based experiment examined the relative microstructure of nacre from different species of mollusc. It is known[41] that in the heterogeneous mixture of macromolecules known as the organic matrix, the composition varies from one molluscan organism to the next. The question under consideration is, does this variation in organic phase composition affect any microstructural features of the nacre, and how does it do so?

To explore this issue, samples of nacre were sectioned from shells of three different molluscan organisms. Nacre samples were obtained from the shells of the nautilus (*Nautilus Pompilus*), red abalone *(Haliotis Rufescens*), and the Pearl Oyster (*Pinctada Margaritifera*). The samples were sectioned, using

[41] M. Cariolu and D.E. Morse, "Purification and Characterization of Calcium-Binding Conchiolin Shell Peptides from the Mollusc, Haliotis Rufescens, as a Function of Development," *J. Comp. Biol. B*, **157**, 717-729 (1988).

a water-cooled diamond wafering saw, and reduced to thickness suitable for study by transmission electron microscopy through sanding, followed by low-temperature ion milling. The TEM study yielded the following results and conclusions, concerning the morphology, microsructure, and microarchitecture of the composite material in the three nacre samples:

(i) Platelet thickness was approximately the same for the abalone and nautilus sample, at approximately 0.5 μm or slightly less. The nacreous platelets from *pinctada* averaged 0.7 μm in thickness.

(ii) The organic matrix layer in nacre of nautilus appears to be substantially wider than that of nacre of *pinctada* and abalone.

The primary conclusion is that the nacre from all three organisms showed remarkable similarity, despite organismal variation and differences in the composition of their respective organic matrices. From earlier research[42] into the composition of the organic matrix, the composition of organic matrices for several different molluscs has been determined. The following table details the amino acid compositions of organic matrices from mollusc shells. The data used in developing this table, it should be noted, originated in several different sources in published literature on molluscan nacre and biomineralization.

[42] M. Sarikaya, J. Liu, and I.A. Aksay, "Nacre: Properties, Crystallography, Morphology, and Formation," Unpublished research.

Table: Amino Acid Compositions of Mollusc Shells

Organism	Where	Asx	Thr	Ser	Glx	Pro	Gly	Ala	Val	Tyr	ref.
H. Rufescens	W	25.0	?	10.2	8.2	?	48.5	4.52	?	?	i.
	N	20.0	2.0	9.2	4.3	3.6	18.4	17.1	?	?	ii.
	P	20.0	11.0	6.8	5.7	5.7	11.0	6.8	?	?	ii.
N. Pompilus	WI	7.1	1.3	9.8	4.5	0.5	35.3	25.0	1.4	0.6	iii./iv.
	N	2.0	1.3	6.3	6.7	0.0	19.7	48.0	2.3	0.0	v.
	NS	26.1	4.8	7.9	6.6	4.6	23.6	4.4	1.5	6.4	vi.
P. Margaritifera	P	9.4	2.9	3.9	2.2	5.6	22.3	3.2	?	5.5	vii.

Key:

N: Nacre Only, P: Prismatic Only, NS: Nacre-Soluble Proteins, W: Whole Shell, WI: Whole Shell, Insoluble fraction only.

References:

i. M. Cariolu and D.E. Morse, "Purification and Characterization of Calcium-binding Conchiolin Shell Peptides from the Mollusc, *Haliotis Rufesccens*, as a Function of Development," *J. Comp. Biol. B*, **157**, 717-729 (1988).

ii. N. Nakahara, G. Bevelander, and M. Kakei, "Electron Microscopic and Amino Acid Studies of the Outer and Inner Shell Layers of *Haliotis Rufescens*," *Venus*, **41**, [1] 34-46 (1982).

iii. M.F. Voss-Foucart, "Essais de Solubilization et de Fractionnement d'une Conchioline (Nacre Mulare de *Nautilus Pompelius*, Mollusque Cephalopode)," *Comp. Biochem.*, **26**, 877-886 (1968).

iv. E.T. Degens, D.W. Spencer, and R.H. Parker, "Plebiochemistry of Molluscan Shell Proteins," *Comp. Biochem. Physiol.*, **20**, 553-579 (1967).

v. S. Weiner and L. Hood, "Soluble Protein of the Organic Matrix of Mollusc Shells: A Potential Template for Shell Formation," *Science*, **190**, 987-989 (1975).

vi. G. Goffinet and C. Jeuniaux, "Composition Chimique de la Function "nacrpine" de la Conchioline de Nacre de Nautilus Pompelius Lamarck," *Comp. Biochem. Physiol.*, **29**, 277-282 (1969).

vii. S. Tanaka, H.Hatano, and O. Itasaka, "Biochemical Studies on Pearl. IX: Amino Acid Composition of Conchiolin in Pearl and Shell," *Bull. Chem. Soc. Japan*, **33**, 543-545.

In separating the organic matrix from the mineral phase (by dissolution of the mineral phase (aragonite) through use of a weak acid such as EDTA), it is impossible to preserve higher-level structure which may contain significant "information" that could affect mineral growth atop the matrix layer. Because of this limitation, it remains unfeasible to make a comparison of the respective structures of the organic matrices from different organisms. Hence, comparison is made (as above) between the relative amino acid compositions of the organic matrices from different nacre samples.

6B, (in Appendix: Figures)

In Figure , a composite micrograph containing images of nacre from all three organisms is presented. In this view, features of the nacre from different species can be distinguished.

Goal 3: Comparison of Microstructure: Aragonite from Nacre, and Aragonite of Geologic Origin

To complete characterization of nacre, and aragonite, from mollusc shell, we compared features in the microstructure of biogenic aragonite with microstructural features of geological aragonite. We have commented, already, on prominent differences in the morphology of aragonite from biogenic and from geologic sources. Biogenic aragonite in nacre occurs in flat, thin, polygonal platelets, whereas geological aragonite assumes a columnar, hexagonal morphology. In addition to this morphological comparison, we have explored whether there are substantial differences in the fine-scale features and

defect structures in these two distinct materials. If differences do exist at the ultrafine scale level, these differences, in addition to those in the morphology of the two systems, could be associated with the respective conditions of formation under which these materials were generated. I have used TEM analysis, as discussed earlier, to examine the substructural features found in biogenic and in geologic aragonite. A summary of the results of comparison of microstructural features the two systems display is provided in the table, below. (In the table, BA is used to indicate Biogenic Aragonite, and GA is used for Geologic Aragonite).

Microstructural Feature	**Abundance**	**Comments**
Dislocations	BA: Moderate GA: Low or none	
Stacking Faults	BA: Low GA: Moderate	
Grain Boundaries		BA: Incoherent, Separated by Organic, Smooth GA: Jagged, Semicoherent
Twins	BA: Moderate GA: Very High	BA: Hierarchical Twinning GA: Coarse and Fine Twins
Voids	BA: High GA: None	

The following TEM micrographs, found in Figure 7 (*See Appendix: Figures*) show examples of the types of defects found in each material system that are indicated in the table.

(#1) An overview, at high magnification, of aragonite from:

(a) Biogenic source: Mollusc shell nacre (Nautilus)

(b) Geologic source: Aragonite mineral, from Idaho

Several defect structures are visible in the respective materials systems, and are noted in the markings on this micrograph.

(#2) Dislocations in geologic aragonite.

(#3) Grain boundaries in biogenic aragonite (a) and in geologic aragonite (b).

(#4) Stacking Faults in geologic aragonite.

(#5) Voids in Biogenic Aragonite.

(#6) Twins in Geologic Aragonite (a) and in Biogenic Aragonite (b).

In summary, the microstructural fabric of geologic aragonite appears to contain a higher concentration of defects than does that of biogenic aragonite. This may be attributable to pressures and stresses at the site of formation of geologic aragonite that are not experienced by biogenic aragonite in its formation, and this may be due in part, as well, to the influence of organic matter in nacre on the formation of crystalline aragonite tablets.

Goal 4: Comparison of composition, Biogenic and Geologic Aragonite

Composition of distinct types of aragonite (biogenic and geologic) has been determined with use of microprobe Energy Dispersive Spectroscopy (EDS) in TEM. Compositional analysis for aragonite from Nacre of Pinctada, Abalone, and Nautilus is indicated in the EDS plots provided on the following page. In addition, composition of geological aragonite is provided in a separate plot.

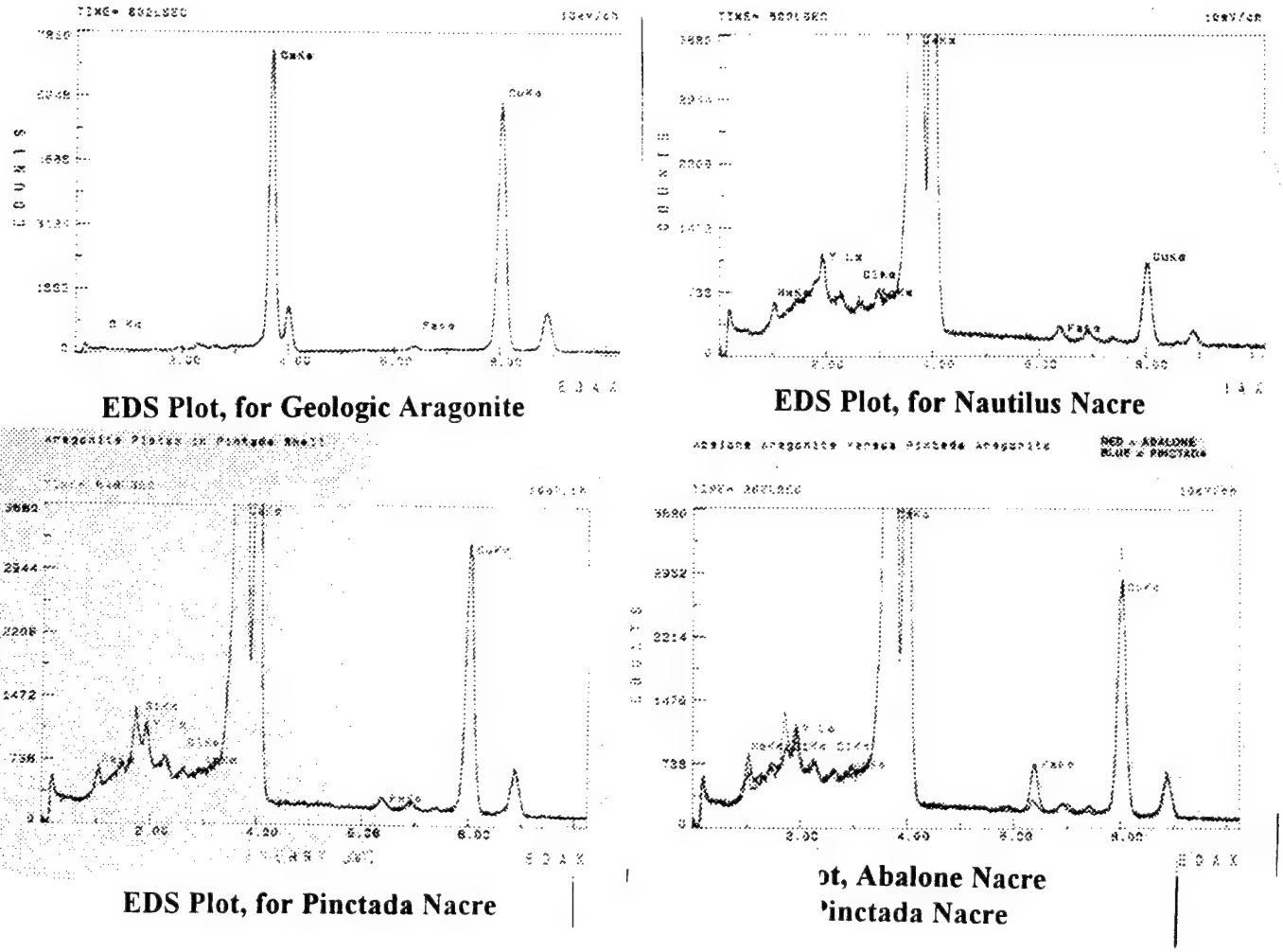

Figure 8: **EDS Plots, Geological Aragonite, Abalone, Pinctada, an Nautilus Nacre**

Future Microscopic Study of these Materials:

•High resolution imaging (using TEM) of both materials, to compare structure,

•Comparison of lattice parameter, using convergent beam electron diffraction (CBED) technique, and

•Comparison of chemical environment of calcium, through use of electron energy loss spectrum (EELS) method.

3.2 Investigation of Biomineralization (Accomplished and Planned Research)

3.2.1 Synthetic Systems: $CaCO_3$ Precipitation in Solution

Part 1: Without Habit-Modifying Ionic Components

Using the method of supersaturation of calcium-carbonate aqueous solution through carbonation with respect to CO_2 (discussed earlier, known as the Kitano technique), a range of parent-solution compositions were produced, and the characteristics of the precipitate produced from such solutions was examined. The choice of which compositions for parent solutions that would be assessed followed a strategy in which the goals were:

First, to vary the level of magnesium present in solution, thereby producing different Mg^{2+}:Ca^{2+} ionic ratios in solution, until the relationship between the relative abundance of these two elements and the mineralogy of the resultant precipitate (either calcite or aragonite) was established.

Second, to examine the product of precipitation from a solution whose composition closely mimicked that of seawater.

Third, to return to a simplified solution whose primary constituents in solution were Ca^{2+} and Mg^{2+} ions (at correct ratio to yield aragonitic precipitate, as established by the first set of experiments) and CO_3^{2-} ions. To this parent solution composition, selected inorganic ions found in sea water were added, one at a time. In this way, we investigated the effect (as growth modifiers) of specific inorganic ions. The inorganic ions were included in the parent solution at concentrations half, one time, and two times their respective concentrations in seawater.

Results of Experiments

Part 1: Ca/Mg Solutions

In the initial phase of experiments in which morphology of precipitate particles is controlled by and related to parent solution composition, the influence of magnesium on characteristics of precipitate was examined. Solutions initially were supersaturated in Ca^{2+} and CO_3^{2-} (by CO_2 carbonation). To these solutions, Mg, in the form $MgCl_2$, was added. The relative proportion of Ca^{2+} and Mg^{2+} in these solutions was varied systematically. Experiments which generated precipitate were run from solutions which contained no magnesium, and magnesium at concentrations 1.0X, 5.0X, and 7.5X the concentration of calcium in the parent solution. The calcium concentration ($[Ca^{2+}]$) for these solutions was 10 mM, which approximates the concentration of this component in seawater.

Photos of precipitate generated from solutions containing only CO_3^{2-}, Ca^{2+}, and Mg^{2+} are presented in Figure 9 (in *Appendix: Figures*). The most regular, faceted crystal particles were grown from the initial solution without any magnesium. As magnesium content for the solutions was increased (in solutions where the Mg:Ca ratio was 1:1, 5:1, and 7.5:1), the precipitate particles, as shown in Figure 9, became increasingly acicular and irregular.

Mineralogy of the precipitates, determined by XRD of dried and powdered precipitate, was calcite for the no-Mg solution, for the 1:1 Ca:Mg solution, a mixture of calcite and aragonite, and for the 5:1 and 7.5:1 solutions, aragonite.

The results, in terms of both morphology and mineralogy of particles, is consistent with the theory that magnesium can disrupt nucleation and growth of calcite when present in aqueous solutions, and that in sufficient quantity, the magnesium will make formation of aragonite favorable. The results have enabled us to establish conditions which would permit formation of aragonite from solutions

supersaturated in Ca^{2+} and CO_3^{2-}, by adjusting the Mg^{2+} content of such solutions. These "recipes" for growth of aragonite precipitate will, in turn, be useful for subsequent experimentation in growth of particles of aragonite of controlled shapes as seen in mollusc shell nacre.

Part 2: Particles grown from Parent Solution in which Mg:Ca Ratio was 5:1, with Addition of Selected Inorganic Ion Species, as Growth Modifiers

Additional experimental work on habit modification for precipitated $CaCO_3$ solid investigated the effects of four different ionic species, namely Sr, Li, K, and Ba. The matrix below details the set of 12 experiments which were conducted, in which these ions were added (from solid halide compounds) to a parent solution with a 5:1 Mg:Ca ratio. The ions chosen represent the major ionic constituents of seawater (aside from Na^+ and Cl^-). These ions were individually included in the parent solutions at concentrations near levels found in seawater. SEM micrographs of morphology of typical precipitated particles from each ionic addition are shown in Figure 10 (in *Appendix: Figures).*

Compo., Mother Solution, Calcium	Conc., Magnesium	Volume of Mother Solution	Ion Species Added	From What Compound	Dilute Solution Conc., Ion Addition	Amount Solution Added	Conc. of Ion Relative to Seawater	Actual Ion Concentration
4.5 mM	22.5 mM	100 ml.	Sr	$SrCl_2 6H_2O$	0.01 M	1.514 ml.	1.0 X	0.1514 mM
4.5 mM	22.5 mM	100 ml.	Sr	$SrCl_2 6H_2O$	0.01 M	3.028 ml.	2.0 X	0.3028 mM
4.5 mM	22.5 mM	100 ml.	Sr	$SrCl_2 6H_2O$	0.01 M	0.757 ml.	0.5 X	0.0757 mM
4.5 mM	22.5 mM	100 ml.	Sr	$SrCO_3$	0.01 M	1.514 ml.	1.0 X	0.1514 mM
4.5 mM	22.5 mM	100 ml.	Sr	$SrCO_3$	0.01 M	3.028 ml.	2.0 X	0.3028 mM
4.5 mM	22.5 mM	100 ml.	Sr	$SrCO_3$	0.01 M	0.757 ml.	0.5 X	0.0757 mM
4.5 mM	22.5 mM	100 ml.	Li	LiCl	1.0 M	2.3 ml.	not sure	.023 mM
4.5 mM	22.5 mM	100 ml.	Li	LiCl	1.0 M	8.0 ml.	not sure	.080 mM
4.5 mM	22.5 mM	100 ml.	Li	LiCl	1.0 M	23.0 ml.	not sure	.23 mM
4.5 mM	22.5 mM	100 ml.	K	KCl	0.001 M	9.445 ml.	1.0 X	9.445 mM
4.5 mM	22.5 mM	100 ml.	K	KCl	0.001 M	18.89 ml.	2.0 X	18.89 mM
4.5 mM	22.5 mM	100 ml.	K	KCl	0.001 M	4.7225 ml.	0.5 X	4.7225 mM

One of the aims of the investigation of the effect of habit modifiers was to uncover a specific composition whose precipitate resembled the particles generated in nacre, produced through biologically-controlled precipitation. These particles (in nacre) are platelet-like, approximately 0.5 μm thick, 5-10 μm in breadth across their flat surfaces (dimensions gathered through TEM examination of nacre samples), and polygonal in shape (as viewed facing the flat surface). We plan to utilize the composition which produces such nacreous-like platelets in subsequent mineralization experiments where organic molecular components are included in the parent solution The Sr^{2+} - influenced precipitate did show such platelet-like particles in some of the precipitate generated. Images (via SEM) of Sr^{2+} influenced precipitate particles are shown, below.

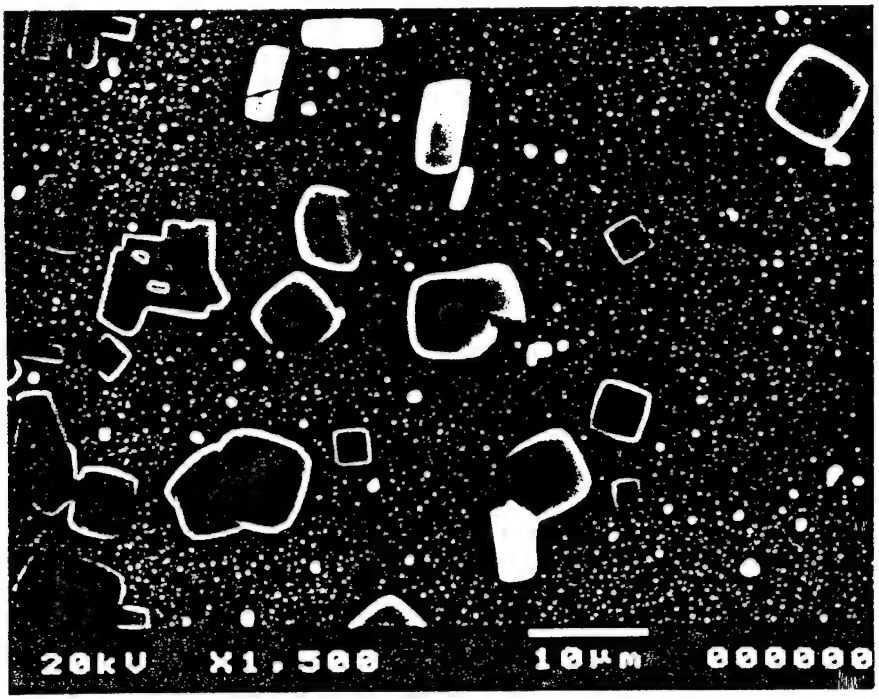

Figure 11: Photos, Platelet-like Particles from Addition of Sr

3.2.2 Biomineralization Strategies in Presence of Organics

Part 4: Mineral Growth in Presence of Organic Molecular Additives

Following exploration of the character of precipitation from solutions containing Ca2+, Mg2+, and selected inorganic ions/growth modifiers, we have started to examine the effect of orgainc macromolecules in similar solutions on morphology of precipitates. Initial results for addition of macromolecules extracted from mollusc shell nacre are presented in Figure 11 (?) (in *Appendix: Figures*).

The macromolecules added in these experiments represent a portion of the organic component of molluscan shell nacre. Specific fractions of extracted molecular components from organic matrices of abalone shell were isolated by:

(a) Crushing (dried) abalone shells

(b) Dissolving (removing) the mineral portion of the shells with weak acid (EDTA)

(c) Eliminating the dissolved $CaCO_3$ by membrane dialysis

(d) Isolating residual proteins from EDTA solvent.

The protein extracted in this manner was added to 10 mM Ca^{2+}, 50 mM Mg^{2+} solution at concentrations 0.25 μg/ml, 0.5 μg/ml, 1.0 μg/ml and 2.0μg/ml. The resultant morphology of typical small particles precipitated from these solutions is shown in Figure 12. (In *Appendix: Figures*). Using such an approach, as seen in the micrographs, it was possible to produce platelet-like polygonal particles approximating in shape the crystalline platelets found in nacre. These experiments have been performed for a few protein concentrations only. The precipitation experiments involving protein will be replicated and additional vartiations in composition examined, to allow for more complete assesment of the influence of proteins on $CaCO_3$ precipitates from solution.

IV. Future Studies

(I) Structure of Nacre

a. In-depth analysis of the microstructural features of aragonite from molluscan nacre and from geologic sources. Classification of defect structures found in the the two respective forms of aragonite. Comparison of microstructures.

b. Examination of the interface region between calcitic and aragonitic portions of the abalone shell.

c. Single-crystal X-ray diffraction study of blocks of nacre and of aragonite. Comparison of profiles from this study. Information from this sudy will give some indication of the orientational ordering found in nacre and a comparison to alignment of crystalline grains in geologic aragonite.

(ii) Formation of Nacre

(iii) Synthetic Assembly of Small Particles, Thin Films, and Nacre-like Structures

a. Growth of precipitates from solution with protein added to it. In these types of experiments, supersaturated solutions containing Ca^{2+} and CO_3^{2-} and specific inorganic ions at near-seawater concentrations would be reduced. To these solutions, small amounts of organic molecules extracted from mollusc shell would be added. In similar manner to initial mineral growth experiments, solubility of $CaCO_3$ would then be reduced by terminating carbonation of these solutions. Morphology of precipitate particles generated from this process could be characterized by SEM to determine the possible influence and control over morphology exerted by these proteins.

b. Growth of precipitate on substrates with prepared assemblies of organic macromolecules attached to them. It is possible to create regularly spaced arrays of functional molecules which are attached to substrate surfaces. (One method to prepare such an activated substrate is to first create an organized monolayer of organic molecules in a Langmuir apparatus, then to transfer this monolayer to the surface of a rigid substrate, such as glass). By placing such surfaces in a solution supersaturated with Ca^{2+} and CO_3^{2-} ions, and allowing precipitation of crystalline solid to take place on this substrate, one could explore the influence of specific species of molecules thought to interact with ions from solutions and to moderate the transformation of these ions to solid material. This process is suspected to take place in biomineralized growth of shells, where, for example in nacre, aragonite tablets form on an organic matrix from fuid in the extrapallial space. Though it may be difficult to utilize actual macromolecules extracted from mollusc shells in such a process, due to the difficulty in isolating these and the small quantities of organic matter available after isolation has occurred, it would be feasible to use similar surfactant molecules with known active headgroups to produce an organized molecular assembly for future mineral growth.

c. Growth of mineral particles under organized surface monolayers (Langmuir monolayers).

Additional microscopic investigation of nacre would include an attempt to explore the growing edge of nacre at the highest resolution, through use of atomic force microscopy. Because the AFM instrument is capable of imaging samples in a fluid medium, it could be possible to observe the inner surface of the shell in a solution mimicking extrapallial fluid, thereby preserving or closely simulating conditions found in the living organism. Such an experiment could provide key information about nucleation and growth of aragonite tablets in the shell, and possibly about the role of the organic matrix in this process. Additional TEM could be employed to examine and investigate orientation telationships between the mineral and organic phases in nacre, by gathering diffraction data from both phases simultaneously. Such an experiment poses significant challenges for the electron microscopist, however, because diffraction from the organic phase is difficult to attain due to the sensitivity and instability of this phase under electron beam irradiation. Success in this experiment would require careful and clever treatment of the sample under the electron beam.

There remain a number of experiments involving mineral growth from aqueous solution that can be applied when suitably isolated and prepared organic constituents (i.e., proteins and other organic molecules) from mollusc shells are available. These experiments will begin to answer questions on the role of organic components in the regulation of crystal particle formation in biomineralization processes. These include:

(i) Mineral growth onto organized self-assembled supernatant monolayers of selected organic molecules (Langmuir Films), possibly using organic molecules extracted from powdered abalone nacre.

(ii) Mineral growth atop seed crystals, compared to mineral growth atop seed crystals whose faces have been treated with proteins.

(iii) Studies of protein binding to sufaces of mineral crystals, and observation of differential absorption depending on which plane face of the crystal the proteins are attaching to.

Quantification of surface attachment by proteins could be made through use of proteins which have been modified by attachment of fluorescent sidegroups, and observation of the attached protein surface density by a spectrophotometer.

(iv) Examination and experimentation with self-assembly of isolated components of the organic matrix layer, in Langmuir films

(v) Design and construction of a more sophisticated large single-crystal growth apparatus, which would be useful to produce regular, faceted crystals of size in the centimeter range, rather than simply observig characteristics of small precipitate particles. With such an apparatus, one could explore the influence of proteins dissolved in parent solution on the morphology of growing crystals.

V. Acknowledgements

I would like to acknowledge Dr. M. Sarikaya for his support of my graduate research study, for providing several ideas to pursue in the course of experimental work, and for leading my efforts with his strong interest, wide knowledge, and activities in biomimetics research. I also recognize the support of R. Humbert (from the Medical Genetics Department, in Dr. Sarikaya's Research group) for contributions in the areas of protein chemistry, genetics, and understanding of the organic portion of the biogenic composite systems we study. K. Katti, for her instruction, insight, and asistance in problems related to electron microscopy and crystallography, and G.H. Kim, for patient assistance in teaching me several techniques and aiding my work in experiments involving TEM.

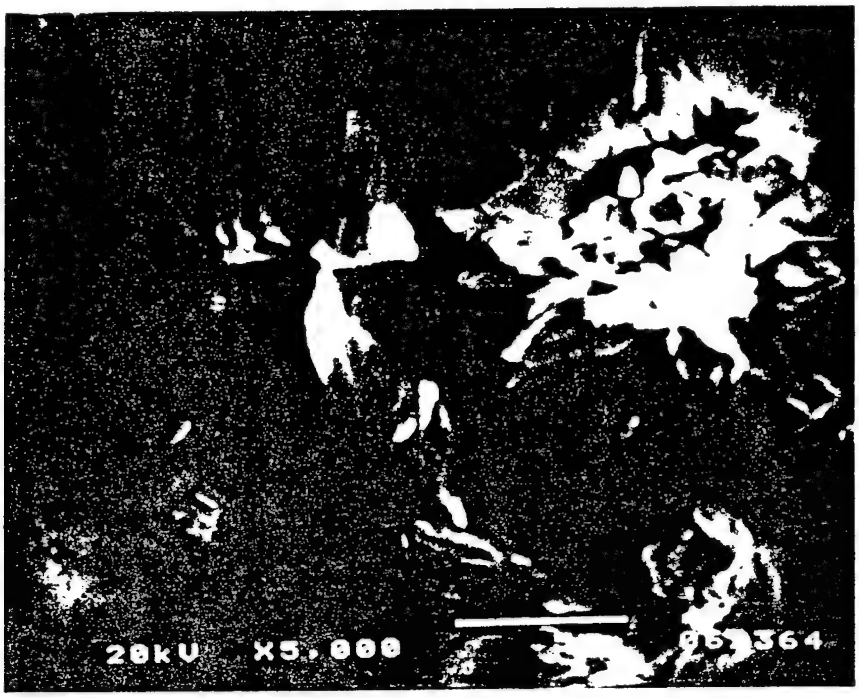

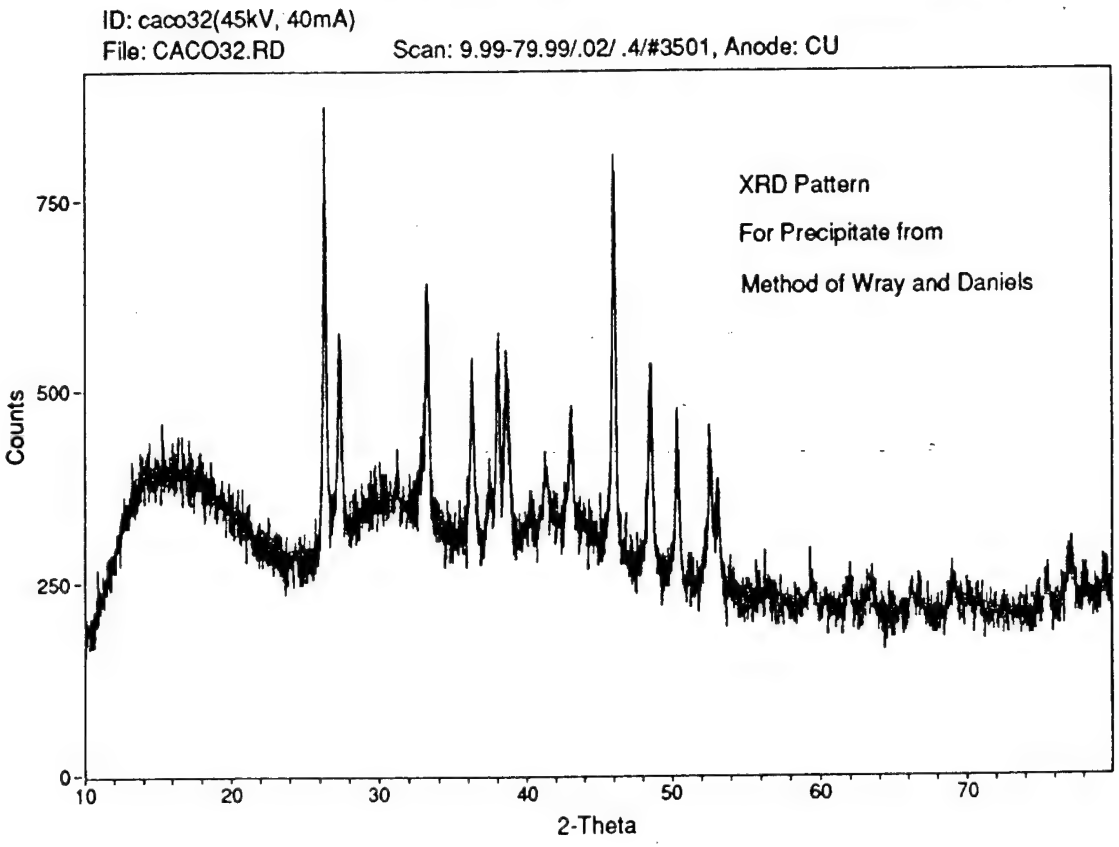

Figure 4: (1) SEM Images, Particles Precipitated by Method of Wray and Daniels (Method 1)
(2) XRD Pattern, Confirming these Particles are Aragonite

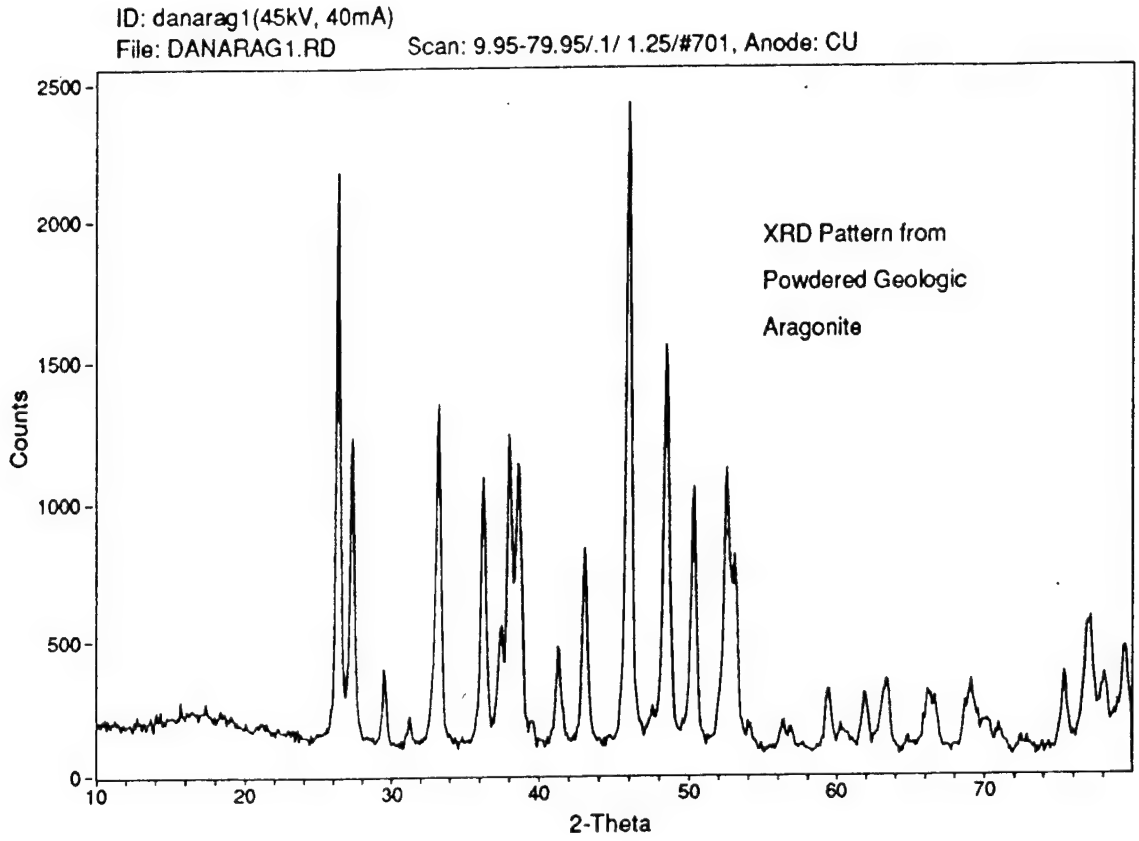

Figure 4. XRD Pattern from Powdered Geological Aragonite

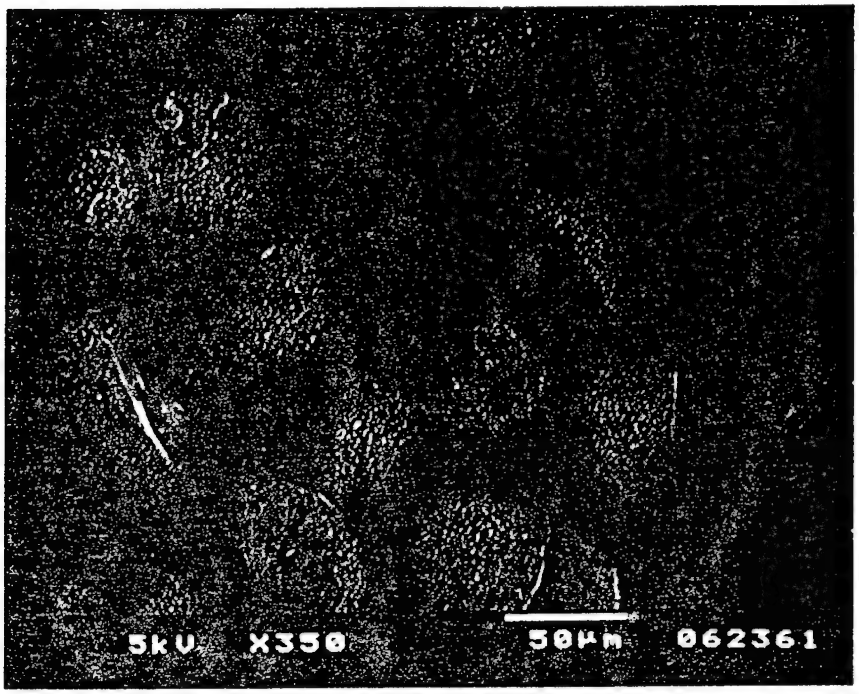

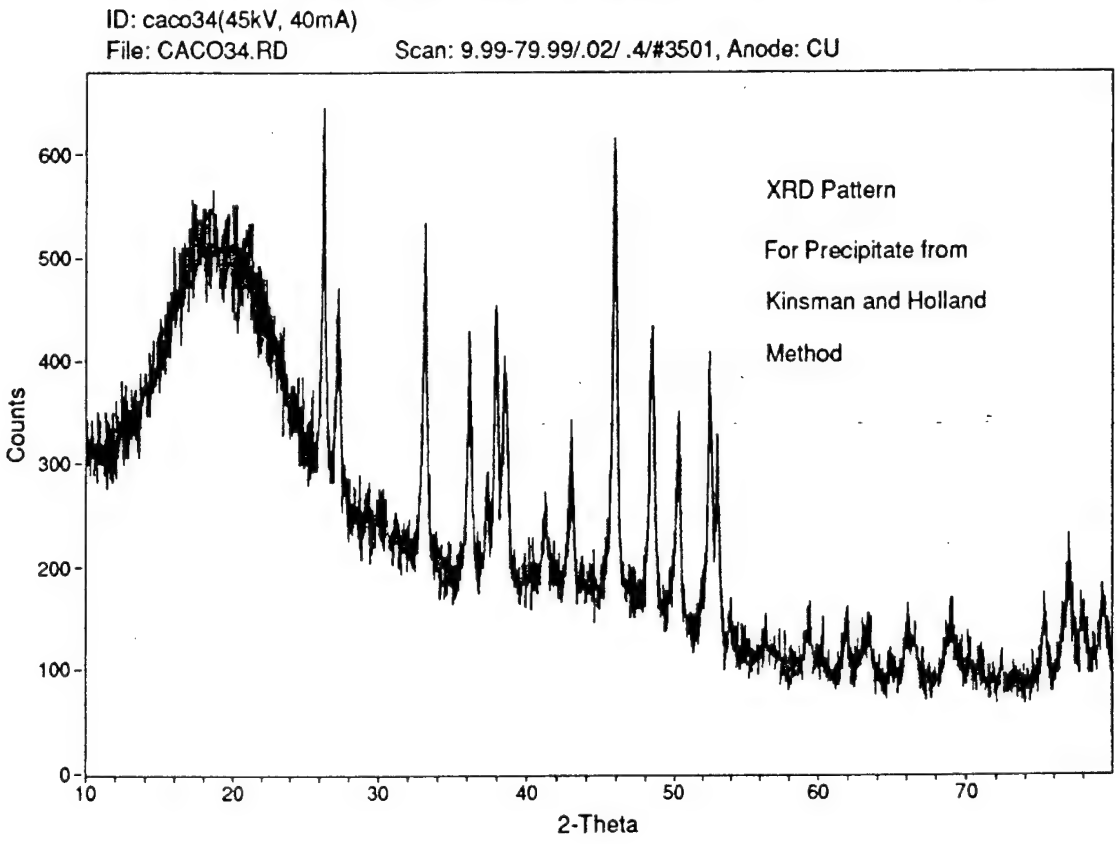

Figure 5: **(1) SEM Images, Particles Precipitated by Method of Kinsman and Holland** *(Method 2)*
(2) XRD Pattern, Confirming these Particles are Aragonite

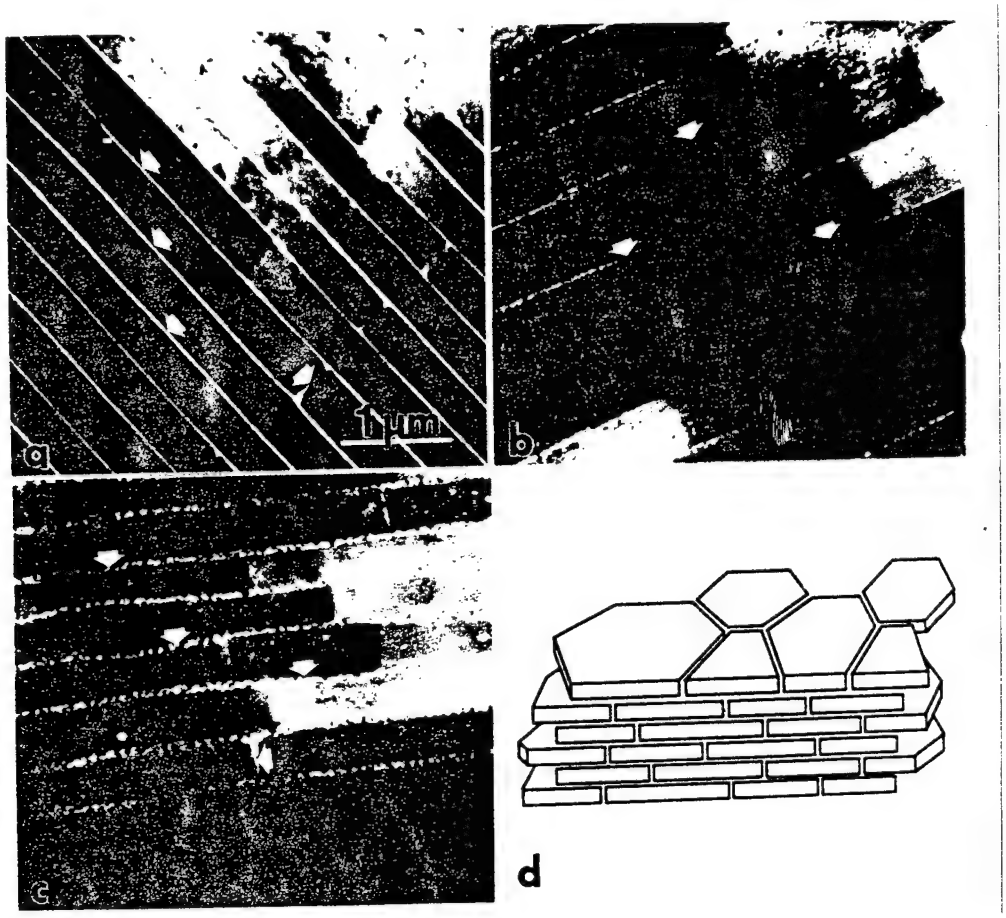

Figure 6B: **Composite View, TEM Bright-Field Images, Nacre from three different Molluscs**
(a) Abalone
(b) Pinctada
(c) Nautilus

Figure 7: **TEM Images of Defets and Microstructural Features in Biogenic Aragonite and in Geologic Aragonite (Microstructural Comparison)**

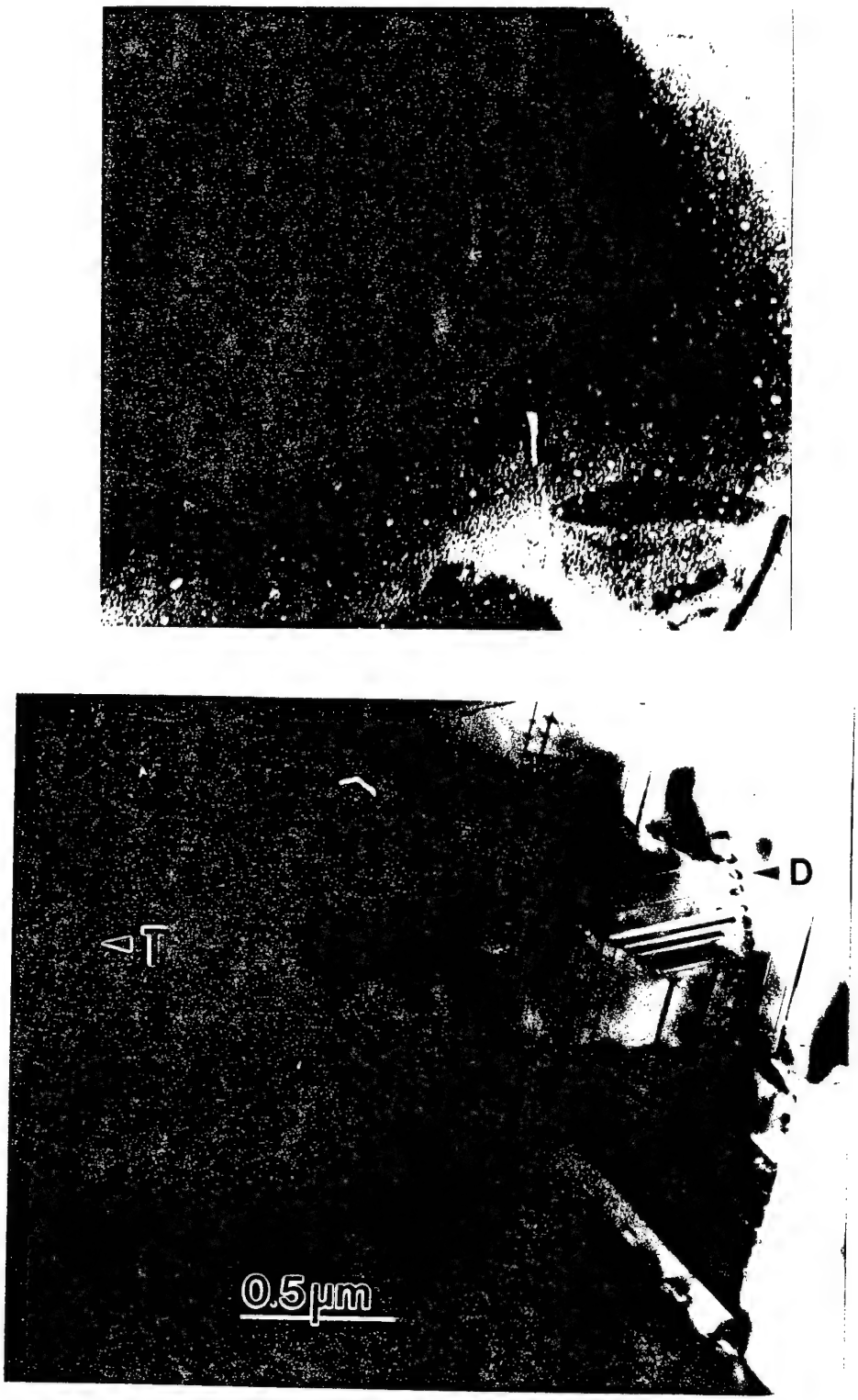

(#1) Defect Structures Visible in High Magnification Views, Biogenic and Geologic Aragonite

T: Twin
D: Dislocation
P: Pore

(#2) Dislocations in Geologic Aragonite

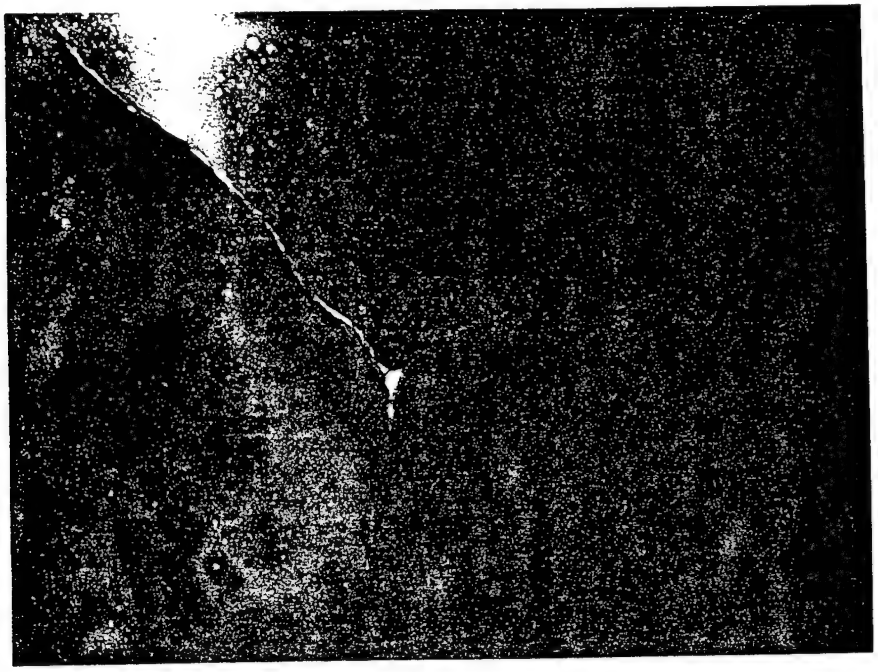

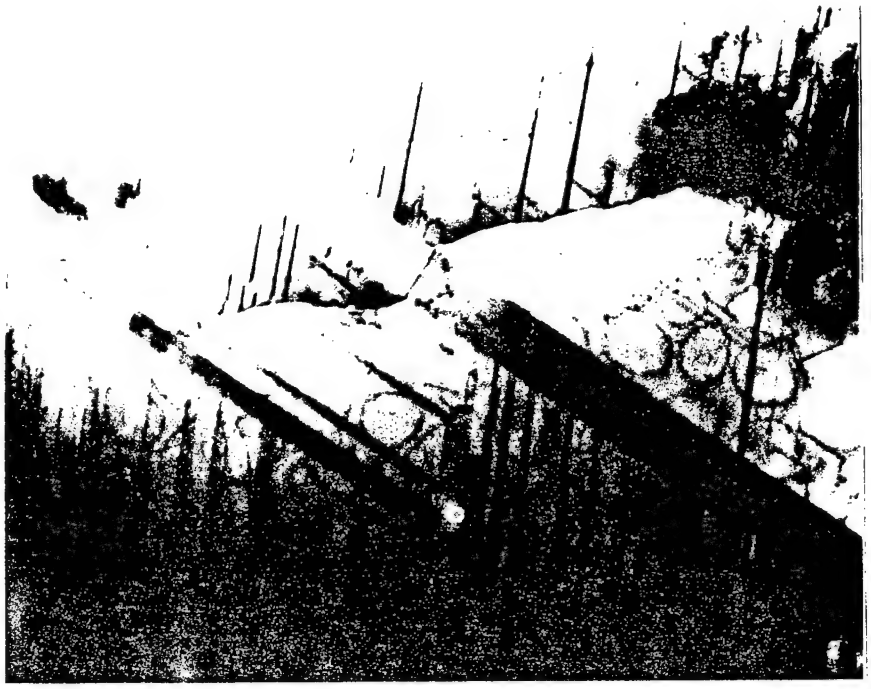

(#3) Grain Boundaries in

a. Biogenic Aragonite (TOP)

b. Geologic Aragonite (BOTTOM)

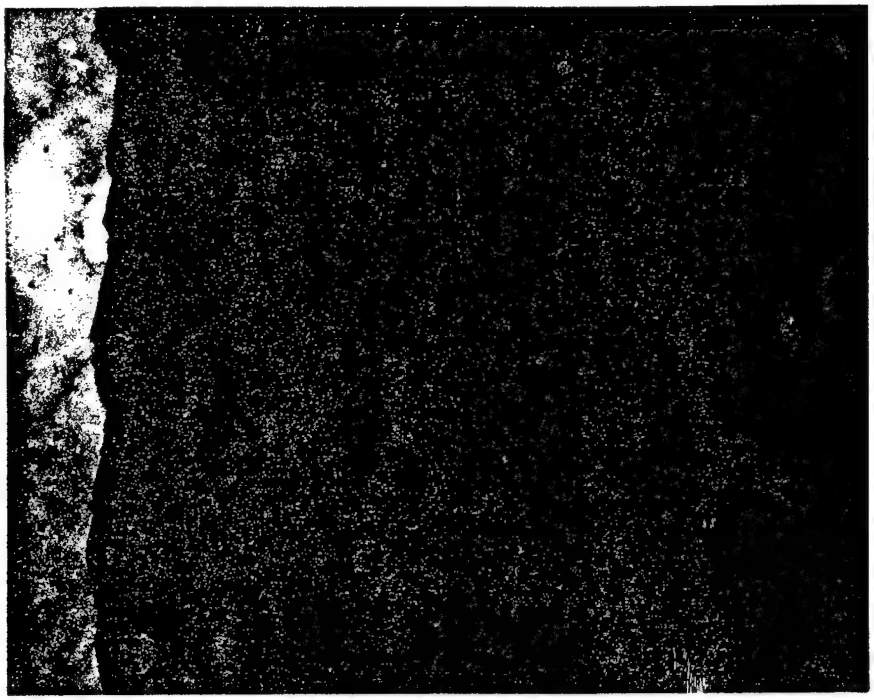

(#4) Stacking Faults in Geologic Aragonite

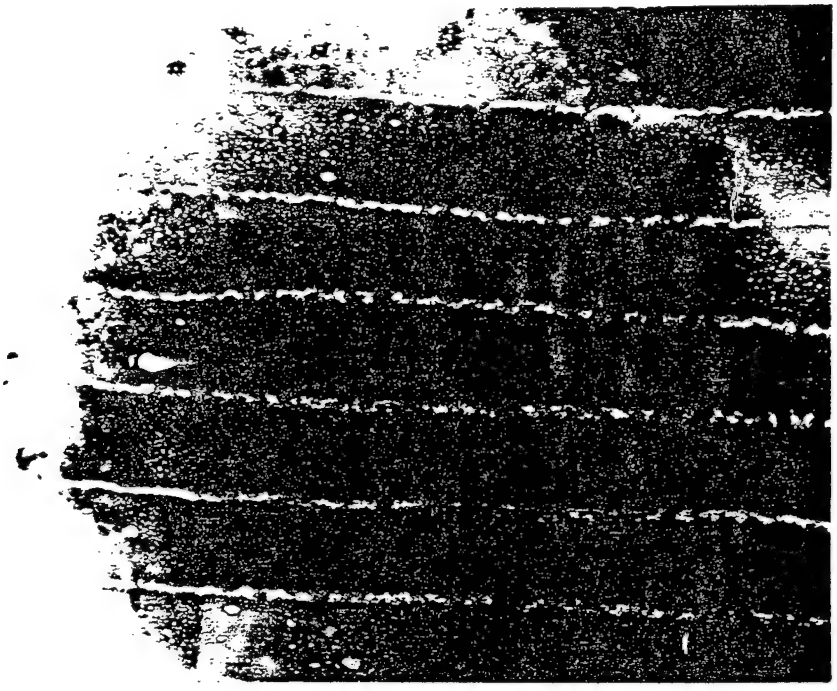

(#5) Voids in Biogenic Aragonite

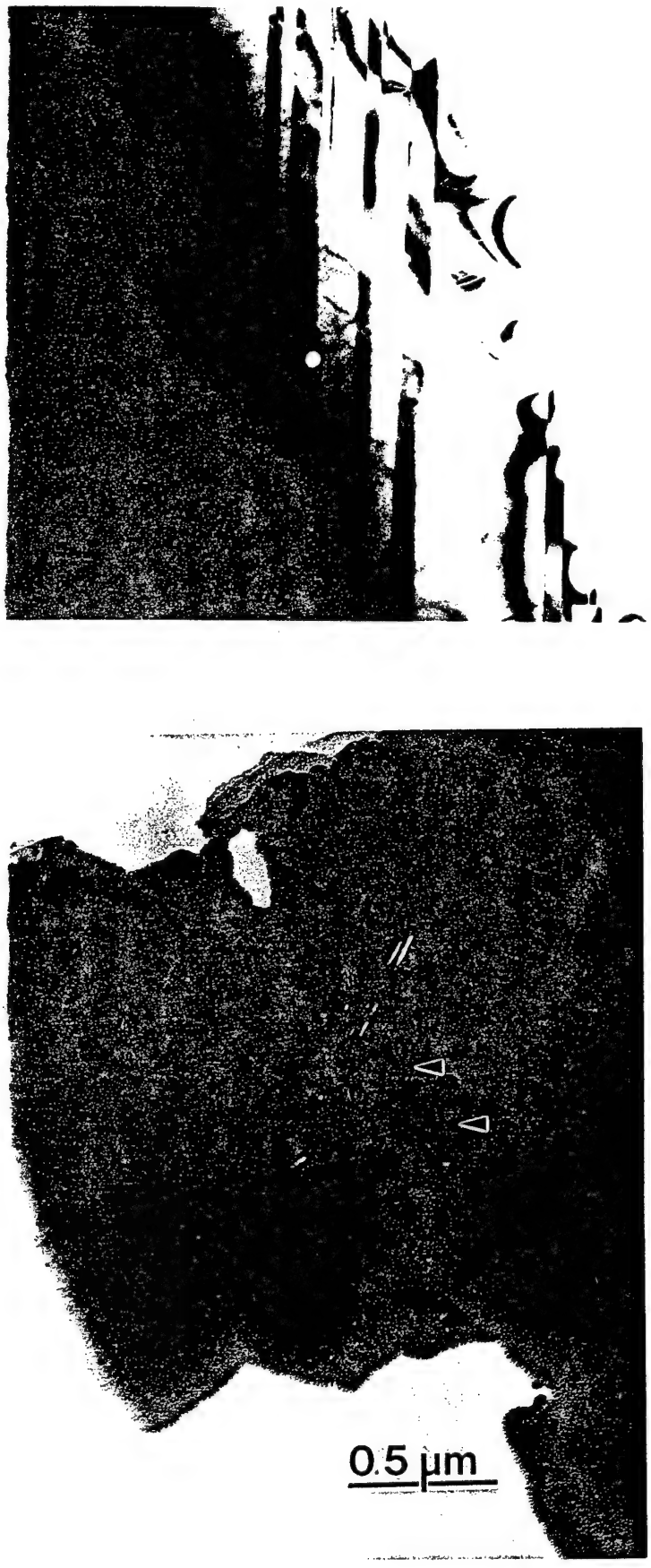

46) Twins in Geologic Aragonite (top) and Biogenic Aragonite (bottom)

Figure 9: Photos, Precipitate from
0:1, 1:1, 5:1, and 7.5:1 Mg:Ca Solutions

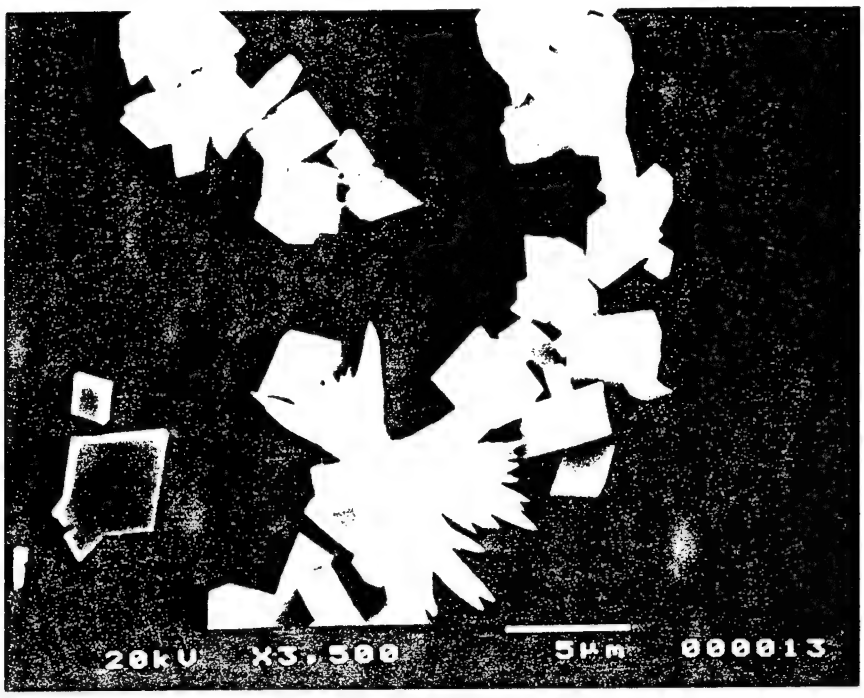

Ppt. From 0:1 Mg:Ca Solution

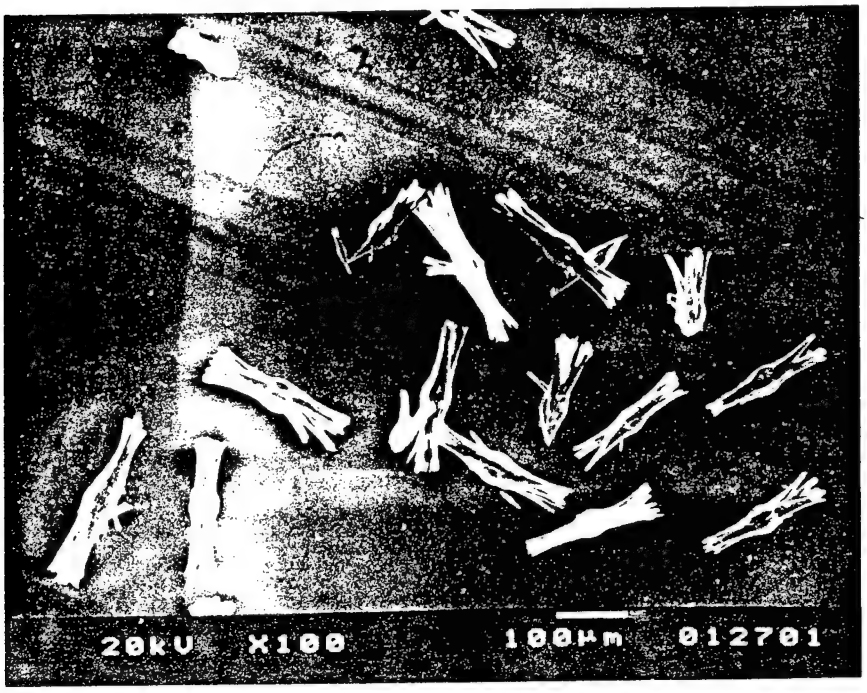

Ppt. From 1:1 Mg:Ca Solution

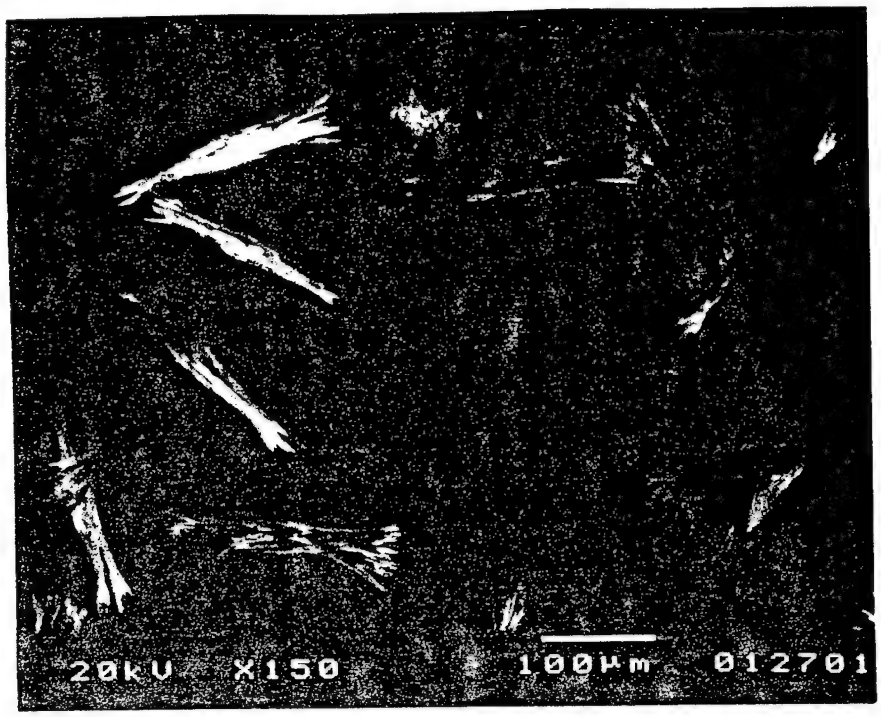

Ppt. From 5:1 Mg:Ca Solution

Ppt. From 7.5:1 Mg:Ca Solution

Figure 10: SEM Images, Particles from Addition of Ions Sr, K, Ba, and Li

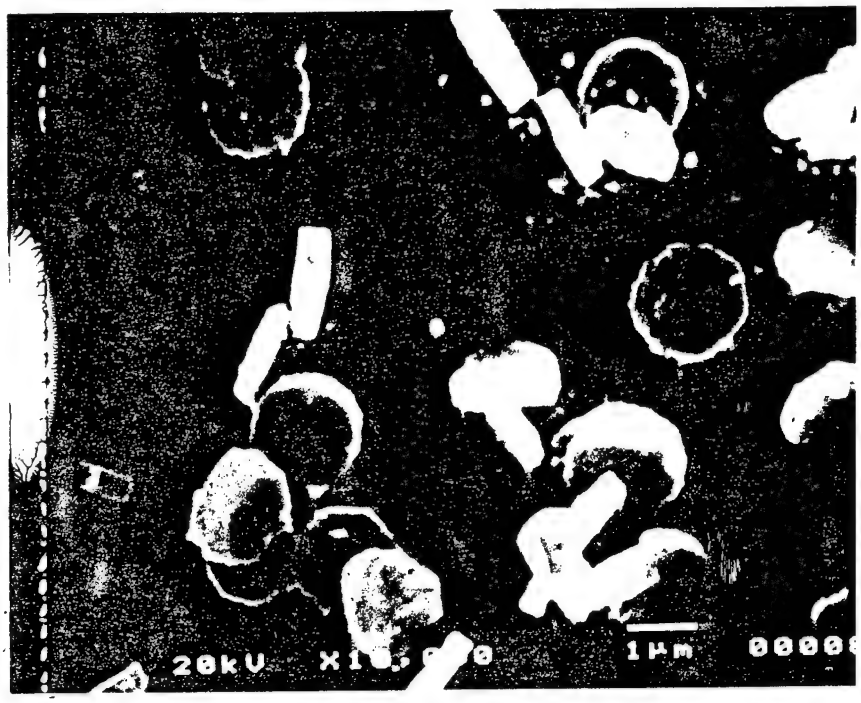

Addition of Sr

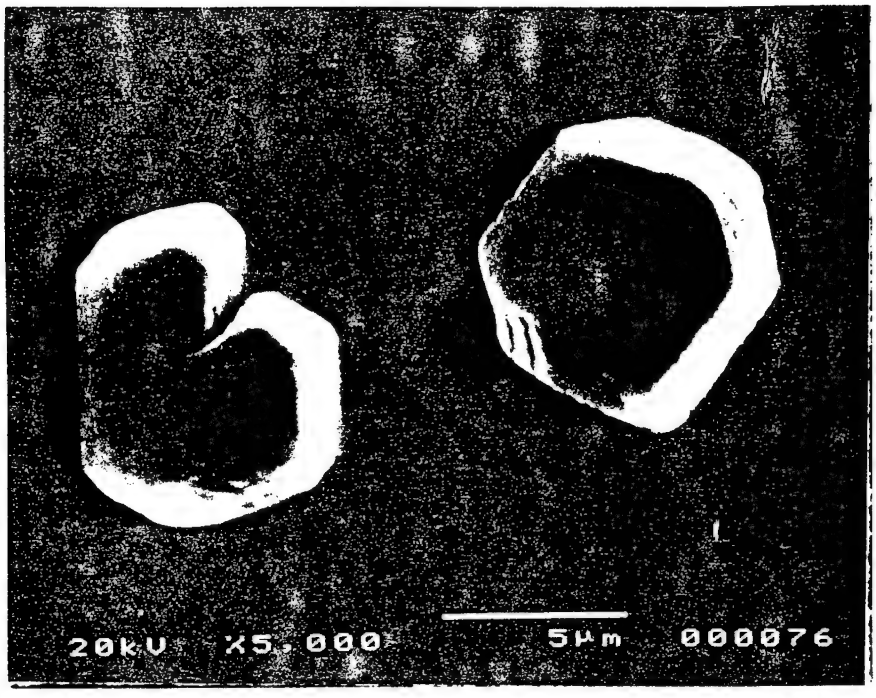

Addition of K

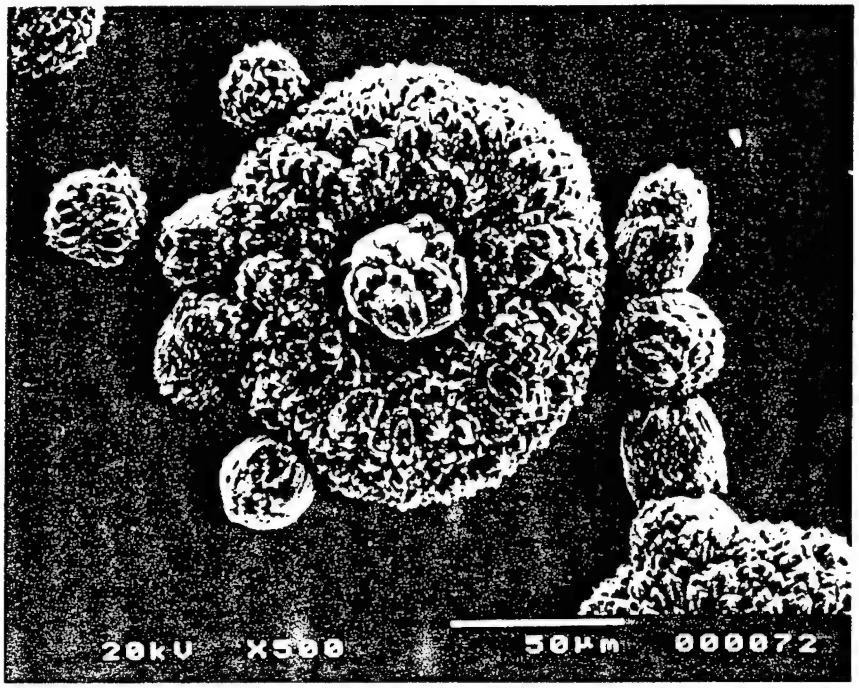

Addition of Ba

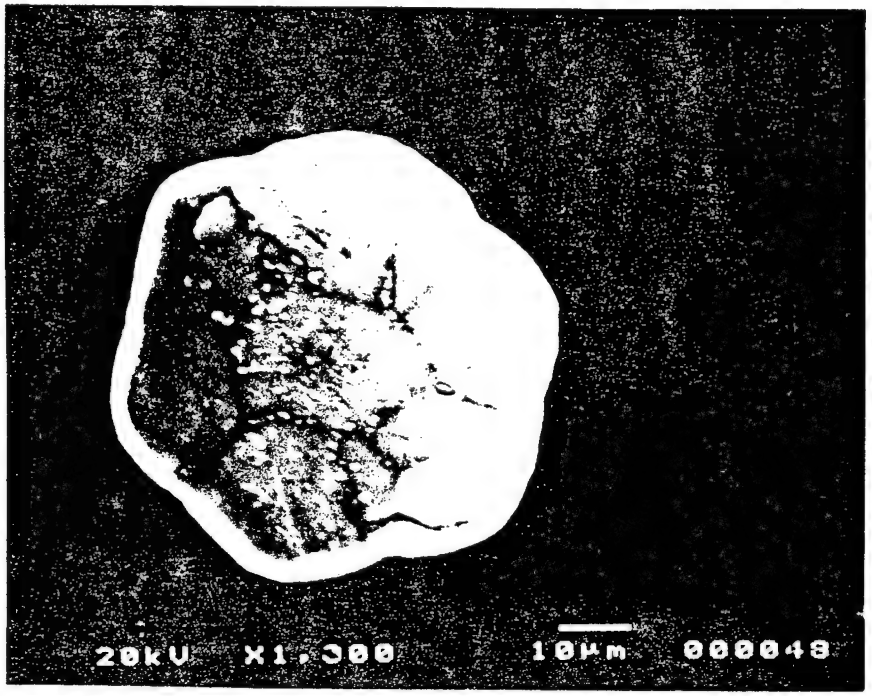

Addition of Li

Figure 12: SEM Images, Particles from Solutions with Added Abalone Proteins

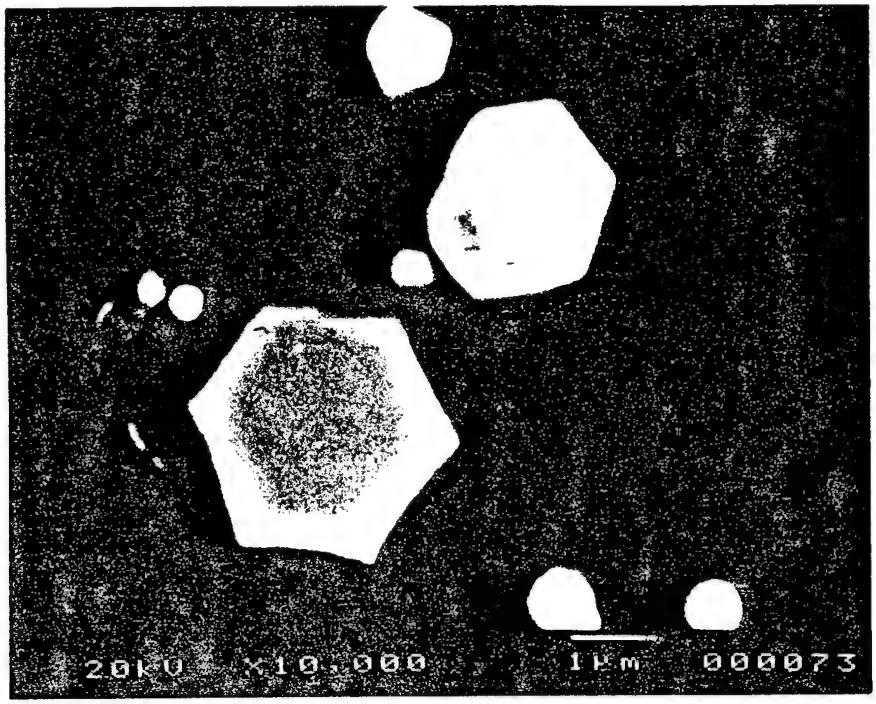

Experiment #1: No Magnesium, [Ca2+] = 10 mM
Abalone Protein: 0.5 µg/ml

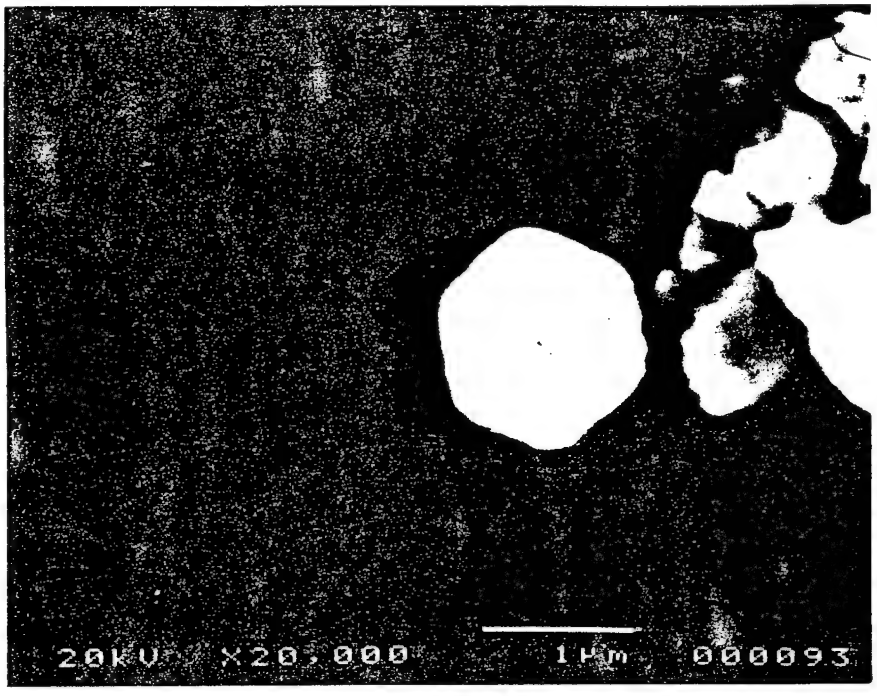

Experiment #2: 5:1 Mg:Ca Ratio, [Ca2+] = 10 mM
Abalone Protein: 0.5 µg/ml

Making of a Biological Armor: Mollusc Shell

Benjamin A. Shapiro and Mehmet Sarikaya

Department of Materials Science and Engineering,
Box 352180, University of Washington, Seattle WA 98195, USA

Abstract

The micromechanical behavior of a biological hard tissue, a molluscan shell, was examined with respect to its micro- and macro-structure for the purpose of obtaining lessons for novel armor design. Microindentation methods were applied to this system to measure mechanical properties, including, microhardness, damage tolerance, elastic recovery, and elastic modulus. In an effort to determine the effects that the inorganic phase has on the mechanical behavior of the mollusc, i.e., red abalone (Haliotis rufescens) its inorganic components, two crystallographic forms of $CaCO_3$, were similarly tested in their pure mineral forms, i.e., calcite and aragonite. Data are provided which highlights the mechanical behavior of this system, and comparisons are drawn as to illustrate this system's superiority in damage tolerance, hardness, and toughness over the mineral constituents from which it is made. Ultimately, it is suggested that the incorporation of an organic phase allows for optimal regulation of the properties that are critical to the system's function as a natural armor, and hence the survival of the mollusc species that produces it . Furthermore, comparisons are made in the structure of the "biological" and "synthetic" armors, and suggestions are made for possible improvements in the advanced armor design.

I- INTRODUCTION AND BACKGROUND

A. Nanocomposite Materials

Technological materials are rarely used in their pure forms since their physical and chemical properties depend primarily on their microstructures. The object in designing and processing materials, therefore, is to tailor their properties for specific applications through structural control. In practice, however, this control is generally limited to a specific length scale: for example, lattice structure, impurities and defects at the atomic scale, interface structure, precipitates and second phase particles at the nanometer scale, grain structure, size and shape at the micrometer scale, and finally overall architecture of the sample at the macro scale.

Recently, it was discovered that materials with controlled structural variations at the nanometer scale exhibit unprecedented physical properties, including optical, electronic, magnetic, and elastic characteristics.[1,2] Fundamental reasons for property improvements, including the nanoscale effects are not well understood. Although some current synthetic techniques can achieve controlled composite microstructures in a limited extent, it is, however, still difficult to produce materials structures with desirable interface properties and with a high degree of control of the lattice and defect structures at the nanometer scale. In this sense structural design is usually accomplished at a single length scale, with possible full control, and over several scales in synthesis, with limited control. In addition, these materials are typically processed for one particular property, such as for certain mechanical properties, and they are rarely multifunctional for more than two properties. In order to meet the demands of current and future technologies for materials with superior physical properties we will need to apply new strategies for producing components with more complex structural designs that accommodate applications which demand multipurpose uses.

Biological systems offer model materials strategies in structural design for engineering applications.[3-4] Biological systems are a rich source of inspiration for design and processing concepts for developing novel synthetic materials where structural control is established over a wide length scale. Among the many novel features which biological materials exhibit[5] is a structural design that is controlled at a continuous length scale from molecule to final tissue in a hierarchical manner.[6,7] It is likely that it is this continuum of structural design organisms, in

many cases, which provides the biological material with its multifunctional characteristics.

One example of such a material is molluscan, or conchiolin shell.[8-10] The molluscan shell are secreted by a variety of gastropods, cephalopods, and bivalves, including, *Haliotis rufescens* (red abalone), *Nautilus pompelius* (nautilus), and, *Pinctada margaritafera* (pearls oyster), respectively, and primarily function as a defense from environmental factors including natural predators.[11-12] A predatorial attack typically comes in the form of an attempted compressive overload of the shell, and thus high toughness and damage tolerance, in addition to hard surface, are critical for the gastropods survival. Recent measurements indicated the exceptionally high toughness of some biological hard tissues, including mollusc shell.[13] For example, the nacre section of abalone and pinctada shells display fracture toughness (4-point bend) values of bout 12 and 16 MPa-$m^{1/2}$.[13] Certain mechanisms, in particular platelet sliding and ligament formation, have been identified by which this material is able to achieve high toughness behavior.[10,13,14] While this finding is at least intriguing, it should not be surprising, as there are many examples of survival driven behavioral evolution in nature.[10] It is important to note that, like modern synthetic composites, it is ultimately the *structural design* which allows for the development of critical behavior defining mechanisms within the biological material. Here, exceptional mechanical behavior is the result of a highly ordered hierarchical structure. This structure allows for the optimal mechanical contribution of each phase within the composite region. While this approach has been the basis for synthetic composite design it has not been fully realized in industrial applications.[13,17] The application of hierarchical, continuously controlled structures, to synthetic composite design, will significantly enhance the quality and usefulness of these materials.

While there has been some investigation into the mechanisms operative in toughening of molluscan nacre structure, the development of a thorough understanding of the overall system in terms of their various mechanical functions remains to be accomplished.[13,14] The questions that must be addressed center around not only how the structure is able to provide the critical mechanical behavior, but how is the creature able to produce the material (i.e., mollusc shell) itself as a system, including all the inorganic and organic phases, their two- and

three-dimensional morphology, and microarchitecture.[10] It is the goal of this research to address the first issue and, in doing so, contribute to the understanding of, and application possibilities that lie within the molluscan structural design.

B. Structure of the Mollusc Shell

Red abalone shell can be thought of as a two ply composite material (Fig. 1).[9,10] The two distinct regions or "plys", although having similar elemental compositions, i.e., Ca, C, and O, have quite dissimilar structural characteristics. The outer region is called[9] prismatic (Figure b, d, e, f, and h), while the inner region is referred to as nacreous (Fig. 1 a, b, c, f, and g)). Both regions contain inorganic $CaCO_3$ as the crystal filler particles which are housed in a matrix largely containing proteins and polysaccharides.[15,16] The micro- and nano-structural elements of each region are significantly different, the most obvious distinction being the morphological and crystallographic form of the $CaCO_3$ crystallites.[10]

The prismatic region is constructed in a manner similar to a unidirectional short fiber reinforced synthetic composite.[17] Single crystals of calcite (rhombohedral $CaCO_3$, R3m) are, for the most part, aligned in the <100> crystal direction and bonded together by a thin organic matrix layer (Fig. 1b, d, f, g, and i)).[18] These crystals are approximately 1-2 μm in [100] direction and 1-20 μm in length in [001] (or [010]) direction, thus have an aspect ratio of approximately 10:1. The columnar calcite crystals are aligned along the axis normal to the shell surface (Figures 1 and 2), but are staggered in the (curved) plane of the shell to form stacked layers, which are bound on all sides by a thin (few nm thick) layer of matrix. In this sense the prismatic region is similar to a multiple ply unidirectional short fiber composite,[17] having approximately 1-2 vol. % matrix, where all plies are oriented in the same direction.[18]

In contrast, the nacreous section of the shell contains twinned pseudohexagonal-shaped single-crystal aragonite platelets (orthorhombic $CaCO_3$; Pmmm).[18] The platelets are approximately 0.25 μm thick along [001] direction and 2-10 μm in edge-length along [110] axis of the orthorhombic cell (Fig. 1b, c, e, g, and h).[10] Therefore, the aspect ratio of the individual aragonite platelet is 0.1 (ration of the

length in the **c**-axis to the length along **a**- (or **b**-) axis. The organic matrix is in the form of a fairly uniform, about 100 Å-thick, film that surrounds the aragonite platelets. The organic matrix itself is a composite material containing proteins, polysaccharides, and possibly phospholipids.[10,20] The microarchitecture of the nacreous region, therefore, is a brick-mortar structure, where the organic component (mortar) acts to bind the inorganic aragonite bricks.[9,10,14] The volume of the matrix in nacre is considerable greater at approximately 2-5%.[21-23] Both the prismatic and nacreous structures can be seen in Figures 1 and 2 which highlights the locations of these sections in the shell and their detailed microstructure, including the SEM and TEM images (Figures 1g and h/i respectively).

The molluscan shell design, therefore, is highly spatially ordered over a wide range of dimensions: two different mineralogies at the molecular scale (calcite and aragonite), substructural variations and lattice defects at the nanometer scale, crystallite particle size and shape (columnar or platelet) at the micro-meter scale, composite structures (alignment, vol. % filler), and finally two-ply composite design (prismatic and nacreous sections) at the macroscale.

C. Ceramic Armor Design

Throughout history armor systems have been designed to protect men, as well as their belongings. Traditional armor was typically made of steel, e.g., in the form of steel chainmail until the introduction of plate armor in the 15th century. A standard plate armor suit was used for both combat and sport, weighed approximately 50 lb., and was made of a variety of steel and iron parts.[24] At the beginning of this century, as projectiles and explosives became standard warfare tactics armor design shifted toward large bulky ceramic structures. Concrete and cement were used for the construction of fixed emplacements to provide protection for troops and vehicles against bullets and explosive blast fragments. The utility of such an armor, however, is limited to cases of fixed defense, where there is no weight penalty to the individual soldier. In order to broaden the applications of ceramic armors, designers were forced to incorporate weight and mobility considerations, and ultimately produced armors which married the two previous design philosophies. In the new era, after World War I, a hard enamel coating was

applied to a metal substrate in the armor design improving the resulting resistance to impact,[25] thus began the development of composite armor systems. These materials, like all composites, are created with the intention of capturing the beneficial, and, at the same time, restricting the detrimental aspects of each of the constituents from which it is made. For example, during the World War II, it was shown that a material combining plate glass and polymer encased Doron (ceramic) was much more effective in stopping projectiles than either material alone.[26-27] The progression from this basic composite macrostructure to modern ceramic composite microstructures has been an important trend in the development of armor and non-armor materials, until to the present time. In a relatively recent two-tier modern ceramic composite armor design (Figure 3), ceramic is the face material with multilayer laminate resin impregnated glass fabric as the backing material.[28] Now it appears that the ceramic faced armor system has been well established, however much work remains in the development of materials micro- and nanostructures which provide superior contributions to this, now, traditional armor system.

Within the composite system, broad armor beneficial properties are sought: low weight, high resistance to penetration, and high damage tolerance. Each region within the composite, however, has a specific function, with specific behavioral requirements.[29] The ceramic facing is naturally stiff, brittle, hard, and strong in compression. The principle employed in the selection of the ceramic face material is that defeat of an armor piercing projectile depends on: overwhelming the hardness of the projectile, sound wave velocity (proportional to the square root of the modulus over the density), and establishment of a minimum thickness required to gain a particular geometric stiffness.[30] In order to be effective, the outer ceramic layer must destroy the integrity of the projectile as it penetrates this region. This is accomplished by the deformation of the projectile such that it has a larger surface area in contact with the ceramic, therefore disseminating the projectile energy more rapidly. It is due to the large compressive yield strength of the ceramic that this is possible. With this in mind, examination of variety of existing ceramics for materials lead boron carbide as the leading ceramic choice, followed by alumina AD 85, and silicon carbide.[30]

The backing material used in the composite armor system must be able to hold the ceramic facing in place throughout its pulverization stage, as well as expend the incident energy presented by the projectile after it has encountered the hard outer layer.[30] Several mechanisms in the backing region which permit this may be: grain boundary bridging, particulate-matrix shear, ligamentation, crack bridging, and delamination of multiple bonded layers. The materials used in this region of the composite have included ductile monolithic metals such as aluminum, as well as polymer reinforced ceramic fabrics.[31] In the case of the later it is believed that the presence of more layers provides greater number of surfaces available for delamination, and therefore more energy is expended. In addition, the bonding characteristics presented by the matrix and filler is critical in the case of laminate backings. Extremely strong bonding will not allow shearing to occur between the matrix and filler particles, while poor bonding does not allow for the material to utilize the high strength and stiffness of the filler particles, so a compromise is reached between the two conditions.

As it is clear, the microarchitectural design in the molluscan shell presents an interesting example of a ceramic faced armor system. First of all, both the face and the backing materials are mainly ceramic. Also, in the mollusc shell, unlike the traditional systems seen thus far, the ceramic facing is not a monolithic material. Like the multilayered laminate backing materials used in many engineering armors, so are both the calcitic facing and the aragonitic backing materials. The microstructural design of these materials has been demonstrated, now what remains to be shown is how each region accomplishes its specific requirements in attaining successful armor design.

D. Experimental Approach

Microindentation hardness tests were performed on the molluscan and geological component materials systems to explain the mechanical behavior, as well as gain better understanding of the influence of the inorganic component on the over functionality of the armor system. The samples with each morphology (prismatic, nacreous, geological calcite, geological aragonite) was tested on two growth planes, the (001) and $(001)_n$ (n for normal direction),using two indentation

geometries, i.e., Vickers and Knoop. These tests were limited to the micro-scale, thus providing information which can be used to distinguish the prismatic composite behavior from that of the nacreous composite behavior. This scale of testing allows segregation of shell information into prismatic and nacre groups, while having no effect on the testing of the geological samples. In this manner comparisons in different behavior can be drawn between the biogenic regions themselves, in addition to those drawn between the mineral and biological forms of $CaCO_3$. By following this approach we illustrate not only the relative variation in micromechanical behavior between the geological and biogenic morphologies, but also the functionally gradient nature of the molluscan design; i.e., mechanical properties vary from one region of the material to another.[32]

I- EXPERIMENTAL PROCEDURES

A. Background

In this work, microindentation methods have been applied to both mollusc shell and geological $CaCO_3$. Both the Vickers and Knoop type indenters were used in order to determine in each sample: (i) microhardness, (ii) elastic recovery parameter, and (iii) relative elastic modulus. Small samples were cut in two crystallographic orientations [(001) and $(001)_{normal}$] and polished to a 0.05 μm surface finish. All samples were tested on a Shimatzu Type M Microindenter with a 0.017 mm/s loading rate, and 0.5 μm measurement resolution.

At this point a brief review of factors which affect hardness/stiffness is in order. Because of the multi-layered composite nature, hardness and stiffness, as measured on the micro-scale, are the result of both crystallite lattice and defect structures as well as microstructural features which span the hierarchical design of this biological material. Some of these factors are intrinsically derived from the individual phases present and some are extrinsically resolved via structural design. In a study such as this, the micro-scale values must be considered in light of several additive contributions at different spatial levels. On the crystalline level it has been noted that the geological form of aragonitic $CaCO_3$ is about 20% harder than that of calcite counterpart.[33] Although this is generally accepted, however, one must also take into account the crystallite defect structure as well as the extent

of any inclusions within the grains, such as precipitates and second phase particles.[34] In addition to these substructural characteristics, attributes such as grain size and shape, and alignment must be considered as well. As noted in metals, refinement of grains typically leads to harder and stronger, but less tough material[35] In addition, in the case of synthetic composite materials, such as fiber-reinforced ceramics, materials exhibit greater stiffness when highly aligned in the incident force direction.[17] In relation to mollusc shell design, all of these factors are present in determining the composite properties of hardness and stiffness; pseudohexagonally twinned aragonitic platelets in the nacreous region, highly-aligned prismatic columnar structure of calcite in the prismatic region, the presence of micron-scale crystallites, and two forms of calcium carbonate. All are not equally responsible for the micro-scale behavior, but all must be considered none the less.

B. Vickers Microindentation

These experiments were originally designed to simply determine the microhardness variation of the two regions in the mollusc shell, and compare them with those obtained for the mineral calcium carbonate counterparts. For this reason the Vickers indenter was selected. Because of the Vickers indenter symmetry, the testing procedure is simplified, however, the extent of quantitative information that can be obtained from this test is minimal (i.e. limited to microhardness values only). Each sample was repeatedly tested under a variety of loads in order to asses the load-size effect which is commonly referred to in static indentation experiments.[36] The load-size effect for biological calcium carbonate is not elaborated in this paper but is left for future work. This analysis allowed for the selection of an appropriate load, such that microhardness values obtained would be as close to the nominal values as possible. As such, a load of 50 gms. was selected and used in all subsequent tests.

Experiments were thus performed on four materials, in two crystallographic planes for each material, both in the c direction (i.e., [001] and [100] in calcitic samples, and [001] and [100] or [110] in aragonitic samples) This was done because of the inherent anisotropy found within the biological samples of calcium carbonate, in both nacreous and prismatic regions. Mineral samples were tested with respect to

their obvious crystallography (Figure 4), while biogenic samples were tested with respect to the crystallography of the calcium carbonate crystals within them (Figures 1 and 2).

The microhardness values obtained via Vickers indenter were calculated using the equation:[37-39]

$$H_v = (1854.4 * P) / d^2 \quad (1)$$

Where, H_v (Kg/mm^2) is the Vickers hardness, P (gm)is the load, and d (μm) is the distance.

C. Knoop Microindentation

In an effort to broaden the amount of information obtainable via the microindentation method, a Knoop indenter was applied to these experiments. As previously described, the use of a Knoop indenter should allow for the quantification of various mechanical properties, elastic and otherwise. As applied to the study of biological composite damage mechanics, elastic recovery behavior and relative elastic moduli are of primary interest.

The starting point for the formulation of the damage characteristics for a brittle system such as mollusc shell is the characterization of the elastic-plastic stress field. Looking at the variation of indenter load, P, with penetration depth, z, the functional relations for the two half cycles (loading and unloading) are defined as follows:[40]

$$P \mu H z \quad \text{(loading)} \quad (2)$$

$$P \mu E (z^2 - z_r^2) \quad \text{(unloading)} \quad (3)$$

Where z_r is the residual indentation depth, and E is elastic modulus. From these relations the following result can be obtained[33]:

$$(z_r/z_m)^2 = 1 - \mu (H/E) \quad (4)$$

It can now be seen that the parameter H/E plays an important role in the characterization of the elastic-plastic field surrounding the indentation.

As previously described, measurements of the elastic recovery at hardness indentations are of interest because of the description they provide regarding the division of energy into reversible and non-recoverable components. In addition, such measurements can also be used in the calculation of Young's modulus on the microscopic scale. As outlined, the parameter of interest is the hardness to modulus ratio H/E. One way of quantifying this parameter is to monitor the load as a function of penetration depth, as prescribed by Eqn. (3). Because this approach requires technology uncommon to most indentation equipment it is not preferred. Another method is to make use of the asymmetric nature of the Knoop microindenter geometry. As such, there exists a length ratio of 1:7.11 between the short and long diagonals of the Knoop indenter.

While the longer diagonal is relatively insensitive to elastic "springback" effect, the shorter one diagonal is not. In this manner one is able to use the long direction as a rule, while monitoring the change in the distance of the indentation diagonal. Such an analysis yields the equation:[39,40]

$$b'/a' = b/a - \mu H/E \qquad (5)$$

Notice that b/a is the nominal diagonal ratio 1/7.11, b'/a' is the ratio of indentation diagonals, and μ is a constant equal to 0.45 for Knoop geometry. Now it can be seen that materials with relatively rigid structures (high H/E) will exhibit greater lateral recovery.

This approach was used for microindentation of both biogenic and geological $CaCO_3$ materials. Microindentation experiments were performed on both nacreous and prismatic mollusc shell, as well as mineral aragonite and calcite, as described above. Microhardness, damage zone size, elastic recovery, and elastic modulus were calculated. It should also be noted that the equation used in determining the Knoop microhardness is similar to that of Vickers.

III- ANALYSIS OF THE RESULTS AND DISCUSSION

A. Microhardness Results

As can be seen in both Figures 5 and 6, and Tables-I and -II, the results of both Vickers and Knoop microhardness experiments are, for the most part, complimentary. In both cases, and on both test planes, the geological aragonite is hardest, followed by the prismatic calcite, nacreous aragonite, and finally geological calcite. While the actual microhardness values are of interest the most significant result of these particular experiments is noticed in examination of the relative hardness trends followed by the materials. In particular, while the biogenic form of calcite (prismatic) shows an increase in microhardness of approx. 30%, the biogenic form of aragonite (nacre) yields a reduction of microhardness by approximately the same amount. The significant implication is that a simple rule of mixtures, which accounts for the additive behavior of volumetric compositions, is not adequate in describing the microhardness behavior. While both biological compositions contain a measurable quantity of soft organic matrix, the effect in one is opposite of that in the other. The explanation of such behavior must then encompass microstructural design.

In the case of prismatic calcite, the columnar design, in addition to a high level of alignment of crystallites, with an aspect ratio of 10:1, allows the material to be significantly more resistive to penetration (compared to the geological calcite with an aspect ratio of 1:1). The crystallites are, in this case, oriented axially toward the incident force (Figures 1 and 2). This alignment, in conjunction with a minimal amount of organic binder, severely limits the plastic deformation possible in the system. In this fashion, the columnar crystals are able to accommodate the majority of stress, thus limiting the corresponding strain, as in the case of a uniaxial short fiber composite.

Nacre, on the other hand, with its textured platelet-lamellar configuration, accommodates most of the penetration force via plastic absorption of the impacting energy. Compared to the aspect ratio, i.e., more than 10:1, of the pseudohexagonal geological rode-like aragonite crystals (Figure 4), the aspect ration of the individual aragonite platelets in the nacre is 0.1. This low aspect ratio and a higher volume of plastic binder, in conjunction with the brick and mortar

microarchitecture, allow for the distribution of stress and strain across the layered structure throughout nacre on the **a-b** plane, perpendicular to the applied stress in the **c**-direction. This phenomenon occurs via platelet shear motion (sliding),[13,15] and platelet compression in the direction normal to the incident force. Ultimately this can bee seen as shear motion between nacreous layers, with accompanying platelet and matrix compression in the direction normal to the incident force (as in the case of (001) penetration), or lamella debonding (accompanied by crack-bridging)[13,15] in conjunction with compression across nacreous layers, in the case of $(001)_n$ penetration.

B. Elastic Recovery and Modulus

Microelastic recovery behavior has been described in terms of a dimensionless parameter b'/a'. This variable illustrates the amount of elastic "springback" in the long diagonal direction of the Knoop indenter, thus providing some information on the extent to which the energy absorbed by the material is reversible. If a material is capable of a high degree of elastic recovery then this material will be less susceptible to plastic overload, as a significant portion of energy, which would otherwise cause plastic deformation, is temporarily alleviated within the stress region. The results of microelastic recovery calculations can be seen in Figure 7, keeping in mind that greater elastic absorption capability is represented by a smaller recovery parameter.

The illustrative trend in this data is that the biological morphologies (the hard tissues) have consistently greater elastic recovery capabilities, mainly because of the presence of macromolecular component in the composite (this is also true in bone).[5] Prismatic calcite shows an increase in elastic recovery of approximately 10%, while that seen in nacreous aragonite is approximately 25% in (001) and 10% in $(001)_n$. This result is not surprising, as these materials are composed of a noted quantity of elastic organic matrix binder. This binder, provides a mechanism for elastic energy absorption and recovery, namely matrix ligament formation. Recall that the volume of matrix is similar in both test planes in the prismatic structure, but in the nacreous structure the matrix thickness is approximately double in the (001) plane. This leads to the similarity of results, by plane tested, as seen in prismatic samples, as well as the dissimilarity noticed in the nacre samples.

It has been recently noted that fine ligaments form within strained matrix volumes, which act to bridge, or connect two regions within the material, thus preventing permanent separation.[13] Such a mechanism ultimately leads to the preservation of structural integrity within the material after the plastic absorption of any remaining energy is accomplished.

In addition to ligament formation, the presence of elastic matrix, in the spirit of the "rule of mixtures",[17] significantly contributes to the materials ability to elastically compress. In the case of a pure mineral, compression capabilities are severely limited. Plastic deformation results, and can be seen in the form of slip plane generation. As the mineral itself has a very high modulus, and with no soft component present, deformation requires much greater energy absorption than does crystallographic cleavage. The result is very little elastic compression of the stressed region. The biogenic sample, on the other hand, contains the small, but critical, soft component volume. When stressed this component readily elastically compresses, thus absorbing energy, and alleviating compressive stress which would be borne by the inorganic component.

The determination of microelastic modulus using the Knoop indentation method follows from the elastic recovery approach. Using the measured values of Knoop microhardness, in conjunction with the recovery parameter equation, we are able to calculate a value for elastic modulus. Again, the illustrative trend is the comparison of geological behavior to that of the biological counterpart. In accordance with the results of the elastic recovery, we see a reduction in modulus in both of the biogenic morphologies. Figure 8 shows the microelastic modulus results. Prismatic calcite exhibits a reduction in modulus of approx. 30% over the mineral form (in both planes tested), while nacreous aragonite is 90% more compliant in the (001), and 60% more compliant in the $(001)_n$. The compliance trend is again similar to that of elastic recovery, as the mechanisms represented are equal. Elastic recovery and moduli data can be seen in Tables-III and -IV.

C. Damage Tolerance

The extent of damage within the materials has been characterized by measuring the apparent area of damage zone on the face of each sample tested. In this manner a qualitative basis is established which allows for the comparative analysis of each system. Micrographs were used in the modeling of damage zones and measurement of zone sizes for each sample. A small area of apparent damage within the material was said to characterize high damage tolerance, whereas a material exhibiting a large damage zone was considered damage intolerant. Images in Figures 9(a through d) show Knoop indentations by which damage zone sizes were calculated. Once again, the biological $CaCO_3$ morphologies exhibit a significantly reduced damage zone than those found in the geological materials. In each case the damage zone was modeled as a simple two dimensional geometric shape, whereby zone size is calculated as area.

In the case of geological calcite the damage zone appears to consist of a highly dense region of local cleavage planes, roughly in the shape of a right triangle (Figure 9c). Prismatic calcite zones, on the other hand, were modeled as isosceles triangles which exhibit local cracking to one side of the indentation (Figure 9d). Among these samples the prismatic structure displays a reduction of damage zone size of approximately 70%. The results are similar for both test planes.

The geological aragonite zones were modeled as semi-circular regions of local cleavage, which again emanated from one side of the indentation (Figure 9a). The nacreous aragonite samples show quite different damage zone characteristics depending on plane tested, and were treated accordingly (Figure 9b). On the (001) test plane the damage zone appeared as a plastically "piled" area that could be seen on both sides of the indentation. This type of feature is similar to a typical outflow of material near the edges of an indentation in a plastic material such as a metal. Each of these areas was modeled as an isosceles triangle and added to yield the total zone size, which as compared to mineral aragonite shows a reduction of 50%. On the $(001)_n$ test plane there is a remarkable deficiency of damage characteristics in the vicinity of the indentations. No measurable damage zone could be seen in this case. This strongly suggests that nearly all the indentation energy is absorbed plastically within the matrix, and the extent of crack formation is minimal, and limited to the formation of numerous small, stable, microcracks at the

platelet/matrix interface.[10,13,15] Furthermore, the damage zone is accompanied by the delamination of the aragonite platelets from the organic layer to allow the creation of new surfaces thereby disseminating the applied load via this energy absorption mechanism.

IV- CONCLUDING REMARKS AND NEW DESIGN PARAMETERS

A. Conclusions from this Work

We have shown that *Haliotis rufescens* mollusc shell is naturally designed as to optimize qualities of a biological armor. While both the prismatic and nacreous regions of the shell are composed of the same inorganic filler ($CaCO_3$), and similar organic matrix (albeit different amounts), they exhibit distinctly different mechanical behavior. On one hand, the outer prismatic region is stiff and hard. It absorbs a great deal of incident energy via crystallite compression and localized brittle fracture. The extent of damage caused by this fracture is severely limited by the highly aligned columnar design. The size, shape, and alignment of the crystallites restricts crack propagation to the immediate area of impact by presenting organized discontinuities within the lamella. Nacre, on the other hand, is a softer and has much more compliant microarchitecture. The low aspect ratio "brick and mortar" design, in addition to a significant volume of soft binder, allows for a large extent of elastic, as well as non-catastrophic plastic deformation within the indentation region. Elastic energy absorption is accomplished via matrix compression, both normal to and in the direction of the incident force, and macromolecular extension via ligament formation . Remaining energy can be plastically absorbed by the matrix via typical shearing processes within a soft component, i.e., sliding of the aragonite platelets over the interlamellar organic film. In this region little stress is borne by the inorganic platelets and an extended tortuous crack path develops which is restricted to the local indentation area.

The main limitation of this research is the inability to directly quantify the contributions made by each component within the nacreous and prismatic regions (e.g., contributions by the individual aragonite platelets and the organic matrix). Although our approach has yielded significant evidence as to the influence of the organic component on micromechanical behavior, the quantification of hardness

and elastic properties over the sub-micron scale would prove invaluable. This approach requires application of currently developing mechanical techniques, such as atomic force microscopy nanoindentation. We are in the process of currently developing such an approach, and preliminary analysis has been conducted in our labs using a Digital Instruments Nanoscope III. There are many issues still to be considered and a variety of nanoindentation techniques to be investigated before such work can be successfully completed.

B. A Novel Armor Design: Lessons From Biology

Our results imply, and provide, several novel ideas in the design of new armor and impact resistance materials (as also depicted in Figure 10):

o- Both the face region and the backing region can be made of components with high ceramic-content (being more than 90%! as demonstrated in this case). This is a significant deviation from the traditional design in which, usually, the face region is monolithic (or tiled, hard for projectile stoppage) ceramic and the backing region is metal or polymer, or in more recent designs, high-percentage soft-component containing composite (for energy absorption through plastic deformation). In addition to the beneficial mechanical properties, the use of ceramics on both regions effectively decreases the overall weight of the armor material, and satisfies one of the important requirements in achieving light-weight armor system.

o- Microarchitectural design is accomplished in both of the regions in the two-ply structure in the biological composite to modify their properties so as to tailor the overall micromechanics of the system as a whole. As illustrated in this work, although the hardness of geological aragonite is higher than that of geological calcite, the prismatic region, mainly because of the columnar organization of the calcite crystallites, has significantly higher hardness value than the nacreous region, in which the aragonite crystallites are organized in the form of thin platelets separated by the organic matrix to provide the higher toughness and the damage tolerance for better energy absorption. The final structure appears as an excellent example of a design of functionally-gradient material (now a device) as expected for an ideal impact resistant material.

o- Synthesis of the component systems in mollusc shell structures is accomplished at room temperature in aqueous environments via self-assembly, using the raw materials widely present in nature. This is a major drastic difference between man-made and natural systems. In making traditional engineering materials, microstructures are developed through complex processing strategies at several separate stages that often involve thermo-mechanical treatments, followed by shaping and machining, all energy absorption techniques. Furthermore, in most traditional systems, multi-component structures, such as ceramic-metal or ceramic-polymer composites, are developed through forced-assembly, e.g., mechanical alloying or layering, or via extensive interface reactions as these components are not phase compatible. In the biological systems, however, the materials structures, involving both organic and inorganic components, are developed via self-assembly, often by using significantly small amount of organic macromolecules (that are more expensive to synthesize in terms of energy used). It is the organic macromolecules, including DNA, proteins, polysaccharides, and phospholipids, that act as template, nucleator, growth modifier, or enzyme controller, under the genetic code of the organism, that is responsible for assembly of highly ordered hierarchical composite structures with multifunctional properties.

o- The mollusc shell need not be bulky (voluminous) and heavy, unlike in modern armor and impact resistant materials. The same architectural design of the mollusc shell, calcitic on the outside and nacreous on the inside, is prevalent in many different mollusk species (nautilus, abalone, and bivalves) that live in significantly different habitats and, hence, exposed to different external forces (water pressure) and predators.[41,42] In all these molluscan species, the individual morphology and the size of the ceramic components are similar in both regions of the shell, i.e., calcitic columnar structure in the prismatic region and the aragonitic platelet structure in the nacreous region, although the overall thickness of the shell may vary from one species to another (1 mm in nautilus and 1 cm thick in abalone). It is this very versatility of the individual and overall microstructural design that most likely allowed these species to survive, and do very well, since the creation of mollusks more that 500 million years ago before the Precambrian! How these structures are constructed, at room temperature in aqueous environments, including the collection of raw materials (inorganic ions) and their self- and co-assembly with the organic macromolecules, their nucleation, growth, shape formation, hierarchical architecture, and, finally, creation of the functionally-

gradient material as a system should be, and is, an intense area of investigation for the purpose of learning, more, from nature to design, synthesize, assemble, and process new, and novel, engineering materials.

ACKNOWLEDGMENTS:

This work was performed under a ARO-URI and AASERT under the Grant #s DAAL03-92-G-0241 and DAAH04-95-1-0279, respectively, and AFOSR Grant No. AFOSR-91-0281.

REFERENCES

1. R. P. Anders et. al., *J. Mater. Res.*, **4**, 704-496 (1989).
2. *Metallic Superlattices*, T. Shinjo and T. Takada (eds.) (Elsevier, Amsterdam, 1987).
3. See, for instance, (i) *Microclusters*, S. Sugano, Y. Nishina, and S. Ohnishi (eds.) (Springer and Verlag, Amsterdam, 1987); (ii) *Layered Structures, Epitaxy, and Interfaces*, J. M. Gibson and L. R. Dawson (eds.) Vol. 37 (Materials Research Society, Pittsburgh, 1984) (iii) *Clusters and Cluster-assembled Materials*, R. S. Averback, D. L. Nelson, and J. Bernhole (eds.) Proc. of MRS, Vol. 206 (Materials Research Society, Pittsburgh, 1991);
4. G. Ozin, *Adv. Mater.*, **4**, 612 (1994).
5. *Biomimetics: Design and Processing of Materials*, M. Sarikaya and I. A. Aksay (eds.) (American Institure of Physics, New York, 1995).
6. *Hirarchically-Structured Materials*, MRS Proceedings, Vol. 255, I. A. Aksay, E. Baer, M. sarikaya, and D. Tirrell (eds.) (Materials Research Society, Pittsburgh, PA, 1993).
7. E. Baer, A. Hiltner, and R. J. Morgan, *Physics Today*, **45** 60-67 (1992).
8. See, for instance, (i) *Materials Synthesis Using Biological Processes*, P. C. Rieke, P. D. Calvert, and M. Alper (eds.), Proc.of MRS, Vol. 174 (Materials Research Society, Pittsburgh, 1990); (ii) *Materials Synthesis Based on Biological Process*, M. Alper, P. D. Calvert, R. Frankel, P. Rieke, and D. Tirrell (eds.) Proc. of MRS, Vol. 218 (Materials Research Society, Pittsburgh, 1991; (iii)
9. J. Currey, *J. Zool.*, **173**, 395-406 (1981).
10. M. Sarikaya and I. A. Aksay, "Nacre of Abalone Shell: a Natural Multifunctional Nanolaminated Ceramic-Polymer Composite Material," Chapter 1, in: *Results and Problems in Cell Differentiation in Biopolymers*, Steven Case (ed.) (Springer and Verlag, Amsterdam, 1992) pp. 1-25; .and M. Sarikaya, J. Liu, and I. A. Aksay, in ref. 5, pp.
11. See, for example, (i) *Biominerialization*, K. Simkiss and K. M. Wilber (Academic Press, New York, 1989); (ii) *On Biomineralization*, H. A. Lowenstam and S. Weiner (Oxford University Press, New York, 1989); (iii) *Biominerialization: Chemical and Biochemical Perspectives*, S. Mann, J. Webb, and R. J. Williams (eds.) (VCH Pub., Weinheim, 1989).

12. *Mechanical Design in Organisms*, S. A. Wainright, W. D. Briggs, J. D. Currey, and J. M. Gosline (eds.) (John Wiley and Sons, New York, 1976).
13. M. Sarikaya, K. E. Gunnison, M. Yasrebi, and I. A. Aksay, "Mechanical Property-Microstructural Relationships in Abalone Shell," *Materials Synthesis Using Biological Processes*, P. C. Rieke, P. D. Calvert, and M. Alper (eds.) Proc.of MRS, Vol. 174 (Materials Research Society, Pittsburgh, 1990) pp.109-116.
14. A. P. Jackson, J. F. V. Vincent, and R. M. Tunner, "The Mechanical Design of Nacre," *Proc. Roy. Soc. London*, **B234**, 415-440 (1988)
15. M. Sarikaya, K. E. Gunnison, M. Yasrebi, D. L. Milius, and I. A. Aksay, in *Proc. of the Amer. Soc. for Composites*, Fifth Technical Conference (Technomic Publ., Lancaster, PA, 1990) pp. 176-183.
16. G. H. Kim, Effect of Metallic Phase and microstructure on the Strengthening Behavior of B_4C-Al Cermets (Ph.D. Thesis, University of Washington, 1993).
17. *An Introduction to Composite Materials*, D. Hull (Cambridge Solid State Science Series, Cambridge University Press, NY, 1981) pp. 59-80.
18. D. Frech and M. Sarikaya, unpublished research (University of Washington).
19. J. Liu, M. Sarikaya, and I. A. Aksay, *Hirarchically-Structured Materials*, MRS Proceedings, Vol. 255, I. A. Aksay, E. Baer, M. sarikaya, and D. Tirrell (eds.) (Materials Research Society, Pittsburgh, PA, 1993) pp. 9-18.
20. S. Weiner and W. Traub, *Phil. Trans. R. Soc. London*, **B 304**, 425-434 (1984).
21. N. Watabe, *J. Ultrastruct. Res.*, **12** 351-370 (1965).
22. H. Erben and N. Watabe, *Nature*, **248**, 128-130 (1974) .
23. H. Mutvei, *Biomineralisation*, **6**, 96-100 (1972)
24. C. Losos and B. Bassett, School Arts, 94 25-31 (1994).
25. R. Rolsten, E. Bodine, and J. Dunleavy, *Space and Aeronautics*, **50** 55-63 (1968).
26. A. Webster, *Diphasic Armor. 1. Glass Doron: Status Report* (Research Division, Bureau of Medicine and Surgery, US Navy Dept., Washington, DC, 1965).
27. A. Alesi and E. Barron, *Plastic-Ceramic Composite Armor for Vietna*, Proc. 23rd Tech. Conf. of SPI (Reinforced Composites Div., Washington, DC, 1968).
28. R. Cook, *Hard Faced Ceramic and Plastic Armor*, US 3509833 (Goodyear Aerospace, Akron, OH, 1970).

29. R. Liable, *Ballistic Materials and Penetration Mechanics* (Elsevier Scientific Pub. Co., NY, 1980) pp. 136-139.
30. ibid., pp. 139-141.
31. L. Landingham and A. Casey, *Final Report of the Light Armor Materials Program*, UCRL-51269 (Lawrence Radiation Lab., Univ. of California, Livermore, CA, 1972).
32. T. Hirai, *Ceramic Transactions: Functionally Gradient Materials* (ACS, Westerville, Ohio, 1993) pp. 11-19.
33. A. Szymanski and J. Szymanski, *Hardness Estimation of Minerals Rocks and Ceramic Materials*, Materials Science Monographs, 49 (Polish Scientific Publishers, Warszawa, 1989) pp. 295-297.
34. P. Flinn, *Strengthening mechanisms in solids* (American Society for Metals, Metals Park, Ohio, 1962) pp. 17-50.
35. E. Davenport and E. Bain, *General Relations Between Grain-Size and Hardenability and the Normality of Steels*, Grain Size Symposium, 16th Annual Convention of the American Society for Metals (ASM, Metals Park, Ohio, 1934. pp. 879-891.
36. *Micro-Indentation hardness Testing*, B. Mott (Butterworths Science Publications, London, 1956) pp. 101-139.
37. *Hardness Estimation of Minerals Rocks and Ceramic Materials,* A. Szymanski and J. Szymanski, Materials Science Monographs, 49 (Polish Scientific Publishers, Warszawa, 1989, p. 64.
38. Ref. 28, p. 9.
39. *Ceramic Hardness*, I. McColm (Plenum Press, NY, 1990) p. 10.
40. B. Marshal and B. Lawn, "Indentation of Brittle Materials," in *Microindentation Techniques in Materials Science and Engineering*, P. Blau and B. Lawn (eds.) (ASTM Special Technical Publications, Philadelphia, PA, 1985) p. 32.
41. *Ecology and Evolution of the Gastrochaenacea (mollusca, bivalva) with notes on the evolution of the endolithic habitat*, J. Carter (Yale University Press, New Haven, CT, 1978).
42. *Molluscs*, E. Morton, 5th Edition (Hutchinson, London, 1979).

FIGURE CAPTIONS:

Figure 1 - Microstructure of Red Abalone. (a) The mollusc (b) and (c) The platelet and columnar morphologies of biogenic aragonite and calcite, respectively; (d) and (e) are nacreous and prismatic sections of the shell, respectively. (f) Secondary electron image (scanning electron microscopy) of a fractured surface of the shell exposing both the prismatic (PR) and nacreous (NR) sections of the shell. (g) and (f) are transmission electron microscopy bright field images of the reveal the laminated and columnar structures of the nacreous and prismatic portions of the shell, respectively.

Figure 2 - Schematic illustration of the prismatic and nacreous sections of red abalone shell indicate the overall dimensions of the sections and the orientations of the crystallites with respect to the surfaces of the shell.

Figure 3 - Schematic illustration of common armor design showing the face-ceramic and the backing material.

Figure 4 - Commonly encountered geological morphologies of geological aragonite (a) and calcite (b) crystals.

Figure 5 - Vickers microhardness of various $CaCO_3$-materials.

Figure 6 - Knoop microhardness of various $CaCO_3$-materials.

Figure 7 - Elastic recovery of various $CaCO_3$-materials.

Figure 8 - Elastic modulus of various $CaCO_3$-materials.

Figure 9 - SEM secondary electron images of the Knoop indentations in (a) geological calcite, (b) biogenic calcite, (c) geological aragonite, d) biogenic aragonite.

Figure 10 - Bioinspired design of an ideal armor material.

Geological Minerals

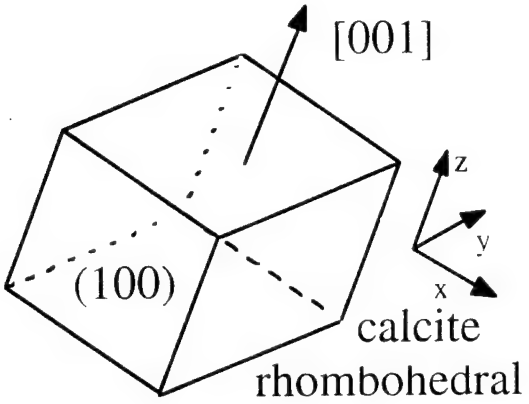

calcite
rhombohedral

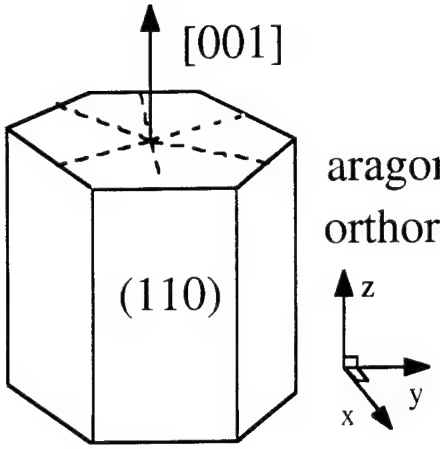

aragonite
orthorhombic

Table I - Microhardness of various $CaCO_3$ bearing materials.

Material - (001) Plane	Vickers Microhardness	Knoop Microhardness
	(Kg/mm^2)	(Kg/mm^2)
Mineral Aragonite	447	340
Biogenic Aragonite	174	177
Mineral Calcite	158	135
Biogenic Calcite	215	210

Table II - Microhardness of various $CaCO_3$ bearing materials

Material - (100) Normal	Vickers Microhardness (Kg/mm^2)	Knoop Microhardness (Kg/mm^2)
Mineral Aragonite	278	201
Biogenic Aragonite	170	141
Mineral Calcite	159	128
Biogenic Calcite	203	168

Table III - Elastic properties of various $CaCO_3$ bearing materials

Material - (001) Plane	Microhardness* Hk - (Kg/mm^2)	Elastic Recovery b'/a' - (μm/μm)	Elastic Modulus Er - (Kg/mm^2)/(GPa)
Mineral Aragonite	340	0.133	20,950/205
Biogenic Aragonite	177	0.102	1,956/19
Mineral Calcite	135	0.132	7,384/74
Biogenic Calcite	210	0.123	5,314/52

Table IV - Elastic properties of various $CaCO_3$ bearing materials

Material - (001) Normal	Microhardness* Hk - (Kg/mm^2)	Elastic Recovery b'/a' - (μm/μm)	Elastic Modulus Er - (Kg/mm^2)/(GPa)
Mineral Aragonite	201	0.132	10,010/98
Biogenic Aragonite	141	0.124	3,885/38
Mineral Calcite	128	0.134	9,379/92
Biogenic Calcite	168	0.124	4,650/46

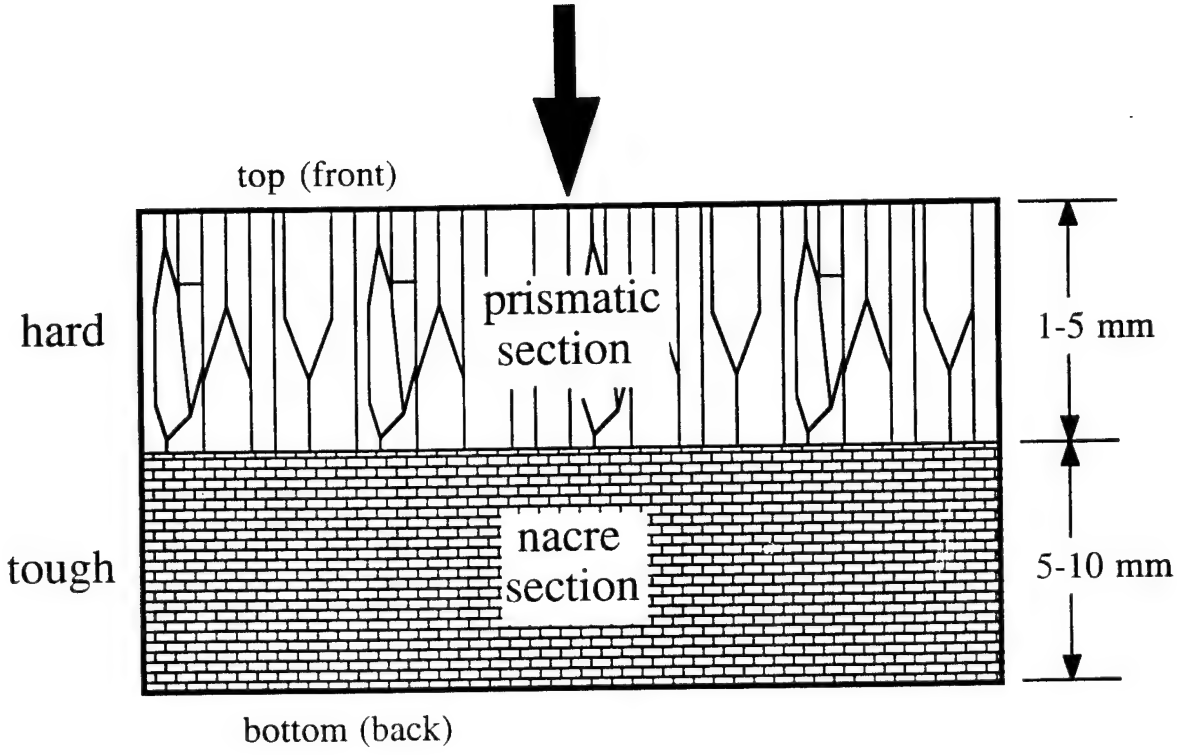
top (front)
hard
prismatic
section
1-5 mm
tough
nacre
section
5-10 mm
bottom (back)

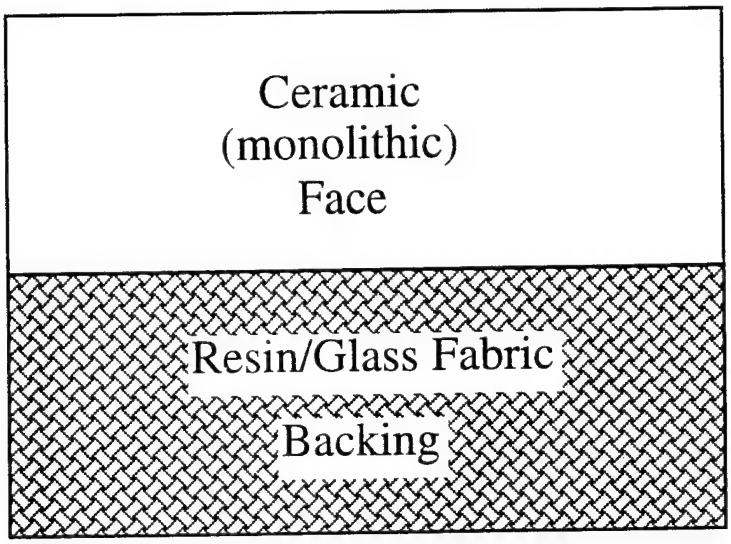

Figure 3

Geological Minerals

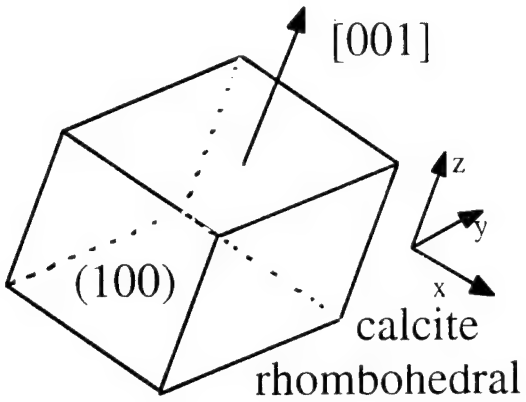

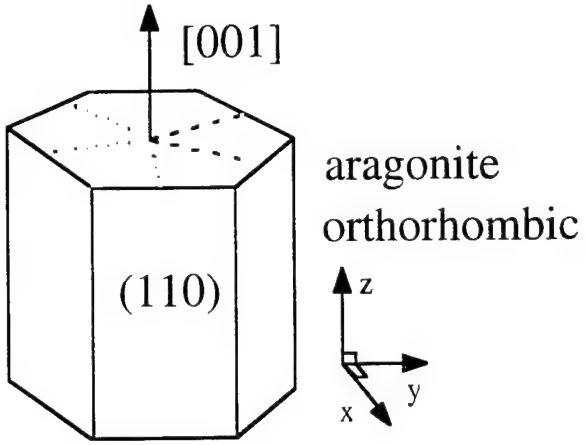

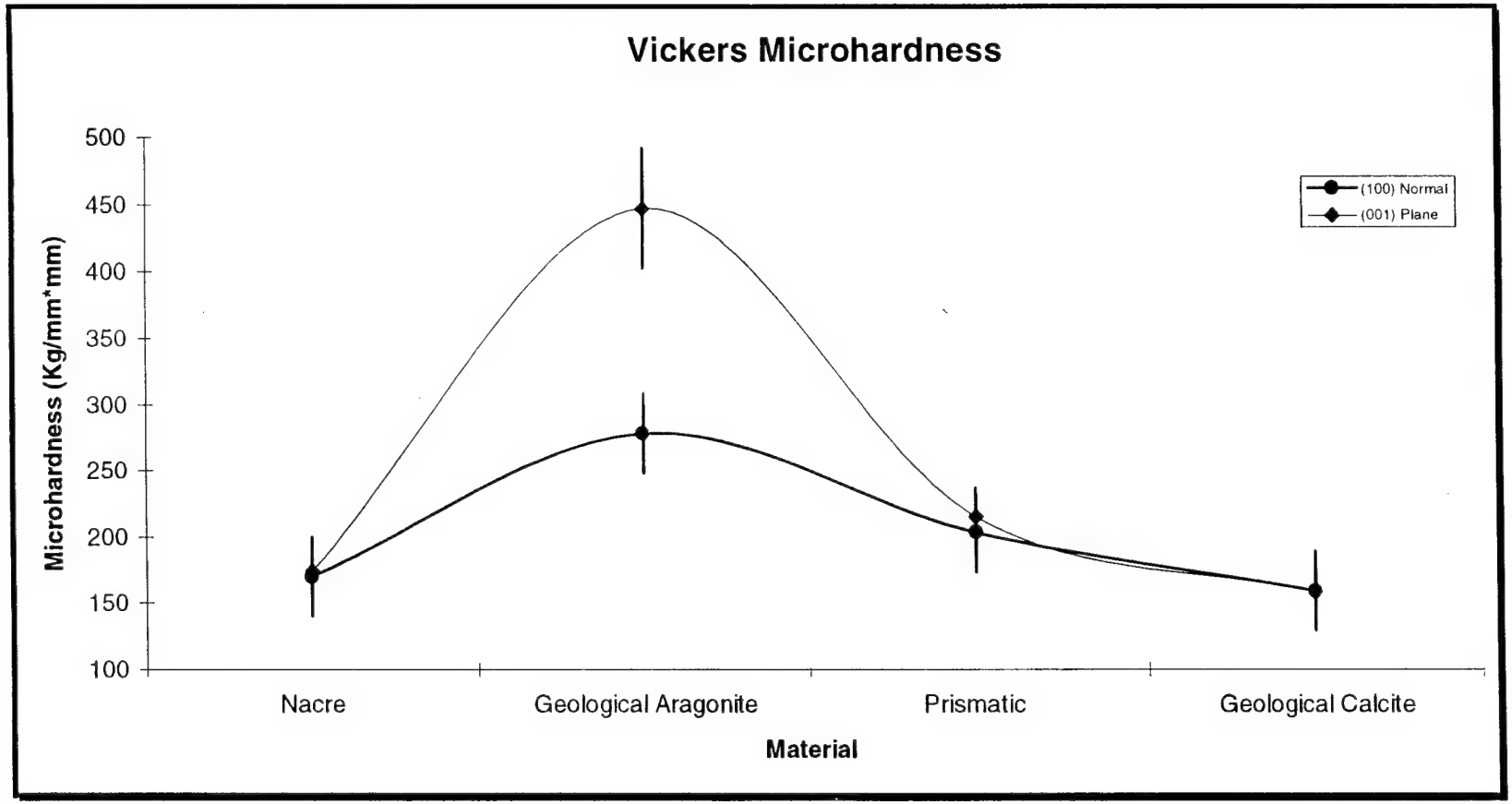

Figure 5 - Vickers microhardness of various $CaCO_3$ bearing materials

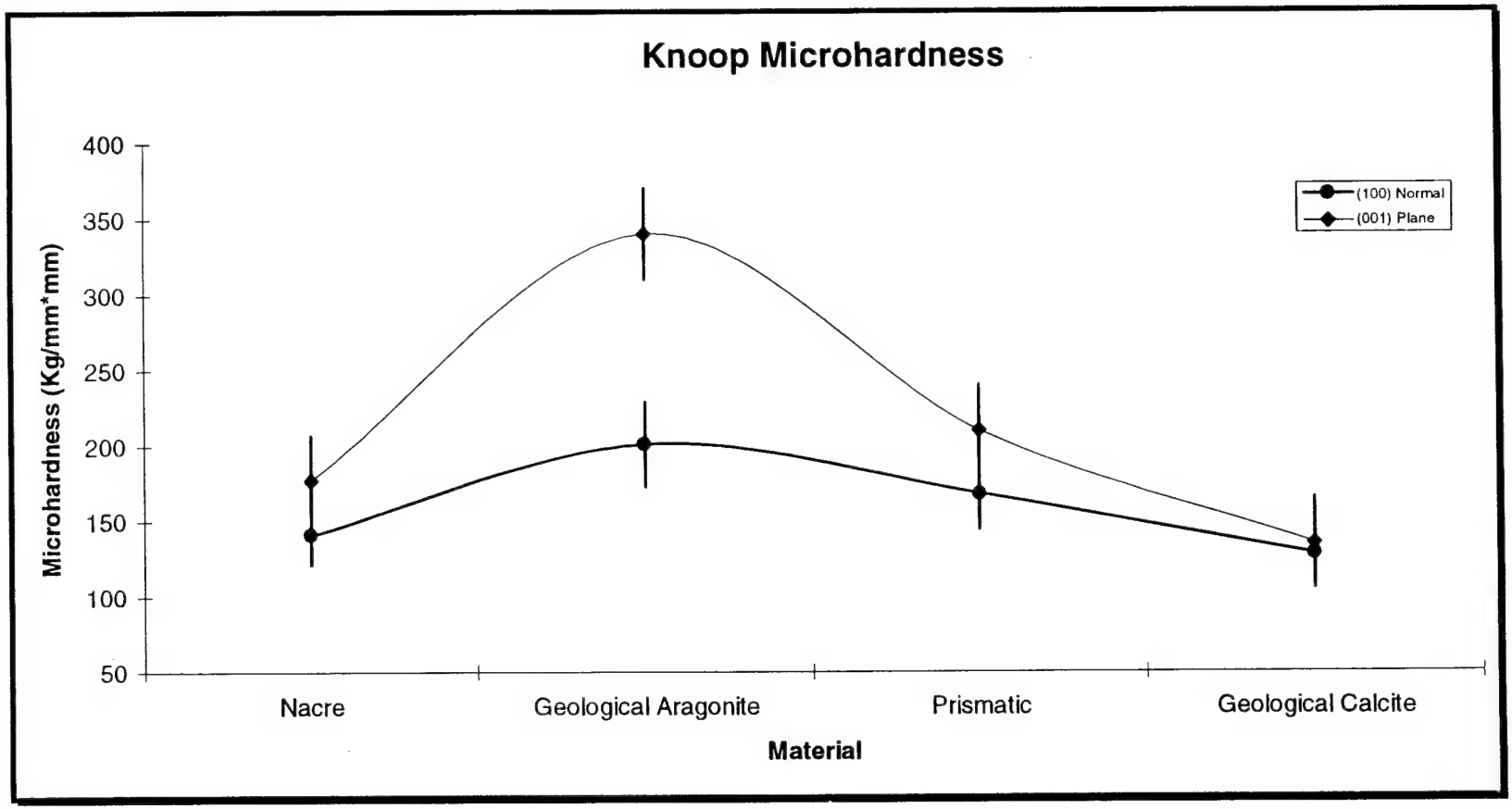

Figure 6 - Knoop microhardness of various $CaCO_3$ bearing materials

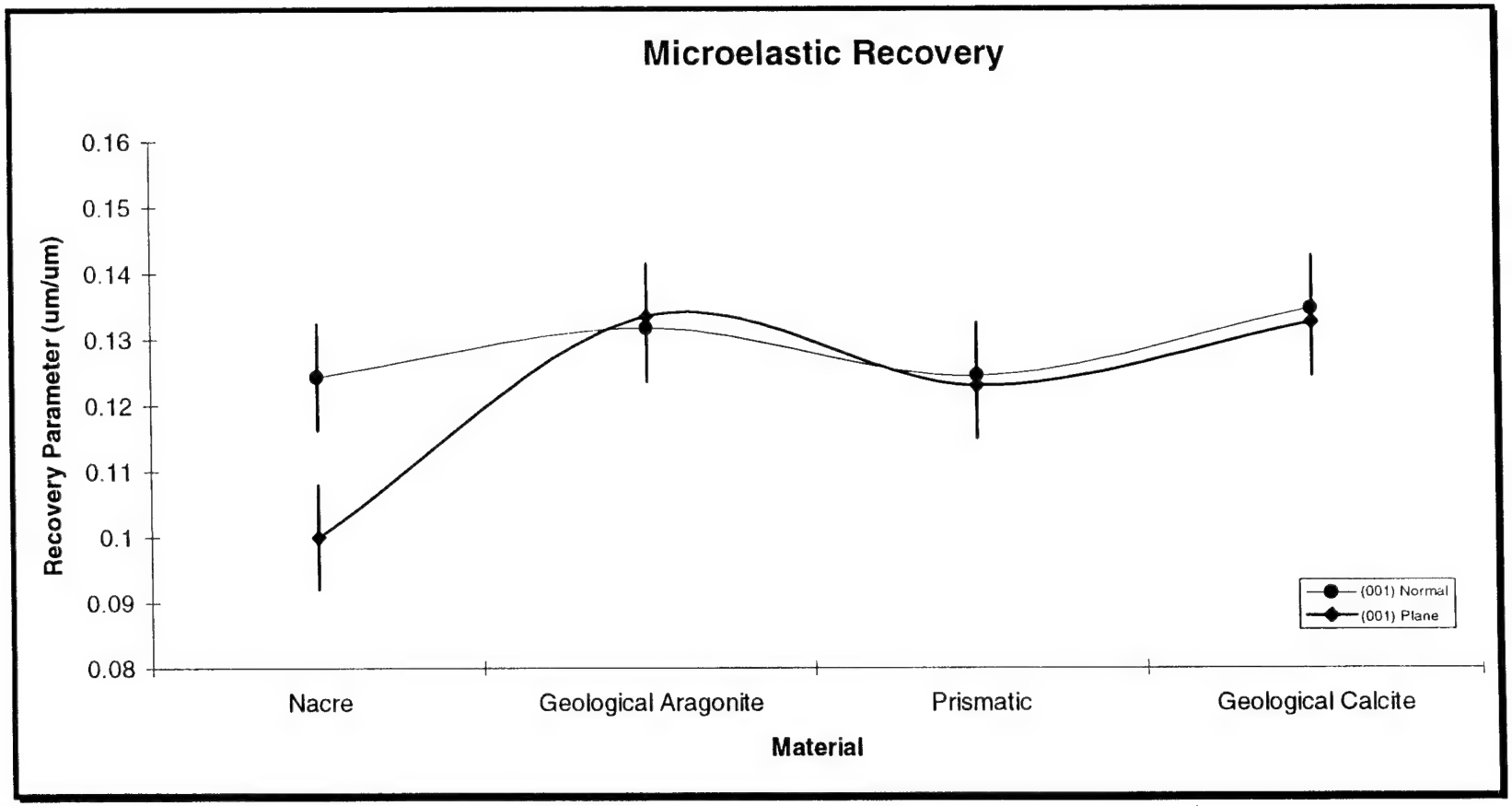

Figure 7 - Elastic recovery of various $CaCO_3$ bearing materials

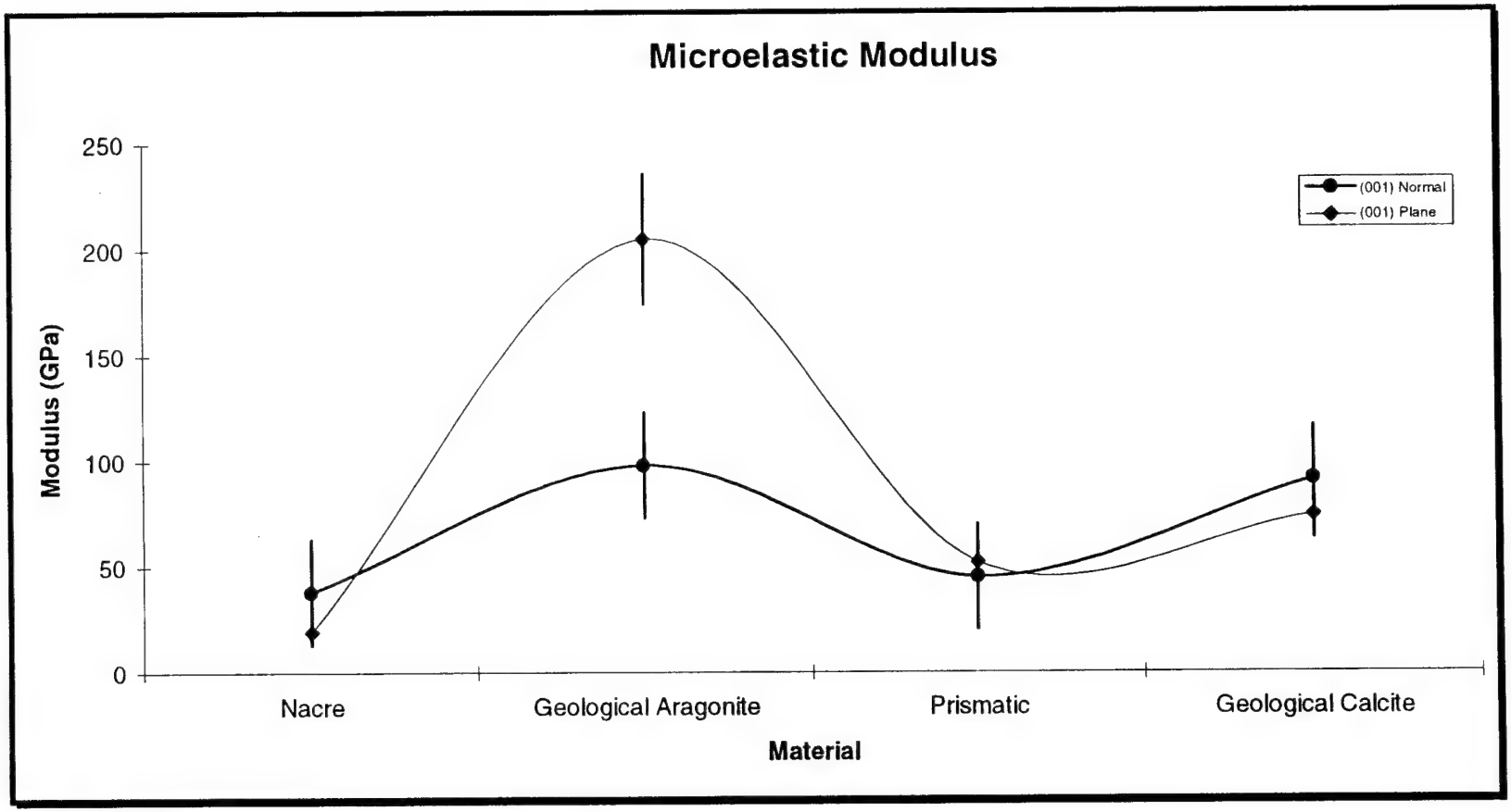

Figure 8 - Elastic modulus of various $CaCO_3$ bearing materials

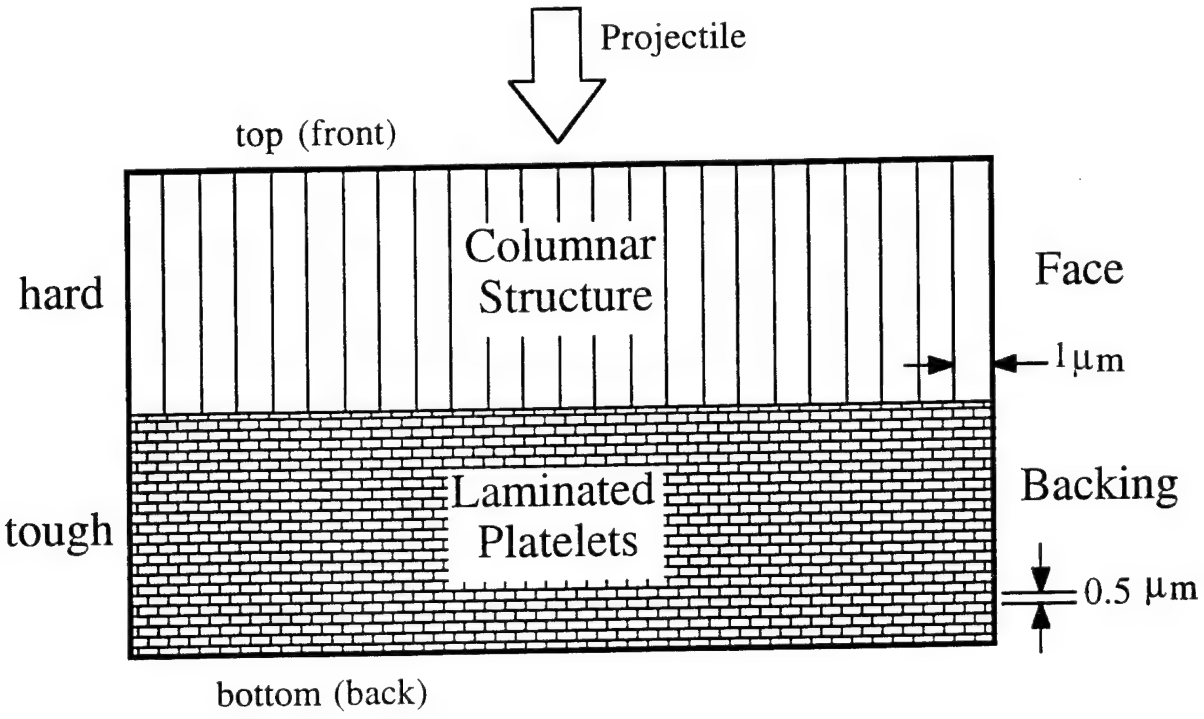
Projectile
top (front)
hard
Columnar
Structure
Face
1 μm
tough
Laminated
Platelets
Backing
0.5 μm
bottom (back)

Construction of a Mineralization Apparatus
Senior Project

MSE 499
by Demetriah Webster
Mehmet Sarikaya

October 25, 1995

Abstract:

A mineralization apparatus was constructed to precipitate a calcium carbonate solution for seeded crystal growth. The apparatus includes features such as pH and temperature control, and solution circulation. A red dye test was performed to confirm that the solution flowed in the desired pattern through the tubing of the apparatus. The temperature change in the solution necessary for precipitation was successful using the constructed water cooler. Temperature and pH control devices are functional but could be more accurate by using a laboratory heater and a pH/temperature meter probe and a water bath.

Introduction:

Crystal growth is a complicated yet common biological process that occurs in nature. Evidence of these processes were found in ceramic-organic composites such as the nacre structure, or mother of pearl, where two structural forms of calcium carbonate were observed[8]. In order to understand how this biological process occurs, attempts to replicate them are performed in the laboratory.

Crystal growth of calcite and aragonite crystals is replicated by means of precipitation of a calcium bicarbonate solution. It occurs when a solution is supersaturated due to many physical or chemical changes to the solution. These changes may be in heat, pH, and/or the addition of ions to the solution. Raising the pH[6] and lowering the temperature[1] of the solution will cause precipitation. Adding ions to the solution will assist or hinder the growth of the crystal such as calcium, strontium[5], and magnesium[3]. The apparatus built in this project was designed to research the effects of precipitation and crystal growth using under specific temperatures, pH levels, and concentrations of additional solutions. The specific objective of this apparatus is to precipitate a calcium carbonate solid from an aqueous solution.

As this precipitation occurs, several reactions take place in the solution. First, carbon dioxide (CO_2) gas is bubbled into distilled water with a semi-permeable bag of calcium carbonate crystals[6].

$$\mathbf{CO_2 + H_2O \rightarrow H_2CO_3}$$

the carbon dioxide reacts with water yielding carbonic acid (H_2CO_3). The next reaction is the dissociation of carbonic acid:

$$\mathbf{H_2CO_3 \rightarrow H^+ + HCO_3^-}$$

Each carbonic acid molecule donates a hydrogen ion to the solution yielding hydrogen carbonate (HCO_3^-) ions. Next, the hydrogen carbonate molecule

$$\mathbf{HCO_3^- \leftrightarrow H^+ + CO_3^{2-}}$$

dissociates leaving carbonate ions to react with the dissolving calcium carbonate crystals. This interaction yields the desired calcium bicarbonate solution.

$$Ca^{2+}{}_{(aq)} + HCO_3^-{}_{(aq)} \rightarrow CaCO_{3\,(s)} + H^+{}_{(aq)}$$[9].

At this point, pH is important and must be neutral in order to mimic the saltwater environment where calcium carbonate crystals nucleate and grow in nature. Once its maximum solubility is reached, precipitation of calcium carbonate occurs. Solutions such as calcium chloride ($CaCl_2$), magnesium chloride ($MgCl_2$), and strontium chloride ($SrCl_2$) salts, contents found in skeletons of marine organisms[5-6], are added to the calcium carbonate solution to further mimic the natural process. Varying the amounts of these added salts can effect the resulting lattice structure of the crystal.

Materials and Methods:

The resulting apparatus constructed is a cross between the U-tube Method by Kruger and Finke, and its updated version invented by Valeton[1]. It has the following features: temperature and pH control, a CO_2 gas connection, and solution circulation. Solution circulation is also necessary for temperature control and for uniform crystal growth[1]. Because glass can react with the solution[2], acrylic tubing was used to construct the vessels in this experiment.

The apparatus has four chambers, two of which are reservoirs for temperature control, and two are vessels that contain the calcium carbonate solution (see Appendix, Figure 1). The large reservoirs will keep the temperature constant to avoid evaporation[1]. The two horizontal tubes allow the solution to circulate through both vessels.

The water cooler on the bottom horizontal tube cools the solution is it travels from the secondary vessel to the primary vessel. This drop in temperature causes precipitation. The water cooler has two barb fittings that are connected to plastic tubing creating a circuit through which water is circulated. A water pump and the connected plastic tubing are submersed in a cooler of ice water to cool the passing solution (see Appendix, Figure

2). To constantly monitor the temperature of the cooled solution, a hole was drilled in the cap of the primary vessel for a thermometer.

Another hole was drilled through the cap of the primary vessel to create a connection for continuous bubbling of carbon dioxide in the solution as mentioned in the previous section.

Constant circulation is required for uniformity of crystal growth. The 60 RPM motor and the attached propeller in the primary vessel pull the precipitated solution up to continue the circulation cycle to the secondary vessel. The speed of the motor is slow so that the solution can circulate without agitating the seed crystal.

A seed crystal can be placed at the bottom of the primary vessel were the crystal growth will take place. The precipitated solution will flow into the primary vessel so that crystal growth can occur. A semi-permeable sack can be placed through the top of the secondary vessel to provide the additional ions needed for the precipitation of the solution.

The pH tester was purchased to test the pH of the solution. Samples of the solution must be removed with a pipette through the third drilled hole in the primary vessel and placed into a vile for testing. The detection solution is added and the color of the new solution determines the pH. Samples of water with a minute amount of vinegar were used to test this device. To test the circulation of the apparatus, the vessels were filled with water and red dye was placed into the secondary vessel after the motor was started. The performance of the water cooler was then tested by placing thermometers into both vessels for 1 minute during circulation.

Results:

The following figures are schematic drawings of the constructed apparatus:

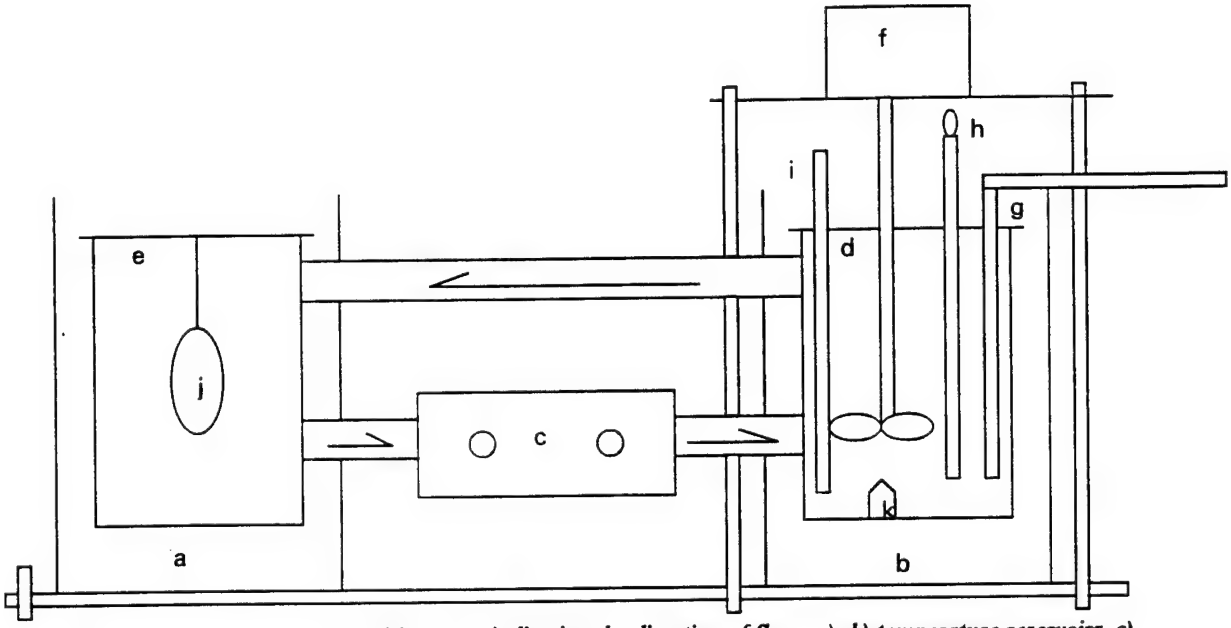

Figure 1: Mineralization apparatus with arrows indicating the direction of flow. a)- b) temperature reservoirs, c) water cooler, d) primary vessel, e) secondary vessel, f) motor and attached propeller, g) CO_2 connection leading to source, h) temperature, i) pipette for pH testing, j) bag of $CaCO_3$ crystals, k) seed crystal.

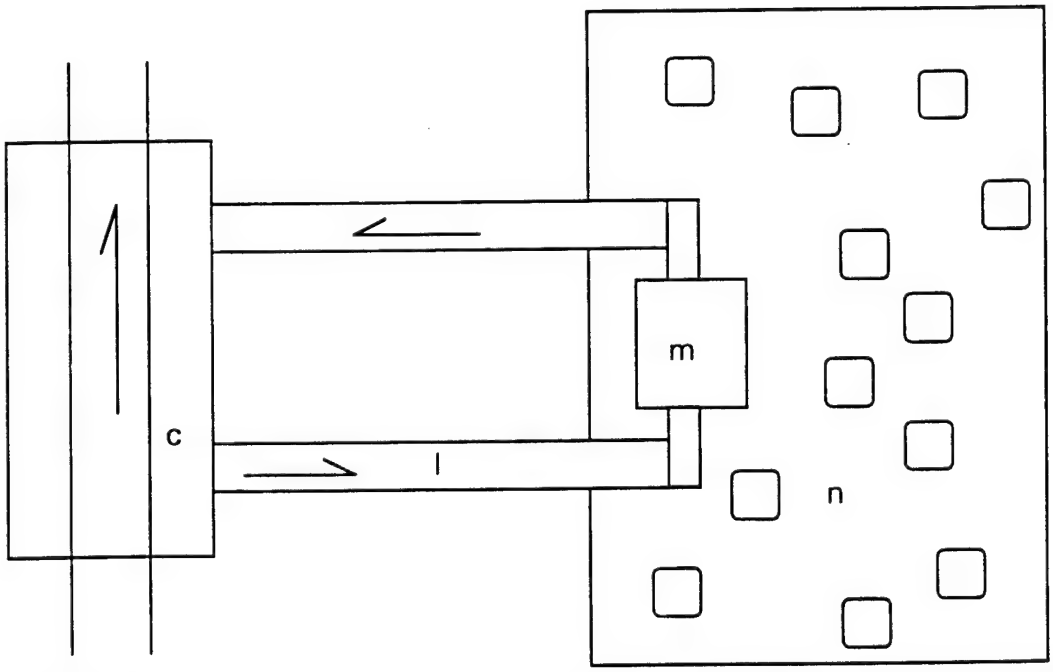

Figure 2: A simplified schematic of the water-cooling system with arrows indicating the direction of flow. c) water cooler, l) plastic tubing, m) water pump, n) cooler filled with cold water and ice.

The circulation forced the red dye through the bottom vertical tube from the secondary vessel into the primary vessel and up through the top vertical tube. The color of the solution showed that the pH of the solution is acidic.

Discussion:

The red dye experiment demonstrates the apparatus's ability to circulate the solution. The settling of the dye in the secondary vessel occurs because the solution in this area falls out of the circulation cycle; the location of the vertical tubing is too high for the solution to flow into the tubing. This is unfortunate but this settling is a trade-off for increased agitation to the seed crystal due to the force of the circulating solution. The temperature and pH control are useful, but a more accurate method for measuring these two parameters would make successful precipitation repeatable. I suggest investing in a pH/ temperature meter and a laboratory heater to maintain constant monitoring of the solution's and the crystal's environmental conditions.

Although differential temperature control was achieved with this apparatus, there is no method for keeping the reservoirs at a constant temperature. Placing the entire apparatus in a temperature-controlled water bath would solve this problem.

Conclusion:

The apparatus constructed successfully provides a controlled environment for precipitation and crystal growth of calcium carbonate crystals. The pH and temperature control features are functional but methods could be used for more accurate control of the conditions. The flow pattern of red dye test shows that the circulation system works properly. The water cooler successfully cools the passing solution in order for precipitation to occur, but a water bath with temperature control is recommended for constant temperature environment.

References:

1. Buckley, H.E. Crystal Growth. New York: John Wiley & Sons, Inc., 1951.
2. Christ C.L. and Hosteller P.B. "Studies in the MgO-SiO2-CO2-H2O (II): The activity-product of magnesite." American Journal of Science 1970,268: 439-453.
3. G. Falini, M. Gazzano, and A. Ripamonti. "Crystallization of calcium carbonate in presence of magnesium and polyelectrolytes." Journal of Crystal Growth 1994, 137:577-584.
4. Katz, Amtai. "The interaction of magnesium with calcite during calcite during crystal growth at 25-90°C and at one atmosphere." Geochimica et Cosmochimica Acta 1973, 37: 1563-1586.
5. Kojima, Yoshiyuki, Akiko Sadotomo, Tamostu Yasue, and Yasuo Arai. "Control of Crystal Shape and Modification of Calcium Carbonate Prepared by Precipitation from Calcium Hydrogencarbonate Solution." Journal of the Ceramic Society of Japan,Int. Edition 1992, 100:1128-1135.
6. Kitano, Yasushi and Nobuko Kanamori. "Synthesis of magnesian calcite at low temperatures and pressures." Geochemical Journal 1966 1:195.
7. Kitano, Yasushi, Nobuko Kanamori, and Tamotsu Oomori. "Measurements of distribution coefficients of strontium and barium carbonate precipitate and solution-Abnormally high values of distribution coefficients measured at early stages of carbonate formation." Geotechnical Journal 1971, 4:183-206.
8. Sarikaya, Mehmet. "An Introduction to Biomimetics: A Structural Viewpoint." Microscopy Research and Technique 1994, 27:360-375.
9. Walker, Justin B.A., Brigid R. Heywood, and Stephen Mann. "Oriented Nucleation of $CaCO_3$ from Metastable Solutions under Langmuir Monolayers." Journal of Materials Chemistry 1991, 1(5) 889-890.

Analysis of Biological and Geological Calcite and Aragonite through Atomic Force Microscopy

Arizona State University
Research for Undergraduates Program

M.T. Katchur
Professor B. Ramakrishna
Professor V. Pizziconi
Professor M. Sarikaya, University of Washington
August 5, 1995

Abstract: Atomic Force Microscopy (AFM) was used an extension of previous Biomimetics research to observe the biological aragonite formed in Red Abalone (*Haliotis rufescens*), Black lipped Pearl Oyster (*Pinctada margaritifera*) and Nautilus (*Nautilus pompilius*) shells and to compare these nacreous formations to the structures found in geological calcite and aragonite. Previous images of the structures have been imaged by SEM, TEM and optical microscopes, but many questions about the internal layering of these microcomposites still remain.

The organized assemblies of the biological systems described above are of recent interest for the insight they lend in developing processes to control the size, morphology and cluster formation of inorganic compounds.[1] The highly ordered formation of nacre, the inner aragonite layers of mollusc shells, is of particular interest due to the extremely high fracture resistance and toughness properties, which are comparable at ambient temperatures to high technology structured ceramics.[2, 4] These properties are a result of a "brickwork" formed by the inorganic platelets of the aragonite and an organic matrix "mortar".[4, 5, 6, 7] The organic matrix is considered to be the causal agent for many of the characteristic features in biomineralization. The effects that have been attributed to the organic matrix include crystal nucleation, size and crystal morphology, and crystal orientation.[3]

It has previously been suggested that the nucleation and growth of the inorganic crystals within the organic layers may not be single crystal formations but a mosaic crystallite structure, or microdomains.[3, 4, 16, 19] In nacre, in particular, the aragonite lattice may incorporate organic molecules.[4, 16] We believe that during this study it has been possible for us to image the crystallites, or microdomains in the Red Abalone shell with the Atomic Force Microscope (AFM).

Introduction

Biomineralization is the process by which organisms convert ions in solution into solid materials.[3] During the process of forming minerals the organisms create microenvironments that affect the nucleation, growth, mineralogy and morphology of the inorganic phase.

The organized assemblies of biological systems lend insight into developing processes to mimic the control of the organisms when synthesizing inorganic compounds. Recent work has been accomplished in biologically mimicked organized assemblies where the mimicking does not attempt to duplicate biomembranes, but to recreate or imitate only its essential components in an effort to develop solutions to practical problems.[1] The biomembranes have been somewhat successfully mimicked through the use of Langmuir-Blodgett films, bi-layer lipid membranes, micelles, microemulsions and vesicles.[1]

The great interest in this area is derived from the superior properties of the biological microstructures, and from the organism's ability to control the size, shape and mineralogy of different structures. Several factors may contribute to the desirable combination of properties present in the nacreous layers. These might include the intertwined presence of both the organic and inorganic components, the highly organized and intricate microarchitecture found in the layers, and finally the scale (size) or fraction of each component (organic and inorganic) present.[4] The result yields a microcomposite material combining the strength of the inorganic component with the elasticity of the organic component.[17]

One organism can produce a range of organic-inorganic structures, such as shell, teeth, bone and cuticles. Many of these structures are formed from the same mineralogies, but unlike the crystals found in the geological forms, the

biological inorganics adopt different morphologies and mineralogies suited for each particular scenario.

Biomineralization begins with an organic matrix, secreted as a substrate by the membrane or organism. The matrix acts as an organized surface that controls the mineralization. This can be thought of as the pre-organization of the system.[17] During this stage the matrix proteins can favor the development of certain isomorphs, and can also inhibit the growth of specific crystal faces.[20] Some of these proteins are soluble, and may become covered by mineral, and trapped in the growing crystal leading to intracrystalline matrix development.[16] Eventually, this sequence would strongly influence the toughness and strength of the mature crystal.[19]

The next stage in the fabrication of biological minerals is templating. This step involves the use of the pre-organization of the organic matrix for the controlled nucleation and growth of the inorganic clusters from aqueous solution.[17] The orientation of the crystal growth is controlled by interfacial molecular recognition which assists in the construction of the nuclei. The morphology of the crystal and direction of growth is governed by the direction in which the energy of the growth is at a minimum.[3, 17]

As many nuclei centers develop within a microspace of the matrix, the lattice of each nuclei become similarly oriented as the nuclei grow and become crystallites. As the crystallite grow, they compress the organic matrix between neighboring crystallites continuing to form the intracrystalline matrix. This mosaic of crystallites, or microdomains, can be interpreted as a single crystal surrounded by an intercrystalline matrix, because of their similar orientations and properties.[3]

Finally, the inorganic crystal growth may also depend on inorganic modifiers. Influences on this step include: [3]

~the rate of supply of ions to the nucleating solution

~diffusion of ions to the growing crystal surface

~adsorption or integration of atoms into the crystal surface

~the effect of inhibitors that may be present

The molluscs mineralize over 26 structures other than the shell, and each one of these structures is formed directly by a single layer of epithelial cells. In order to accomplish this, the cells must be involved in both the movement of the mineral ions to the deposition site, and also in the secretion of the organic matter that will become the matrix for the deposited minerals.[3] The epithelial cells in the mantle tissue alternately secrete the organic and inorganic components into the extrapallial space, which is an internally closed cavity between the mantle and shell.[2]

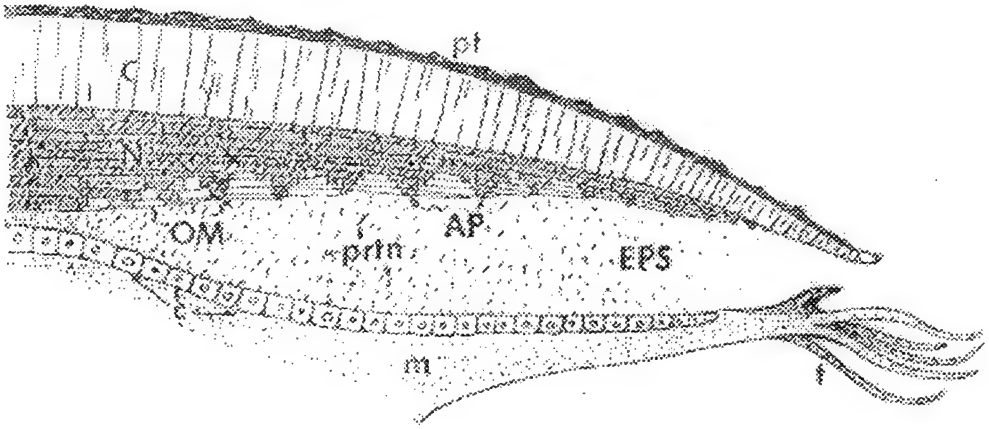

figure 1. (M. Sarikaya, 1995) A schematic drawing of the growing edge of the abalone shell. C: prismatic layer; N: nacreous layer; EPL: extrapallial space; pt: periostracum; c: cells; prtn: proteins; m: muscle of the foot; t: tentacles; OP: organic matrix; AP: aragonite platelets.[4]

The calcium carbonate present in the molluscan shell is derived from calcium and bicarbonate ions in the extrapallial fluid according to the reaction[3]

$$Ca^{2+} + HCO_3 \rightarrow CaCO_3 + H^+$$

Inside the extrapallial space, the concentrations of calcium and carbonate ion are raised to levels exceeding the solubility product causing precipitation and crystal formation to occur. The nucleation and growth of the crystals are

controlled by pH differentials across the membrane.[9] The morphology and size of the nucleating crystals may be affected by both inhibiting ions that are also present in the fluid [10, 11, 12] and by the organic matrix enveloping them.[13, 14, 15] The organic matrix may be separated into two fractions, the soluble and insoluble components. The principal compounds of the soluble fraction are glycoproteins, polypeptides and polysaccharides.[2,3] The insoluble component contains DOPA and has higher concentrations of phenylalanine, tyrosine, glycine, and alanine.[3, 14]

There are two phases of $CaCO_3$ present in the mollusc, these are the calcite and aragonite phases. The nacreous layers in the interior of the mollusc shells are composed of aragonite. Aragonite is a polymorphic phase of $CaCO_3$ that in this case adopts a hexagonal platelike morphology. The platelets range from about 1μm to 5μm, but sometimes up to 10 μm across [4, 16], and are approximately 0.5 μm in thickness. The platelets in nacre are typically arranged in either columns (abalone or nautilus), or in sheets (pinctada). The stacking sequences of the platelets are not random, but are layered together with the organic matrix to form the microarchitecture described previously.[4]

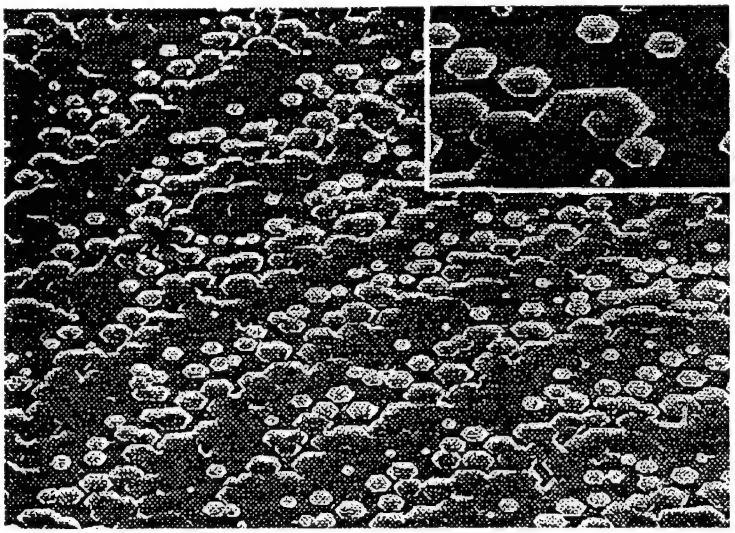

Figure 2a. (Wise,1970) *Pinctada radiata* crystals arranged in sheets. SEM image.[3]

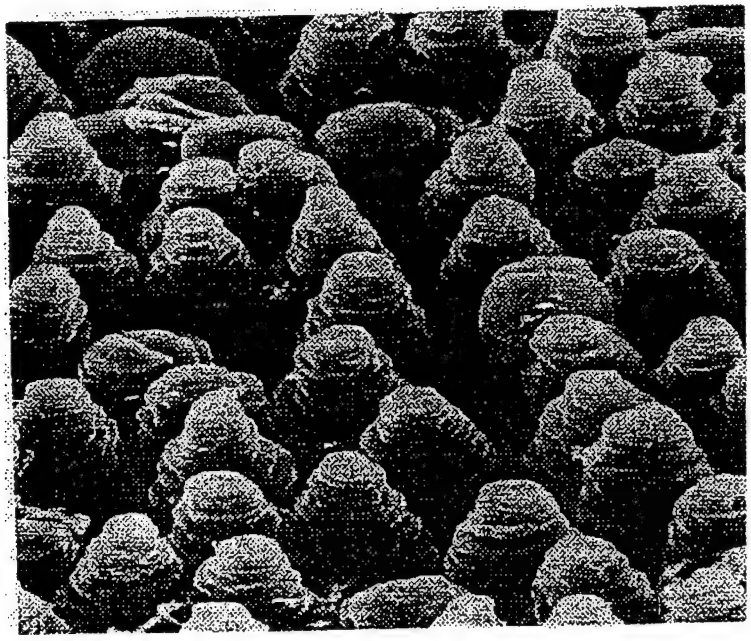

figure 2b. (Wise, 1970) Nacreous shell of the gastropod *Turbo castanea* showing stacked formations. SEM image.[3]

The calcite phase is columnar, rather than platelike, and appears on the exterior portion of the shell. Both the calcite and aragonite phases are composed of oriented crystal lamellae, each surrounded by an intercrystalline organic matrix. The organic matrix not only surrounds each crystal, but intracrystalline matrices also penetrate and envelop the smaller crystallites within them, as discussed previously.[16]

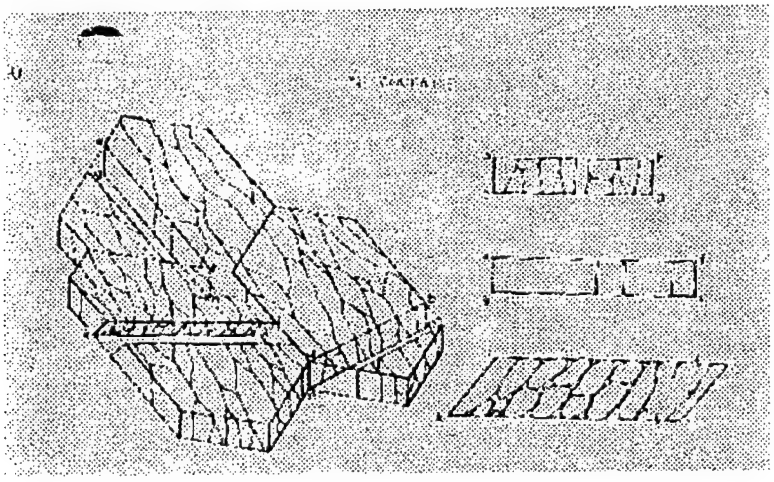

figure 3. (Watabe, 1965) Schematics of crystal platelets showing intracrystalline organic matrix and crystallites.

Kitano and Hood (1962) have shown that aragonite is the preferred phase to nucleate from supersaturated seawater, mainly due to the presence of Mg^{2+}, which inhibits the formation of calcite.[16] The Mg^{2+} and other inhibiting ions, such as Sr^{2+} present in seawater may also affect the morphology and mineralogy of the nucleating crystals.[12]

In this study we have been primarily concerned with the observation in mollusc shells of the inorganic aragonite phase, and the imaging of its boundaries and microdomains within the organic matrix.

Scanning Probe Microscopy

The Atomic Force Microscope (AFM) and the Scanning Tunneling Microscope (STM) are part of the new family of emerging Scanning Probe Microscopes (SPM) that are capable of resolving surfaces down to the atomic level.[25] Besides atomic and molecular shapes, these new devices can also map electrical, magnetic and mechanical properties and tempreature variations.[26]

The first SPM was the scanning tunneling microscope (STM), developed by G. Binnig and H. Rohrer during 1981 at the IBM Zurich research laboratories.[24] The STM is based on the tunneling capabilities of electrons. To scan a surface using the STM, an extremely sharp tip (of tungsten or platinum-iridium) is brought close enough to the sample surface so that the electron clouds of each are just touching. Since the probability of finding an electron beyond the surface decreases exponentially with distance from the surface, this distance must be very small. A voltage is applied between the tip and the sample, causing electrons to flow, or tunnel through the electron clouds. The distance between the tip and sample is very sensitive, and produces precise measurements by rastering the tip across the surface moving up and down with the topography.[24]

The tip can move in three dimensions with an x, y, z, piezoelectric translator. The distance betwen the sample and the surface is controlled by a voltage applied to the z piezo element. The voltage is determined by a feedback circuit that measures and controls the small current caused by the movement of the tunneling electrons and the low bias voltage applied to the tip.[25] The lateral resolution of the surface is limited by the sharpness of the tip[26]. Ideally, the tip would be sharp enough to have only a single atom sitting securely at the end. Usually, this atom comes from the sample itself, being dislodged by high electric fields that are caused by the applied voltage.[24] If the sharpness of the tip, the precision of the controls, and the fineness of the raster scan are all adequate, the STM can resolve images as small as 0.2 nm.[26] Because of its dependance on current, it is necessary for the sample to exhibit some conductive

properties, or in the case of biological specimens, be immersed in a liquid cell in order to image with the STM. This presents some limitations as even many metals become oxidized.[27]

The AFM, which does not need a conductive sample was introduced by C. Quate, of Stanford University and C. Gerber, from the IBM Zurich laboratory in 1985.[26] The AFM records the interatomic forces between the apex of a cantilevered tip (a shard of diamond mounted at the end of a silicon nitride tip) and the atoms in the surface of a sample.[25] The AFM can be operated in two modes; either in contact mode where the AFM senses the repulsive forces (generated by the overlap of the electron cloud at the tip with the electron cloud at the sample surface atoms) between the tip and the sample by actually touching the sample, or in non-contact mode, where the tip senses the attractive forces between the tip and sample and the feedback system keeps the tip from touching and damaging the sample. This second method comes at the cost of decreased lateral resolution.[25, 26] The small repulsive forces (10^{-6}-10^{-9} N) are recorded by measuring the minute deflections of the cantilever tip. The deflection of the spring in the in the force sensor can be measured with electron tunneling, an interferometer or by the deflection of a laser beam reflected off a mirror and received by a photodiode. The electric signal must vary rapidly with deflection, and the feedback mechanism responds to the changes in the beam's path by activating the piezoelectric motor. The piezo control adjusts the distance of the tip from the sample surface to keep the deflection of the cantilever constant. The deflections of the cantilever are recorded by a computer which translates them into a display of the sample's topography.[25, 26]

SPM has become a much needed alternate to SEM and TEM, since it offers non-destructive methods of imaging, although work is still being accomplished in interpretation of the images. Work in this area is necessary to overcome or realize artifacts of convolutions present in the displays.

Technological applications of SPMs extended largely into the electronics and compact disk industries where methods for quality checks on the micron or nanometric scale on a regular basis are necessary. There is also great interest in SPM in the medical and biological fields for imaging biological structures and molecules. This

study is a good example of the difference in information obtained from the AFM in comparison to that previously obtained by the SEM or TEM.

Though much work has been accomplished in this area, only a few publications are available using SPM techniques. Recent work done by S. Manne et al. [23] have explained what we believe to be microdomains as surface asperities. The asperities described were imaged on the bivalve (*Atrina* sp.), but were not mentioned in the imaging of the gastropod (*Haliotis rufescens*).

Experimental

1. Sample Preparation

The Red Abalone, Pinctada (pearl oyster), and Nautilus samples were each cleaved with a razor blade to produce a fresh surface. The cleaved samples were mounted on standard AFM sample plates using double sided tape. Before imaging, each specimen was cleaned using "Dust Off".

The geological aragonite (orthorhombic lattice structure) had been previously prepared, and a flat native (001) surface was exposes for imaging. The geological calcite (rhombohedral lattice structure) was cleaved and a fresh (001) surface was exposed for imaging. These samples were mounted using the same method as described for the biological specimens.

2. Imaging

A commercial AFM (Nanoscope E from Digital Instruments, Santa Barbara, CA) was used for imaging. We operated in contact mode, with silicon nitride cantilever tips, replaced after each session for optimal results. The AFM imaged in constant height mode.

Results

Some difficulty was encountered in imaging both the biological and geological specimens due to the sample roughness and natural curvature of the shells. The roughness values and grain sizes were calculated using the software that accompanies the Nanoscope II. The diameters were also calculated through manual use of the software. Images and sectional analysis sheets for each specimen may be found in the appendix.

The images below in figure 5. are several examples of the geological aragonite samples. As the scan size is decreased, the size of the crystals are found to be approzimately 150-300 nm in diameter.

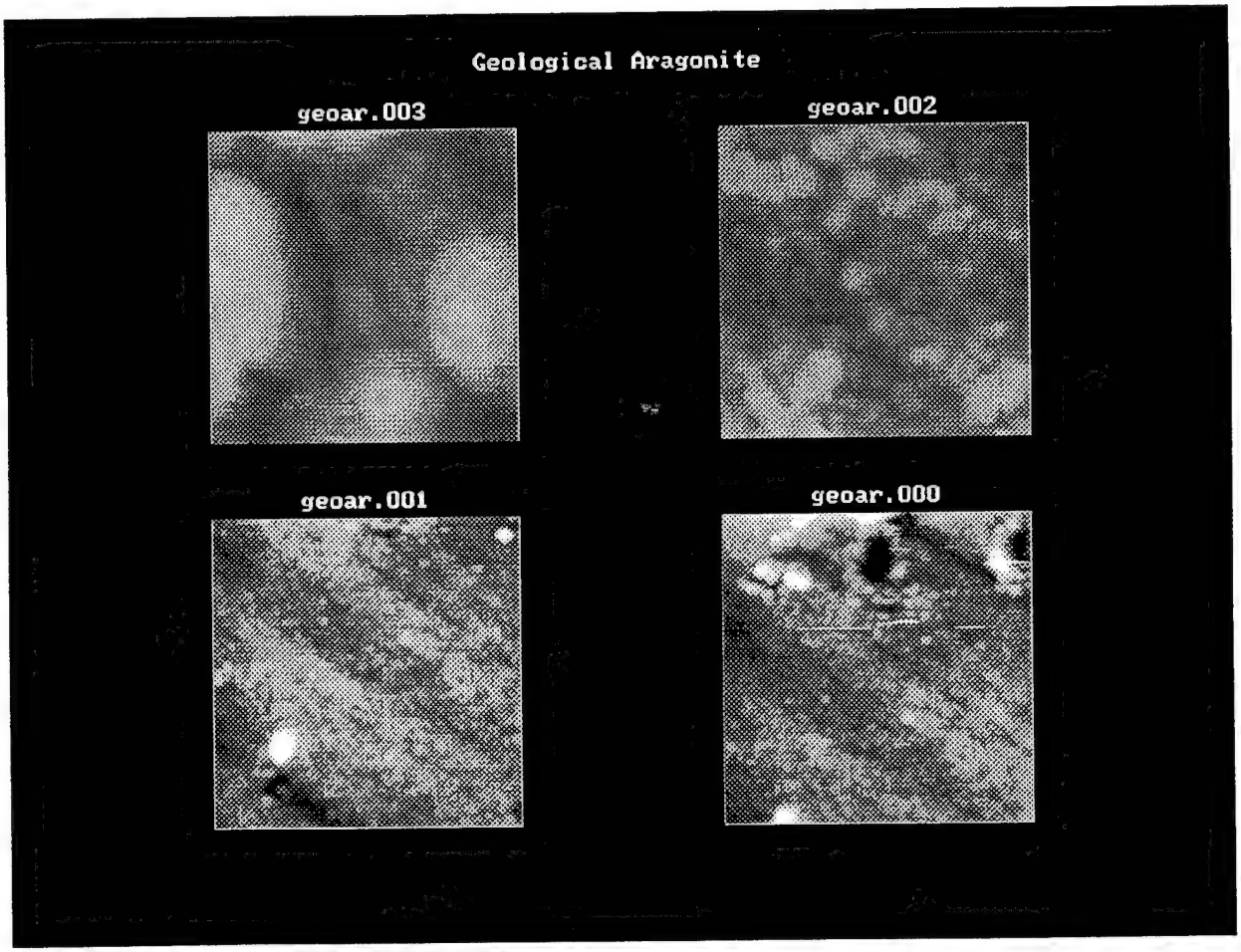

figure 5. Geological Aragonite. Clockwise from the upper left, scan sizes range from 400 nm, 2 μm,10 μm, 10 μm.

Geological calcite was imaged as seen below in figure 6.

figure 6. Geological Calcite. Scan sizes are 200 nm. and 5 μm.

The Red Abalone (*Haliotis rufescens)* was imaged with the J head, in order to obtain larger scan sizes. The Red Abalone contained a network of platelets approximately 5-7 μm across. As smaller scan sizes were used for imaging the platelets, crystallites, or microdomains began to appear, as seen in the latter images in figure 7.

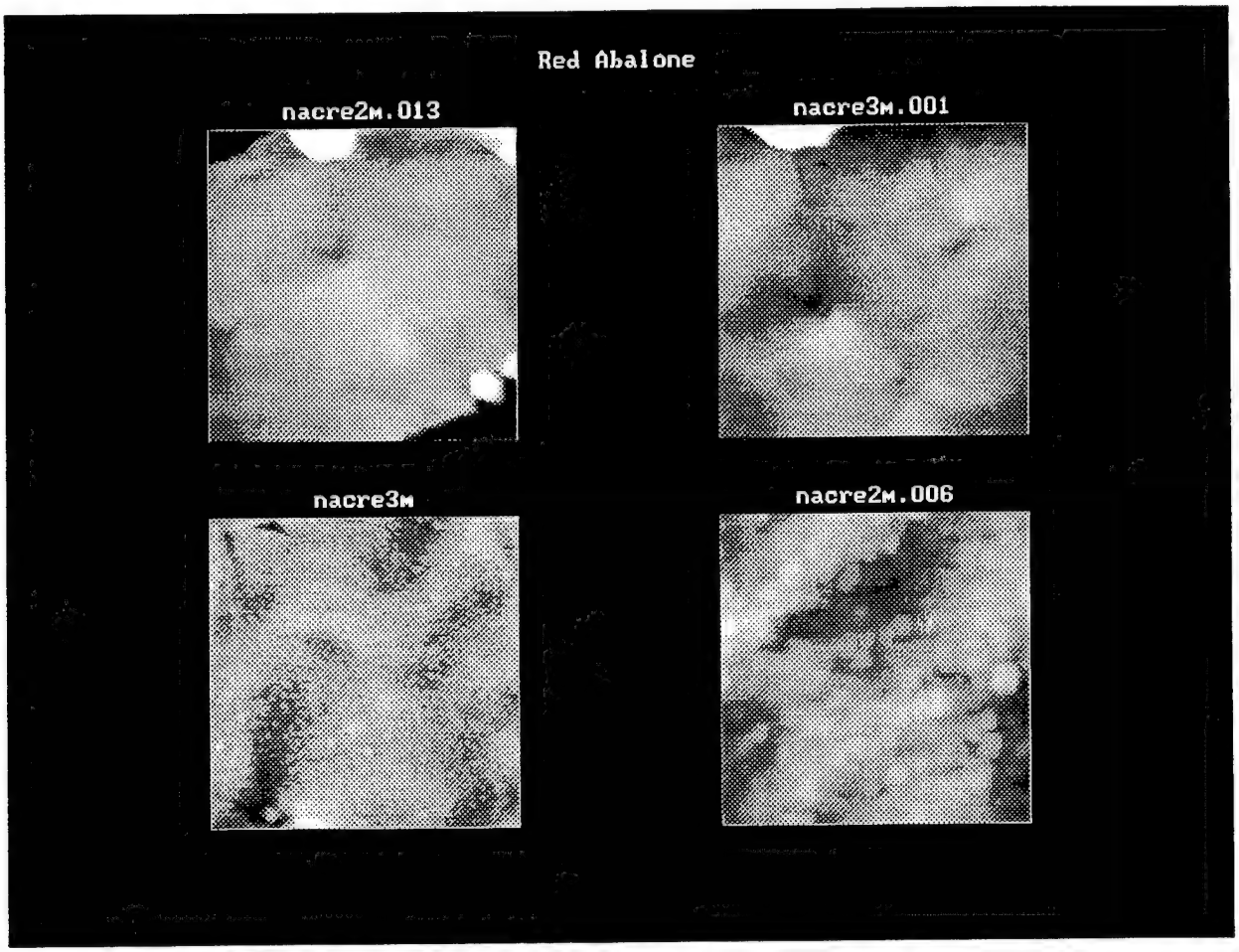

figure 7. Red Abalone. Clockwise from upper left, the scan sizes are as follows; 15 μm, 10μm, 5μm, and 2μm.

The Black lipped Oyster (*Pinctada margaritifera*) was also imaged with the J head. The oyster platelets were approximately 3-5 μm in length. As the scan size decreased, microdomains also began to become apparent in this sample, as imaged in figure 8. A second region was also imaged, as seen in figure 9. The organic matrix is not present here as in the prior images.

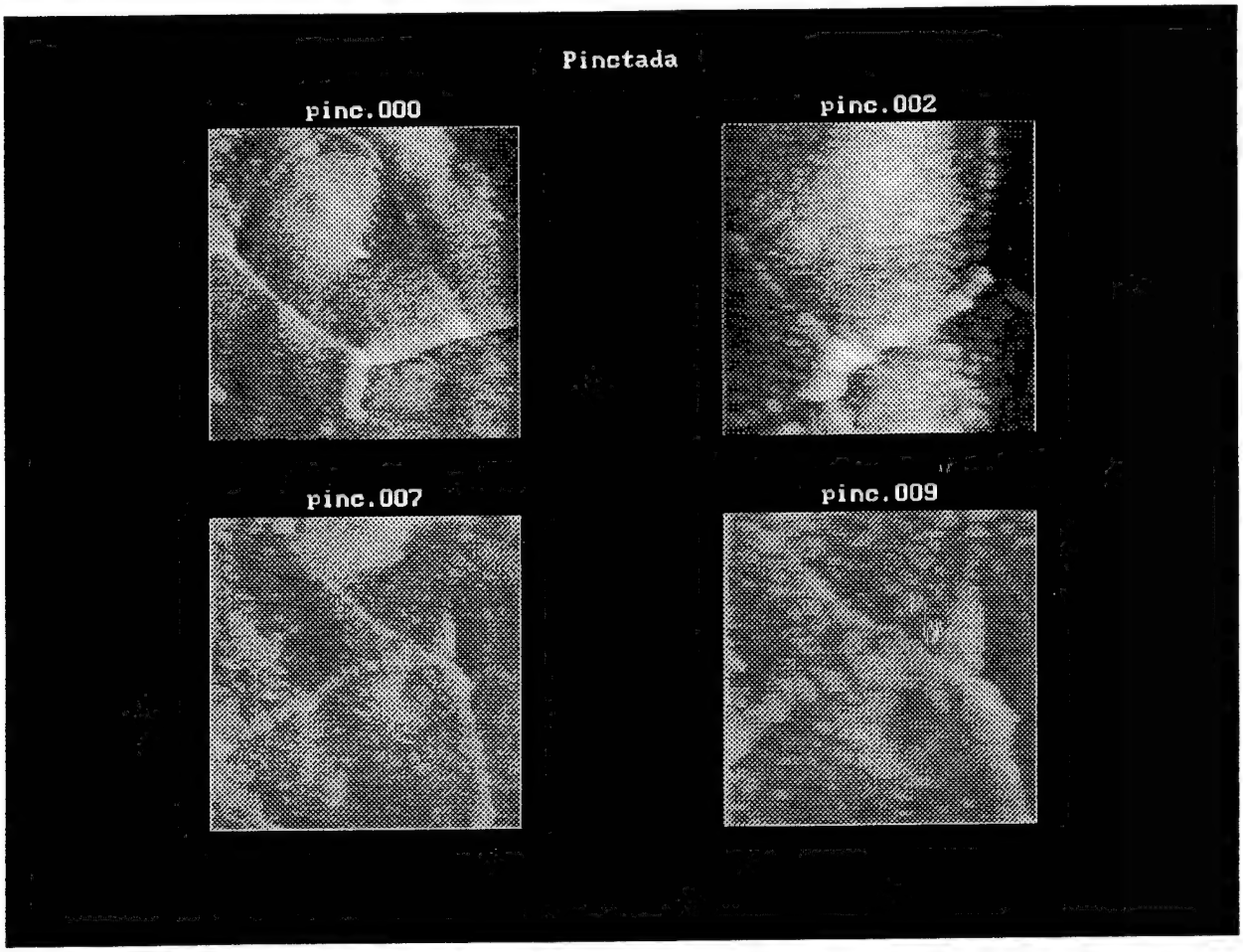

figure 8. Black Lipped Oyster. Clockwise from the upper left, 5 μm, 3 μm, 3 μm, 5 μmm

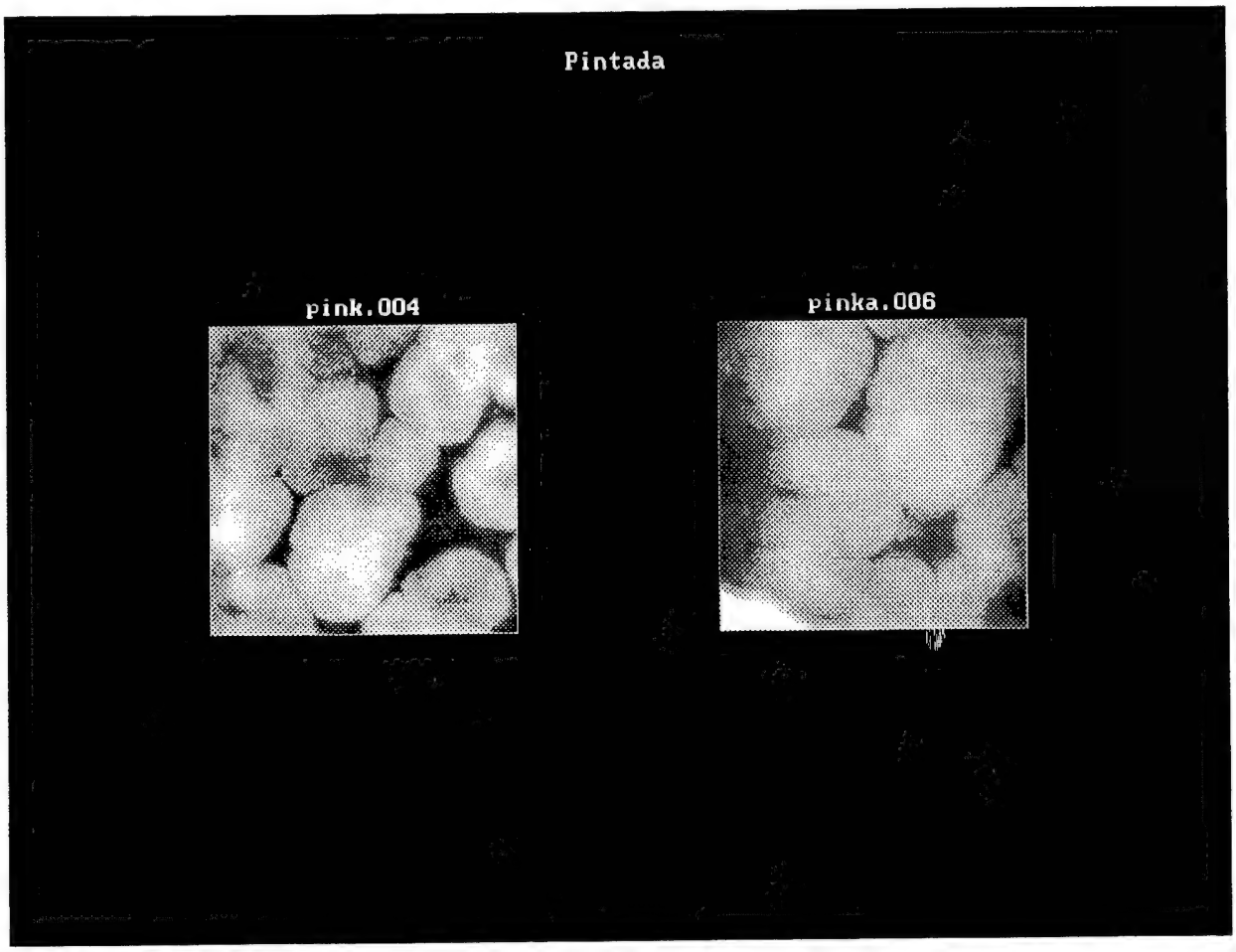

figure 9. Black Lipped Oyster. From left to right, 10 μm and 7.5 μm.

The Nautilus (*Nautilus pompilius*) was the most difficult sample to cleave and to image. Both the J and E heads were used for imaging. The nautilus crystals are approximately 0.7 μm in length. Images may be seen below in figure 10.

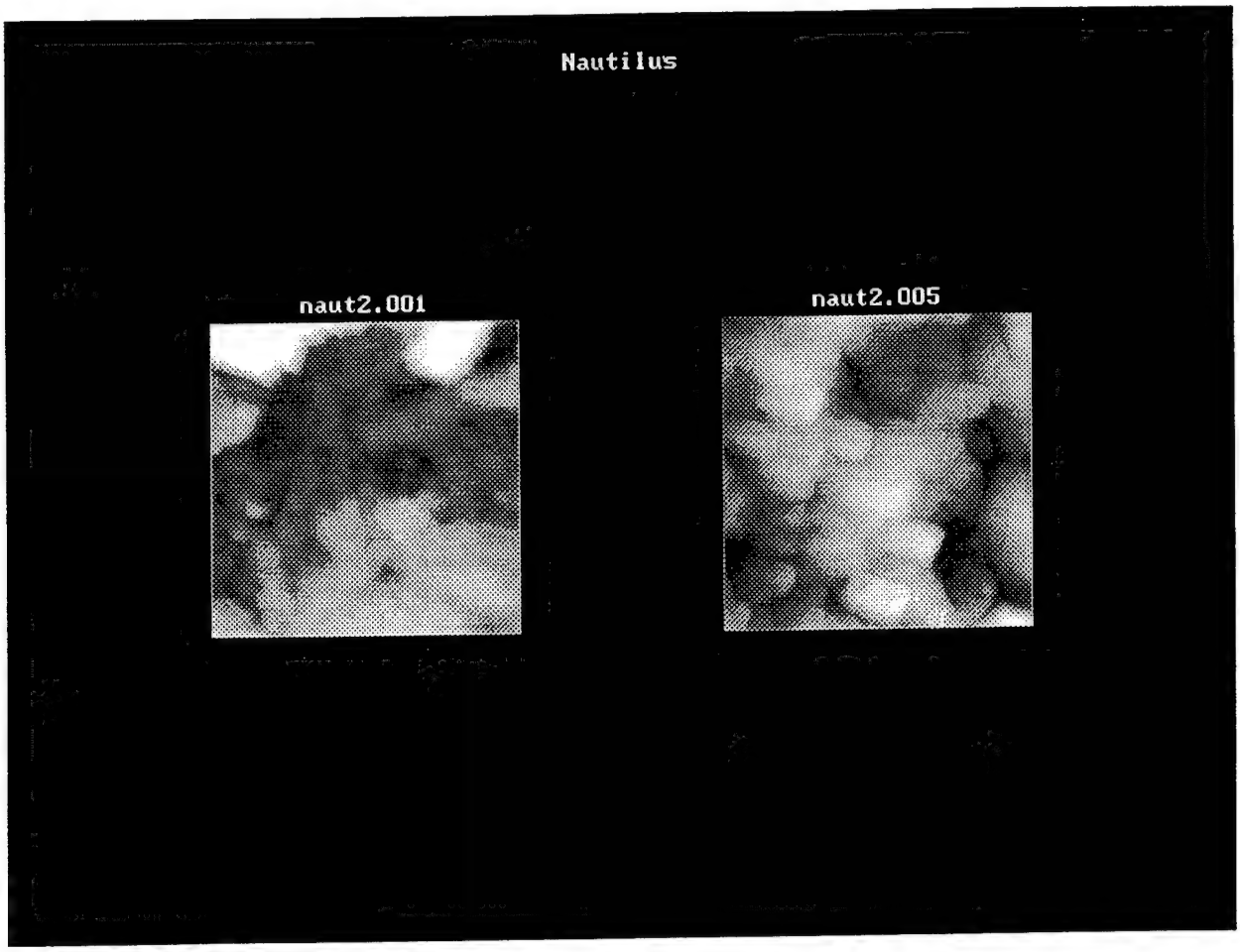

figure 10. Nautilus. From lleft to right, 800 nm. and 5 μm.

The values for platelet size, crystallite size and roughness values may be compared in Table 1. below.

Table 1. Data for Comparison of Nacre

specimen	*Platelet size*	*Crystallite size (nm)*	*Roughness (RMS) for 5 μm scan size*	*Maximum height for 5* μm scan size
geological aragonite	NA	150-300	6.01 nm	38.95 nm
geological calcite	NA	100-125	5.088 nm	59.65 nm
Red Abalone	5-7 μm	100-180	9.26 nm	489.3 nm
Oyster	3-5 μm	150-375	97.4 nm	815.37 nm
Nautilus	0.7 μm	N/A	77.67 nm	1.17 μm

Other AFM results and images, including roughness, sectional and grain size analysis may be seen in the attached appendix.

Optical microscope results were also obtained for the shell samples, and are also presented in the appendix.

Discussion

It is believed that the imaging of the platelets in the 1-7 μm range as seen in prior studies was difficult to accomplish throughout our experiment partly due to intracrystalline fracturing during cleaving. Although the J head was utilized in each case, the several micron range was a large area to scan, especially since each of the samples possessed a certain degree of curvature and the height deviated greatly in many regions. The strong sensitivity of the AFM to surface roughness strengthens the need for extremely level samples. The nautilus sample was the most uneven, this is evident in the optical and maximum height calculations. It was not uncommon for several imaging sessions to pass with few or no useful results. We were fortunate to have found level areas after several attempts, this being accomplished through pure trial and error. The correct combination of scan area size and z range values were crucial in realizing that an informative image was present. Only experience and patience can improve this element of the experimental work. Several times, while imaging larger samples, the force calibration curve would exhibit jagged oscillations, even though the scope mode was varying consistently. It is unknown why this occurred, and could possibly be connected with poor resolution in some of the images.

We were able to image both the platelets (0.7 to 7μm) and crystallites (100-375 nm) present in the nacreous layers of the shells. The crystallites appear as the scan size decreases in the images. Although Watabe (1965) discussed the presence of the crystallites and the intracrystalline organic matrix separating them, very few publications have followed even though much other related work has been accomplished in this area. The platelets are treated in most literature as single crystals, with no mention of the microdomains. Resolution of the crystallites may have been difficult using other techniques such as SEM or TEM.

Two recent studies (S.Manne, et al., 1994) and (R. Giles, et al., 1995) examined similar shells and also obtained images through AFM. It is believed that they dismissed the microdomains as surface asparities due to the scan size used to obtain the images. If a sectional analysis is done on a 5-10 μm scan, the resulting line graph has given height deviations in the range of 20-50 nm. This size range must be treated skeptically, since it is in the range of the tip image size. If the images are obtained at smaller scan sizes (< 1 μm) this size range does not appear. What is evident is that the platelets are composed of smaller domains, which are not in the size range of possible tip convolutions. These images are not overly uniform or directional in appearance, and scale in size with a change in the image scale. The microdomains are in the same size range as the crystals of the geological aragonite, which is not an unlikely result.

Also of interest in the figure 9 images of the Pinctada is the clearly visible matrix between the larger platelets. Although the organic matrix regions are believed to consist of layers of an amorphous material, they appear in these images as particles, in the same size range as the crystallites.

In conclusion, it is apparent that the crystallites compose the nacreous platelets in each of the biological samples. These images should be of interest in the study of the nucleation and growth of the crystals on the organic matrix. They should lead to insight into the construction of the platelets, and therefore clues into the high strength and fracture toughness of these organic/inorganic microcomposites.

References

1. Fendler, J.H. *Chem.Rev.* 1987, 87, 877-899

2. R. Giles, S. Manne, S. Mann, D.E. Morse, G.D. Stucky, P.K. Hansma, *Biol. Bull.* 188:8-15 (Feb.-Mar. 1995) pp. 8-15

3. K. Simkiss and K.M. Wilbur, *Biomineralization,* Academic Press Inc. San Diego, CA , 1989

4. M. Sarikaya and I.A. Aksay, (eds.) *Biomimetics: Design and Processing of Materials,* American Institute of Physics, New York, 1995

5. M. Sarikaya, and I.A. Aksay, *Results and Problems in Cell Differentiation in Bipolymers*, Steven Case (ed.) Springer and Verlag, Amsterdam, 1992 pp. 1-25

6. I.S. Weiner, W. Traub, and H.A. Lowenstam, *Biomineralization and Metal Accumulation*, P Westbroek and E.W. de Jong (eds.) Dordrecht: Reidel, 1983 pp. 205-224

7. S. Weiner and Traub, *Phil. Trans. R. Soc. Lon.*, B 304, 425-434, 1984

8. Mann, S. *Struc. Bonding (Berlin)* 1983, 54, 125

9. Williams, R.J.P., Phil. *Trans. R. Soc. Lon.*, B 304, 411-424, 1984

10. Kitano, Y., *J.Chem. Soc.*, vol. 35, 12 Dec 1962, pp.1973-1979

11. D.J.J. Kinsman and H.D.Holland, *Geochim. Cosmochim. Acta.*, 331, 1969

12. Frech, D.W. University of Washington, doctoral thesis, unpublished work

13. Weiner, *Science* vol. 190, Dec. 5, 1975 pp. 987-9

14. Mann, S. *Nature* vol. 332, March 1988

15. Heywood, Mann, and Rajam, *J. Chem. Soc. Faraday Trans.*, 1991, 87, 735, 743

16. Watabe N., *J. Ultrastruc. Res.* 12, 351-370 1965

17. Mann, S. *New Scientist* 10, March 1990 pp. 42-47

18. Mann, S. *Nature* vol. 365, 7 October 1993 pp. 499-505

19. H. Silyn-Robers and R.M. Sharp, *Proc. R. Soc. Lon., Ser. B.* 227, 303-324 1986

20. L. Addadi and S. Weiner, *Proc. Natl. Acad. Sci. U.S.A.* 82, 4110-4114

21. Wise, S.W., Jr. *Eclogae Geol. Helv.* 63, (1970), 775-797

22. S. Mann, J. Webb, R.J.P. Williams, (eds.), *Biomineralization; Chemical and Biochemical Perspectives,* Basel (Switzerland);VCH, 1989

24. G. Binnig and H. Rohrer, *Scientific American*, Aug. 1985, pp. 50-56

25. P.K. Hansma, V.B. Elings, O. Marti, C.E. Bracker, *Science,* vol. 242, Oct. 14, 1988, pp. 209-216

26. Kumar Wickramasinghe, H., *Scientific American*, October, 1989, pp. 98- 105

27. Y.E. Strausser and M.G. Heaton, *American Laboratory*, 1994, 1-7

Acknowledgements

I would like to thank Amy Powell (University of Washington and fellow REU participant) for helping with the shell images, Richard Vos (Arizona State University, Solid State Science) for performing the optical microscopy, Cecilia Morales and D.W.Frech (University of Washington) for preparing and sending the samples, and Mike McKelvy (Arizona State University, Solid State Science) for assistance in cleaving and preparing fresh samples. Also, David Uhl, Mark Hunter, and Jeff Crane for their patience, suggestions, and assistance while our group learned to image with the AFM. This work was supported by grants from Research Semester for Undergraduates Program of the National Science Foundation.

Appendix

Height Angle Plane Angle Clear Calculator

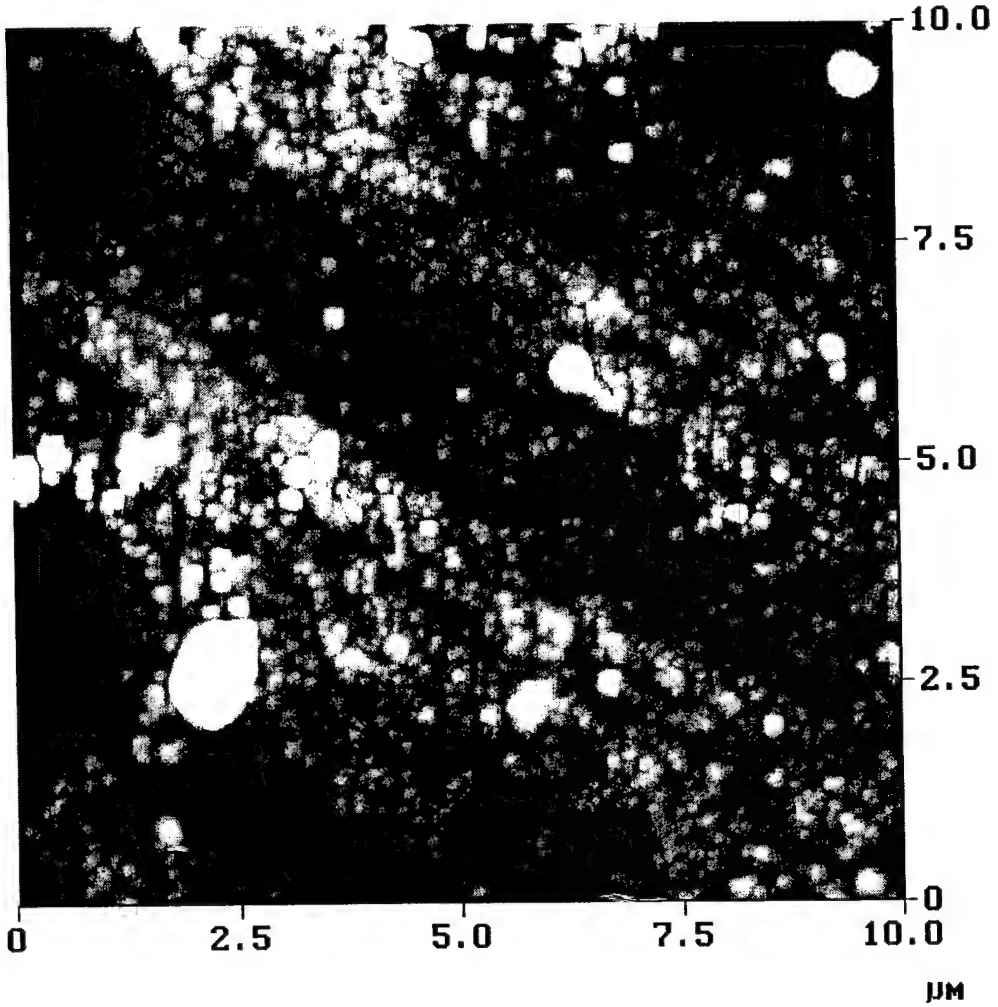

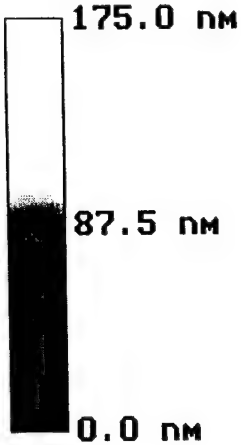

Microscope	AFM
Scan size	10.00 µm
Setpoint	0 V
Scan rate	1.001 Hz
Number of samples	512

Geological Aragonite
geoar.001

Height

Height Angle Plane Angle Clear Calculator

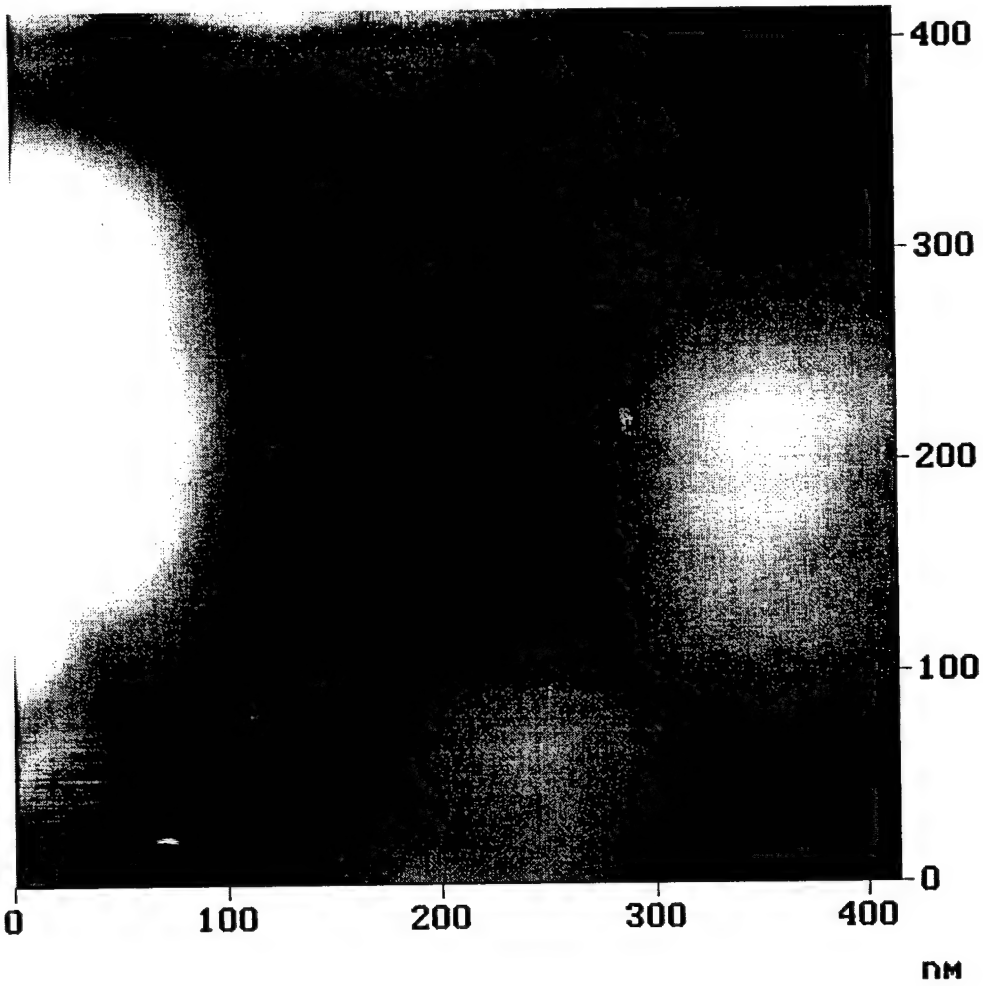

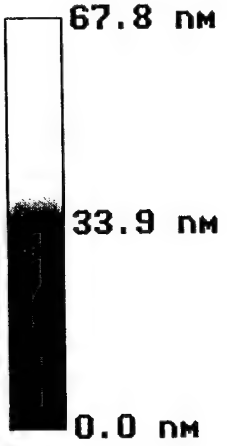

Microscope	AFM
Scan size	414.2 nm
Setpoint	0 V
Scan rate	1.001 Hz
Number of samples	512

Geological Aragonite
geoar.003

Height

Height Angle Plane Angle Clear Calculator

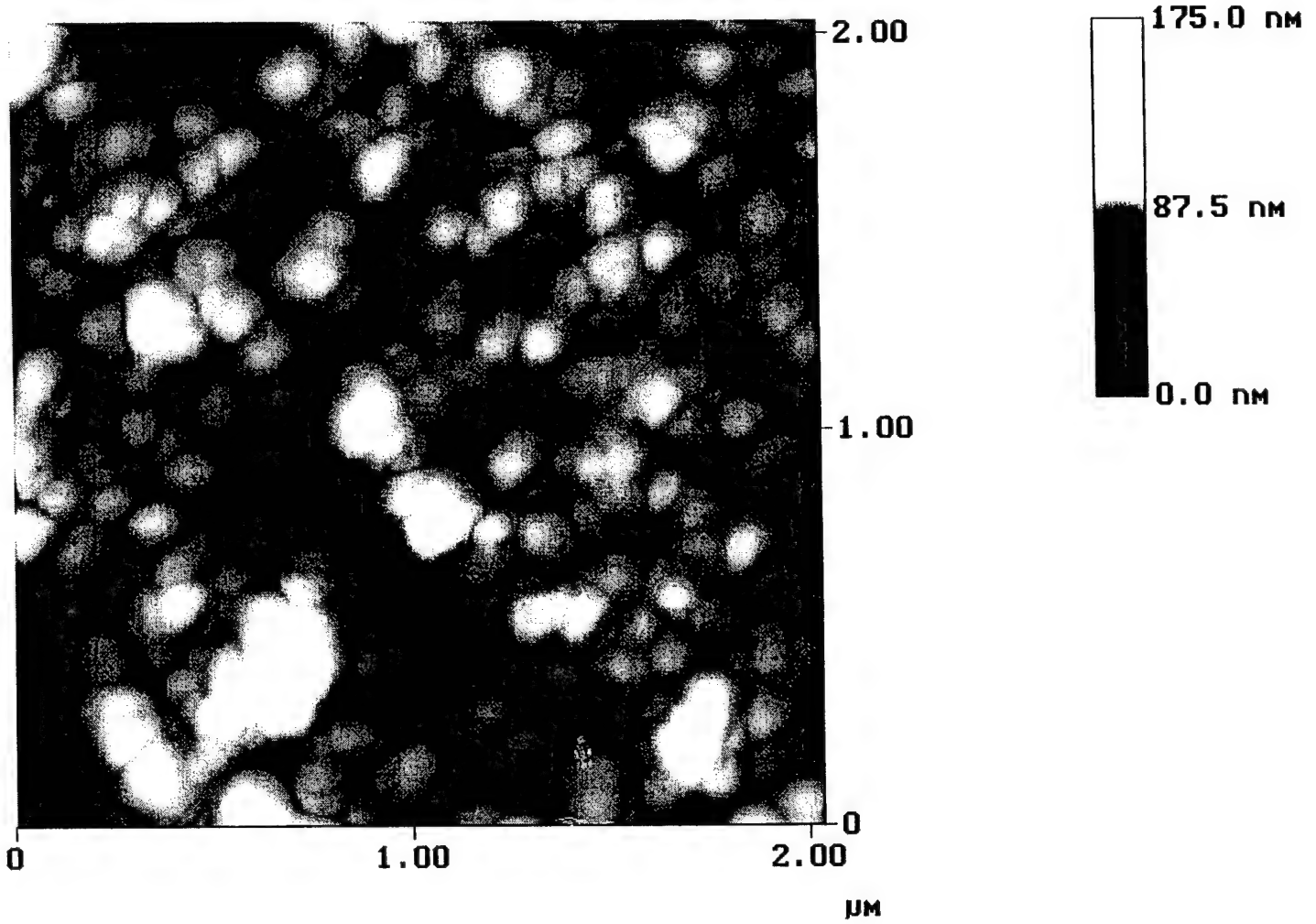

Geological Aragonite

Height

Cursor Marker Spectrum Zoom Center Line Offset Clear

Section Analysis

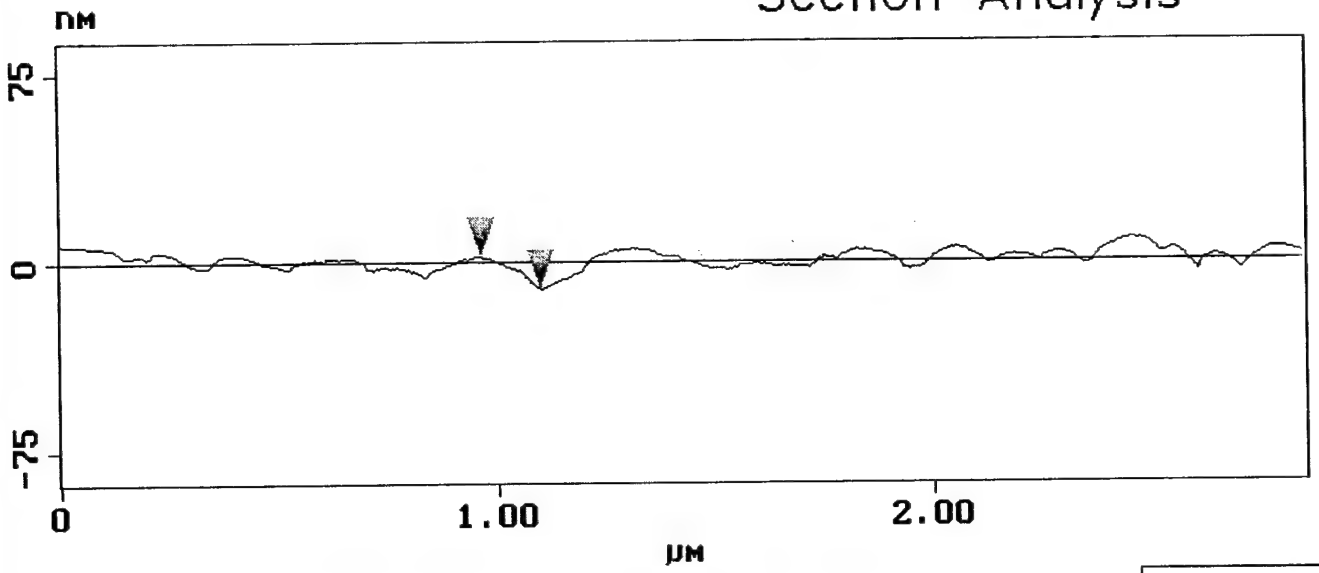

L	135.15 nm
RMS	3.881 nm
lc	DC
Ra(lc)	0.660 nm
Rmax	3.110 nm
Rz	2.523 nm
Rz Cnt	4

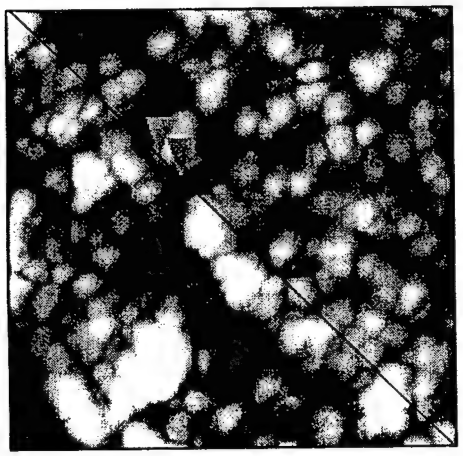

Spectrum

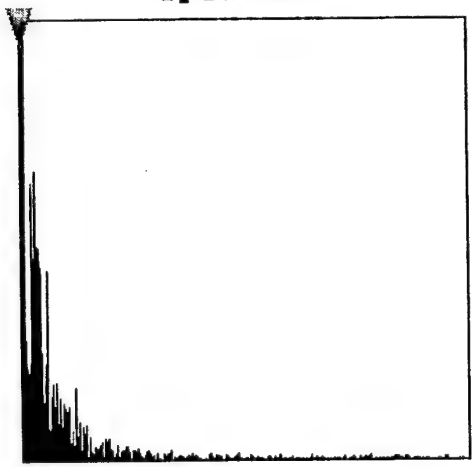

Horiz distance(L)	135.15 nm
Vert distance	12.443 nm
Angle	5.260 deg
Horiz distance	
Vert distance	
Angle	
Horiz distance	
Vert distance	
Angle	
Spectral period	DC
Spectral freq	0 Hz
Spectral amp	1.758 nm

Geological Aragonite

Cursor: fixed Zoom: 2:1 Cen line: Off Offset: Off

Execute Height Clear

Grain Size Analysis

Height Threshold

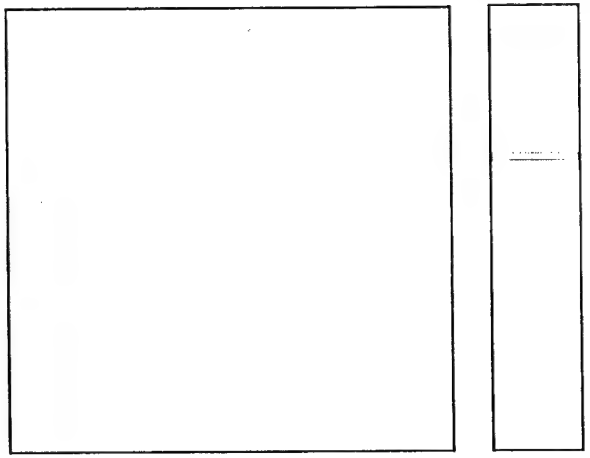

Histogram

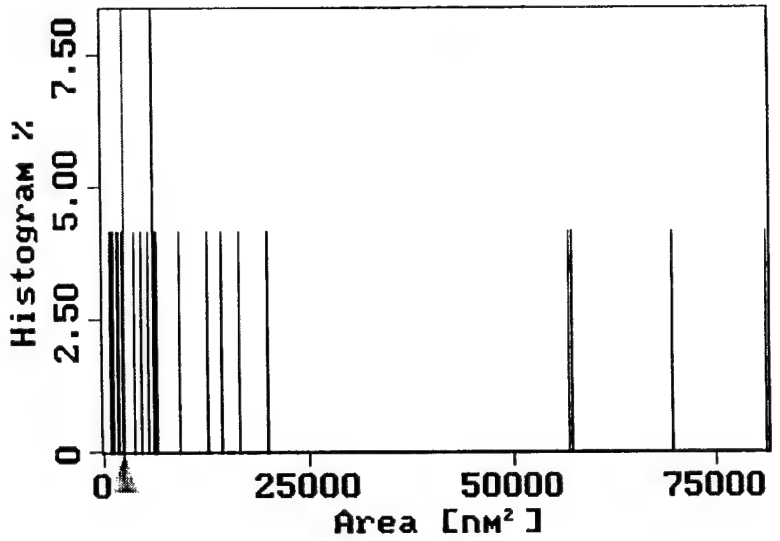

Grain size mean	1.634e+004 nm²
Grain size std dev	2.324e+004 nm²
Number of grains	24
Height threshold	8.000 nm
Grain size	2.560e+003 nm²
Histogram %	8.333
Ht threshold min	-24.200 nm
Ht threshold max	24.200 nm

Geological Aragonite

Slope off

Peak Surface Area Summit Zero Crossing Stopband Execute Clear

Roughness Analysis

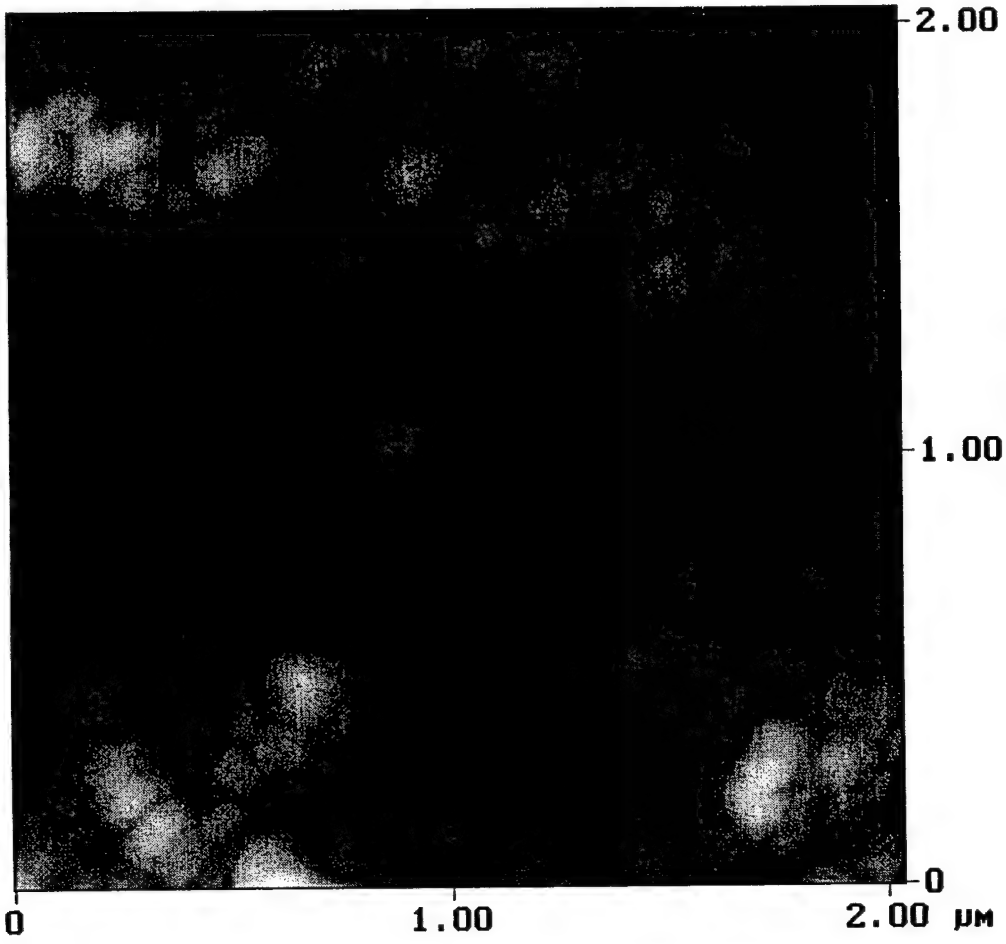

Image Statistics

Z range	40.876 nm
Mean	0.158 nm
Rms (Rq)	6.013 nm
Mean roughness (Ra)	4.822 nm
Max height (Rmax)	38.947 nm

Box Statistics

Z range	23.474 nm
Mean	-3.391 nm
Rms (Rq)	4.518 nm
Mean roughness (Ra)	2.226 nm
Max height (Rmax)	16.185 nm
Box x dimension	350.49 nm
Box y dimension	426.16 nm

Peak off Area off Summit off Zero Cross off

Height Angle Plane Angle Clear Calculator

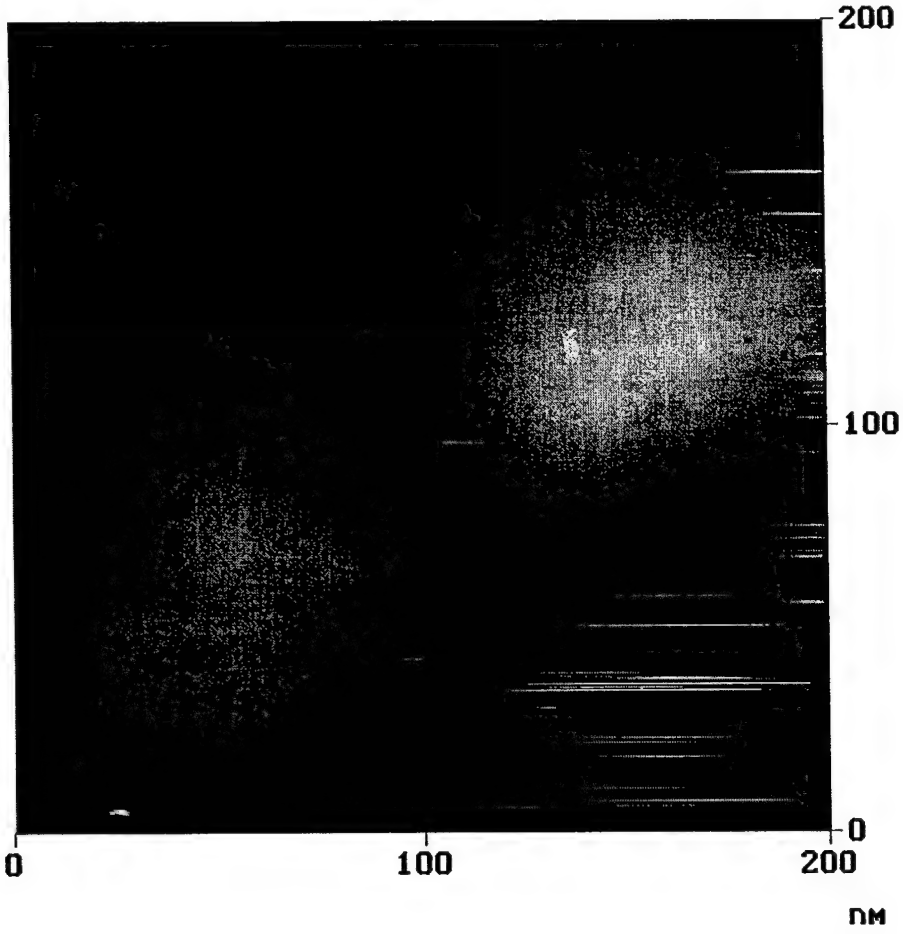

Microscope	AFM
Scan size	200.0 nm
Setpoint	0.5000 V
Scan rate	1.969 Hz
Number of samples	512

Geological Calcite
geocal.001

Height

Peak Surface Area Summit Zero Crossing Stopband Execute Clear

Roughness Analysis

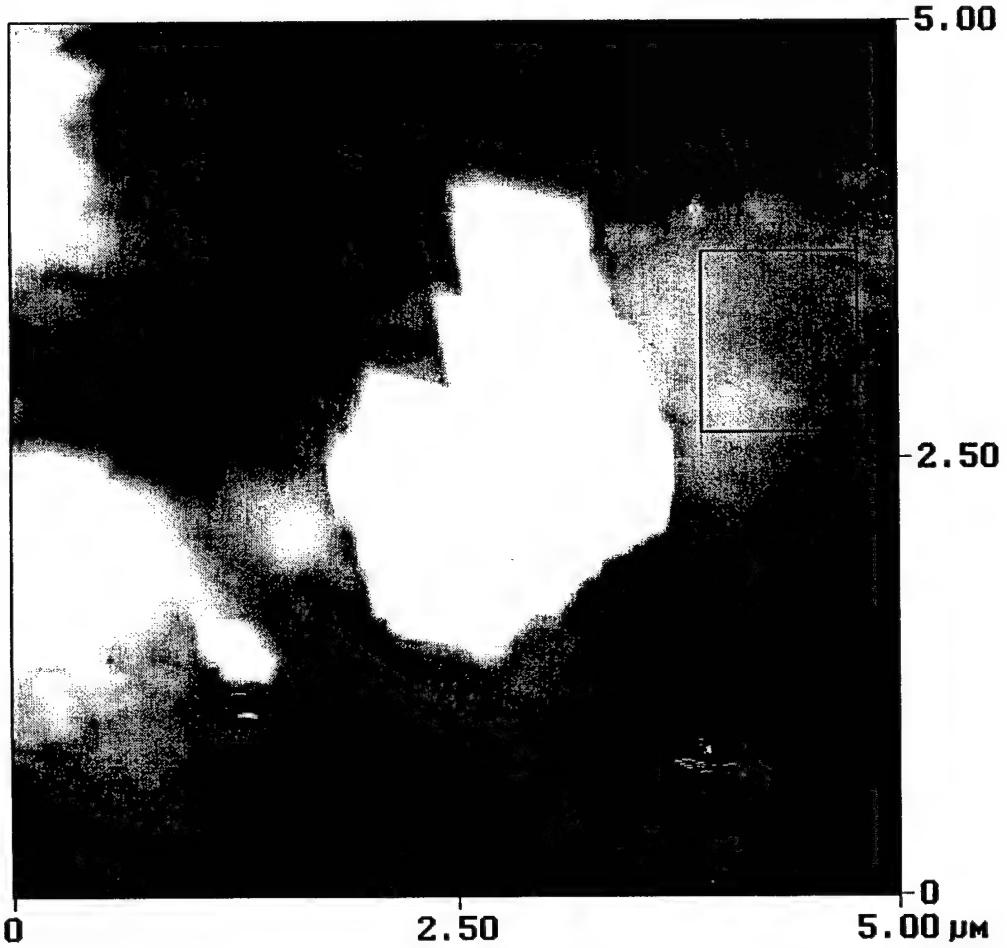

Image Statistics

Z range	830.30 nm
Mean	0.097 nm
Rms (Rq)	128.44 nm
Mean roughness (Ra)	90.168 nm
Max height (Rmax)	838.02 nm

Box Statistics

Z range	83.745 nm
Mean	33.454 nm
Rms (Rq)	16.273 nm
Mean roughness (Ra)	5.107 nm
Max height (Rmax)	54.695 nm
Box x dimension	890.41 nm
Box y dimension	1.037 µm

Peak off Area off Summit off Zero Cross off

Microscope	AFM
Scan size	5.000 µm
Setpoint	0.5000 V
Scan rate	1.969 Hz
Number of samples	512

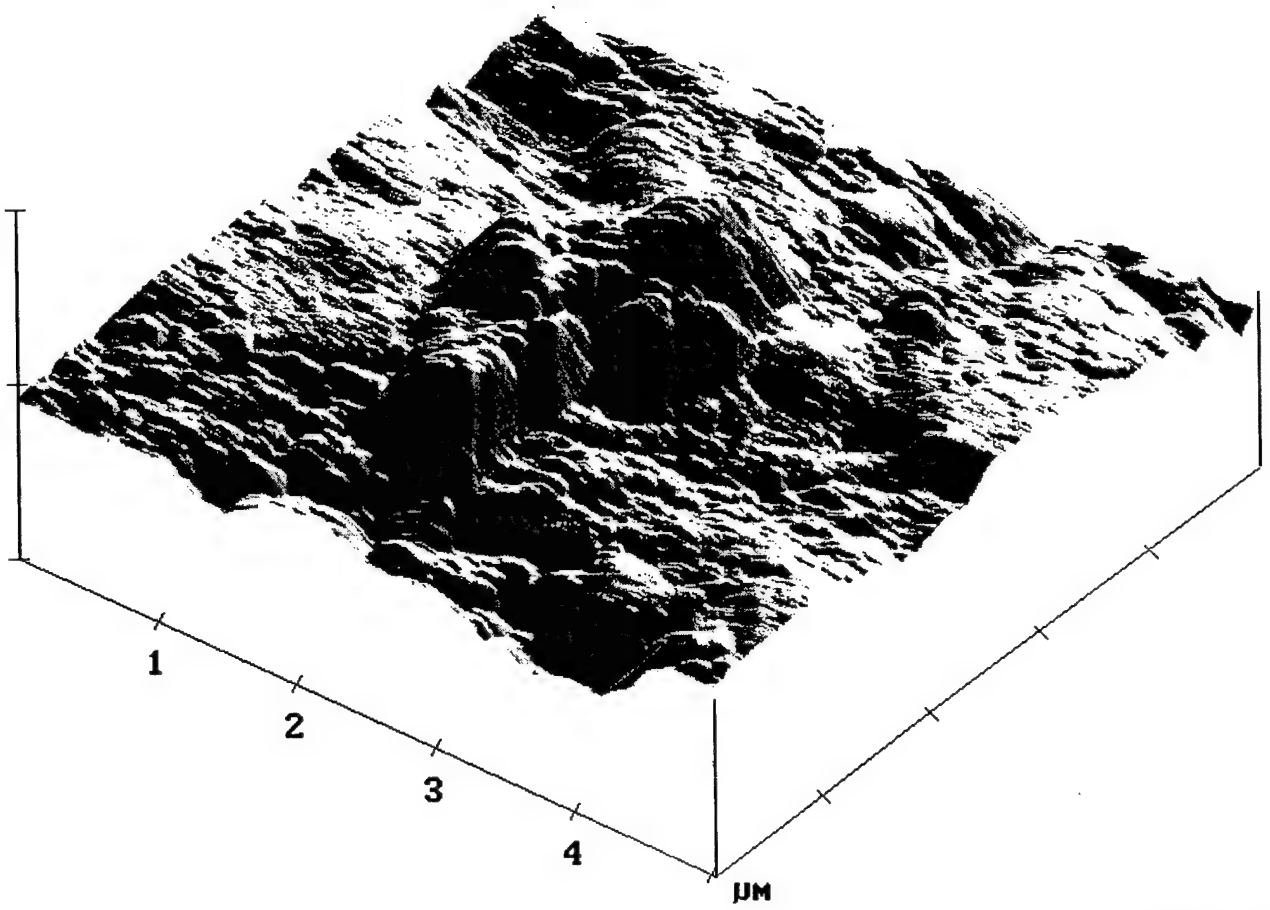

X 1.000 µm/div
Z 1.000 µm/div

Geological Calcite
07110747.001

Peak Surface Area Summit Zero Crossing Stopband Execute Clear

Roughness Analysis

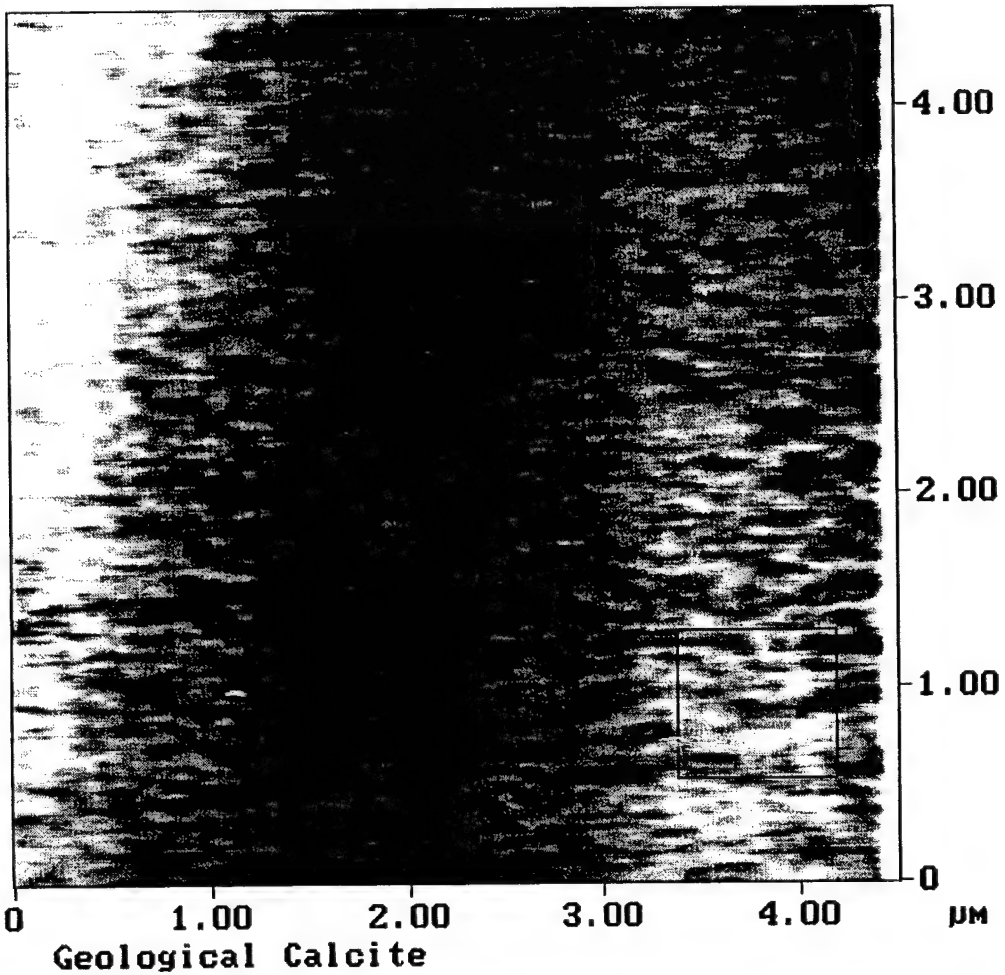

Image Statistics

Z range	59.399 nm
Mean	0.091 nm
Rms (Rq)	5.088 nm
Mean roughness (Ra)	3.746 nm
Max height (Rmax)	59.652 nm

Box Statistics

Z range	17.702 nm
Mean	2.875 nm
Rms (Rq)	2.746 nm
Mean roughness (Ra)	2.161 nm
Max height (Rmax)	17.494 nm
Box x dimension	801.54 nm
Box y dimension	766.31 nm

Peak off Area off Summit off Zero Cross off

Height Angle Plane Angle Clear Calculator

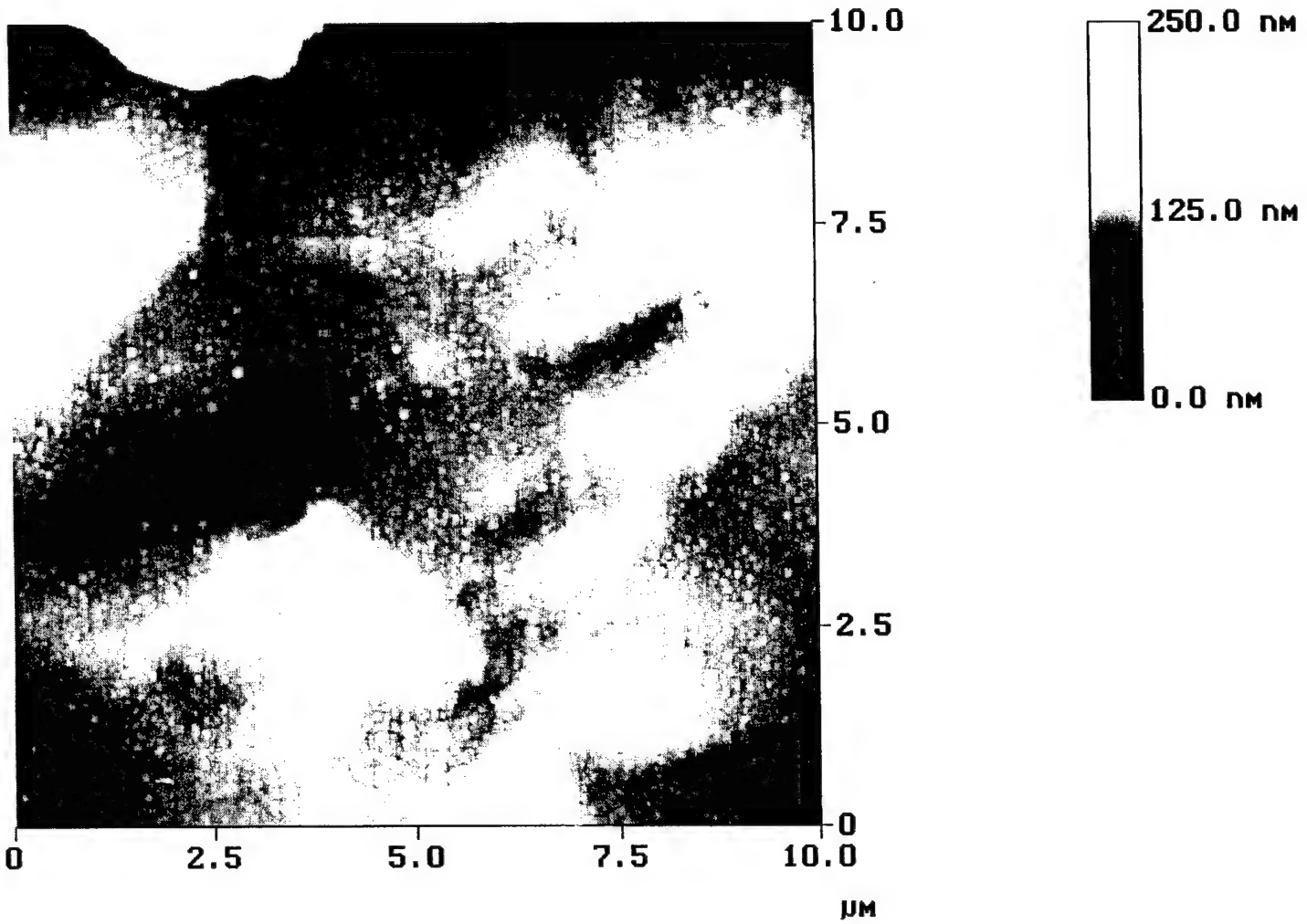

Red Abalone

Height

Peak | Surface Area | Summit | Zero Crossing | Stopband | Execute | Clear

Roughness Analysis

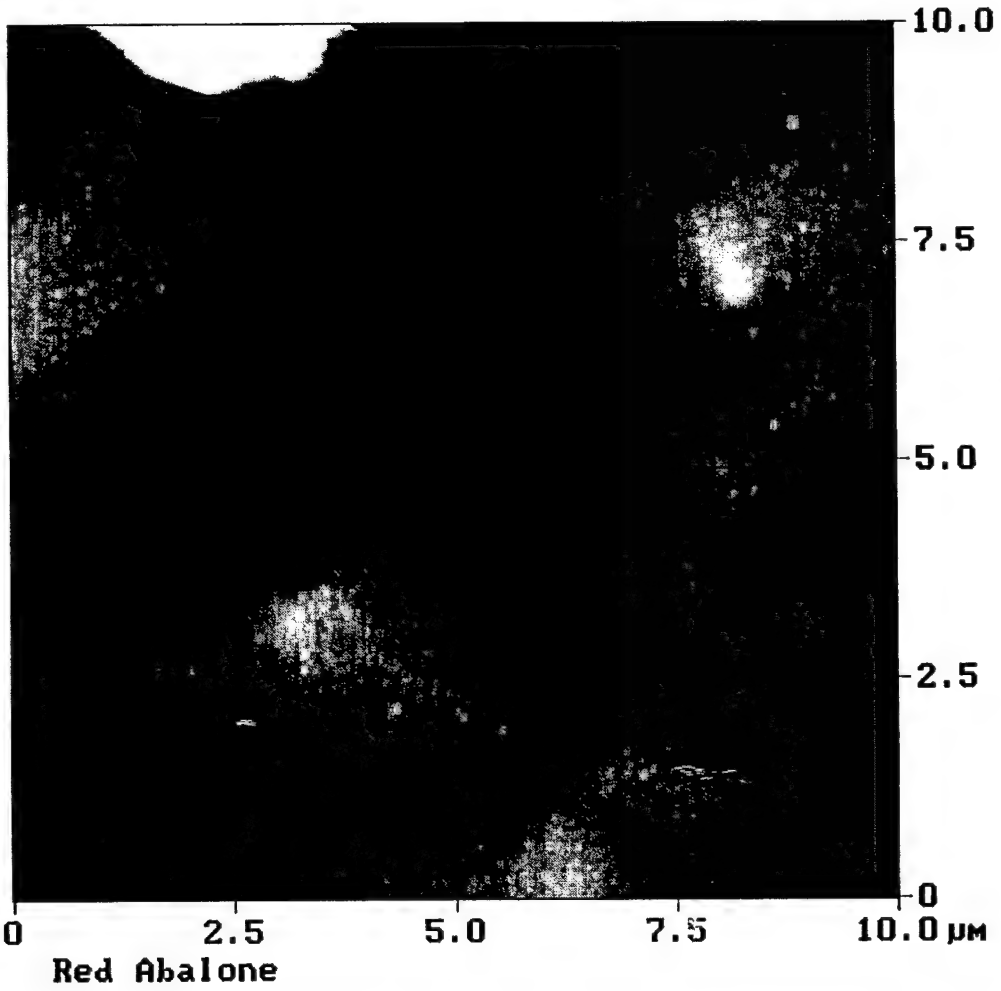

Image Statistics

Z range	489.30 nm
Mean	-0.012 nm
Rms (Rq)	43.030 nm
Mean roughness (Ra)	24.271 nm
Max height (Rmax)	489.30 nm

Box Statistics

Z range	61.243 nm
Mean	4.378 nm
Rms (Rq)	11.760 nm
Mean roughness (Ra)	4.882 nm
Max height (Rmax)	44.575 nm
Box x dimension	1.937 µm
Box y dimension	1.018 µm

Peak off | Area off | Summit off | Zero Cross off

Cursor Marker Spectrum Zoom Center Line Offset Clear

Section Analysis

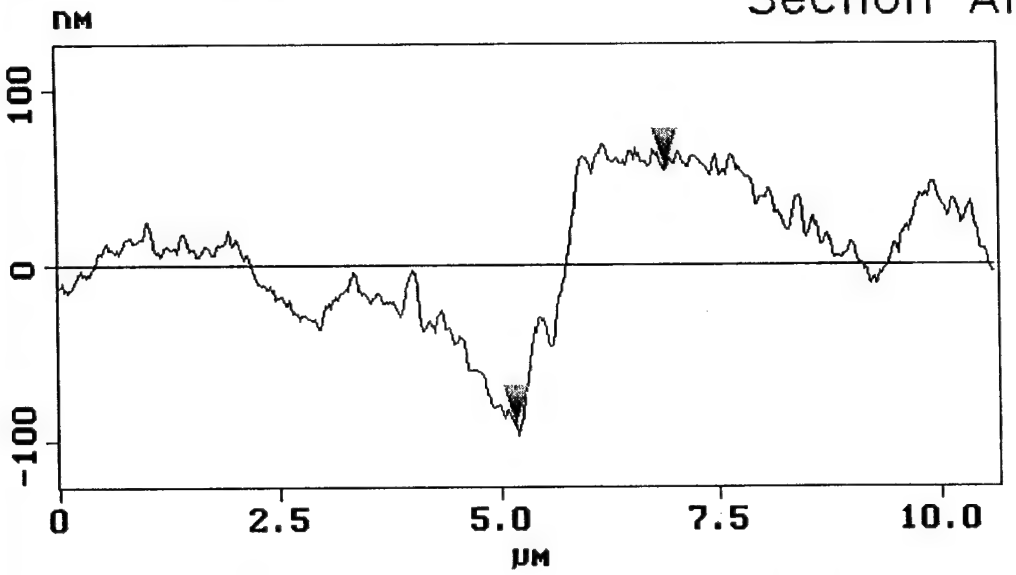

L	1.738 µm
RMS	51.238 nm
lc	DC
Ra(lc)	20.767 nm
Rmax	91.928 nm
Rz	55.992 nm
Rz Cnt	6

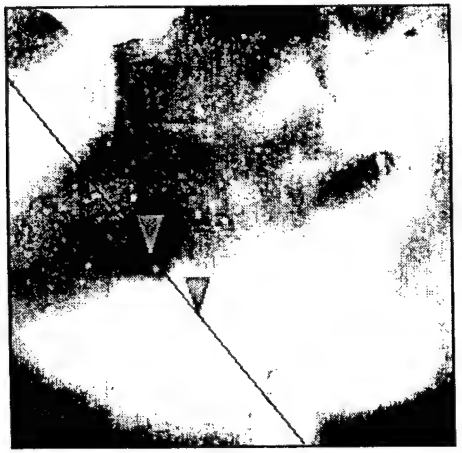

Spectrum

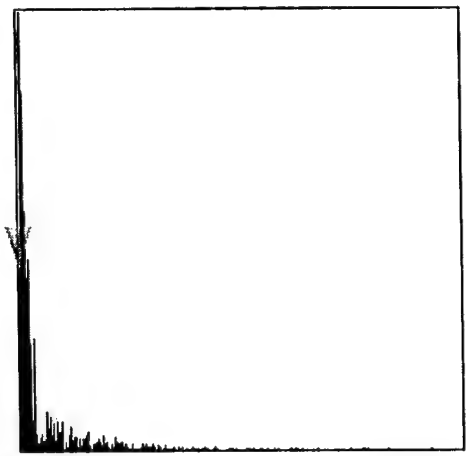

Horiz distance(L)	1.738 µm
Vert distance	146.28 nm
Angle	4.810 deg
Horiz distance	
Vert distance	
Angle	
Horiz distance	
Vert distance	
Angle	
Spectral period	DC
Spectral freq	0 Hz
Spectral amp	9.770 nm

Nacre 2/7/95

Cursor: fixed Zoom: 2:1 Cen line: Off Offset: Off

Cursor Marker Spectrum Zoom Center Line Offset Clear

Section Analysis

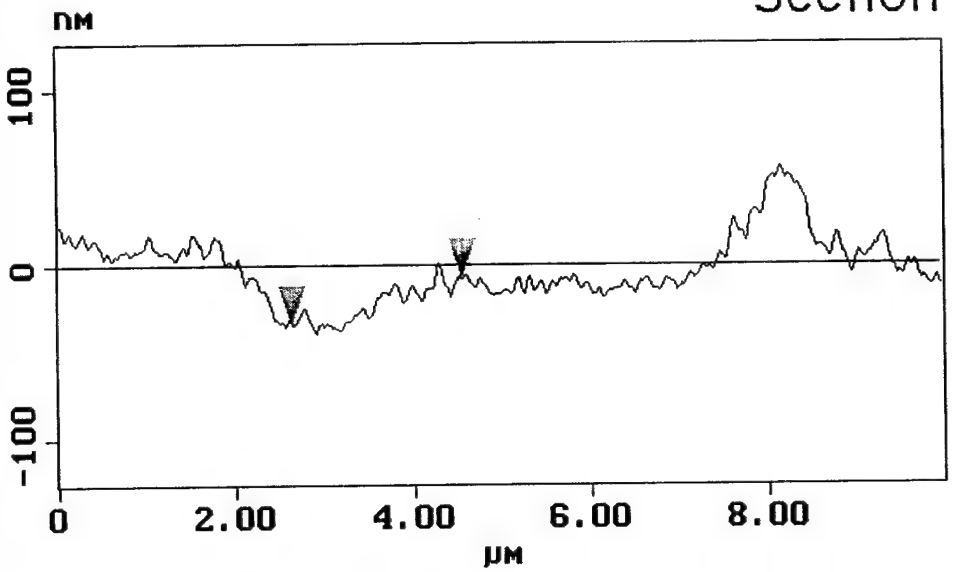

L	1.914 µm
RMS	10.155 nm
lc	DC
Ra(lc)	4.006 nm
Rmax	20.829 nm
Rz	13.839 nm
Rz Cnt	valid

Spectrum

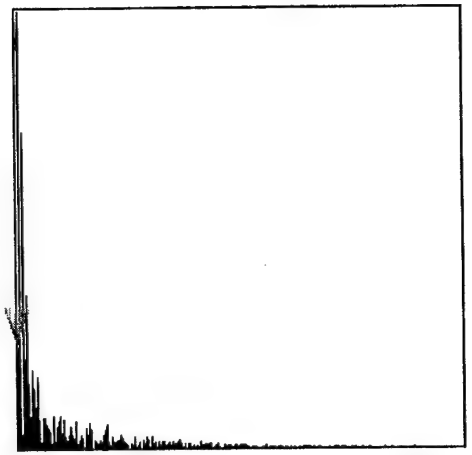

Horiz distance(L)	1.914 µm
Vert distance	26.106 nm
Angle	0.781 deg
Horiz distance	
Vert distance	
Angle	
Horiz distance	
Vert distance	
Angle	
Spectral period	DC
Spectral freq	0 Hz
Spectral amp	3.137 nm

Nacre 2/7/95

Cursor: fixed Zoom: 2:1 Cen line: Off Offset: Off

Height Angle Plane Angle Clear Calculator

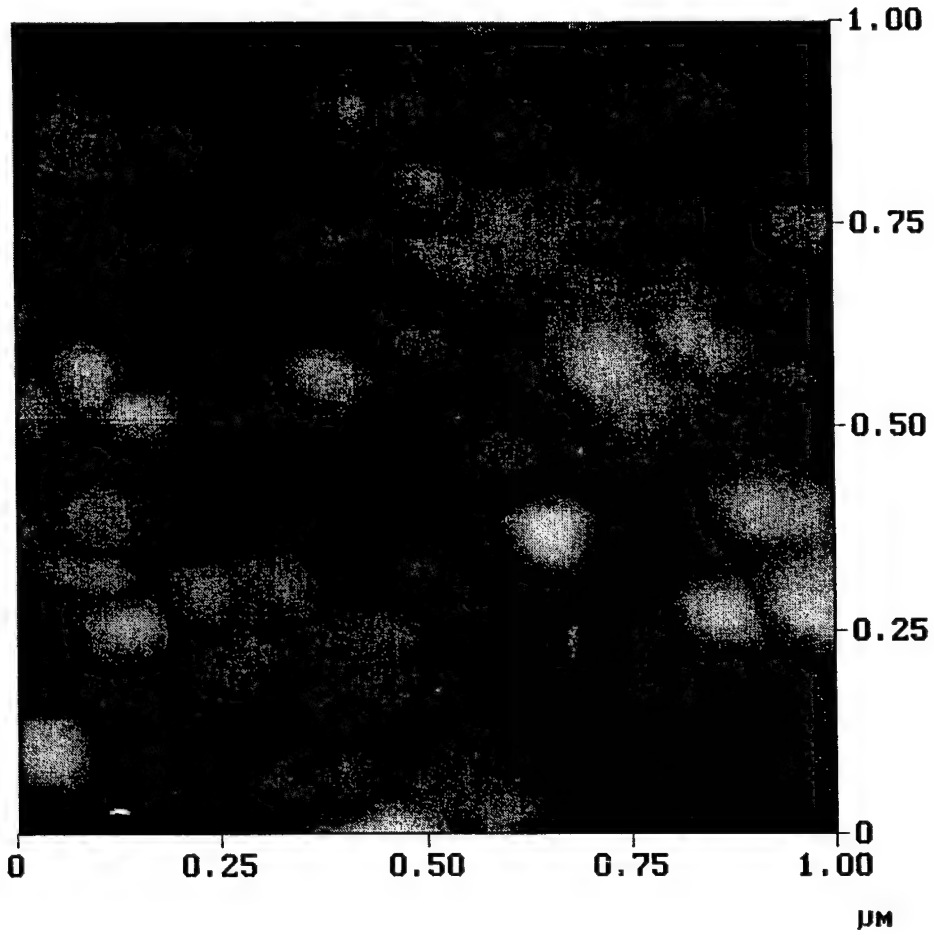

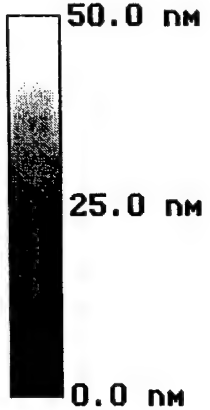

Microscope	AFM
Scan size	1.000 µm
Setpoint	0.5000 V
Scan rate	1.001 Hz
Number of samples	512

Red Abalone
nacre2.011

Height

Height Angle Plane Angle Clear Calculator

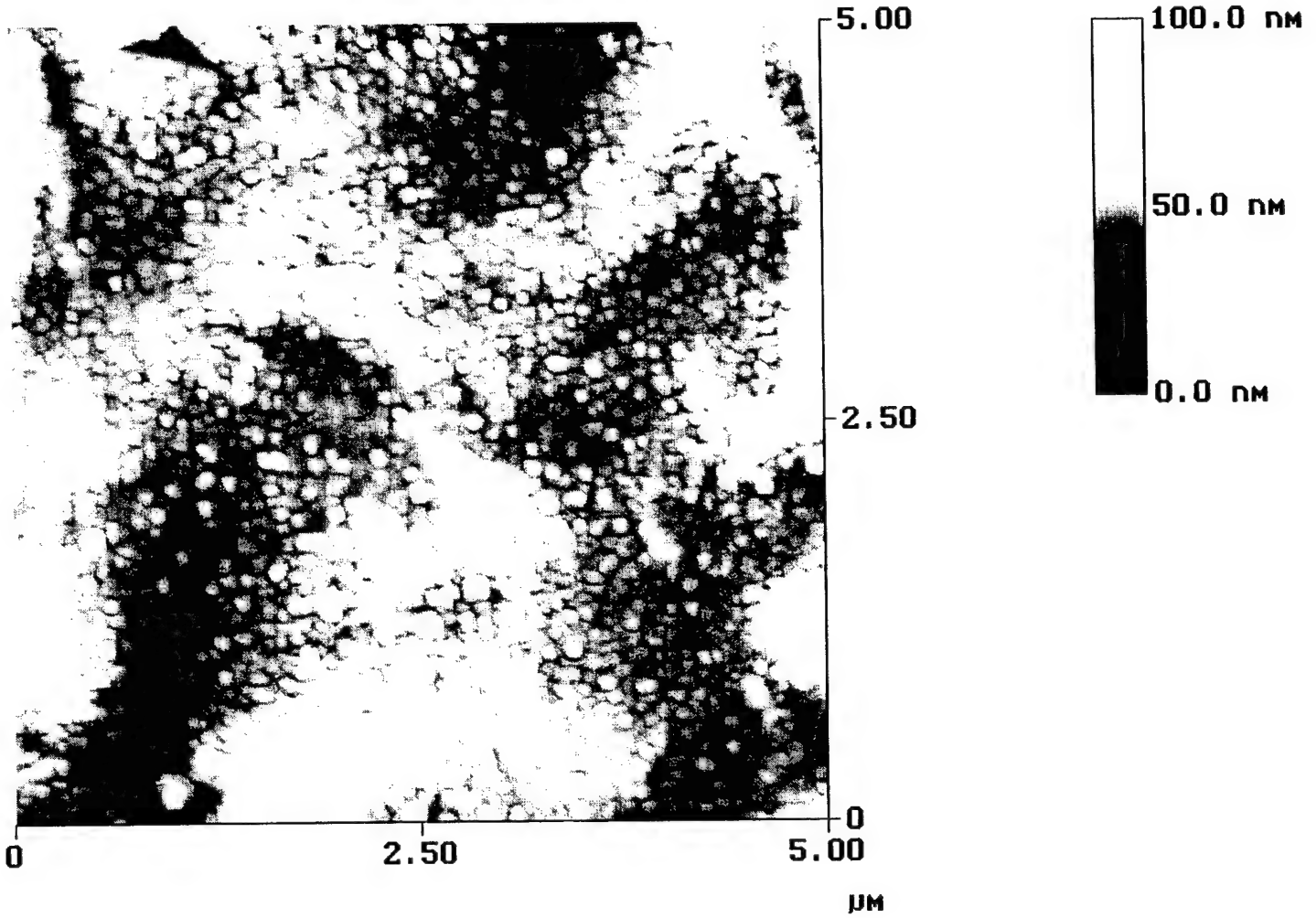

Height

Peak Surface Area Summit Zero Crossing Stopband Execute Clear

Roughness Analysis

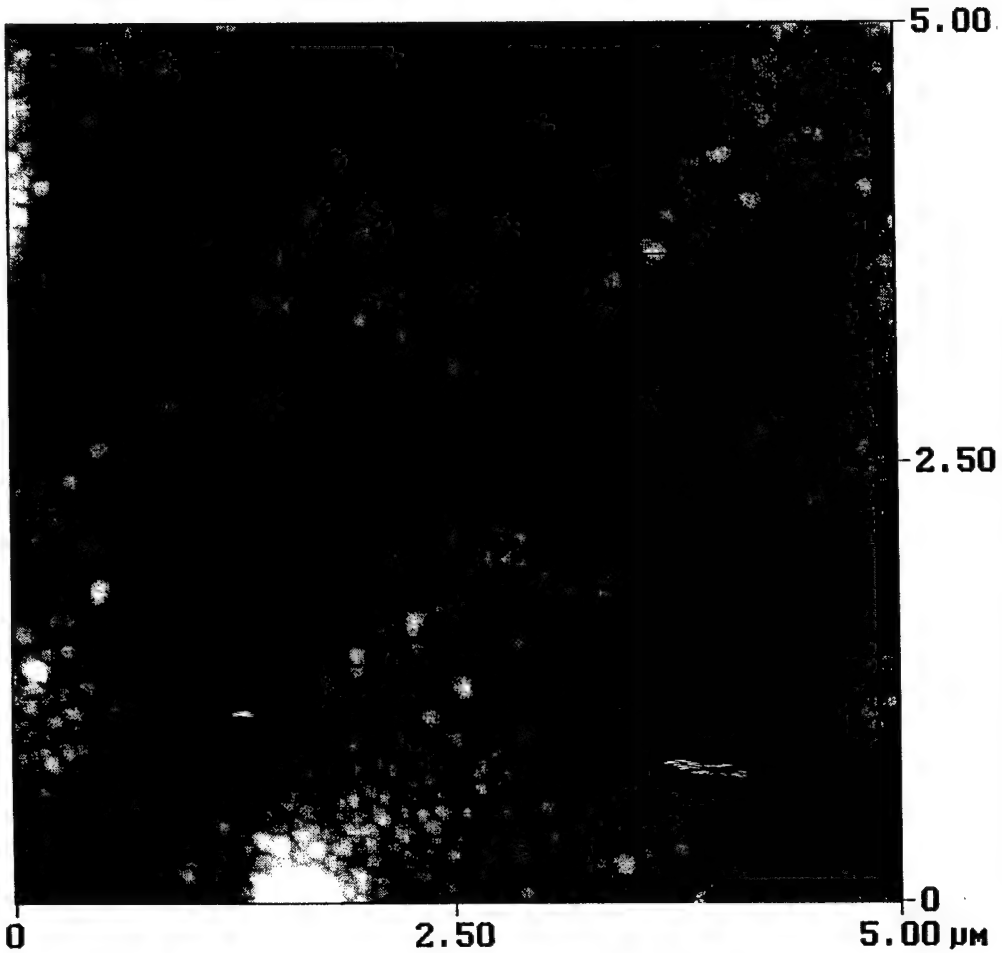

Image Statistics

Z range	109.32 nm
Mean	0.0009 nm
Rms (Rq)	9.262 nm
Mean roughness (Ra)	6.901 nm
Max height (Rmax)	109.34 nm

Box Statistics

Z range	40.593 nm
Mean	-2.980 nm
Rms (Rq)	5.708 nm
Mean roughness (Ra)	4.201 nm
Max height (Rmax)	38.643 nm
Box x dimension	1.370 µm
Box y dimension	861.06 nm

Peak off Area off Summit off Zero Cross off

Cursor Marker Spectrum Zoom Center Line Offset Clear

Section Analysis

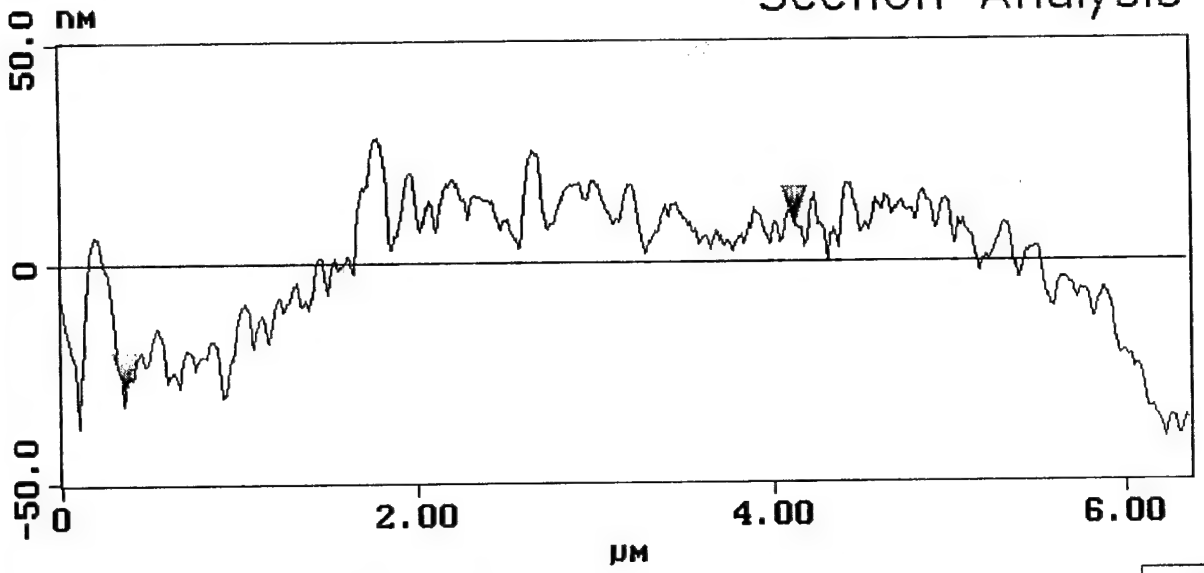

L	3.770 µm
RMS	14.278 nm
lc	DC
Ra(lc)	8.604 nm
Rmax	50.705 nm
Rz	21.187 nm
Rz Cnt	valid

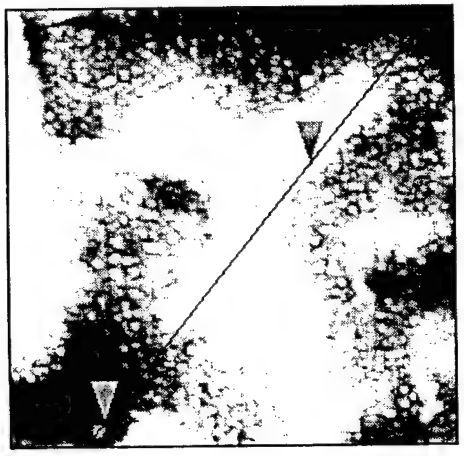

Spectrum

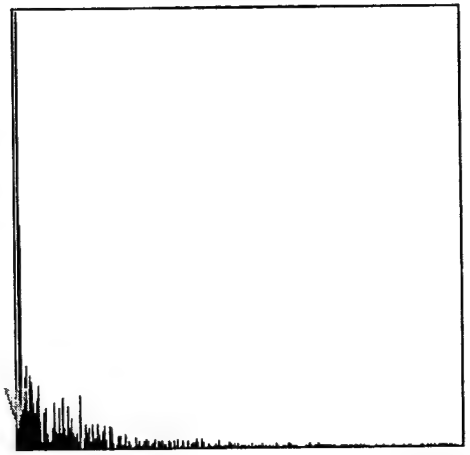

Horiz distance(L)	3.770 µm
Vert distance	36.707 nm
Angle	0.558 deg
Horiz distance	
Vert distance	
Angle	
Horiz distance	
Vert distance	
Angle	
Spectral period	DC
Spectral freq	0 Hz
Spectral amp	0.561 nm

Cursor: fixed Zoom: 2:1 Cen line: Off Offset: Off

Peak Surface Area Summit Zero Crossing Stopband Execute Clear

Roughness Analysis

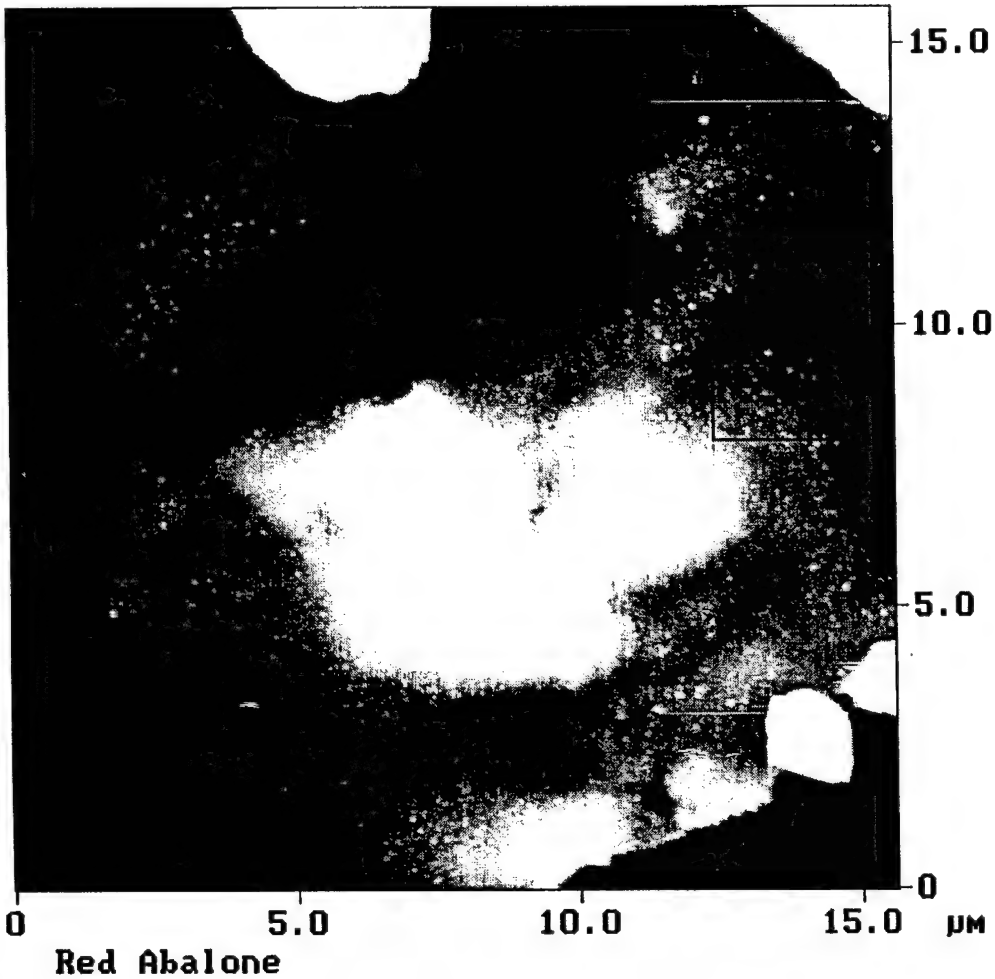

Image Statistics

Z range	1.610 µm
Mean	0.116 nm
Rms (Rq)	122.75 nm
Mean roughness (Ra)	58.850 nm
Max height (Rmax)	1.628 µm

Box Statistics

Z range	66.149 nm
Mean	20.800 nm
Rms (Rq)	10.494 nm
Mean roughness (Ra)	4.682 nm
Max height (Rmax)	47.483 nm
Box x dimension	2.512 µm
Box y dimension	1.348 µm

Peak off Area off Summit off Zero Cross off

Execute Height Clear

Grain Size Analysis

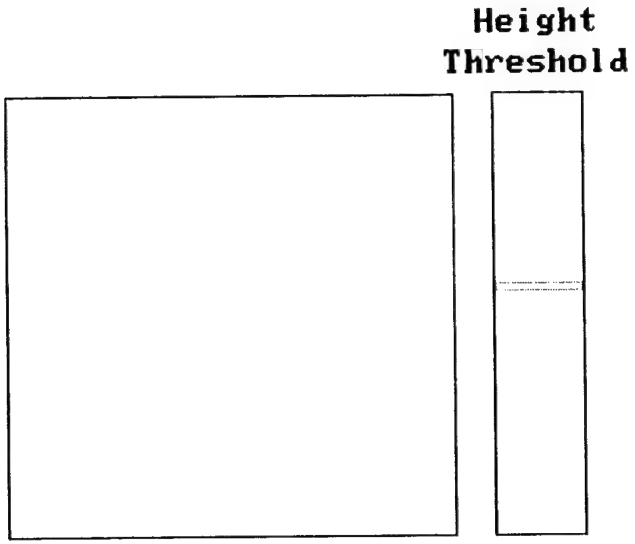

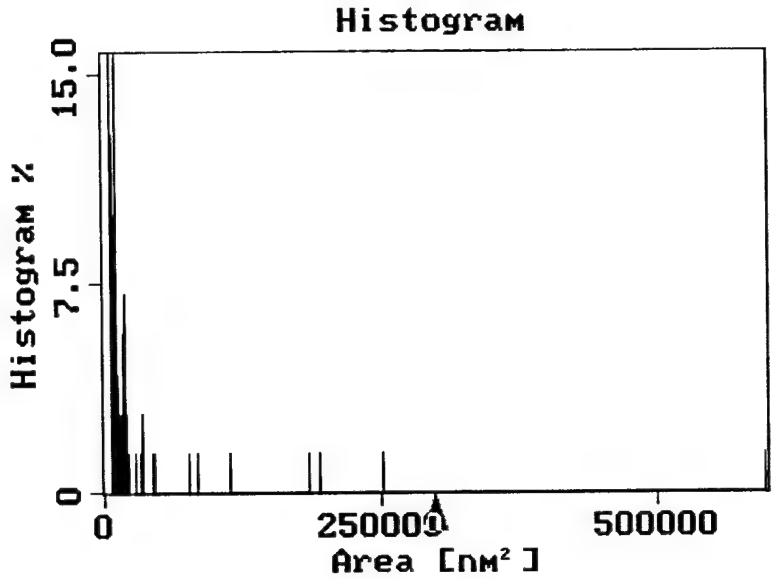

Grain size mean	3.397e+004 nm²
Grain size std dev	8.081e+004 nm²
Number of grains	70
Height threshold	10.000 nm
Grain size	2.994e+005 nm²
Histogram %	0.000
Ht threshold min	-79.398 nm
Ht threshold max	79.398 nm

Red Abalone

Slope off

Height Angle Plane Angle Clear Calculator

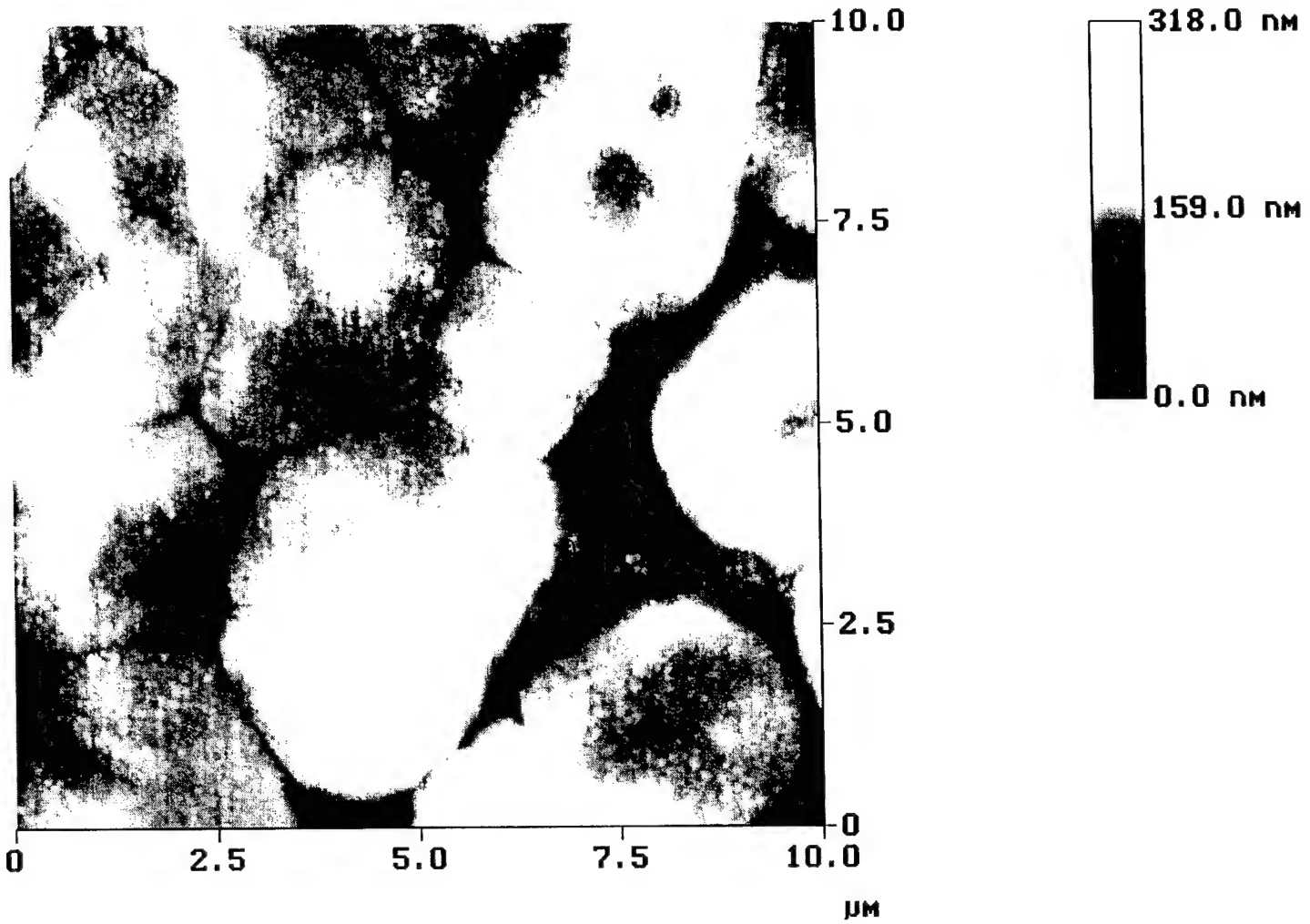

Pinctada

Height

Cursor Marker Spectrum Zoom Center Line Offset Clear

Section Analysis

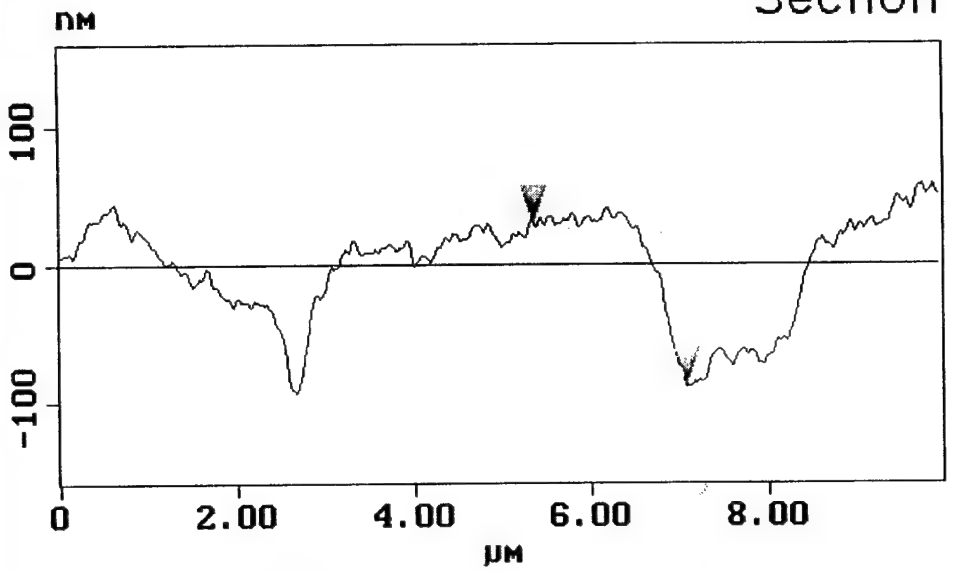

L	1.738 µm
RMS	36.125 nm
lc	DC
Ra(lc)	18.650 nm
Rmax	87.696 nm
Rz	59.795 nm
Rz Cnt	4

Spectrum

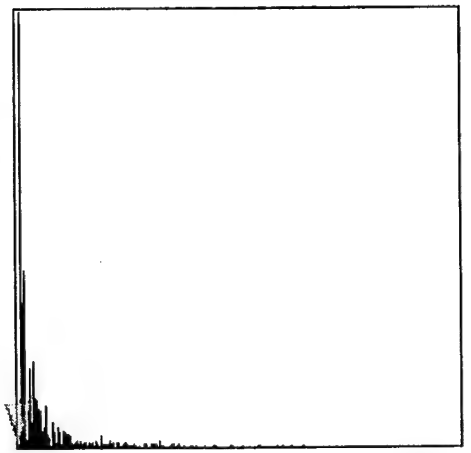

Horiz distance(L)	1.738 µm
Vert distance	118.23 nm
Angle	3.891 deg
Horiz distance	
Vert distance	
Angle	
Horiz distance	
Vert distance	
Angle	
Spectral period	DC
Spectral freq	0 Hz
Spectral amp	0.245 nm

Pinctada

Cursor: fixed Zoom: 2:1 Cen line: Off Offset: Off

Height Angle Plane Angle Clear Calculator

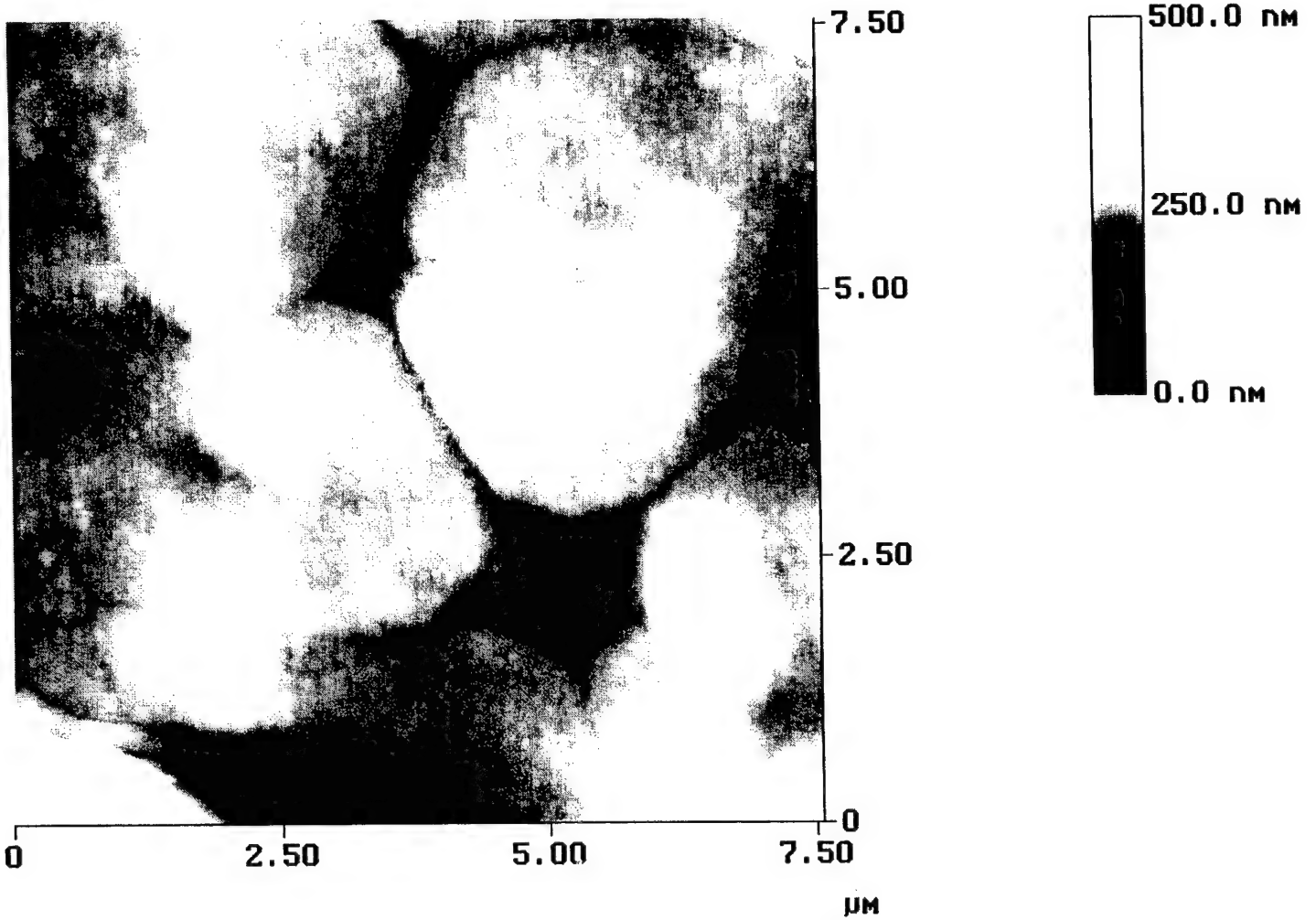

Pinctada

Height

Cursor Marker Spectrum Zoom Center Line Offset Clear

Section Analysis

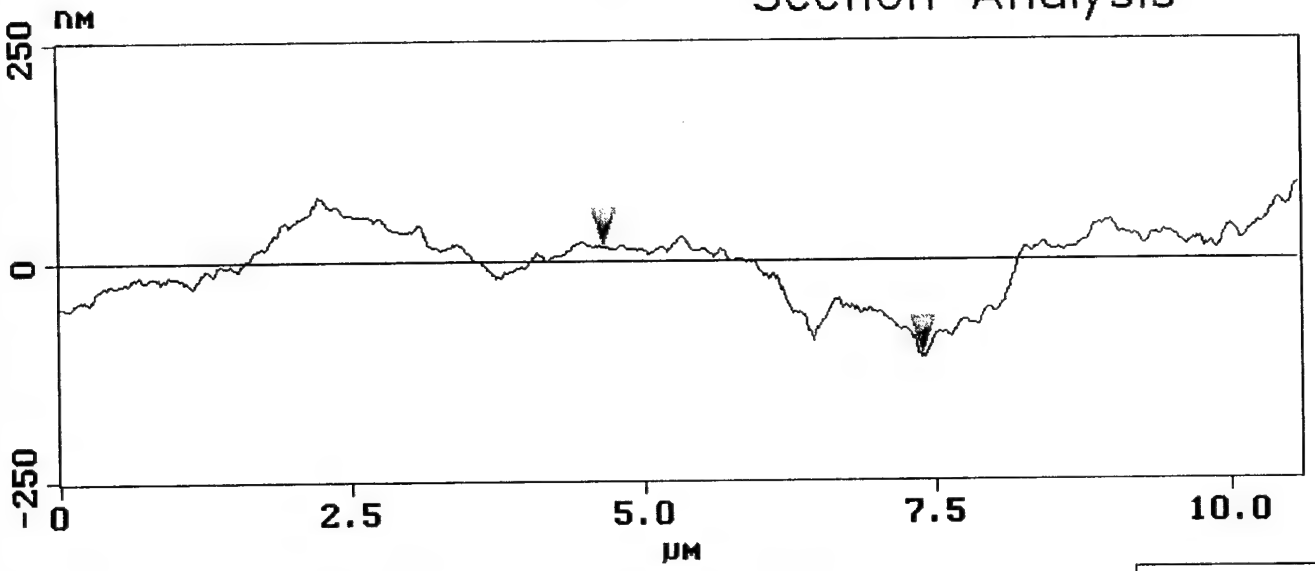

L	2.730 µm
RMS	38.883 nm
lc	DC
Ra(lc)	12.465 nm
Rmax	68.016 nm
Rz	26.455 nm
Rz Cnt	valid

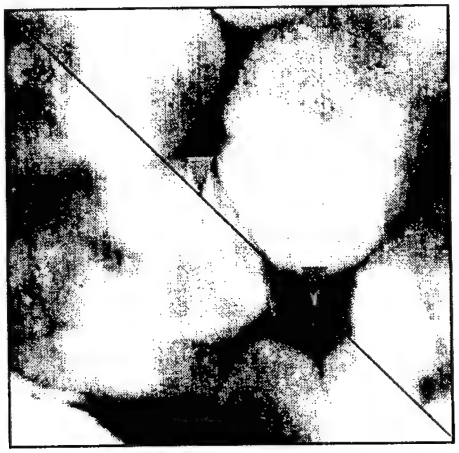

Spectrum

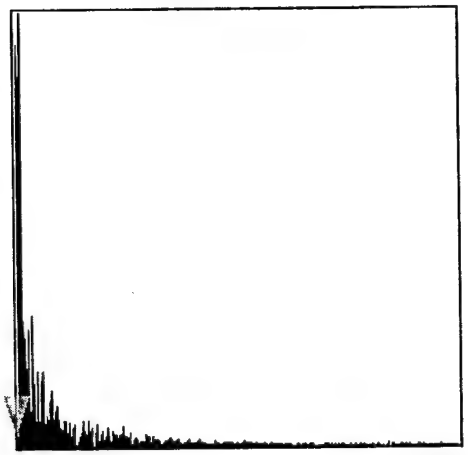

Horiz distance(L)	2.730 µm
Vert distance	125.29 nm
Angle	2.628 deg
Horiz distance	
Vert distance	
Angle	
Horiz distance	
Vert distance	
Angle	
Spectral period	DC
Spectral freq	0 Hz
Spectral amp	0.611 nm

Pinctada

Cursor: fixed Zoom: 2:1 Cen line: Off Offset: Off

Height Angle Plane Angle Clear Calculator

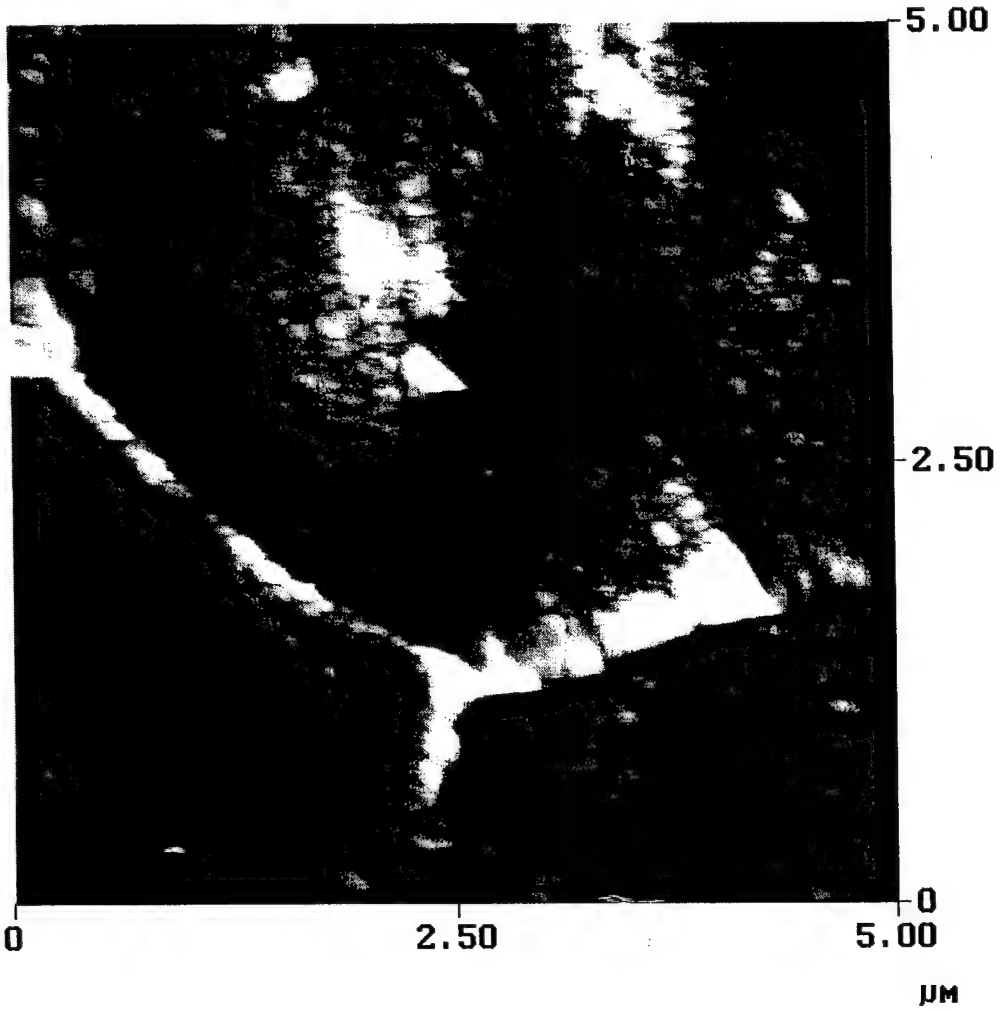

Pinctada

Height

Peak Surface Area Summit Zero Crossing Stopband Execute Clear

Roughness Analysis

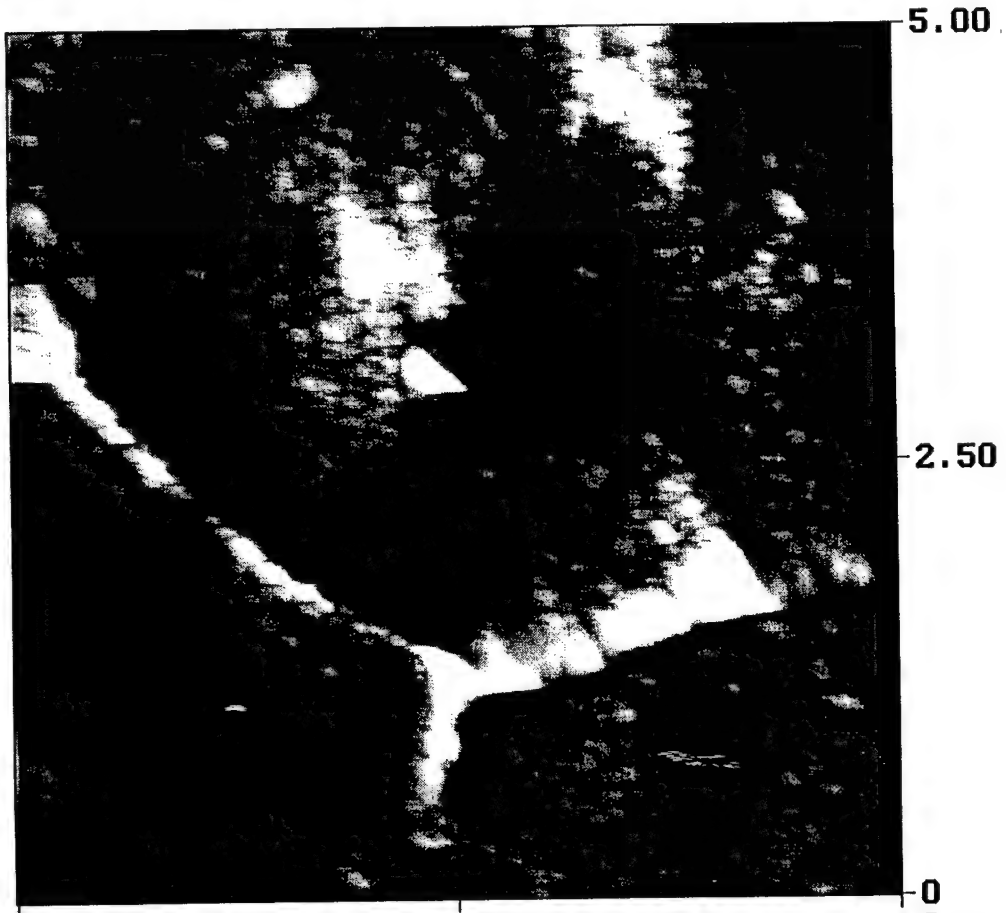

Image Statistics

Z range	807.36 nm
Mean	0.131 nm
Rms (Rq)	97.374 nm
Mean roughness (Ra)	73.426 nm
Max height (Rmax)	815.37 nm

Box Statistics

Z range	
Mean	
Rms (Rq)	
Mean roughness (Ra)	
Max height (Rmax)	
Box x dimension	
Box y dimension	

Peak off Area off Summit off Zero Cross off

Cursor Marker Spectrum Zoom Center Line Offset Clear

Section Analysis

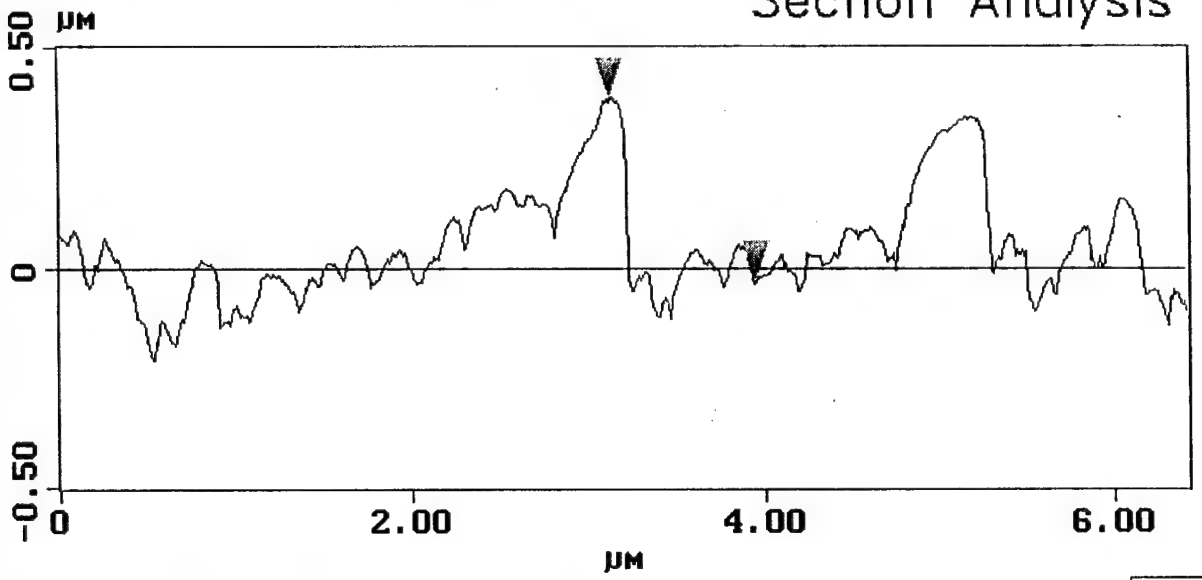

L	810.55 nm
RMS	124.65 nm
lc	DC
Ra(lc)	84.005 nm
Rmax	448.99 nm
Rz	279.68 nm
Rz Cnt	4

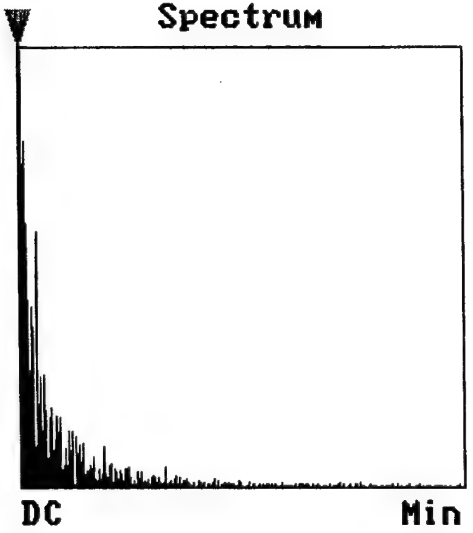

Horiz distance(L)	810.55 nm
Vert distance	415.74 nm
Angle	27.154 deg
Horiz distance	
Vert distance	
Angle	
Horiz distance	
Vert distance	
Angle	
Spectral period	DC
Spectral freq	0 Hz
Spectral amp	69.290 µm

Pinctada

Cursor: fixed Zoom: 2:1 Cen line: Off Offset: Off

Execute Height Clear

Grain Size Analysis

Height Threshold

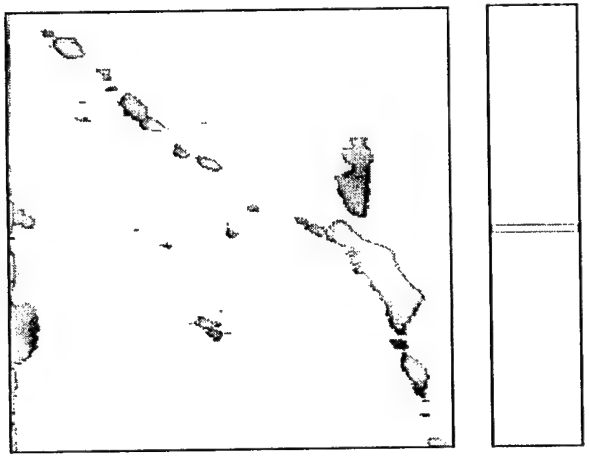

Histogram

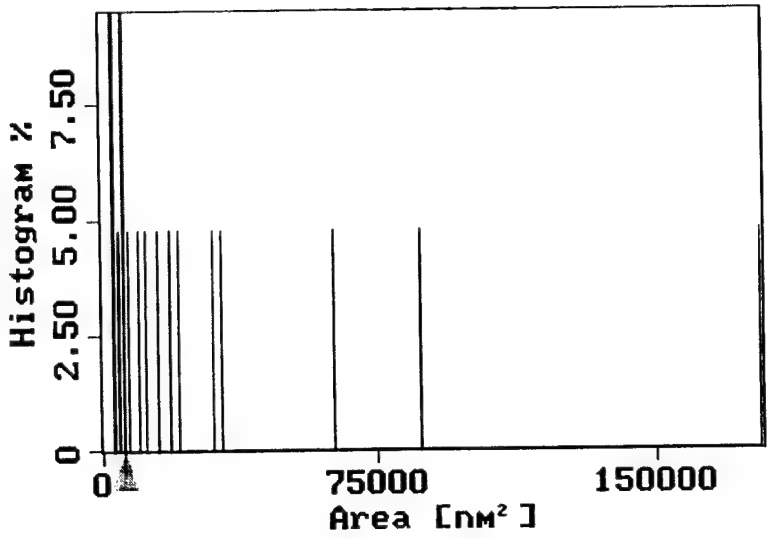

Grain size mean	2.466e+004 nm²
Grain size std dev	4.029e+004 nm²
Number of grains	21
Height threshold	-6.241 µm
Grain size	6.097e+003 nm²
Histogram %	9.524
Ht threshold min	-399.438 µm
Ht threshold max	399.44 µm

Pinctada

Slope off

Height Angle Plane Angle Clear Calculator

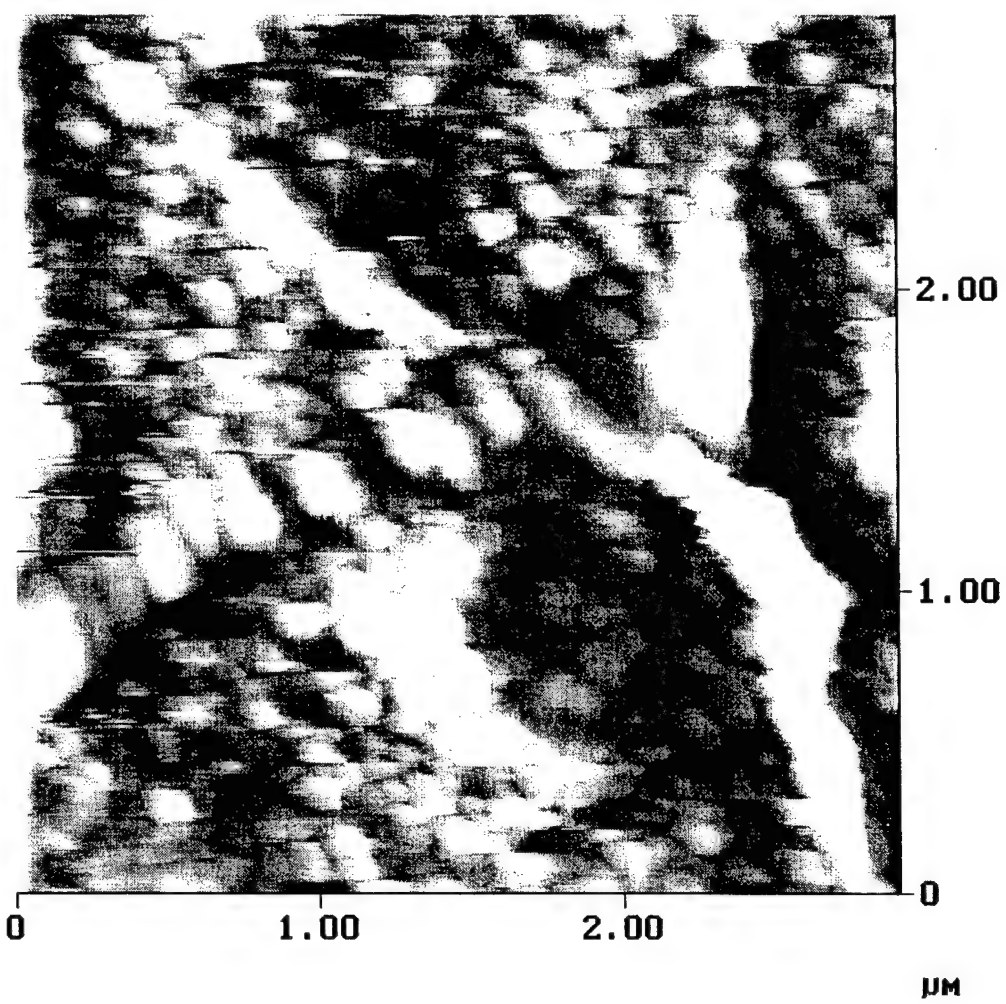

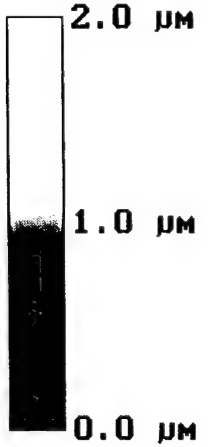

Microscope	AFM
Scan size	2.916 µm
Setpoint	0 V
Scan rate	2.654 Hz
Number of samples	512

Organic intercrystalline matrix in Pinctada
pinc.009

Height

Cursor Marker Spectrum Zoom Center Line Offset Clear

Section Analysis

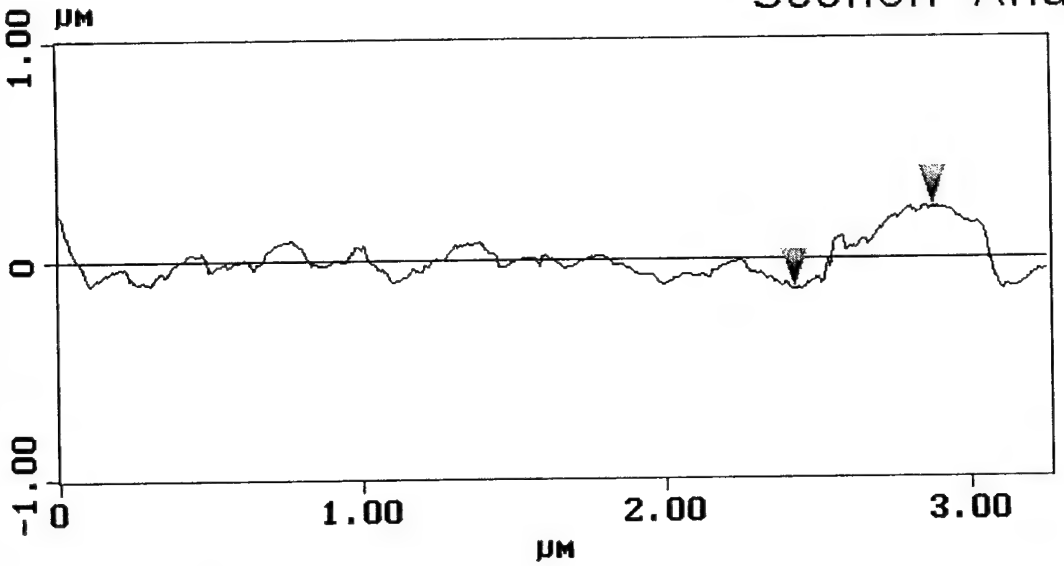

L	455.60 nm
RMS	124.22 nm
lc	DC
Ra(lc)	26.337 nm
Rmax	164.55 nm
Rz	79.368 nm
Rz Cnt	8

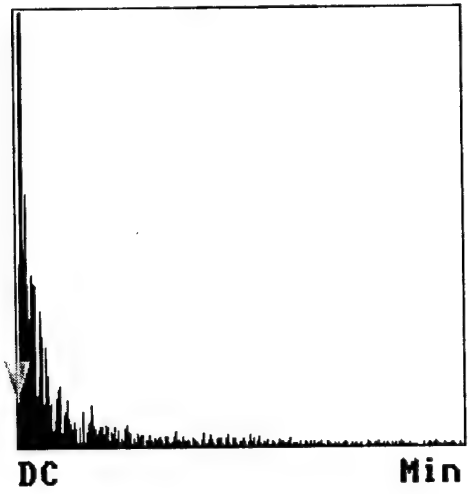

Horiz distance(L)	455.60 nm
Vert distance	373.47 nm
Angle	39.343 deg
Horiz distance	
Vert distance	
Angle	
Horiz distance	
Vert distance	
Angle	
Spectral period	DC
Spectral freq	0 Hz
Spectral amp	4.779 µm

Organic intercrystalline matrix in Pinctada

Cursor: fixed Zoom: 2:1 Cen line: Off Offset: Off

Peak Surface Area Summit Zero Crossing Stopband Execute Clear

Roughness Analysis

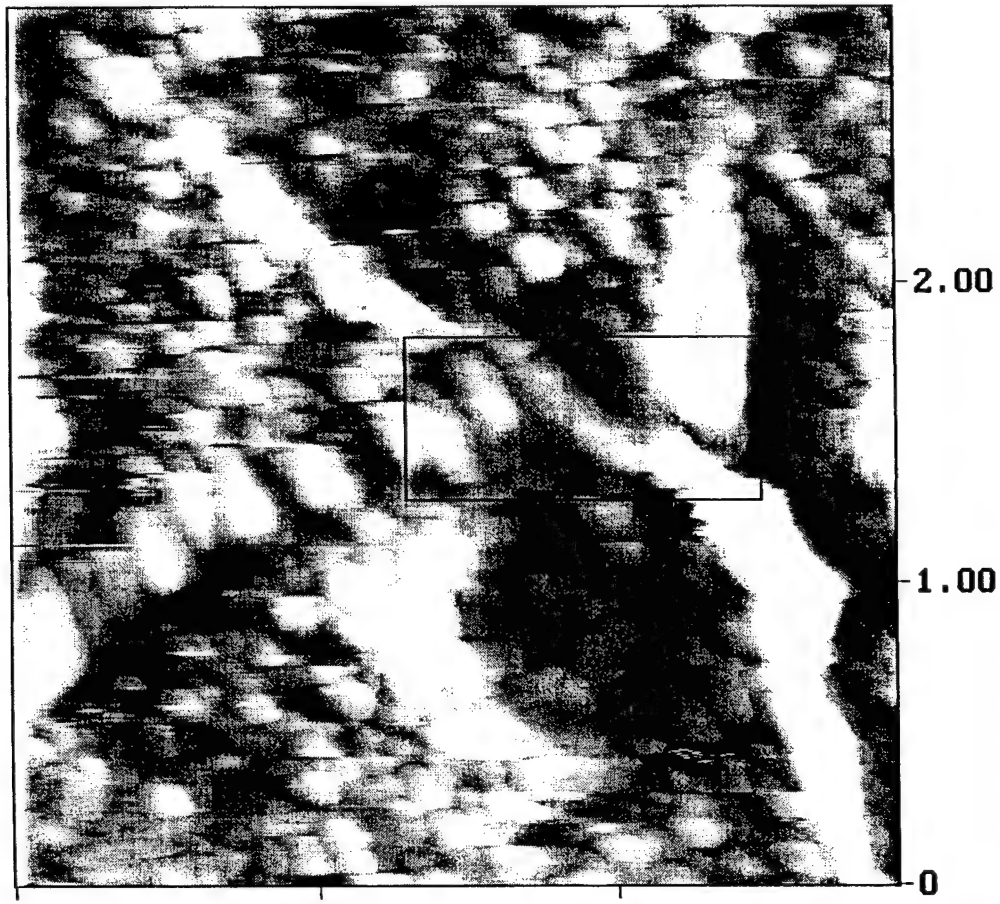

Organic intercrystalline matrix in Pinctada

Image Statistics

Z range	637.25 nm
Mean	0.003 nm
Rms (Rq)	78.349 nm
Mean roughness (Ra)	61.216 nm
Max height (Rmax)	637.09 nm

Box Statistics

Z range	617.02 nm
Mean	13.143 nm
Rms (Rq)	85.700 nm
Mean roughness (Ra)	63.656 nm
Max height (Rmax)	627.58 nm
Box x dimension	1.175 µm
Box y dimension	542.09 nm

Peak off Area off Summit off Zero Cross off

Height Angle Plane Angle Clear Calculator

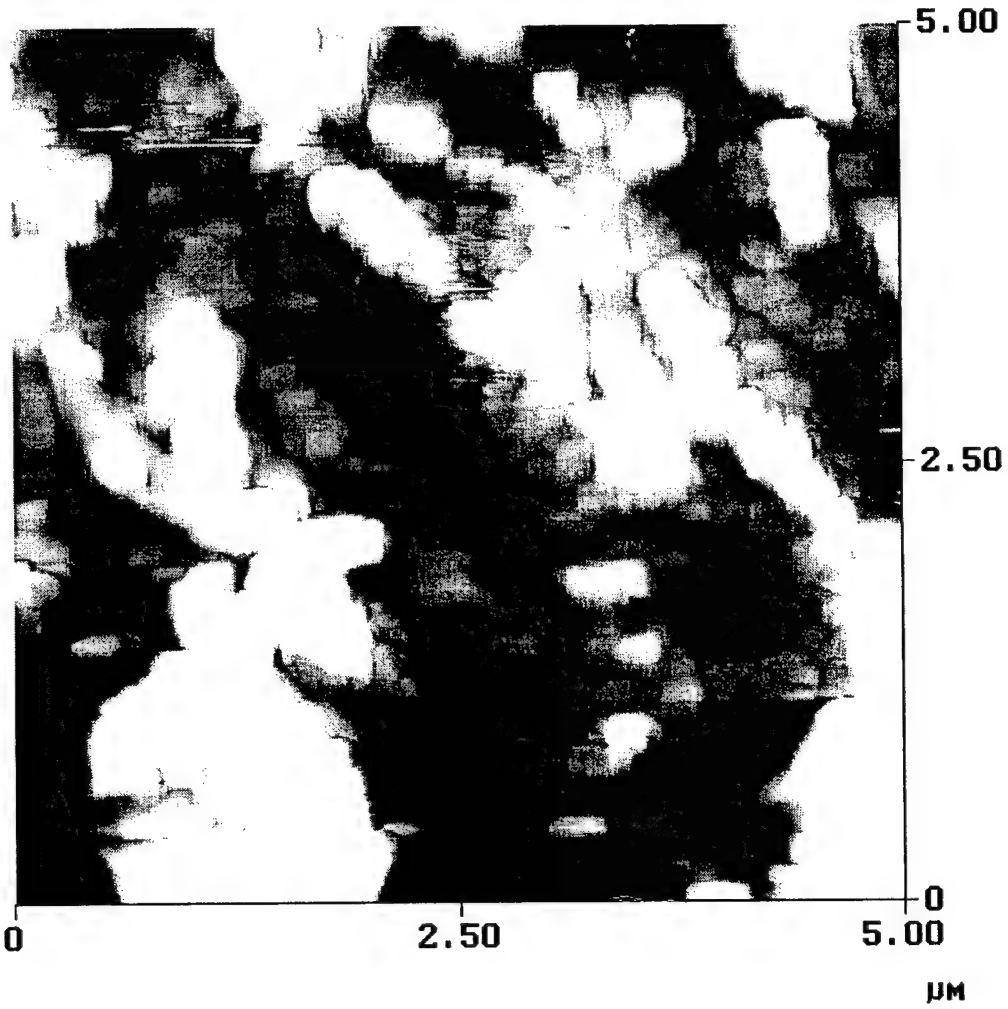

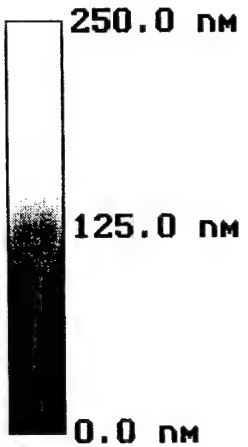

Nautilus

Height

Peak Surface Area Summit Zero Crossing Stopband Execute Clear

Roughness Analysis

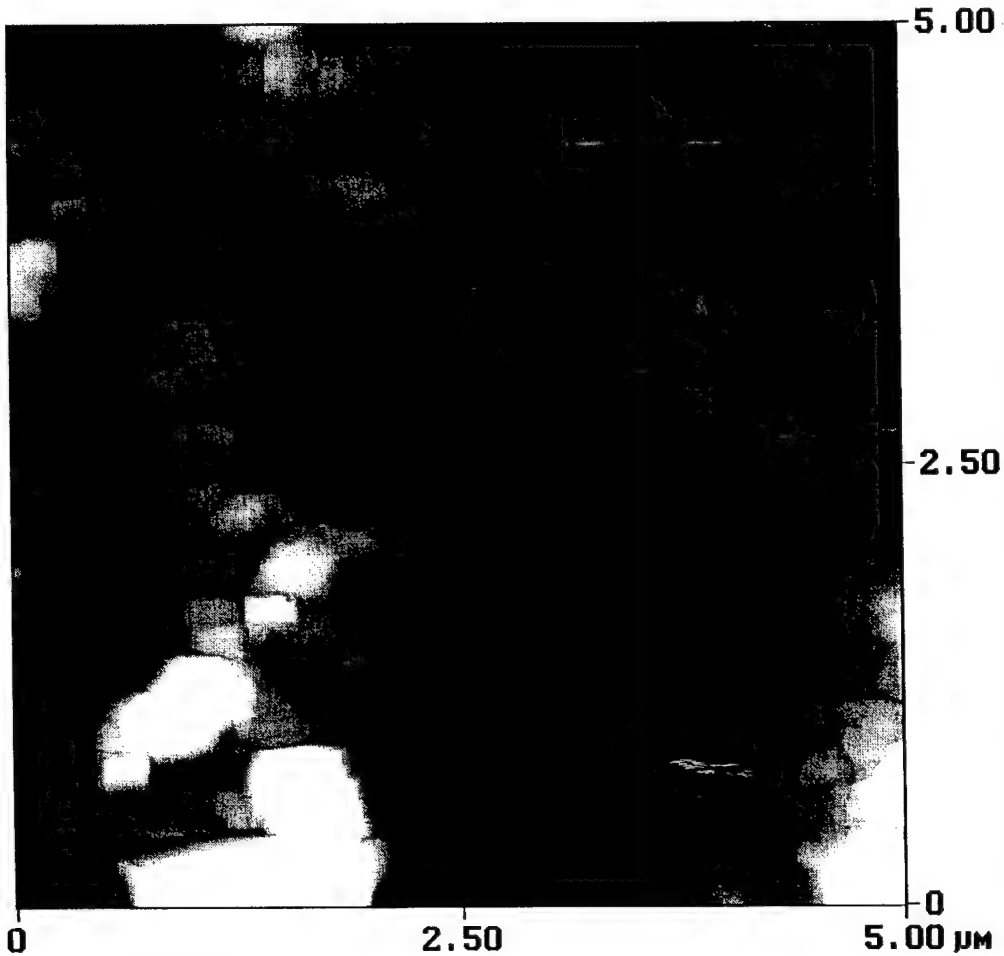

Image Statistics

Z range	1.172 µm
Mean	-0.009 nm
Rms (Rq)	77.662 nm
Mean roughness (Ra)	49.463 nm
Max height (Rmax)	1.172 µm

Box Statistics

Z range	93.023 nm
Mean	6.686 nm
Rms (Rq)	20.570 nm
Mean roughness (Ra)	11.652 nm
Max height (Rmax)	67.634 nm
Box x dimension	1.125 µm
Box y dimension	606.65 nm

Peak off Area off Summit off Zero Cross off

Cursor Marker Spectrum Zoom Center Line Offset Clear

Section Analysis

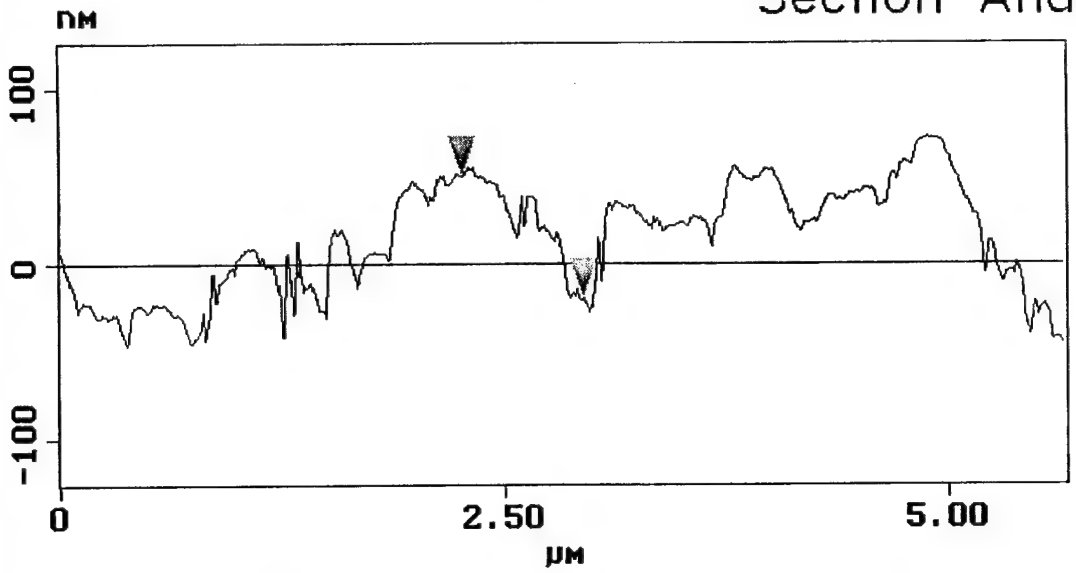

L	683.59 nm
RMS	23.031 nm
lc	DC
Ra(lc)	6.993 nm
Rmax	34.784 nm
Rz	20.678 nm
Rz Cnt	8

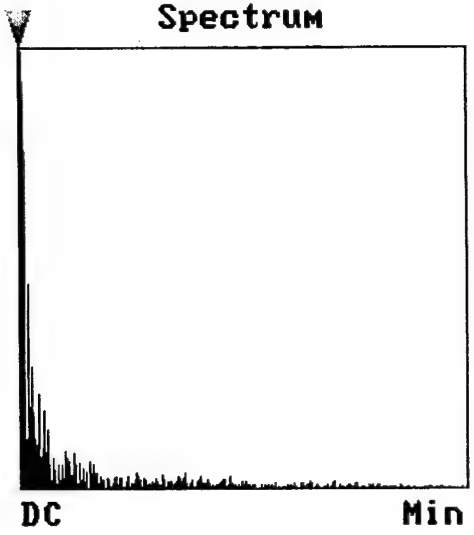

Horiz distance(L)	683.59 nm
Vert distance	69.629 nm
Angle	5.816 deg
Horiz distance	
Vert distance	
Angle	
Horiz distance	
Vert distance	
Angle	
Spectral period	DC
Spectral freq	0 Hz
Spectral amp	0.021 nm

Nautilus

Cursor: fixed Zoom: 2:1 Cen line: Off Offset: Off

Peak | Surface Area | Summit | Zero Crossing | Stopband | Execute | Clear

Roughness Analysis

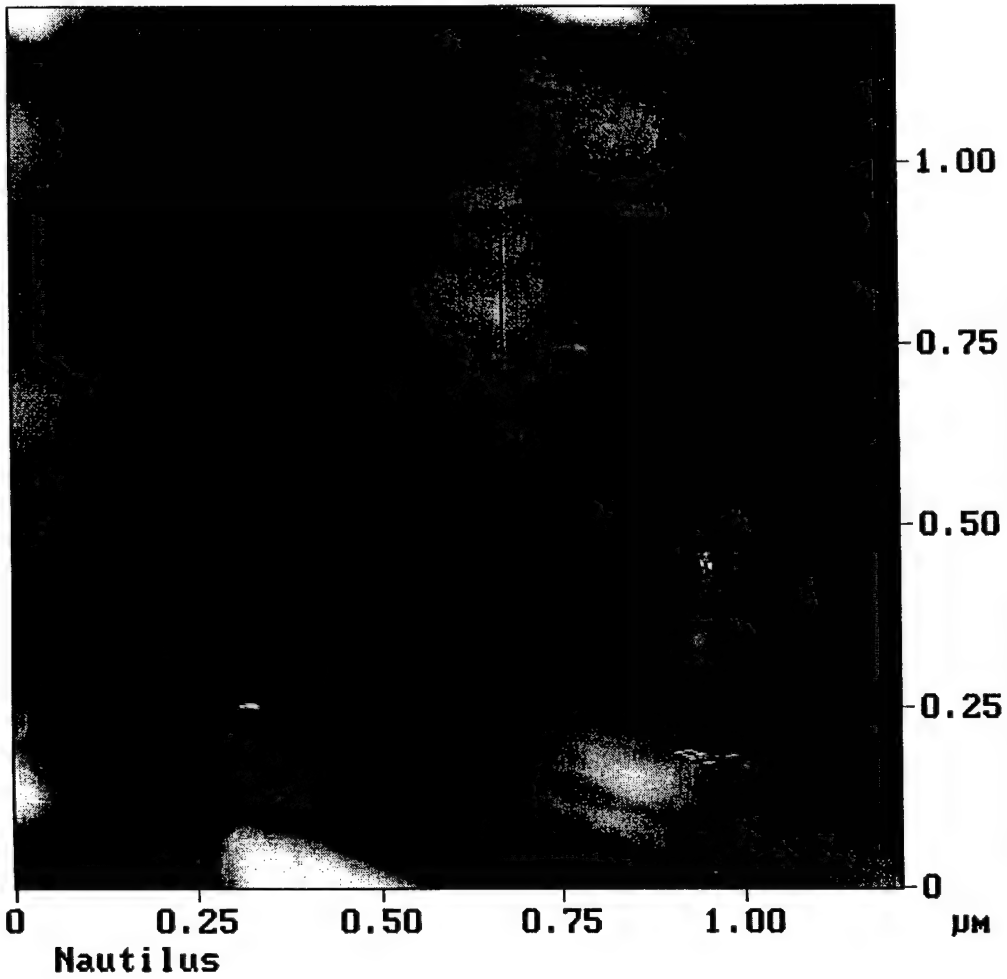

Image Statistics

Z range	94.808 nm
Mean	-0.000002 nm
Rms (Rq)	10.074 nm
Mean roughness (Ra)	7.761 nm
Max height (Rmax)	94.808 nm

Box Statistics

Z range	45.782 nm
Mean	0.480 nm
Rms (Rq)	9.050 nm
Mean roughness (Ra)	6.600 nm
Max height (Rmax)	40.066 nm
Box x dimension	391.77 nm
Box y dimension	227.94 nm

Peak off | Area off | Summit off | Zero Cross off

Execute Height Clear

Grain Size Analysis

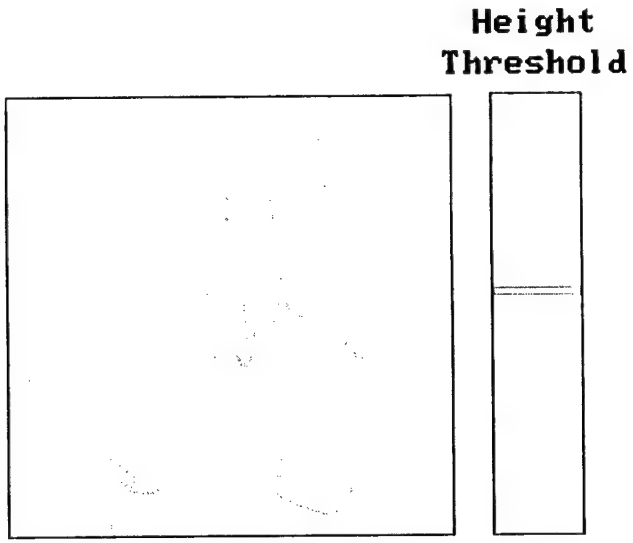

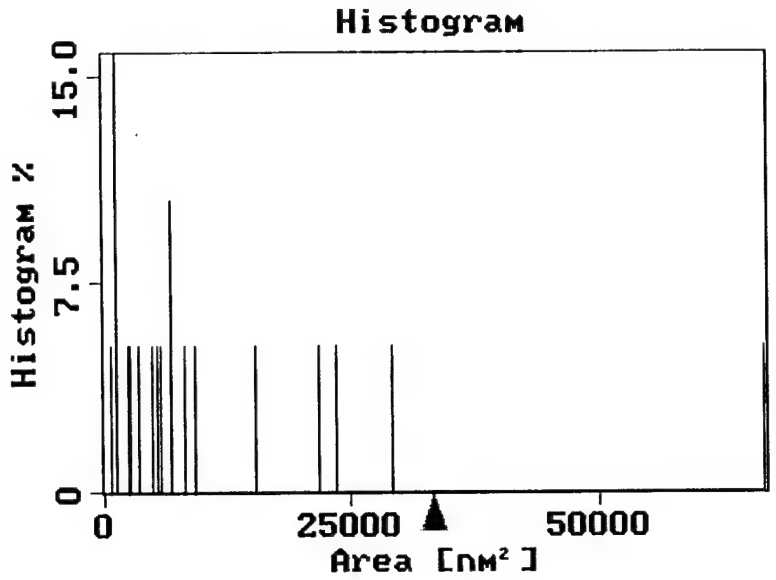

Grain size mean	1.140e+004 nm²
Grain size std dev	1.531e+004 nm²
Number of grains	19
Height threshold	9.998 nm
Grain size	3.335e+004 nm²
Histogram %	0.000
Ht threshold min	-93.925 nm
Ht threshold max	93.925 nm

Nautilus

Slope off

Height Angle Plane Angle Clear Calculator

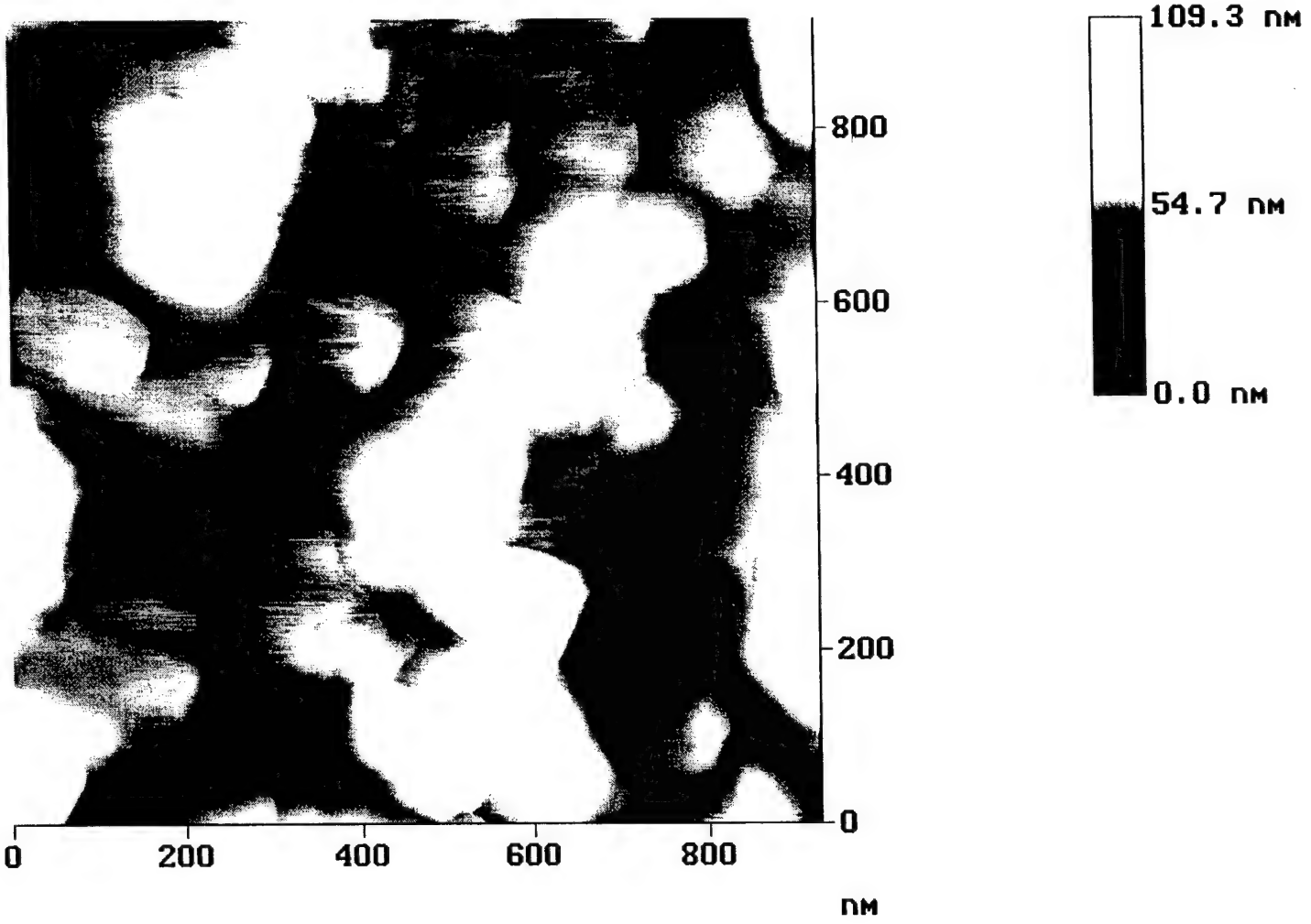

Nautilus

Height

Peak Surface Area Summit Zero Crossing Stopband Execute Clear

Roughness Analysis

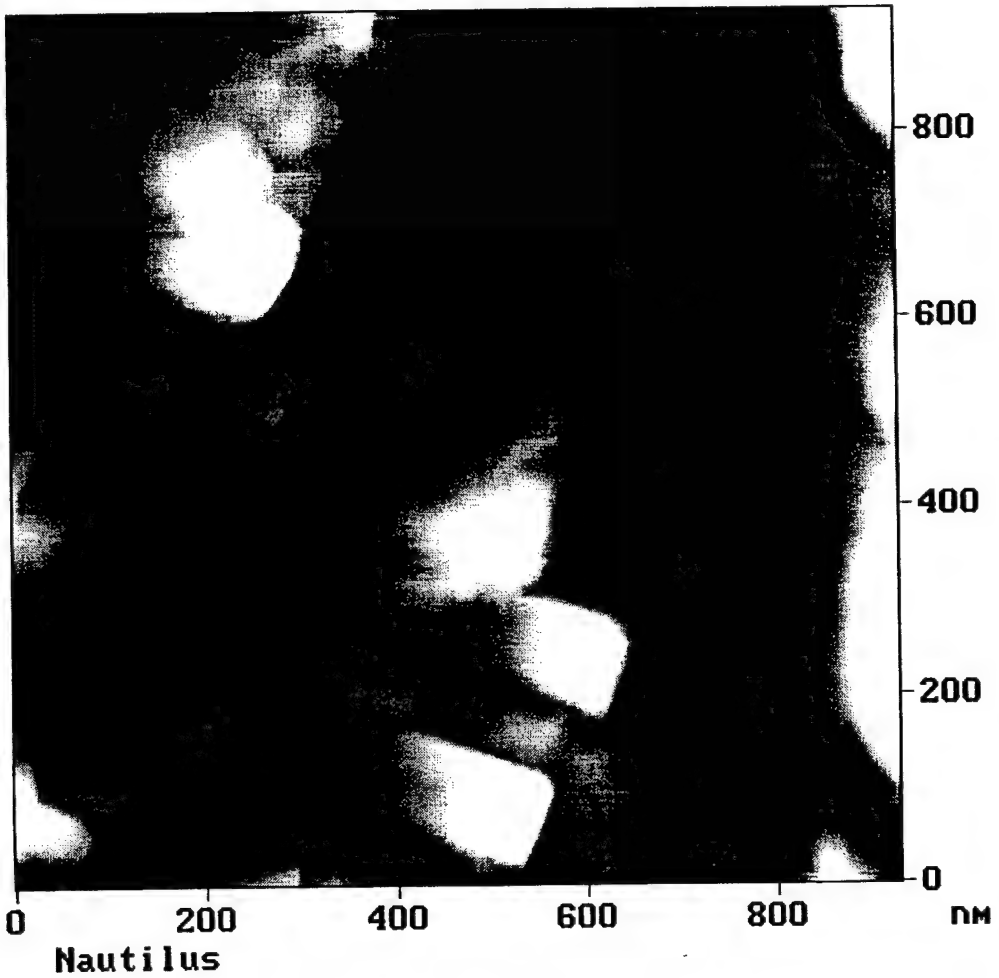

Image Statistics

Z range	60.181 nm
Mean	0.000000 nm
Rms (Rq)	9.041 nm
Mean roughness (Ra)	7.001 nm
Max height (Rmax)	60.181 nm

Box Statistics

Z range	21.262 nm
Mean	-1.766 nm
Rms (Rq)	3.830 nm
Mean roughness (Ra)	2.307 nm
Max height (Rmax)	16.837 nm
Box x dimension	259.91 nm
Box y dimension	183.57 nm

Peak off Area off Summit off Zero Cross off

Cursor Marker Spectrum Zoom Center Line Offset Clear

Section Analysis

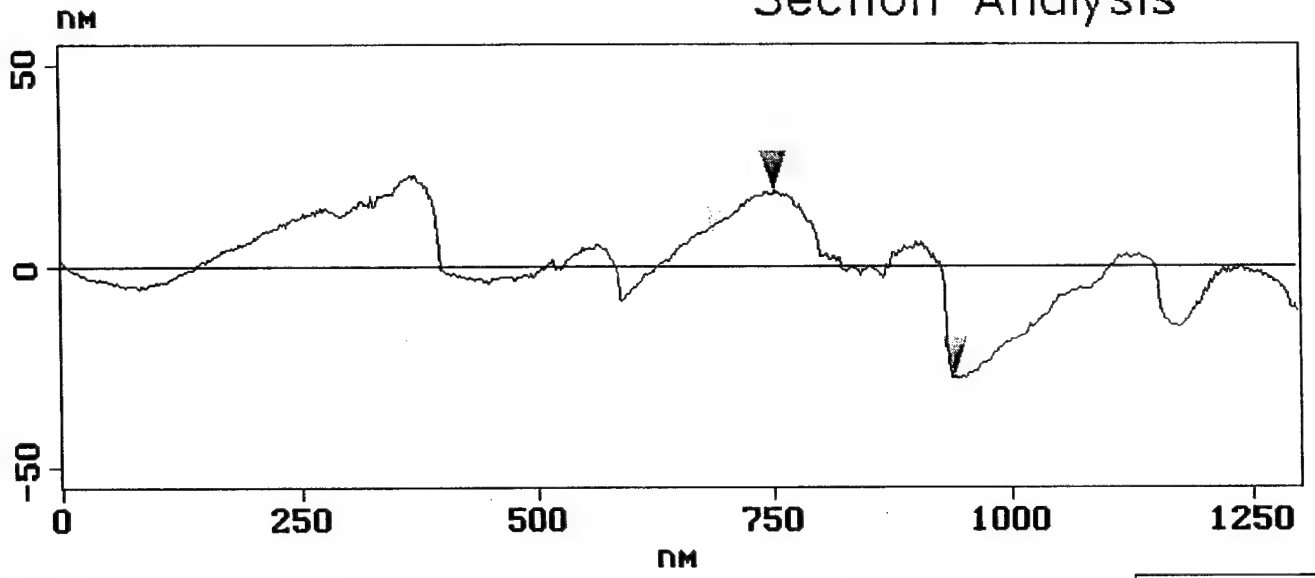

L	188.65 nm
RMS	9.253 nm
lc	DC
Ra(lc)	5.411 nm
Rmax	29.513 nm
Rz	20.749 nm
Rz Cnt	4

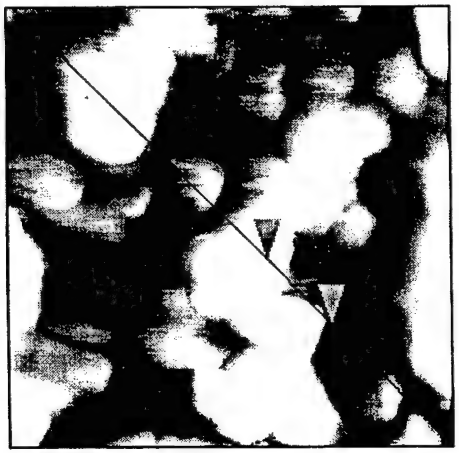

Spectrum

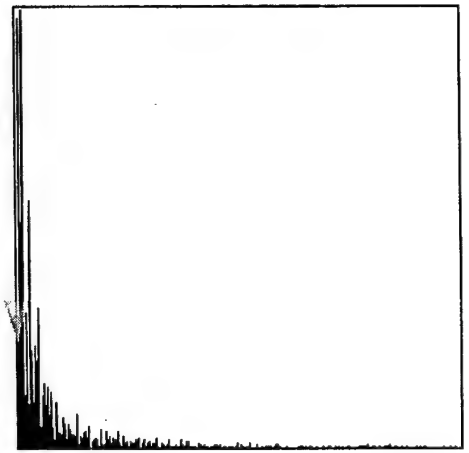

DC Min

Horiz distance(L)	188.65 nm
Vert distance	46.058 nm
Angle	13.720 deg
Horiz distance	
Vert distance	
Angle	
Horiz distance	
Vert distance	
Angle	
Spectral period	DC
Spectral freq	0 Hz
Spectral amp	1.420 nm

Nautilus

Cursor: fixed Zoom: 2:1 Cen line: Off Offset: Off

Height Angle Plane Angle Clear Calculator

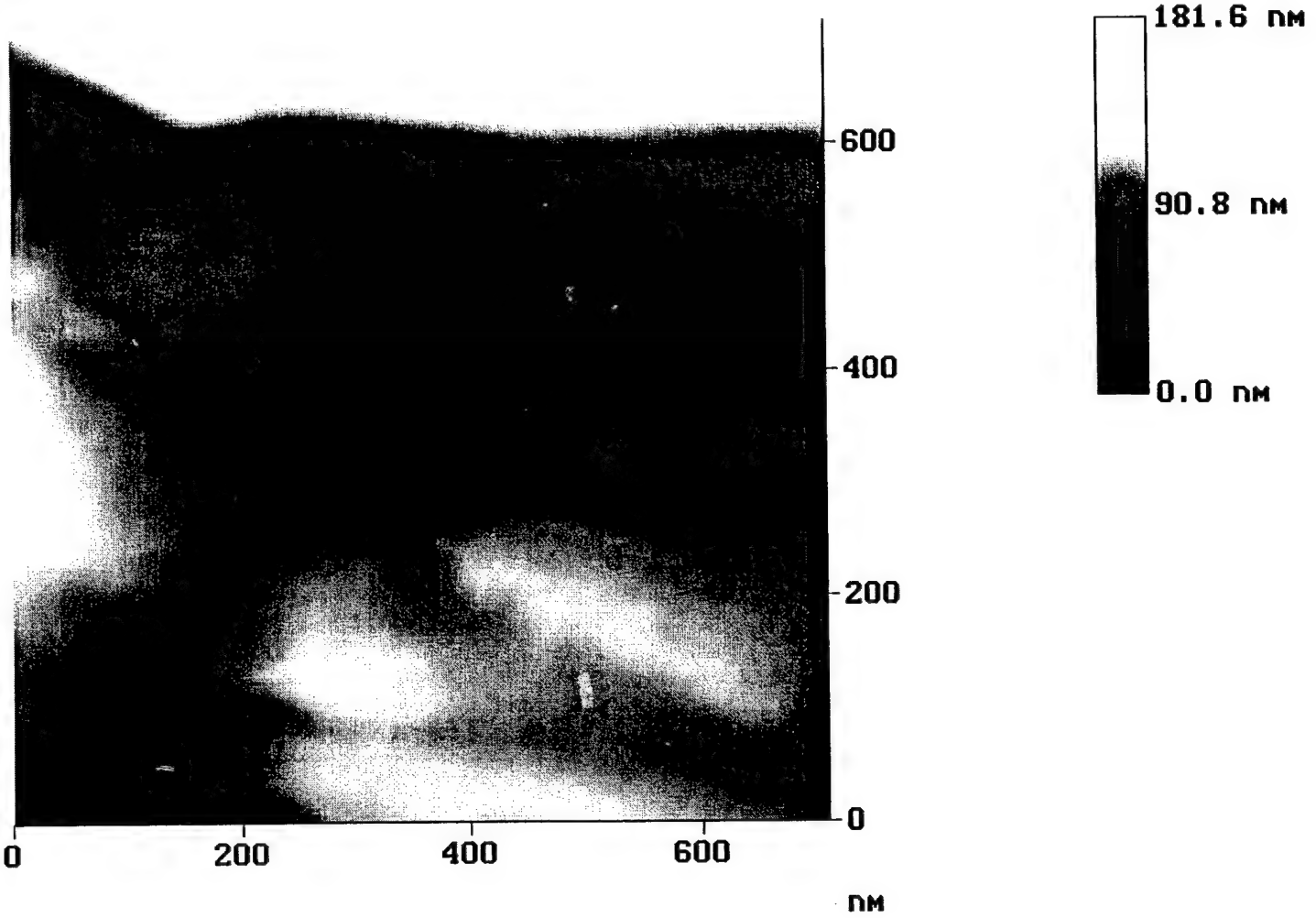

Nautilus

Height

Cursor Marker Spectrum Zoom Center Line Offset Clear

Section Analysis

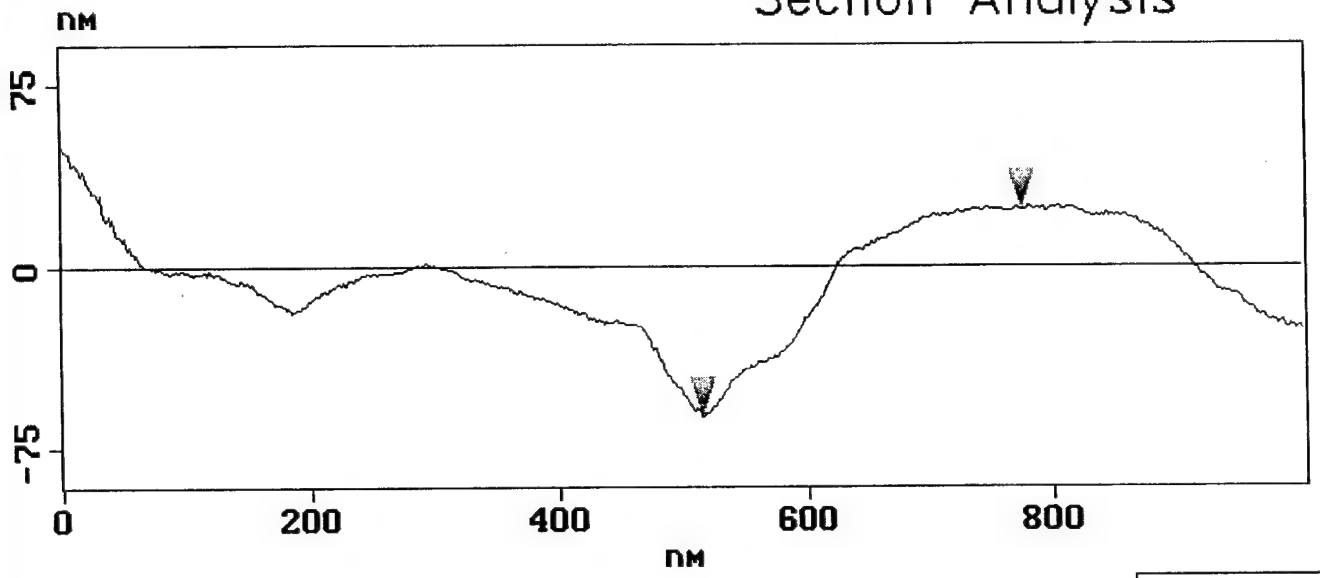

L	262.05 nm
RMS	28.361 nm
lc	DC
Ra(lc)	7.380 nm
Rmax	33.427 nm
Rz	32.846 nm
Rz Cnt	2

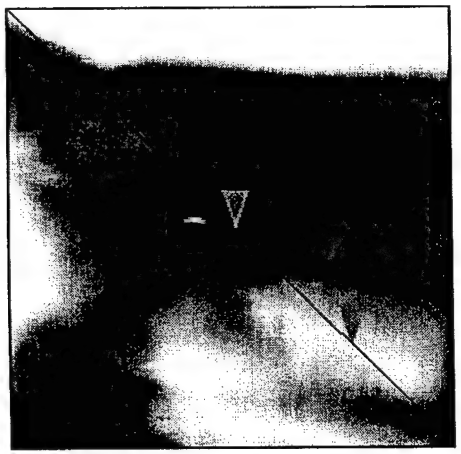

Spectrum

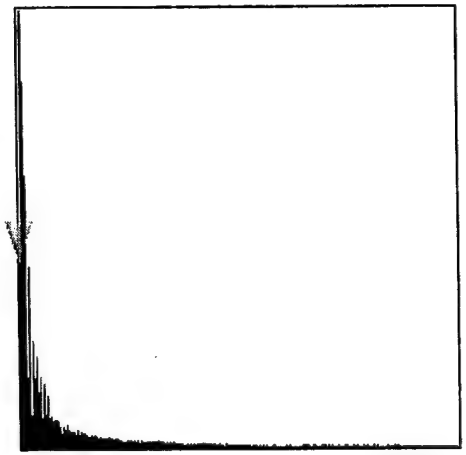

DC Min

Horiz distance(L)	262.05 nm
Vert distance	85.394 nm
Angle	18.049 deg
Horiz distance	
Vert distance	
Angle	
Horiz distance	
Vert distance	
Angle	
Spectral period	DC
Spectral freq	0 Hz
Spectral amp	5.793 nm

Nautilus

Cursor: fixed Zoom: 2:1 Cen line: Off Offset: Off

Prismatic-Nacreous Interface in Red Abalone Shell: A Crystallographic and Morphological Investigation by TEM

D.W. Frech and M. Sarikaya
University of Washington
Department of Materials Sciences and Engineering

Abstract

The transition region between the prismatic and nacreous regions in red *ablaone (Haliotis rufescens*) has been investigated by transmission electron microscopy imaging and electron diffraction. The goal of this study was to obtain a better insight into the microstructural properties of the interface. The interface region is where morphologically and mineralogically dissimilar phases of $CaCO_3$ meet, *i.e.*, on the outside of the shell, there exist columnar grains of calcite and on the inside, the layered platelets of aragonite, constituting, respectively, prismatic and nacreous regions of the shell. Both these sections contain about 2% organic matter mostly separating the individual crystallites. The study focused on the transition from calcite to aragonite, involving local morphological and crystallographic features found in this region. The character of the aragonite crystallites found near the interface change dramatically until nacre of ideal and consistent microarchitecture is found within 10-20 μm of the interface. The microstructure which develops in the post-interface transition region features zones of granular disordered aragonite, widely-spaced layers of aragonite grains with columnar morphology, early nacre (layered aragonite crystals) with insonsistent, though somewhat platelike shape, and gradual development of consistent nacreous microstructure of parallel-sided aragonite platelets approximately 0.5 μm thick separated by parallel organic layers. Evidence of the effects of both thin structural core of the organic matrix, in limiting thickness of mineralized layers, and of the functional organic molecules (thought to attach to the core layer), in directing mineralogy of the precipitating phase (calcite or aragonite) have been found. It appears that a complete combination of both components of the organic matrix is required to produce the highly consistent nacreous microstructure, though the process of templating still remains in question.

Introduction

The shell of the organism red abalone (*Haliotis rufescens*), a well-studied example considered to exemplify formation processes and features of biomineralized materials systems, is comprised of an outer region, of thickness 0.5 mm to 3.0 mm[1] (in the shells of mature animals) consisting of fine calcite crystallites, and an inner region known as mother-of pearl (or, nacre) which is a highly organized

organic/inorganic microcomposite material. The microscopic scale structure of nacre and the processes of its genesis have been studied extensively primarily due to the extraordinary mechanical properties it exhibits and the unusual morphology and organization of its inorganic (aragonite crystal platelets) and organic (protein and polysaccharide sheets, thickness ~50 nm)[2]. The exact processes which govern and dictate the growth of highly specialized microarchitecture found in the nacreous section of abalone and other shells are not completely explained at this time. Previous works[3] have asserted that a cooperative interaction takes place between organic macromolecules deployed/secreted by the molluscan organism and Ca^{2+} and CO_3^{2-} ions which form solid $CaCO_3$ (aragonite) crystallites of highly consistent morphology and specific crystallographic orientation when nacre is formed from the solution near the shell surface. (The structure of nacre consists of platelets approx. 0.5 μm in thickness and 5-10 μm in breadth, assembled with sheets of organic material separating the individual platelets. A cross sectional view of this material reveals a "brick and mortar" microarchitecture).

Recent experimental work[4] in growth of nacre atop artificial substrates inserted into the EPF in live abalone indicates that shell formation in red abalone proceeds from crystallization of an initial layer of oriented calcite crystals which is followed by production of nacre, containing small (0.5 μm thick, 5-10 μm in breadth) crystalline platelets of aragonite separated by thin sheets of organic matter The transition from the calcitic to nacreous regions in abalone shell involves selective crystallization of one distinct polymorphic variation of $CaCO_3$: calcite (crystal class rhombohedral, space group 167) or aragonite (crystal class orthorhombic, space group 62)[5]. Because of the relatively short-range transition between these crystal types, the interface and difference in crystalline structure present are thought to demonstrate the selectivity and control exerted by the organic components in the process of biomineral growth.

In this study, the microstructure and crystallography of the interface region have been examined using transmission electron microscopy and electron diffraction. The conclusions and findings from this study suggest that the release of organic macromolecules and their control over the formation of the highly organized nacreous structure does not reach its full extent instantaneously at a precise line of interface. Within the aragonite zone immediately adjacent to calcite at the interface, there is some irregularity and disorder not found in nacre from the central regions within the shell's inner layer. The disordered features at the interface are occasionally interrupted by zones of nearly ideal nacre immediately adjacent to calcite at the interface, but for the majority of the interface, examination revealed that nearby aragonite it is not structured with the same consistency as that from the central nacre. Features found in the near-interface aragonite zones are listed below:

(a) A region of aragonite with small, unoriented crystallites is located between the calcitic crystal region and the first *platelets* formed.

(b) There is no recognized crystallographic correlation between calcite and neighboring aragonite crystal at the interface.
(c) For the first platelets of nacre which form after the transition from calcite to aragonite (usually, depositied after the thin region of unoriented, polycrystalline aragonite), their geometry is not consistent.
(d) Calcite and aragonite are found intermixed and intercalated at the interface.
(e) Sheets of protein (organic matter) have been found deposited within calcite crystalline regions near the interface, in parallel layers as they are found in "regular" nacre.
(f) In initial layers of aragonite found near the interface, though edges of platelets are parallel, the actual blocks between the organic sheets do not contain single-crystalline domains.

These results suggest that the switching from calcitic columnar crystalline texture to aragonite single-crystalline platelets separated by thin organic layers in an abrupt step may be an idealization of a transition which involves a more gradual progression and several distinct types of formation. It appears that the nucleation and growth of platelets, in stacked layers, of aragonite:

i) requires deposition of an organic sheet with nucleating sites in localized positions.
ii) becomes gradually defined over a distance 5-10 μm, sometimes more, into the nacreous region.

Furthermore, the shape of the particles of aragonite forming nacre do not seem to immediately result from habit modification previously hypothesized[6] to be due to organic molecules interacting with specific surfaces of growing crystallites. Directly across from single-crystalline calcite regions, well-formed single-crystal blocks of aragonite do not appear. Rather, some irregular, polycrstalline aragonite crystalline layers, eventually followed by single crystal calcite blocks in regions where organization of organic layers is more consistent, is typical. In fact, since nucleation (rather than growth) is not regulated in this region, then the aragonite crystallites have morphology, size, and crystallography features that are irregular (we have the aragonite growth in this region "frustrated biomineralization".

Experimental Procedure

A. Sample Preparation

The principal requirement for producing a sample suitable for examination by transmission electron microscopy is making a specimen of the material which is thin enough to permit transmission of electrons accelerated in a collimated beam by the instrument (TEM). To produce such samples, we started

with bulk samples of mollusc shell (from either abalone, pinctada, or nautilus). Because of the presence of organic matrix and water in this material, both the preparation and TEM investigation require extreme care to prevent radiation damage.

Initial Thinning

Sections (rectangular beams or pieces of size and shape that can be handled by the wafering saw) were cut from the shells using a water-cooled, hi-speed diamond saw, first, to produce manageable pieces for further sectioning. The upper layer of these beamlike sections was calcite (the shell outer surface), and the lower layer was nacre. Thin (approx. .025 in. thick) wafers were cut from these sections using a low-speed, water-cooled saw, equipped with a diamond-coated wafering blade. The wafers had the approximate aspect ratio of a sheet of plywood, in which the sheet was composed of a flat calcitic zone and an adjacent flat aragonitic zone. Pieces from these thin sections were thinned further by sanding them, starting with 600-grit SiC abrasive paper, and finishing with 1200-grit abrasive paper. Mechanical thinning in this fashion was carried out until the sample was as thin as it could be made while still capable of withstanding the strain of the abrasive process without breaking into smaller fragments. Refinements on this sample perparation process included bonding the thin wafer to glass slides with cyano-acrylate adhesive (soluble, later, in acetone, to remove the thinned piece), and polishing and thinning the piece using abrasive SiC slurry. Typical final sanded thickness was .002 or .001 in. (or less). Following thinning, with an oval hole in its center, using silver paint.

Ion Beam Milling and Final Thinning

The final step in thinning the specimen was ion-beam milling. Small sections were cut from the wafer-thin sample using a razor blade, and were mounted onto a 3 mm Cu disk (which would later serve as the specimen holder in the TEM sample stage) which had an oval hole in its center. The sample was bonded to the edge of the oval hole in the copper disk with silver paint, so that a portion of the sample projected over the edge of the oval hole. The line of interface in these small sections was centered over the oval hole so that it would be most effectively thinned in subsequent ion-beam milling. The sample, mounted on the copper disk in this manner, was then placed into a Gatan ion-beam miller. Focused ion beams of argon atoms accelerated to 6 KV struck the sample surface at a glancing angle of between 10 and 20 degrees. Throughout the bombardment of the sample by the ion miller beam, the sample holder was cooled to approximately 77 K by liquid nitrogen to prevent damage to the sample. Final preparation of the sample for TEM involved application of carbon coating to the sample; this was performed in a carbon

evaporator. The thin layer of (conductive) carbon deposited on the sample surface prevented charge from building up on an otherwise insulative specimen.

B. Electron Microscopy

All experimental TEM information was acquired using a Philips 430T transmission electron microscope, operating at 200 KV. During the experiments, the sample was cooled using a liquid nitrogen reservoir attached to the sample stage, reducing the sample temperature to approximately 77 K, to avoid radiation damaging its mineral or organic phases.

Bright field imaging was used extensively for inspection and overview of areas of the sample. In this mode, contrast is generated between regions of the sample which diffract more or less strongly. This principle allows for recognition of different grains and of regions of different mineralogy and composition (organic/inorganic phases). Most imaging was conducted at magnification levels between 10,000 and 60,000 X.

Electron diffraction (particularly selected area diffraction) was used to establish orientation relationships between different regions within the interface, and to identify the crystalline phase (aragonite or calcite) present. Crystal texture, orientation, and polycrystalline character of the biominerals can be determined by analysis of the diffraction information gained through this approach.

Results and Discussion

From TEM examination of the interface region, several new unanticipated features have been uncovered in early stages of aragonite mineralization and in the interrelationship between calcite and aragonite at the interface. The images of these features, crystallographic analysis, and interpretation are provided for each (mentioned in the introduction) in the subsections following.

Initial Unoriented Aragonite Mineralization at the Edge of the Calcitic Crystal

Adjacent to the line separating aragonitic and calcitic zones, higher magnification images show that the first aragonite to form occurs in an uneven layer from 0.2 μm to 5 μm in thickness. Between this polycrystalline layer and its neigboring single-crystalline calcite domains, the interface was not separated by a distinct organic sheet. . However, a distinctly thick organic sheet is found between these zones and underlying layers of aragonite which begin to assume more regular shape and which are interspersed with organic layers between each mineral layer[7]. Images of such zones of "intermediate" mineralization are shown Figure 1 (at end of text, all figures in Figures Section) in (3) TEM micrographs in taken from different locations along the interface.

Selected area electron diffraction (SAED) patterns acquired from these zones reveal that the crystallites are in relatively random orientation, as evidenced by the broken-ring appearance of the diffraction pattern. By comparison with simulated ring diffraction from aragonite and from calcite, it was concluded that the mineral phase present in these zones is aragonite. This represents therefore the initial deposition of aragonite immediately following the transition from calcite. Diffraction from these regions and a simulated ring pattern is provided in Figure 2.

From examination of the T.R., and subsequently deposited layers of aragonite found below it, it is apparent that a sheet of organic matrix is not necessary to initiate crystallization of aragonite and the transition from calcitic mineralization, but that growth of layered aragonite, as found in nacre, must be accompanied by periodic deposition of organic nucleators, and a distinctly thick organic layer that precedes the growth of the first and subsequent aragonitic strata following intermediate mineralization zones in the T.R.

At the cup-shaped nucleus of where growth of new aragonite crystals begins, the aragonite crystallites formed are platelike, but with a slightly upward-bulging curve in their center,following the contours of the nucleating site. It is only after several successive layers that aragonite crystalline tablets assume a flat morphology.

Lack of Crystal Correlation at the Interface

From diffraction gathered from near-interface crystals of aragonite and calcite, the possibility of a near matching between atomic arrangements at the interface,or a coincidence between calcite and aragonite has been practically eliminated. For most of the near-interface calcite, the crystals are relatively large and of single domain and orientation. Diffraction from several areas of a region 5-10 μm in extent yields the same pattern at consistent sample stage tilt, as shown in Figure 3; this indicates that this domain consists on one large single crystal (Furthermore, there is a lack of grain boundaries, interruptions, and other features in this region). However, away from the interface, we have found that the calcite crystallites have a crystallographic correlation. At the same time across the line of interface, we are presented with multiple small aragonitic crystallites of inconsistent orientation. In the more organized case, platelets, rather than needle-like crystallites, also of nonuniform orientation, are found. In either of these cases, it would not be possible to have the multiple crystals of aragonite in registry with a single crystal plane or characteristic pattern of sites in the same calcite crystal; no coincident site lattice between calcite and aragonite, at the interface, is demonstrated through all of the imaging and diffraction results.

Figure 4 illustrates the case of a domain of polycrystalline aragonite (its mineralogy determined from a selected area diffraction pattern , also a ring pattern, not shown, acquired from this area) sharing an interface with a larger single-crystalline domain of calcite. From a higher magnification image of the aragonite polycrystalline zone, multiple crystallites, in slightly different crystalline orientation can be

recognized by their darker or lighter appearance, which is attributable to diffraction contrast. Figure 5 shows a zone of several platelets in random orientation all sharing a line of interface with a common single calcite crystal grain.

Nonuniform Platelets Adjacent to Interface

A lack of consistent and rectangular shape to the platelets of nacre in close proximity to the calcitic zone is typical of the initial aragonite formed after switching the mineralization from calcite to aragonite at the interface. A TEM bright-field image of a region exhibiting disorder typical of the earliest layered aragonite sections formed is provided in Figure 6. The thickness of platelets in these regions is not consistent nor is the cross-sectional shape of the platelets rectangular. The platelets appear often polycrystalline rather than single-crystalline, as they appear deeper in nacre. The organic sheets delimiting the top and bottom surfaces of the platelets are not in parallel orientation. In short, the transition from calcite to aragonite is not necessarily accompanied by genesis of flat, polygonal, interdigitating aragonite crystals of thickness 0.5 μm. For comparison, a TEM bright field image of a cross section of abalone nacre from the central region of the inner nacreous layer is also provided in Figure 6.

Radical variation of aragonite layer thickness is also characteristic of the earliest formed aragonite. The layers in some cases initially deposit with fairly consistent, submicron thickness, and subsequent deposition becomes erratic with layers several microns thick occurring next. Within these near-interface mineral layers, the aragonite is comprised of fine, needle-like grains oriented with long axes oriented along the normal to the layers. The morphology of the crystallites in these early aragonite layers resembles acicular calcite. Typically after some of this variation, the regular nacreous structure emerges in layers deposited later, wherein layer thickness is approximately 0.5 μm.

Theories on the role and presence of interlamellar and intercrystalline organic matrix put forth by Bevelander and Nakahara[8] support the findings in the early aragonitic layers and platelets. A thicker matrix, providing separation between individual crystallites on the same layer as well as between layers, appears to be required to generate single-crystalline blocks, while thin interlamellar sheets can produce distinct layers, but without generating individual "bricks" of aragonite which are essential to the microarchitecture of the microcomposite.

The relative thickness of the organic layers (thin in the regions of initial aragonite mineralization where acicular aragonite crystallites are found within layers, but which are much thicker at the onset of regions in which regular nacreous platelets form) supports the hypothesis that the organic matrix is a bi-component system, in which the structural core is composed of sheets of protein featuring a periodic higher-order structure and possibly β-sheet type conformation. Attached to this framework are active acidic macromolecules (containing substantial protions of aspartic and glutamic acids) which directly interact with ions to regulate growing crystals. Thinner bands of organic lamella could be interpreted to be

the structural core of the organic matrix, without attached active macromolecules. The mineralization resulting from the presence of the structural core lamella only is poorly controlled (see images of needle-like aragonite within layers). Thicker organic layers then consist of both core sheets and attached active organic molecules, and their effect is to produce single-crystal, oriented blocks of aragonite and after a short period of disorder, regular nacre.

Intercalation of Calcite in Aragonite

Near the initial line of calcite/aragonite transition, there appear regions where within layers of aragonite, calcite crystals are deposited. Figure 8 gives a TEM bright-field view of a small calcite grain surrounded by aragonite grains (the calcite zone is found within one layer of aragonite, between organic sheets separating otherwise aragonitic crystal). Apparently, switching from one crystal type to another is not immediate nor is it reversible at the initial interface. Calcite exists in contact with and surrounded by the same proteins and organic matter which seem to promote formation of aragonite.

Sheets of Protein Interpenetrating Calcitic Crystal

In selected areas sheets of organic/protein material are found interspersed within calcite crystal, in parallel, layered disposition as they are found within layers of aragonite crystal in nacre. These bands of organic material appear to be finer than those found at the major, definite transition line at the interface, below which layered aragonitic crystal typically is found. Figure 9 provides a bright-field image of a region of near-interface calcite which has such layers within it. By diffraction, the region was confirmed to be comprised of calcite, as shown from the SAD pattern and simulated pattern from calcite zone axis [220-4] shown in Figure 9. This diffraction pattern was acquired from the region directly between the organic layers, marked by a circle in Figure 9. A higher magnification view, Figure 10, of the junction between single-crystalline calcite containing these anomalous organic sheets and the neighboring domain shows that these bands continue across this junction into a layered region containing thin bands of aragonite in "formative" nacreous microstructure. The organic material found here is apparently not sufficiently influential to direct and/or switch the crystallizing polymorph, by producing aragonite instead of calcite, at every mineral surface which it contacts.

The presence of these organic sheets concurs with the findings of Mutvei[9] who recognized earlier the presence of such regularly spaced intracrystalline organic sheets within the calcitic region of shell from H. rufescens, through analysis of polished and etched samples of shell by SEM. Though in Mutvei's findings the sheets were reported to be well defined, we have found that these sheets appear substantially thinner than organic matter separating aragonite blocks in nacre. This may be interpreted in terms of the

distint intercrystalline and interlamellar matrix components previously proposed by Bevelander and Nakahara[10]. In this view, an electron "lucent" inner sheet is surrounded by an electron dense outer layer in the interlamellar matrix, and similar electron dense material, without a supporting sheet, separates platelets between their edges on the same layer. We have found a thin,, relatively transparent layer, which can be interpreted as only the interlamellar sheet, within the calcite. This conclusion is supported by Figure 10, wherein the parallel sheets intercalated within calcite are seen to continue across a boundary into aragontie, where these sheets separate layers of aragonite crystal. The aragonitic crystal region does not contain single-crystal platelets (characteristic of nacre); there is an apparent lack of separation on the same layer by the (absent) intercrystalline matrix.

Conclusions

The small aragonite crystals in the zones of "intermediate" mineralization in the transition zone possess a random orientation. Thin band of separation between the single-crystal calcite overlying these regions and the granular aragonite does not have the flat, layered appearance of the organic sheets. It is possible that this mineralogy (aragonite) is created through the presence of active organic molecules only,.without the structural framework of the organic sheets.

The morphology of the aragonite crystalllites in the transition zone region shows a progressive transformation toward the flat, platelet-like morphology over a range of several to tens of microns as one examines regions which lie away from the interface. From these observations, the first organic sheets released by the organism do not offer total control of the characteristic shape of near-interface aragonite particles. Along a small proportion of the interface line, one can see immediate formation of "regular" nacre, composed of single-crystalline platelets of aragonite of consistent thickness, immediately following the line of calcite/aragonite transition. However, typically there exists a short-range region of disordered aragonite, featuring occasionally a granular zone of aragonite mineralization followed by a thick band of protein and platelets of inconsistent morphology and strata of nonuniform thickness. Layer thicknesses in the near-interface nacre do not appear to be restricted as strictly as in the central-zone nacre. It appears that the separation of the subsequent layering of initial aragonite is attributable to deposition of new organic sheets, not due to the modified shape of aragonite crystal under organic influence, which has been thought in past to be flat and hexagonal or polygonal.

While the role of the organic sheets from the prior observations does not seem to include total control over particle shape, size, and disposition, deposition of organic sheet does seem to be necessary in order to promote the growth of aragonite *in layers* as it is found in nacre. Other components of the organic matrix appear to be capable of promoting switching from calcitic to aragonitic mineralogy, as is seen in

"transition" regions and their mineralization (there is no intervening sheet between these regions and the neighboring calcite crystallites), but these organic constituents are not capable of producing layers.

A templating mechanism, performed by the organic layers and resulting in the "pseudo-epitaxial" growth of mineral in contact with these layers, has not been elucidated in this investigation A more general conclusion on the control/mechanism of formation of the nacreous platelets that emerges from the evidence of this study:

i) Platelet shape, or at least the thickness of the platelets, is controlled by the separation of the organic layers.

ii) Some control over switching of crystallizing polymorphic form of $CaCO_3$ is avaliable without deployment of organic sheets. This conculsion agrees with the results of Belcher et al. (1996)[11] in which organic material (selectively extracted soluble polyanionic proteins) removed from the nacreous aragonite in red abalone shell was found capable of causing polymorphic calcite-aragonite switching when deployed in *in vitro* crystal growth experiments.

iii) Probably, some single-crystalline blocks of aragonite grow in preformed organic containment structures (where very quiescent conditions exist) which begin to develop after the initial transition zone is extablished. The interlamellar sheets are seen in all aragonite formed after the calcite/aragonite transition except in the initial transition zone (granular) mineralization. However, the earliest aragonite layers do not consist of single-crystal stacked tablets, rather, acicular aragonite crystals of dimensions ___ by___ compose the layers, which are hence polycrystalline. When later "regular" nacre develops, single blocks of aragonite are separated along the same layer by organic matter. This suggests that compartments of organic matter may preexist before mineralization of aragonite or these compartments may form when aragonite displaces organic matter found between lamella as growing tablet-like crystals spread and fill the space between interlamellar sheets.

iv) No general conclusion on what feature is responsible for consistent orientation of the platelets of aragonite, within regular nacre, along the [001] direction. Templating by well-organized organic sheets, set up as a pre-existing scaffolding within which crystalline particle deposit, is still possible.

[1] C. Zaremba *et al.*, *Chem. Mater.*, 1996, **8**, 681, and M. Sarikaya, Nacre paper, ...

[2] S.A. Shepherd *et al.*, *Marine and Freshwater Research*, 1995, **46**, 607-615.

[3] For Example, S. Mann, *Nature*, 1988, **332**, 119-124, S. Weiner and W. Traub, *Phil. Trans. Roy. Soc. Lond. B*, 1984, **304**, 425-434, S. Weiner and W. Traub, *FEBS Letters*, 1980, **111**, 311-316, and S. Weiner, Y. Talmon, and W. Traub,.*Int'l Journal of Biol. Macromolecules*, 1983, **5**, 325-328.

[4] M. Fritz *et al.*, *Nature*, 1994, **371**, 49.

[5] R.W.G. Wyckoff, *Crystal Structures*, Vol. II (New York: John Wiley and Sons, 1964), 359-366.

[6] Footnote on possible habit modification of particles of $CaCO_3$ found in nacre by epitaxial control of organic molecules, by adsorption to surfaces, or by other mechanism of their influence.

[7] In synthetic "flat pearls" grown in-vitro by other researchers (Endnote 1), the absence of such a sheet separating oriented calcite prisms and granular aragonite found along portions of the calcite/aragonite interface was noted as well. However, these results have been gathered from actual shell samples validating the use of flat pearls as analogues for growth of natural abalone shell.

[8] H. Nakahara, An Electron Microscope Study of the Growing Surface of Nacre in two Gastropod Species, *Turbo cornutus* and *Tegula pfeifferi*, *Venus*, 1979, **38** [3] (1979), 84-92, and G. Bevelander and H. Nakahara, An Electron Microscope Study of the Formation of the Nacreous Layer in the Shell of Certain Bivalve Molluscs, *Calcified Tissue Research*, 1979, **3**, 84-92.

[9] H. Mutvei, Structure of Molluscan Prismatic Layers, *in Origin, Evolution, and Modern Aspects of Biomineralization in Plants and Animals*, R.E. Crick, Ed. (N.Y.: Plenum Press, 1989), 137-151.

[10] G. Bevelander and H. Nakahara, 1969, *Calc. Tissue Res.*, **3**, 84-92.

[11] A. Belcher *et al.*, *Nature*, 1996, **381**, 56-58.

List of Figures

Figure 1
Bright Field TEM Images
Fine Polycrystalline Aragonite Mineralization
Adjacent to Single Crystal Calcite at Interface
Preceding Deposition of Platelets

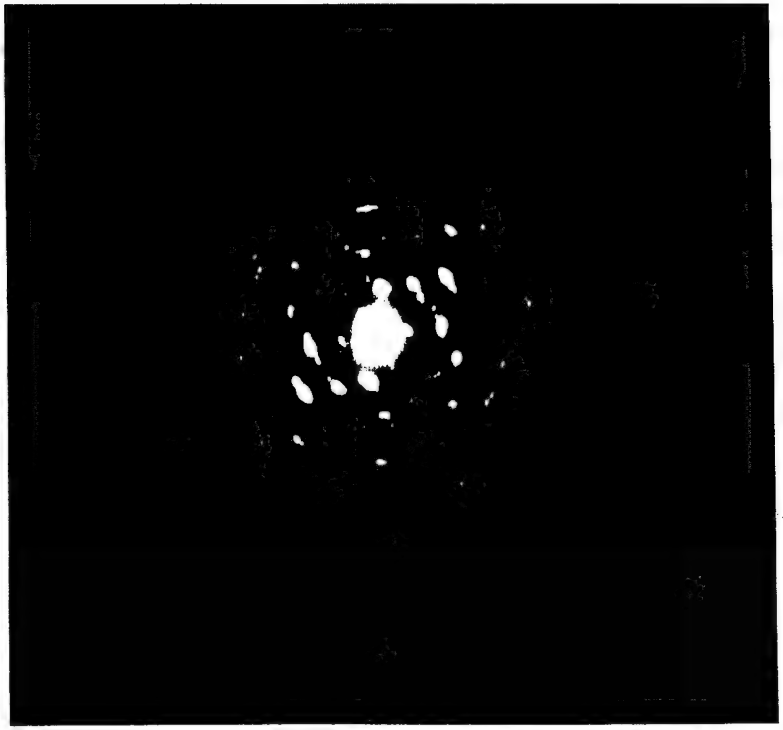

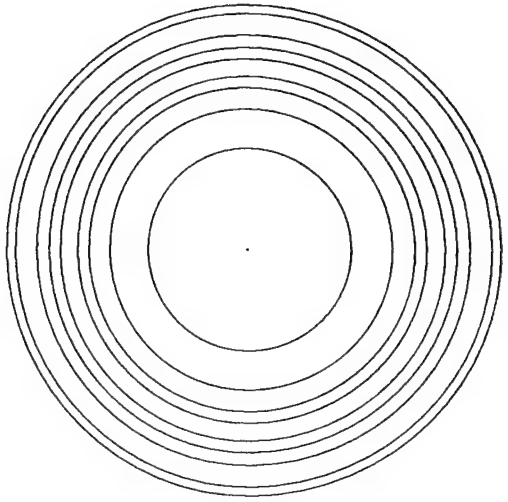

Figure 2
(L) Selected Area Diffraction Pattern from the Transition Zone Region, shown in Figure 1
(R) Simulated Ring Diffraction Pattern from Aragonite

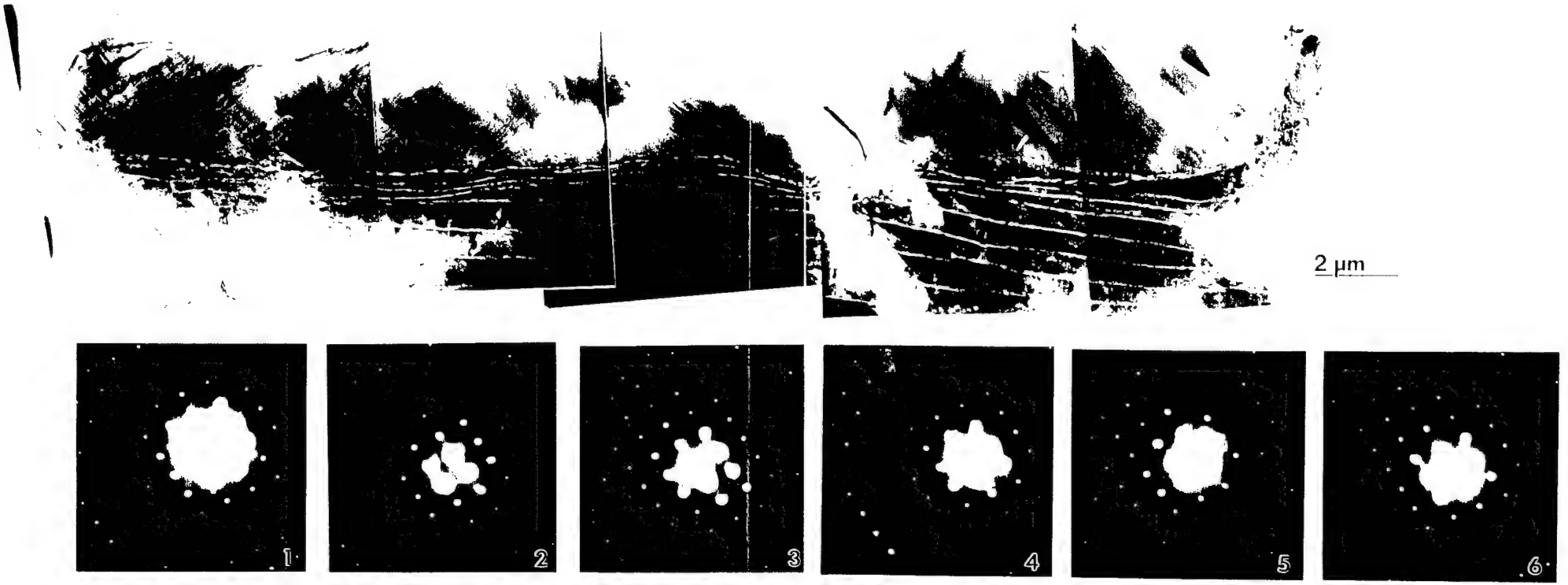

Figure 3
(A) Bright Field TEM Image, Large Single-Crystalline Calcite Domain near Interface
(B) Selected Area Diffraction Patterns Acquired from Several Regions in the Calcite Crystal Grain in the Previous Image. Locations where Diffraction taken are marked in TEM BF Image by circles.

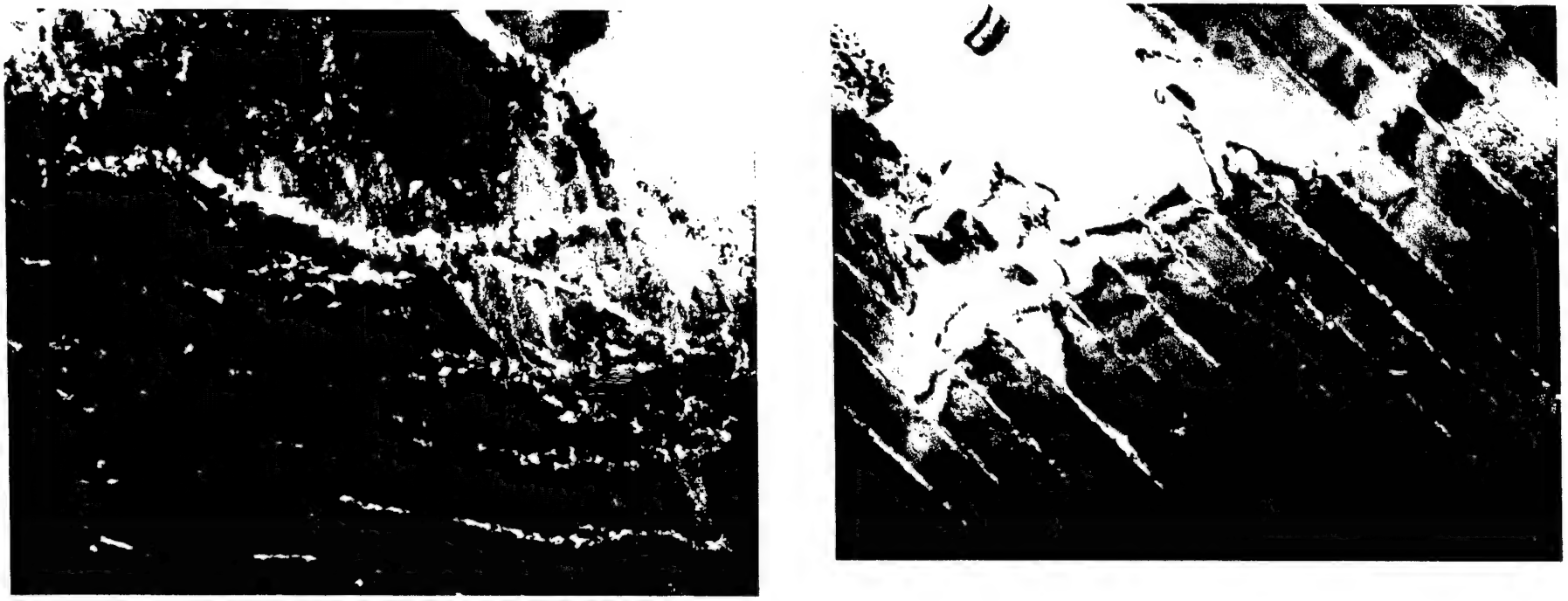

Figure 6

(L) Aragonite platelets in early nacre found near interface, exhibiting nonuniform morphology
(R) Platelets in nacre from central regions of inner shell layers, where the shape and thickness of platelets is quite consistent.

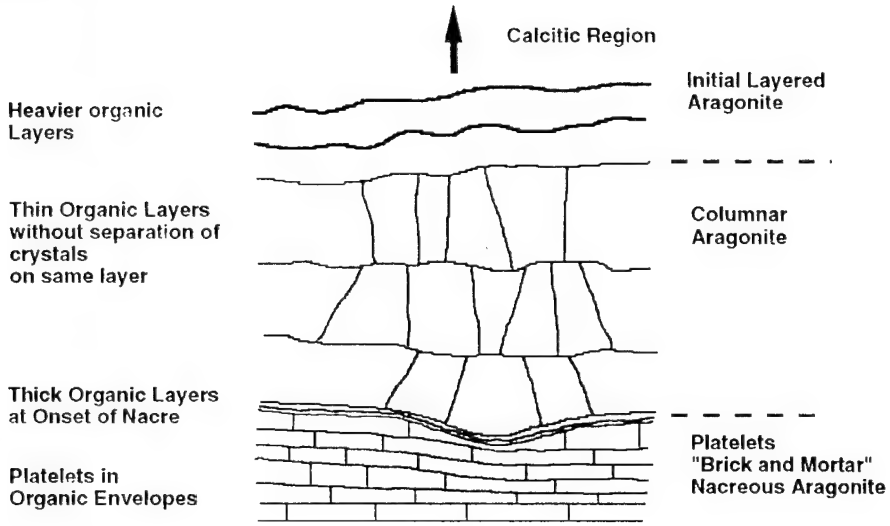

Figure 7

(A,B) Bright Field TEM Images, illustrating Zones of varying aragonite layer thickness near the interface. (C) Schematic illustration depicting irregular zones in near-interface nacre

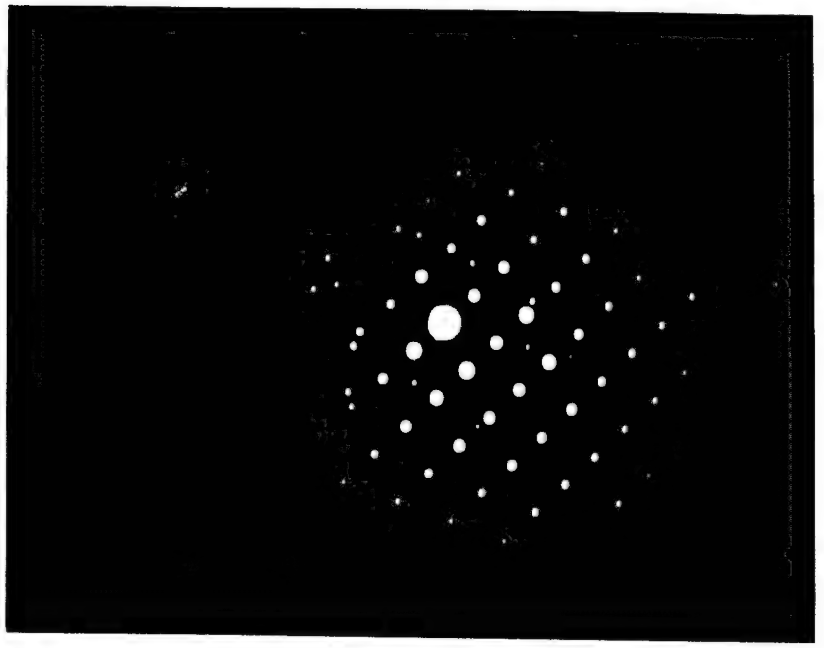

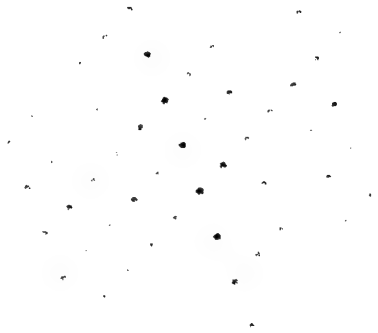

Figure 8

(A) Calcite Grain surrounded by Aragonitic Crystal near interface
(B) Selected Area Diffraction Pattern calcite crystal in aragonite
(C) Simulated Diffraction Pattern, [220-4] Zone Axis, from Calcite

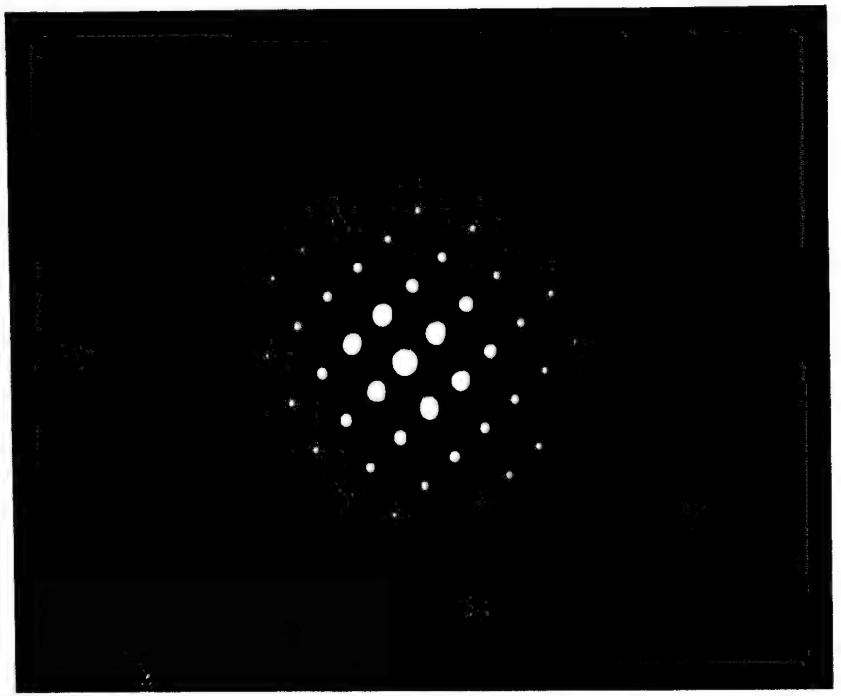

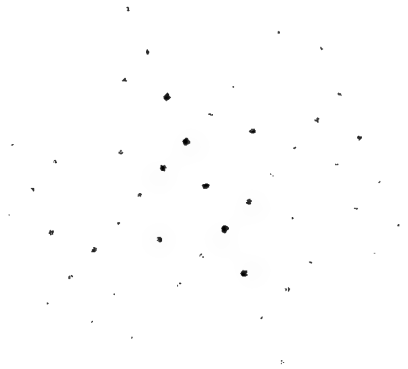

Figure 9

(A) Bright Field TEM Image, Parallel organic layers intercalated within near-interface calcite

(B) Selected Area Diffraction Pattern, from crystal (calcite) between layers shown in TEM BF Image

(C) Simulated Diffraction Pattern, [220-4] Zone Axis, from Calcite

Figure 10
Bright Field TEM Image, Showing Organic Layers continuous between Calcitic and Aragonitic Phases

Appendix - VI: Manuscript submitted

LAYERED ARAGONITIC PARTICLES FROM MOLLUSC SHELL EXTRACTS.

Richard Humbert*, Mehmet Sarikaya#, and Clement E. Furlong*.

Departments of *Genetics, Medicine, and #Materials Science and Engineering,

University of Washington, Seattle, WA 98195, USA

Key Words: layered aragonite, mollusc shell

The most prominent ultrastructural characteristic of nacre (mother-of-pearl) features sub-micrometre thick layers of aragonitic platelets ($CaCO_3$) separated by 10 nm thick macromolecular organic layers.[1] Organic material extracted from nacre, when added to artificial seawater supersaturated with carbonate, organizes the formation of layers in ooid-like spherical particles. Electron diffraction experiments indicate organizational alteration of the mineral phase. Structural and compositional similarities between layered particles and nacre are sufficient to suggest that similar processes could explain the early evolution of the molluscan shell. The ability to generate layered structures should form the basis for the synthesis of useful engineering materials.

Biomineralized structures have recently attracted the interest of materials scientists because they represent examples of changes in or control of mechanical and physical properties imposed by introduction of relatively small amounts of biopolymers.[2-4] In nacre, proteins and polysaccharides constitute 0.1 - 5 wt % of the material with the remainder being calcium carbonate.[5] The significance of nacre as a structural material stems from its excellent mechanical properties - comparable to or better than some structural ceramics.[6,7] Observations regarding particles found in rocks and marine sediments[8-12] (ooids) led us to examine the effect of molluscan macromolecular extracts on mineralization in vitro.

Soluble organic extracts were prepared from shells of red abalone, *Haliotis rufescens*, nautilus, *Nautilus sp.*, and Atlantic razor clam, *Siliqua costata*. Nacre was mechanically separated from other shell structures, powdered, and demineralized in 5% NaAcetate pH 3.0 under vacuum. Soluble material was diafiltered to near dryness with an Amicon YM10 membrane, washed 3X with NaAcetate pH 3.0, 2X with 10 mM TrisCl pH 8.0, resuspended in 10 mM Tris pH 8.0 and passed through a 0.2 µm filter. Serial 2-fold dilutions of extract ranging from 50 µg/ml protein to 0.3 µg/ml were prepared in 5 ml filter sterilized artificial

seawater in 18 x 150 mm borosilicate tubes. Addition of 200 µl of 0.1 M Na_2CO_3 supersaturated the system with $CaCO_3$.

A limited number of potential calcium-binding proteins were seen after electrophoretic analysis of organic extracts (Fig. 1). The proteins from different molluscan classes were not obviously related, being rather small in abalone extract and larger in nautilus and razor clam. The extracted protein represents only a small portion (about 0.5%) of the total shell protein.

Particles or thin sections of particles formed from molluscan extract, but not controls, exhibited concentric layers of refractive index change (Fig. 2a). Within 4 days at ambient temperature, several hundred spherulitic particles grew on the sides of control tubes. As the concentration of molluscan shell extract was increased, both the number of particles and the growth rate decreased. At protein concentrations below that at which mineralization was inhibited, a few large (~500 µm) hemispherical particles were observed after about two weeks (Fig. 2b). The effective concentration range between particles equal in size to control particles and inhibition of growth is small, 0.5 - 10 µg/ml protein. Inclusion of non-molluscan protein (bovine serum albumin), amino acids, or other small organic molecules in mineralization experiments did not give significant growth inhibition or layered particle formation .

The particles we have studied do not yet represent complete reconstitutions of nacre. In both control (Fig. 2c) and layered particles, pressure from a sharp blade caused predominantly radial fracture; nacre is more fracture resistant. In layered particles, fracture sometimes occurred along the concentric layers (Fig. 2a). Etching of fracture faces of layered particles in the presence of protein fixatives revealed ridges protruding from the bulk surface separated

by 1.2 - 9 μm (Figs. 2b and d). In the absence of protein fixatives, the surface etched evenly. Prominent extensions of aragonitic needles from the surface of control particles (Fig. 2c), were largely absent on particles from molluscan extracts. A chromogenic amino-group reagent was incorporated into concentric layers when attached to abalone protein (Fig. 2e). In the transmission electron microscope, layers of electron transparency were observed corresponding to the layers visible in the light and scanning electron microscopes (Fig. 2f). The microstructure consists of small elongated crystals extending into or through layers. Layers appear to represent a region of more concentrated protein rather than a strictly separate structure.

Transmission electron diffraction patterns recorded from ultramicrotomed (but not strained) particles from abalone extract and from control indicate that the $CaCO_3$ particles are aragonite (orthorhombic) in both cases (Fig. 3). In the abalone extract sample, fine particles are organized radially and slightly elongated with a preferred crystallographic texture not observed in the control. Texturing and elongation indicate a significant degree of control of particle growth by nacreous organic extract.

Striking similarities exist between ooids[11,12] (spherical particles with lamellar structure found in rocks and sediments) and nacreous structures. The amino acid composition of shell proteins including abalone[5,13,14] and nautilus[15] tends to be rich in aspartic acid, with proposed involvement in calcium binding.[16-19] Organic matter comprises 0.1 weight % of natural Bahamaian ooids, 30% of this was aspartic acid-rich protein.[9] From the amino acid composition data, it was suggested that similar processes applied to ooid formation and carbonate biomineralization.[9] Nacre and ooids share similarities which do not apply to other biomineralized structures. Both are composed of layers of aragonite separated by thin organic layers, with the aragonite c axis perpendicular to the major organic layer,[7,20,21] and aligned

in the growth direction. Humic acid was found to organize artificial radial carbonate ooid formation from artificial seawater (these studies, data not shown)[8,10]. Carboxylation of aspartates eliminated ooid formation.[22]

The nacreous structure has been a remarkably successful evolutionary design. Nacre is found in members of the Monoplacophora, Gastropoda, Pelecypoda, and Cephalopoda.[23] At the ultrastructural level, relatively small changes are observed between groups which diverged about 500 MYr bp. In current forms, macromolecular components appear to self-assemble and form layers[1] or compartments[24] which are subsequently filled with growing aragonite tablets.[16-18,24,25] Using an analogy derived from metallurgy, spontaneous formation of calcium carbonate in a mucilaginous phase was proposed to explain molluscan shell evolution.[23] Planar layered aragonite similar to the particles formed in these studies could have evolved into the nacreous structure as shown in Fig. 4. The radial aragonitic crystals with crystallographic texture of control particles could be relevant to prismatic ultrastructural evolution. This speculative model explains the presence of two carbonate structures in molluscan shells based on experimentally observed phenomena. Examination of the ultrastucture of early shells is precluded by diagenetic alteration of specimens from this epoch.

The evolution of nacre occurred about 550 Myr bp in Cambrian seas. Although our experiments used artificial seawater of modern formulation, the sequence of minerals in marine evaporites, ionic composition of halite inclusions and ratios of strontium and carbon isotopes in marine limestones place constraints on oceanic inorganic composition and have led to the conclusion that seawater composition has not changed drastically since the Cambrian.[26] Carbonate rocks deposited during the Cambrian are common. The molluscan shell may have evolved in one of the abundant Cambrian shallow tropical seas similar to the

Bahama shoals where ooid formation occurs today.

Detailed understanding of nacre formation may allow for the design of new materials in which polymers regulate the formation and properties of technological ceramic-based materials to produce nanoscale-laminates with desirable properties.[1-4] Humic acid, previously shown to produce layered carbonate structures,[8,10, 22] is a substance which largely defies characterization and which would be difficult to use technologically. The individual proteins in our molluscan extracts, when fully characterized, could form the basis for the reproducable synthesis of novel materials.

References

1. Sarikaya, M. & Aksay, I. A., in *Results and Problems in Cell Differentiation: Structure, Cellular Synthesis, and Assembly of Biopolymers,* Case, S. T., ed. **19**, 1-25 (Springer-Verlag, Amsterdam, 1992).
2. Alper, M. et al., eds. *Materials Synthesis Based on Biological Process* (Materials Research Society, PA, Pittsburgh, 1991).
3. Aksay, I. A. et al., eds. *Hierarchically Structured Materials* (Materials Research Society, Pittsburgh, PA, 1992).
4. Calvert, P. & Mann, S. *J. Mater. Sci.*, **23**, 3801-3815 (1988).
5. Keith, J., Stockwell, S., Ball, D., Remillard, K., Kaplan, D., Thannhauser, T., & Sherwood, R. *Comp. Biochem. Physiol.* **105**B, 487-496 (1993).
6. Jackson, P., Vincent, J. F. V., & Turner, R. M. *Proc. Roy. Soc. London B* **234**, 415-440 (1988).
7. Sarikaya, M. et al., in *Materials Synthesis Using Biological Processes* (ed. Rieke, P. C. et al.) 109-116 (Materials Research Society, Pittsburgh, PA,1990).
8. Suess, E. & Fütterer, D. *Sedimentol.* **19**, 129-139 (1972).
9. Mitterer, R. M. *Geochim. Cosmochim. Acta* 36: 1407-1422 (1972).
10. Ferguson, J., Bubela, B., & Davies, P. J. *Chem. Geol.* **22**, 285-308 (1978).
11. Davies, P. J., & Martin, *K. Geol.* **4**, 120-122 (1976).
12. Newell, N. D., Purdy, E. G., & Imbrie, J. *J. Geol.* **68**, 481-497 (1960).
13. Cariolou, M. & Morse, D., *J. Comp. Physiol.* B **157**, 717-729 (1988).
14. Nakahara, H., Bevelander, G., & Kakei, M., *Venus* **41**, 33-46 (1982).
15. Weiner, S., *Calcif. Tiss. Intl.*, **29**, 163-167 (1979).
16. Weiner, S. & Hood, L. *Science*, **190**, 987-989 (1975).
17. Crenshaw, M. A. & Ristedt, H., *Biomineralisation*, **8**, 1-8 (1975).

18. Mann, S., *Nature*, **332**, 119-123 (1988).

19. Wierzbicki, A., Sikes, C. S., Madura, J. D., & Drake, B. *Calcif. Tiss. Intl.* **54**, 133-141 (1994).

20. Wada, K. *Biomineralisation* **6**, 141-159 (1972).

21. Addadi, L. & Weiner, S. *Mol. Cryst. Liq. Cryst.* **134**, 305-322 (1986).

22. Davies, P. J., Bubela, B., & Ferguson, *Sedimentol.* **25**, 703-730 (1978).

23. Taylor, J. D. *Paleontol.* **16**, 519-534 (1973).

24. Bevelander, G. & Nakahara, H. *Calc. Tiss. Res.* **3**, 84-92 (1969).

25. Wise, S. L. *Eclogae geol. Helv.* **63**, 775-797 (1970).

26. Holland, H. D., Lazar, B., & McCaffrey, M. *Nature* **320**, 27-33 (1986).

27. Campbell, K. P., MacLennan, D. H., & Jorgenson, A. O. *J. Biol. Chem.* **258**, 11267-11273 (1983).

ACKNOWLEDGMENTS

We thank Mr. G. Lancaster and Mrs. S. Lara for technical assistance. The work was supported by the U. S. Army Research Office and Air Force Office of Scientific Research .

FIGURE LEGENDS

Figure 1. SDS-polyacrylamide gel analysis of molluscan extracts. Electrophoresis was in 14% acrylamide gels stained with 1-ethyl-2-[3-(1-ethylnaptho [1,2 d] - thiazolin-2- ylidene)-2-methylpropenyl]naptho[1,2d]- thiazolium bromide (Stains-all). Lane 1 - molecular weight standards; bovine serum albumin (66,000), carbonic anhydrase (29,000) and trypsin inhibitor (20,000). Lane 2 - organic extract from abalone. Lane 3 - extranct from nautilus. Lane 4 - extract from razor clam. Lane 5 - abalone extract digested with trypsin before electrophoresis. The bands in the standards lane were stained pink. All the major bands in the molluscan extracts were stained blue. Blue staining has been associated with calcium binding[13,27].

Figure 2. Micrographs of layered particles. (a) Light micrograph of a fractured slice of a particle formed in razor clam extract. Note the fracture plane following layer. (b) Scanning electron micrograph of etched particle from abalone extract (AB particle). The upper face was fractured only. The right and left faces were etched to different extents. Fix/etching was in 10% glutaraldehyde, 2.5% paraformaldehyde, pH 2.9. (c) SEM photo of control particle. The spherulitic structure consists of radially oriented aragonite needles without layers. (d) A closer view of layers in an SEM image of etched AB particle. (e) Light micrograph of AB particle formed when dabsylated material was added to mineralization solution. Incubation of dialyzed extract in 0.1 M CO_3 buffer, pH 8.9 at 70 ^oC with amino group-specific reagent 4-dimethylaminoazobenzene-4-sulfonate (dabs) labeled the protein components of the extract. The labelled material fractionated preferentially into particles in mineralization experiments and was predominately. (f) Transmission electron micrograph of AB particle. Control and molluscan extract particles stained black with Feigl's solution, consistent with aragonitic structure.

Figure 3. TEM images and diffraction patterns of AB and control particles. (a) and (b) are TEM images of AB and control particles, respectively. In AB particles, grains are radially elongated (aspect ratio: 3:1); in control, they are equiaxed. (c) and (d) are selected area diffraction patterns from (a) and (b) , respectively being aragonite (orthorhombic, Pmnc, a=4.94 Å, b=7.94 Å, and c=5.72 Å). Crystallographic texturing (about 30°) in (a) is absent in (b).

Figure 4. Proposed scheme for evolution of the molluscan shell. The proto-mollusc (A) had a proteinaceous precursor to the periostracum of modern shells. At some time (B), the organism gained the ability to produce sites for nucleation of carbonate deposition allowing mineralization of aragonite needles similar to those of control particles. At a later stage (C), acidic proteins in the more protected area under the shell resulted in formation of a layered structure on top of the needles. At the shell margin, seawater currents reduced the concentration of protein, thus needle formation continued in this region. In the ancestral structure, the primary interaction was the physical association of organic and carbonate materials. The initial stages of shell evolution would have been somewhat disorganized and uncontrolled. Increased interactions between organic components facilitated control of growth and elaboration of the shell and improved the mechanical properties. At a later stage, interactions between organic components allowed self-assembly of the organic macromolecules prior to mineral deposition. The long thin aragonitic needles of the precursor to the prismatic region of the shell could be converted to prisms by increased growth rates along the a and b crystal axes. In many species, the prismatic region was converted to calcite at a later evolutionary stage. The layered portion became nacre as self-assembly of organics into compartments preceded aragonite mineralization. At this point, the mollusk had a strong shell deposited in a controlled manner (D) which provided armor far superior to the original proteinaceous shell.

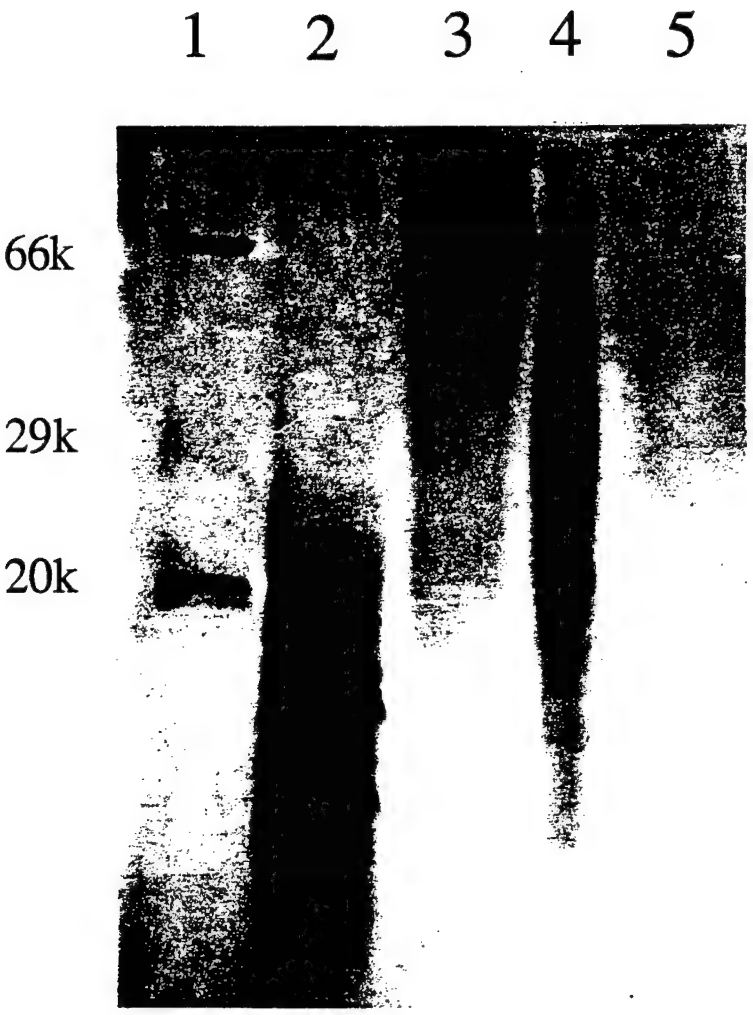

Fig. 1, R. Humbert et al., Layered Aragonitic ...

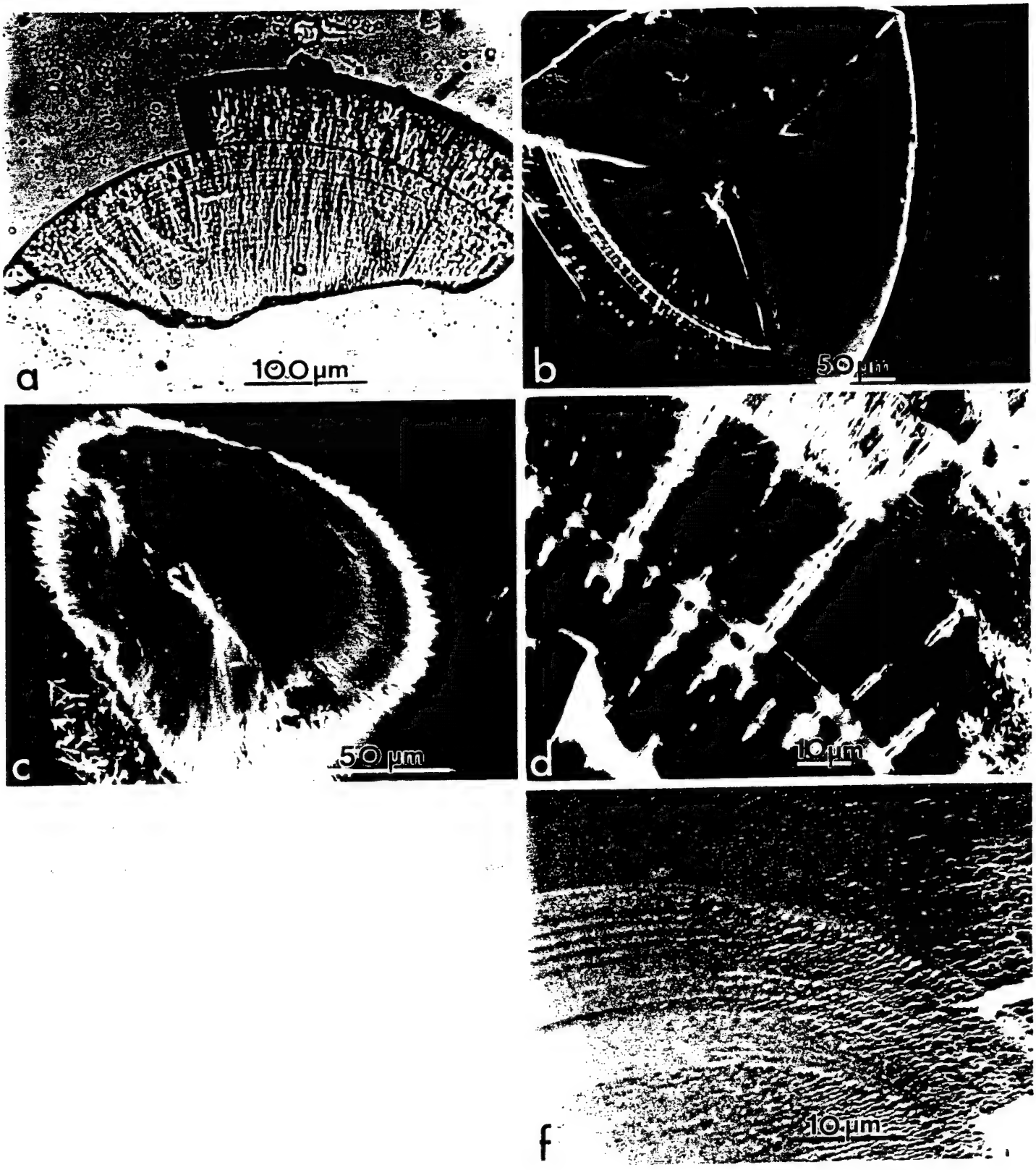

Fig. 2, R. Humbert et al., Layered Aragonitic ...

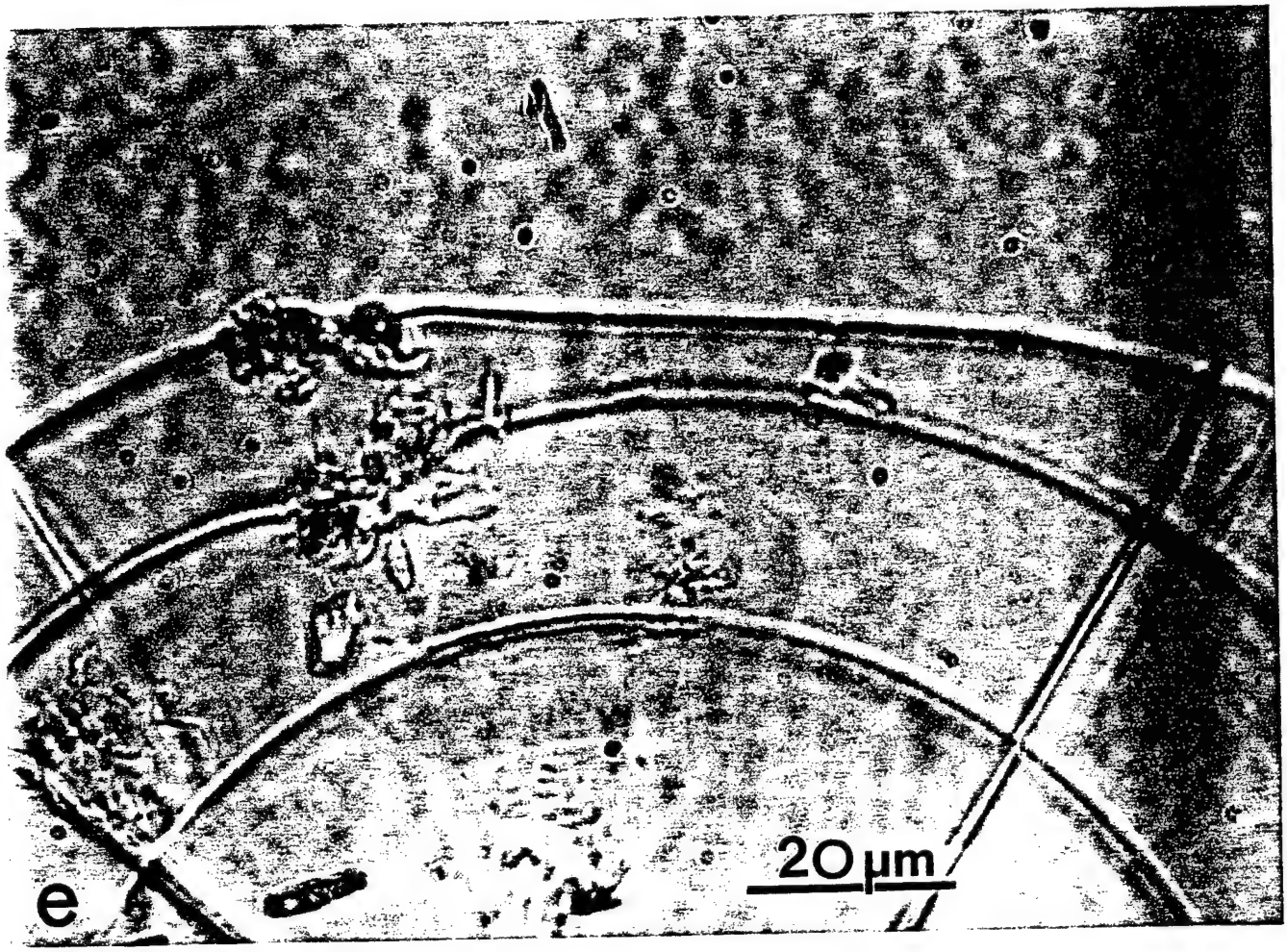

Fig. 2e, R. Humbert et al., Layered Aragonitic ...

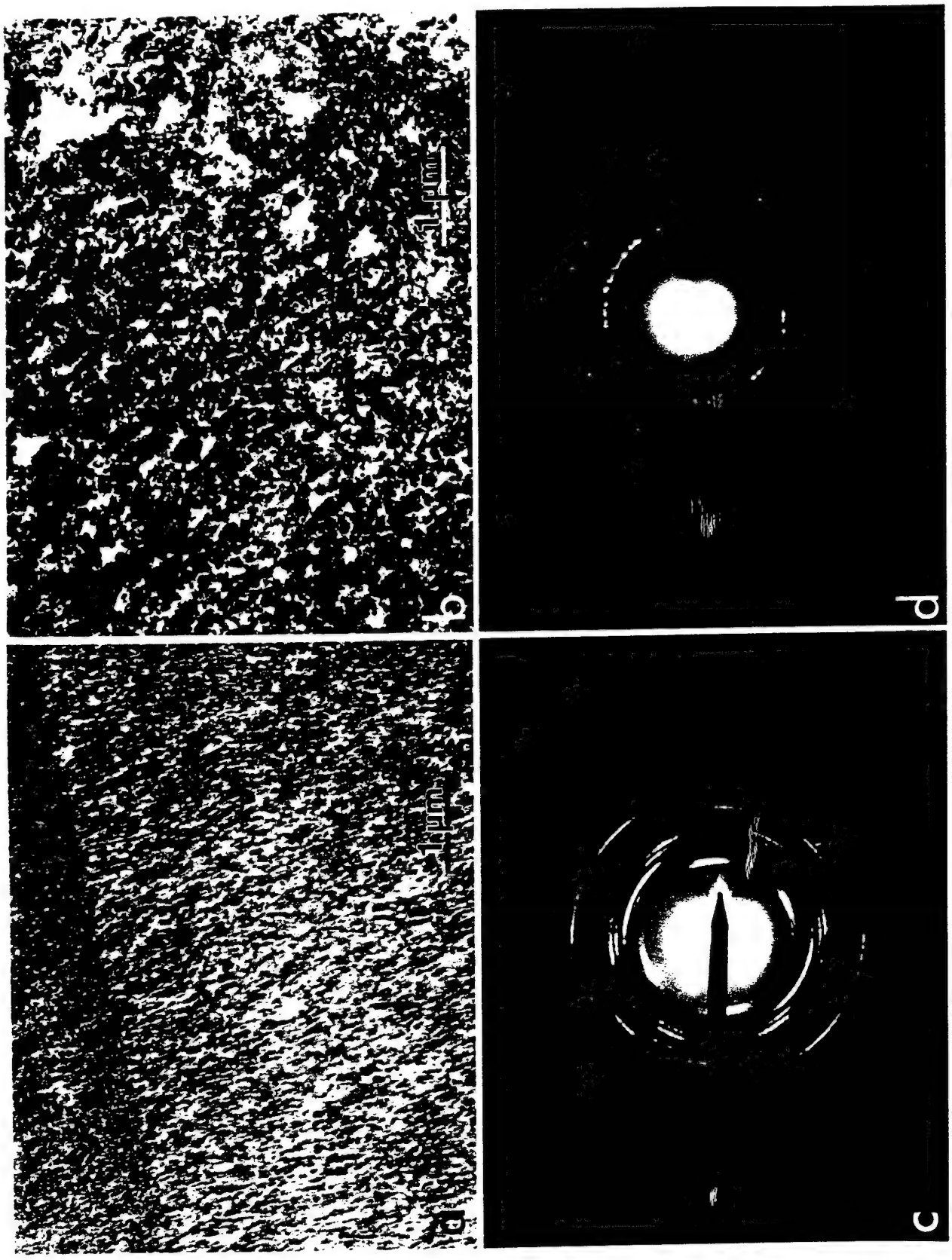

Fig. 3, R. Humbert et al., Layered Aragonitic ...

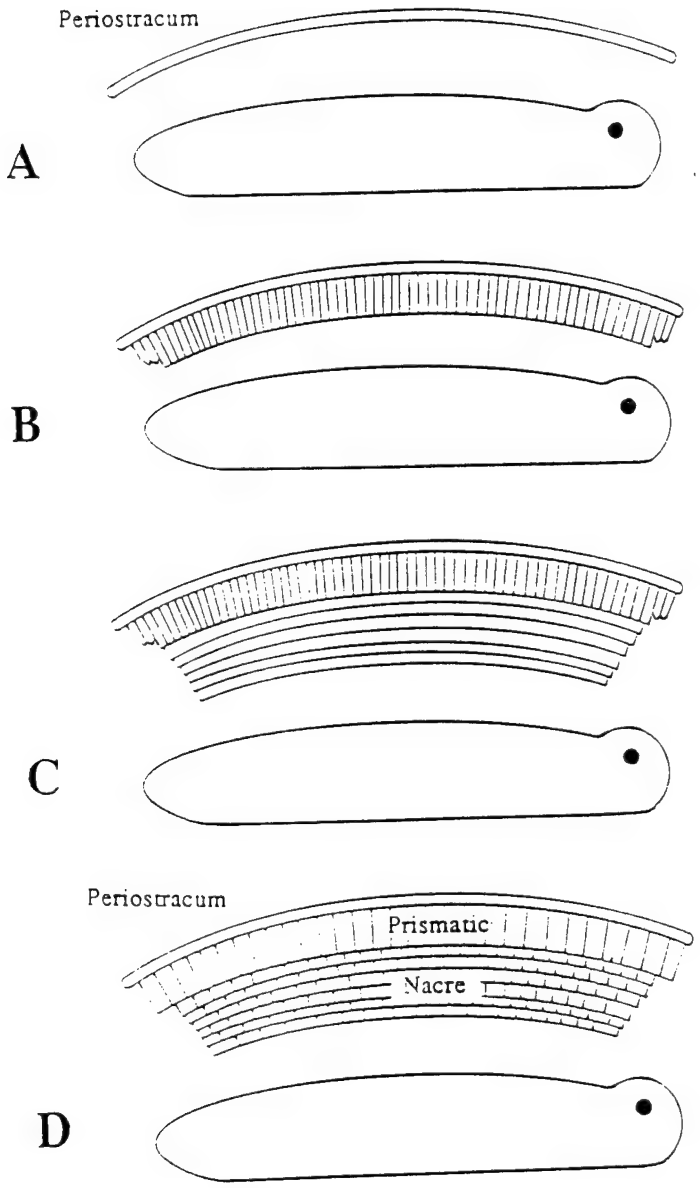

Fig. 4, R. Humbert et al., Layered Aragonitic ...

5. J. J. Cassidy, A. Hiltner, and E. Baer, *Ann. Rev. Mater. Sci.*, **15**, 455 (1985).

6. E. Baer, S. Torp, and B. Friedman, in: *Structure of Fibrous Biopolymer*; E. D. T. Atkin and A. Keller (eds.) (Butterworth, London, 1975, p. 223); S. Trop, E. Baer, and B. Friedman, Proc. Colston Conf., 226 (1974).

7. E. Baer, J. Kastelic, and A. Galeski, *J. Connect. Tissue Res.*, **6**, 11 (1978); E. Baer, J. Kastelic, and I. Palley, *J. Biomech.*, **13**, 887 (1980).

8. A. Hiltner, J. J. Cassidy, and E. Baer, *J. Connect. Tissue Res.*, **23**, 75 (1989).

9. A. Hiltner, J. W. Orberg, and E. Baer, *J. Connect. Tissue Res.*, **11**, 285 (1983).

10. J. W. Orberg, E. Baer, and A. Hiltner, *Connect. Tissue Res.*, **9**, 187 (1982).

11. K. Fackler, L. Klein, and A. Hiltner, *J. Microsc.*, **124**, 305 (1981).

12. R. L. McCally, C. B. Bargeron, W. R. Green, and R. A. Farrell, *Exp. Eye Res.*, **37**, 548 (1983).

Appendix - VII:

Manuscript published: in Biomimetics: Design and Processing of Materials (AIP, New York, 1995)

NACRE: PROPERTIES, CRYSTALLOGRAPHY, MORPHOLOGY, AND FORMATION

Mehmet Sarikaya,* Jun Liu,* and Ilhan A. Aksay§

*Department of Materials Science and Engineering
University of Washington, Seattle, Washington 98195; and
§Department of Chemical Engineering, and Princeton Materials Institute
Princeton University, Princeton, New Jersey 08544-5263, USA

Biological hard tissues are composite materials incorporating both inorganic component (e.g., phosphates and carbonates) and organic component (macromolecular structural units including proteins and polysaccharides). These materials have excellent physical properties mainly because of their hierarchically ordered structures through the dimensional scale from molecular to submeter. These composites are a source of inspiration for design and processing of synthetic materials based on both their structure and processing. In this chapter, we give a general overview of some biological hard and stiff tissues in biomimetics research. We specifically discuss mechanical properties of nacre section of mollusk shells which is a composite of $CaCO_3$ platelets surrounded by an organic matrix. The current understanding of micro- and nanostructures of $CaCO_3$ and the organic matrix, crystallographic relationship between them, and finally the morphology and shape formation of the shell are discussed.

1.0 INTRODUCTION

A central issue in materials science is to develop materials for specific applications through a precise control of their structural features in order to achieve a desired set of properties.[1] Ideally, the structural features are to be controlled from molecular to macroscopic dimensions. In biologically produced composites, nanocomposite structures themselves are the building blocks for larger scale composite structures as a hierarchical "materials system" builds up from nanometer length scale upward. In synthetic composites, a typical length scale for the smallest level of hierarchy is in the micron range. Exceptions to this rule are found in a few synthetic composites where structural hierarchy is pushed into the nanometer range not necessarily by deliberate design but by

more complex than biomimicking and will require a long-term commitment (probably decades of research), not only to learn the intricacies of bioprocessing used by organisms but also to develop new strategies to process materials synthetically from the molecular level up with the same size, shape, complexity, and multifunctionality as the biocomposites. The biomimicking approach, although by no means simple, will require a shorter time commitment (ten years of research or less). Biomimicking involves exploring the structures of biomaterials, correlating their multifunctional properties with the specific structural features. This chapter focuses only on the biomimicking approach.

We describe some of our findings on structural design of the nacre of abalone shell and answer several questions about this unique, but relatively simple, composite. In particular, we focus on the organization of the inorganic component, its possible

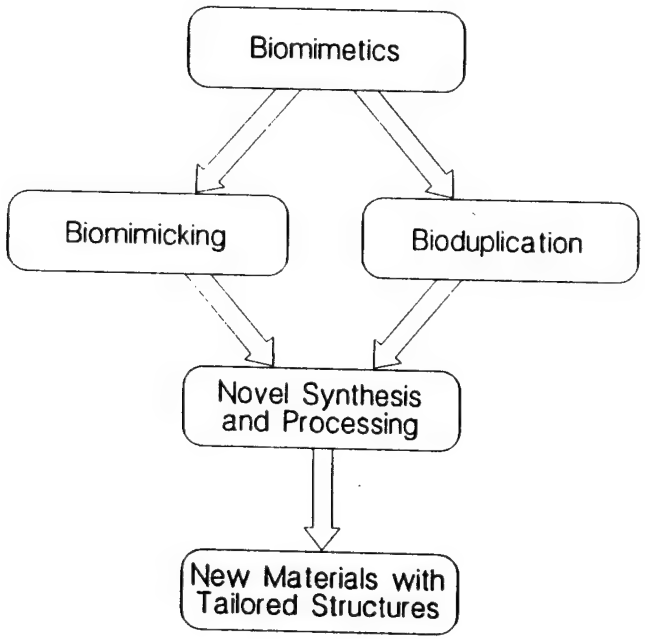

Figure 1. Schematic description of methods of materials design based on biomimetics.

structural relation to the organic matrix, and the growth mechanism of the shell. Before describing a detailed structure of nacre, certain unique aspects of some of the other biological composites are discussed. Our goal is to obtain lessons and design guidelines for the synthesis of future technological materials via biomimetics which, to us, is a natural extension of the materials revolution that is taking place today and is expected to continue well into the next century.

1.2 AN OVERVIEW OF MICRO- AND NANOSTRUCTURAL DESIGN IN BIOLOGICAL HARD TISSUES

Biological materials that are of interest in technological applications are mostly hard and stiff tissues and small particles. These structures are composed of an organic matrix (mostly proteins and polysaccharides) with the inorganic phase interspersed throughout. The formation, morphological development, and crystallography of the inorganic particles are assumed to be controlled by the organic matrix, a hypothesis which has not been indisputably established.[21,31] In the case of stiff tissues, such as insect cuticles,[32] all the components of the composite are organic macromolecules in which the matrix is usually composed of proteins. The stiffness comes from fibrillar polysaccharides, such as collagen and chitin, organized at the nano-, micro-, or higher-scales.[33] Some lower organisms, such as bacteria and algae, produce fine inorganic particles with unique physical properties.[34] As listed in Table-I with their corresponding properties, biological composite materials include all organic components,[35-40] such as spiders' webs,[35] mucus,[36] and insect cuticles;[32,33] inorganic-organic composites, including seashells,[41] teeth,[42] and bones;[43] ceramic composites, such as sea-urchin teeth[44] and spines;[45] and inorganic ultrafine particles, such as magnetic[34,46] and semiconducting[47] particles produced by bacteria and algae, respectively. In some cases, byproducts and enzymes,[48] proteins,[49] and other macromolecules[50] have chemical or physical properties superior to their synthetic counterparts.

Small inorganic particles of biological origin offer analogies with synthetic nanoparticles[11] and mesoscopic systems.[51] There are many organisms that produce ultrafine inorganic particles that perform various functions.[34] One notable example of this is iron clusters that form at the center of ferritin molecular cages (or vesicles) in organisms.[52] In some cases, metal clusters are accumulated as foreign entities that might

Table-I. Categorization of various biological composites, their micro-/nanodesign, and physical properties

Material/composite	Example	Scale	Properties
Small particles	bacterial algal	N N	magnetic, electronic, optical
Ceramic/ceramic	sea-urchin	B	mechanical (wear resistant)
Ceramic/polymer	mollusk bone dentin	N, H N, H N, H	mechanical (tough, strong), ferroelastic
Polymer/polymer			
laminated	cuticle	N, H	mechanical, optical
fiber/matrix	tendon	N, H	mechanical, ferroelastic
fiber/fiber	silk	N	mechanical (tensile)
Liquid crystalline matrix	mucus	N	rheological

N: nanometer; M: micrometer; B: both nanometer and micrometer; H: hierarchical

otherwise be harmful to the host organism, such as CdS in algae.[47] Another example is ultrafine magnetic particles that are found in bacteria.[34,46,53,54] Some species of bacteria that live anaerobically in freshwater and salt swamps move about to seek oxygen and food by a mechanism that makes use of a string of magnetic particles (Fe_3O_4 or Fe_3S_4) as a compass.[46] In *Aquaspirillum magnetotacticum*,[55] for example, each bacterium has about 20-25 particles that are oriented along a string with their magnetization axis along the long axis of the bacterium (Figure 2). Bacteria can move either forward or backward, depending on their configuration with respect to the Earth's magnetic field. In terms of biomimetic applications, some of the significant materials characteristics of these particles are: (i) they are single crystalline (no lattice defects, such as dislocations, twins, or stacking faults),[54,56,57] (ii) they have a uniform particle size of about 500-600 Å, and, thus, are in the single domain (superparamagnetic) region,[55,58] (iii) particle shape is species specific and can be dodecahedral, cubo-octahedral, or hexagonal,[56] (iv) they are aligned as a single string of particles (and occasionally as double strings)[54,59] (v) they form in biological sacks, called magnetosomes.[54] In S-rich regions, some species are known to form an isomorphic form of magnetite, i.e., Fe_3S_4.[60]

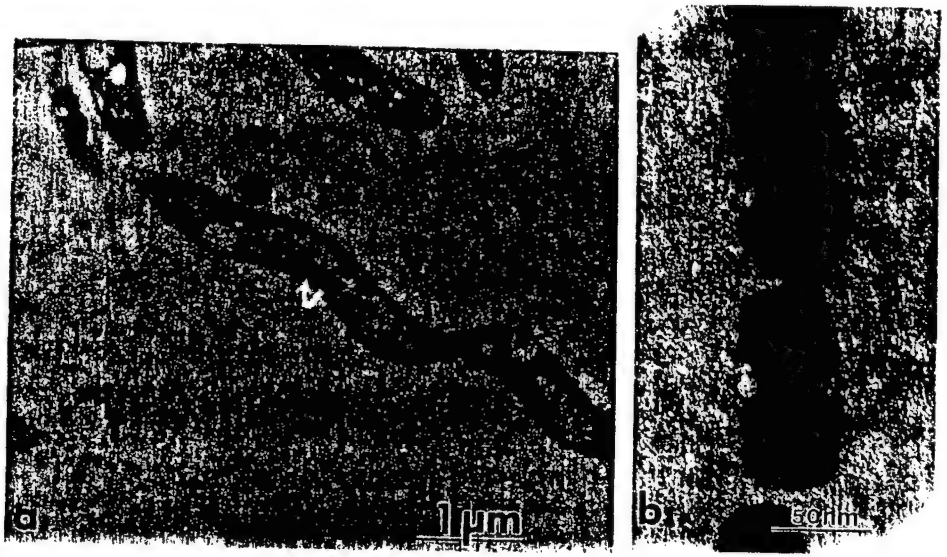

Figure 2. TEM images of *A. magnetotacticum* show a string of fine Fe_3O_4 particles.

The formation of magnetic particles within magnetosome membranes is of great interest especially with respect to forming small synthetic particles under closely controlled synthesis conditions.[61] Small magnetic particles can be formed synthetically in several ways including solution precipitation from precursors, in microemulsions, and using vesicles.[62] In each of these cases, however, the particles formed are nonuniform, often are not fully crystalline, are compositionally nonhomogeneous, and, more importantly, are in an agglomerated state which imposes problems in processing.[63] Processing of small magnetic and other inorganic ultrafine particles via biological routes, therefore, promises advantages in terms of controlling synthesis and morphological properties. The most critical point in the understanding of particle formation in magnetosomes is mechanism(s) by which organic matrix allows the nucleation and controls the growth of these particles. The investigation of structure and composition of the magnetosome membrane and its protein organization, therefore, is important for understanding transport of ions through the membrane and the early stages of particle formation. Current knowledge of the membrane demonstrates that it is a bilayer and is likely to contain proteins that are found in the outer membrane of the bacteria.[64] Other questions

involve details of the early stage of formation of particles (amorphous or crystalline and, possibly, in the hydrated form), selection of their chemistry (e.g., Fe_3O_4 vs Fe_3S_4), the control of their growth, and finally, factors that affect particle morphology, as discussed by Frankel and Bazylinski in this book.[65]

While only a small particle may be wholly inorganic in bacterial magnetite, in some organisms, such as echinoderms[66,67] skeletal components display unique composite structures also involving mostly inorganic phases. In biocomposites, such as sea shells and bones, it is assumed that an organic phase is usually associated with an inorganic phase in an easily recognizable way, with each phase in close proximity to the other.[20,21] In sea-urchin skeletal units inorganic phase appears to be present alone and constitutes the overall component of the skeleton. (In these systems, organic matrix may cover the overall skeletal unit as a sheath (teeth) that may control the growth, or may be present within holes of the spongy-structured inorganic phase (spine) which is dissolved during sample preparation for observation.) These biocomposites, therefore, also provide potential examples in biomimetic applications for ceramic/ceramic composites. In the body and the spine of the sea-urchin [Figure 3(a)], the mineral is a calcitic single crystal forming an intricate architectural design.[68] The most interesting among the structural composites in sea-urchin are its teeth.[69] Five pieces of teeth in the lower center of the body are used to scrape food from the surface of rocks. A cross-section at the cutting edge of a tooth is composed of a matrix of amorphous $CaCO_3$ with crystalline calcitic $CaCO_3$ fibers embedded with their long axes perpendicular to the cutting surface to increase the wear resistance[69,70] of the tooth [Figure 3(b)]. Irrespective of sea-urchin teeth, this design has been in use in synthetic fiber-reinforced composites.[71]

Recent studies reported that organic macromolecules may be occluded within certain sea-urchin skeletal units.[67] With respect to biomimetics, the major questions involve the presence, types, and spatial distribution of organic macromolecules that constitute less than 1 vol. % of the structure. If there exist occluded proteins, or their fractions, then these hard tissues may be regarded as molecular composites, i.e., analogs of nanocomposites.[3] Investigation of sea-urchin at high spatial resolution (in imaging) and elemental resolution (in spectroscopy) is expected to provide better insights into the understanding of these unique structures.

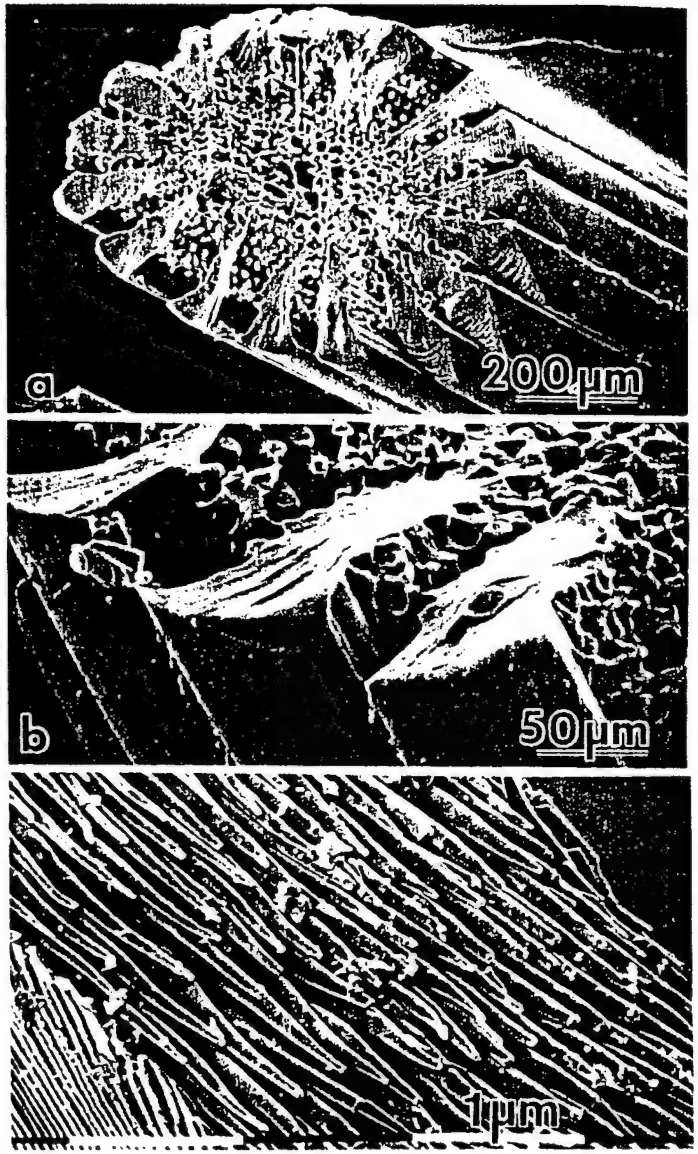

Figure 3. SEM images of a sea-urchin (a,b) spine, showing its intricate structure, and (c) tooth, displaying its composite structure consisting of calcite fibers embedded in an amorphous $CaCO_3$ matrix.

Organic/organic biological composites constitute numerous stiff biological tissues, composites of fibrous organic components embedded in a soft organic matrix, that are analogs of fiber- or particle-reinforced polymeric composites.[71] Tendon,[38,72] which connects muscle and bone, is a classic example. It has six discrete levels of structures organized in a hierarchical manner from molecular to centimeter-scale. Silk, found in cocoons of silk moths and webs of spiders, is another structural material.[35,73i] These unique structures consist of silk fibroin proteins (pleated sheets) organized in a liquid crystalline fashion in an amorphous protein matrix. These are designed, by the organisms, to withstand stresses much higher than those encountered by high tensile strength-metallic or polymeric fibers (see also the paper by Gosline et al.).[73ii]

One of the major classes of organic biocomposites is cuticles.[32,74] Arthropods, such as insects, crustaceans, spiders, millipedes, and others, are evolutionarily very successful, probably because their cuticles cover their bodies from "head to toe." The cuticle, therefore, is the skeleton, for example, of an insect. Its structure resembles that of fiber-reinforced polymer matrix; the fibers are chitin (polysaccharides), and the matrix consists mostly of proteins.[74,75] The composite has a sheet structure in which chitin fibers are arranged in layers. In each layer, the fibers are oriented parallel to each other.[32,33,75] In successive layers, there is a rotation of these parallel fibers only a few degrees, i.e., helicoidal (discussed by Gunderson and Schiavone in this book and references therein).[76] The unique structure of the insect cuticle, as well as cuticles of other classes, may serve as an example for the design of composite materials in which all the components are polymers.

Exoskeletons, in addition to serving as protective "armor" for insects, also form intricate surface structures which give optical effects. For example, in butterfly wings, although the origin of color for the most part is pigmentary, some colors such as blues and violets come from scattering of light from highly ordered surface structures.[77] The structural details on surfaces can take an intricate and ordered combination of layers, scales, and ridges which are arranged to produce optical effects through the interference of light. Coloring through structural variations is an area of study in biomimetics. Furthermore, pigmentation itself is also an area of materials science interest, involving questions such as the origin of pigmentation, the nature of pigments, their size, distribution, and composition within the matrix, and their coloring effects.

In cuticles, there are both biomimicking and bioduplication possibilities for future materials formation. In the case of biomimicking, questions involve the types of structural units at the nano- and microscales, and their spatial distribution. There are already synthetic polymers that may be used as the matrix (such as diblock copolymers),[78] as well as fibrous polymers[79] that can be used as the stiff component. In the case of bioduplication, some subjects of future investigation are composition and spatial distribution of proteins in the matrix, their possible liquid crystalline order, and their synthesis. The nature of chitin, its molecular structure and composition, its structural relationship with the protein matrix, and overall hierarchy of the structure of cuticle will be further areas of biomimetic interest.

The examples of biological composites that contain both ceramic and biomacromolecular phase(s) vary in their form. They are mainly encountered as structural materials in skeletons or as protective covers over the bodies of organisms.[20,21] These include bones[80] in vertebrates, teeth[81] in fish and mammals, and shells in mollusks[20,21,82] One of these biological composites, namely the nacre section of mollusks, is discussed in detail in the rest of the chapter.

1.3 A BACKGROUND ON NACRE STRUCTURE

Nacre is a biogenic composite of a ceramic phase and macromolecules.[30,83-85] Its significance as a structural material stems from its excellent mechanical properties, such as fracture toughness and strength, which are comparable or better at room temperature than those of some high-technology structural ceramics.[83-85] This result is the major driving force in our quest for producing ceramic-based composites (cermets and cerpolys) with mechanical properties better than the existing ones.[30,85]

The major component of nacre is $CaCO_3$, a material with limited engineering value in the bulk form for structural applications (although it is heavily used as a filler in the powder form in cements, papers, paints, and plastics).[86] This unique structure is composed of alternating nanometer-scale laminated layers of thin biomacromolecular matrix and $CaCO_3$ (aragonite) platelets, all highly organized to produce an excellent multifunctional material (armor) for the organism.[83-85] Some of the other known facts about nacre include:[83-85,87-89] (i) the overall shell composite is more than 95 vol. %

inorganic material; (ii) the composite has a brick and mortar architecture with aragonite forming thin, hexagonally shaped multi-edged bricks[30,90] and an organic matrix that is a composite of proteins and polysaccharides (Figure 4);[90] and (iii) the inorganic phase consists of crystallographically highly oriented aragonitic platelets.[30,90i] If the desired synthetically laminated materials based on nacre are to be produced through biomimicking and bioduplication, further knowledge is needed about this unique structure. The areas of investigation may be divided into several categories: *(i) micro- and nanostructural variations*, including: (a) lattice and interface defect structures within the aragonitic phase, (b) composition and structural organization of the organic matrix, (c) interface structural and compositional relationship between aragonite and the organic matrix; *(ii) structure-property relationships*, including: (a) cooperative and separate structural responses of phases (aragonite, organic matrix, and interfaces) under various mechanical stresses, (b) toughening, strengthening, and hardening mechanisms, (c) size, lamination, and organizational effects (nanocomposite behavior and source(s) of multifunctionality); *(iii) biomineralization*, including: (a) identification of the active units within the organic matrix (nucleator proteins), (b) mechanism of self-assembly of the organic macromolecules (also of construction of framework macromolecules), and (c) mechanisms of nucleation and growth; *(iv) shape formation (morphogenesis)* including: (a) hierarchy in structural units and (b) growth mechanism of the shell (based on geometry, crystallography, and size); *(v) biomimicking*, including (a) detailed structural build-up of the shell from the molecular level to macro-scale and (b) its mimicry through novel materials processing strategies; and *(vi) bioduplication*, including (a) separation, purification, compositional (amino acid) and structural identification of each of the macromolecular units in the organic matrix, (b) cloning, reproduction, and self-assembly of structural macromolecules, and (c) processing new materials by using these macromolecules based on both biomineralization and morphogenesis principles. Answers to these questions will shed more light not only on the nanocomposite behavior of nacre but also on the mechanisms of its formation and particularly the degree of control that the organism has over the growth of this highly ordered biocomposite, and their use in the processing of future biomimetic materials.

Although discussed in our earlier papers, for completeness of this book, we begin with a summary analysis of the mechanical properties of nacre. A set of criteria is developed for the structural design of synthetic laminated composites. This is followed by a

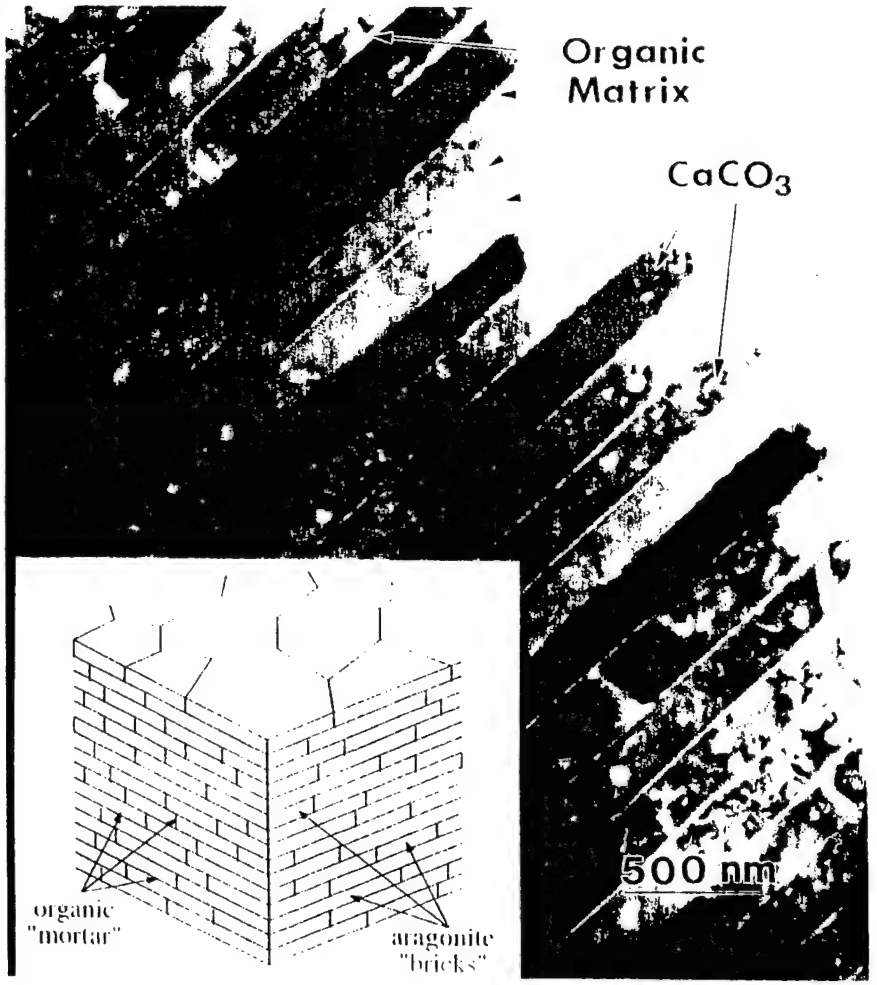

Figure 4. A cross-sectional image of nacre (edge-on configuration) of red abalone. The inset is a schematic three-dimensional view of the structure.

description of the current understanding of the structure of nacre in terms of morphology, composition, and crystallography. Its hierarchy is also discussed in both the hard and soft tissues that lead to a possible structural relationship between the organic and

inorganic components. Finally, an assessment is made of current knowledge, with possible directions, for future studies.

2.0 MECHANICAL PROPERTIES OF NACRE: A NANOLAMINATED CERAMIC-POLYMER COMPOSITE

Nacre structure is found in many families of mollusks, including abalone (*Haliotidae*) of the gastropod family, cephalopods such as nautilus (*Nautilus pompilius*), bivalves such as pearl oysters (*Pinctada*), and blue mussels (*Mytilus edulis Linne*).[91-94] A transverse cross-section of each of these shells displays two types of microstructures: an outer prismatic layer (calcite) and inner nacreous layer (aragonite). We focus our work on the structure and properties of the nacreous layer since this is the part of the shell that displays an excellent combination of mechanical properties as a result of its highly ordered laminated structure. We used mostly red abalone (*Haliotis rufescens*) because in this species the diameter and thickness of the shell containing the nacre are large enough to perform standard mechanical tests.[95] This allows a direct comparison of nacre with engineering structural ceramics and ceramic-based materials. Black-lipped pearl oyster (*Pinctada margaritifera*) shells were also used. Although relatively thin (1 to 5 mm), these shells are much more uniform through the thickness and relatively flat, and, therefore, exhibit less scatter in mechanical tests.

Red abalone samples were collected in Baja California, Mexico. The specimens were estimated to be 10 to 12 years old, had shell diameters of 25 to 30 cm, and shell thickness of about 1.5 cm, including the prismatic and nacreous layers. Mechanical properties in terms of fracture toughness (K_{IC}) and fracture strength (σ_F) in three-point straight notched and four-point bend bars, respectively, were evaluated in the transverse direction - perpendicular to the laminated layers through which a crack is normally expected to propagate in the shell of the mollusk in its natural environment.[96] Fracture toughness and fracture strength of nacre of both abalone and pinctada, and those of some of the well-known ceramics and ceramic-based composites (cermets) are plotted in Figure 5. The average K_{IC} and σ_F values of nacre are approximately 20-30 times that of geologically produced monolithic $CaCO_3$.[84,85]

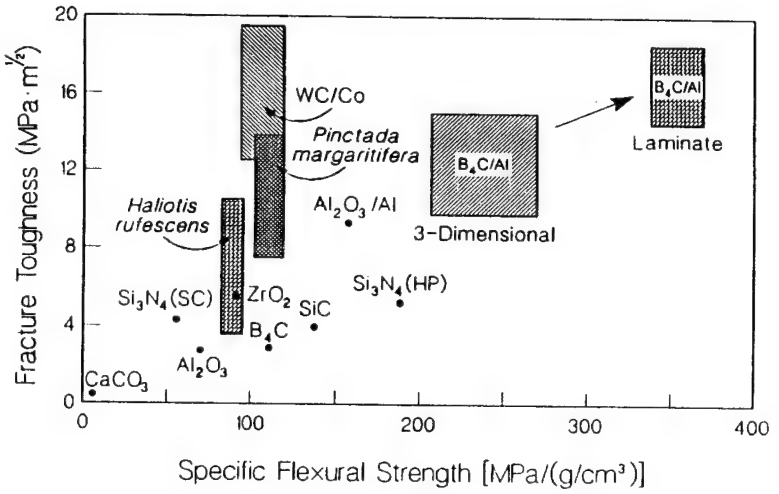

Figure 5. Mechanical properties of nacre of abalone and pinctada (pearl oyster) compared to some major ceramic and cermet materials.

The investigation on crack propagation behavior in nacre[84,85] reveals that there is a high degree of tortuosity not seen in the more traditional brittle ceramics, such as Al_2O_3 or in high toughness ceramics, such as in fiber-reinforced SiC[97] and particulate-reinforced ZrO_2[98] composites. The surfaces of fractured samples indicate that a major crack has meandered around the $CaCO_3$ layers resulting in a rough fractured surface, similar to that seen in fiber-reinforced ceramic composites where a pull-out mechanism operates.[99] Examination of micrographs recorded at higher magnifications indicates either sliding of the $CaCO_3$ layers upon organic matrix, suggesting the resolved stresses are lateral to the layers, or formation of organic ligaments between the layers, when the stresses are normal to the layers (Figure 6). The latter case, stretching, indicates that the interface between the organic and the inorganic phases is strong and that the organic phase acts as a strong binder.[84,85] Sliding, or bridging, of the macromolecular assemblages that make up the composite organic matrix under different modes of stresses is an excellent example of the unique quality of biological materials in terms of their structures and resulting properties. Several toughening mechanisms, therefore, may be proposed:[100] (i) crack blunting/ branching, (ii) microcrack formation, (iii) plate pull-out, (iv) crack bridging (ligament formation), and (v) sliding of $CaCO_3$ layers.

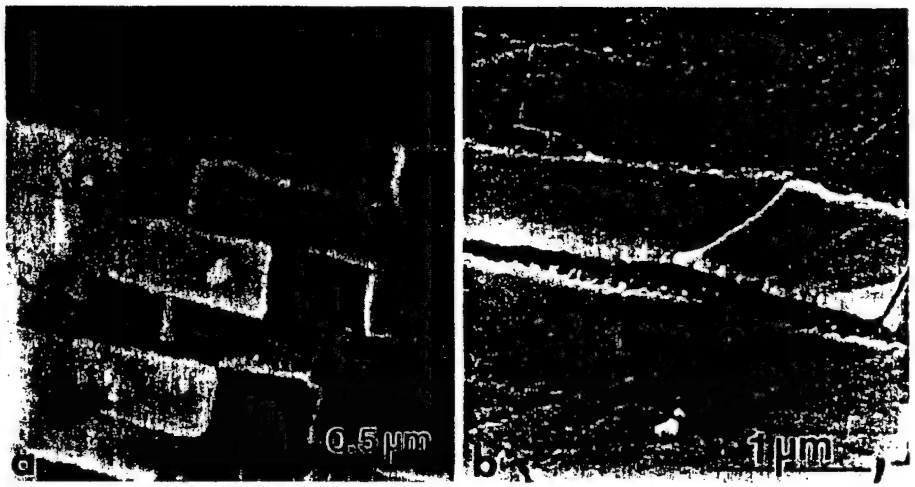

igure 6. SEM images recorded near an indentation performed on an edge-on configuration in acre of abalone. Either sliding of aragonite platelets (a) or ligament formation by the organic hase (b) takes place depending on the resolved applied stress (longitudinal and transverse, spectively). Both mechanisms are responsible for the high toughness of the nacre.

he high degree of tortuosity seen in crack propagation[85] may be due mainly to crack lunting and branching.[97,99] Tortuosity alone, however, is not a major toughening echanism in these composites, because it cannot account for the many orders of agnitude increase in toughness. The major toughening mechanisms, therefore, are iding and ligament formation.[85] Similarities exist between the deformation of a nacreous seashell[30,85] and a metal[101] in the sliding mechanism in terms of forming deformation bands in the bulk that appear as striations on the surface. It is likely that this complex deformation mode may be the main mechanism of energy absorption during the propagation of cracks, which needs to be further investigated quantitatively in terms of its energetics.

The strength of nacre, on the other hand, may be related to several factors, including the size and structure of the aragonite platelets and the interfaces between the inorganic and the organic components. From the limited thickness of the largest flaw (i.e., the thickness of the platelet) 0.5 μm, the increase in the theoretical fracture strength[102] of

aragonite would be about 200 MPa, comparable to the measured value of 185-220 MPa in our studies.[85] Therefore, the rule-of-mixtures[103] may account, at least, for part of the value of the measured strength.[83-85,100]

3.0 DESIGN GUIDELINES FOR PROCESSING BIOMIMETIC LAMINATED COMPOSITES

The lamination microarchitecture of present day impact resistance materials originates from ancient armor.[104] Biological structures, such as those in insects,[32] egg shells,[105] and sea shells[91-94] also have similar architectures, but at much smaller dimensional scale. In fact, the best armor has a double-architectural design in which the front section is hard, for the effective stopping of the projectile, and the back section is soft (but strong) for the absorption and dissipation of the kinetic energy from the projectile.[104] This is basically analogous to the shell of abalone. In cross-section, the hard front consists of long calcite crystals perpendicular to the shell plane (and in the direction of the projectile, ready to confronting it), and the back is tough nacre (laminated aragonite and organic matrix) as schematically illustrated in Figure 7 (also see Figure 10). In a ceramic/ceramic composite design, on the other hand, even in laminated architecture, weak interfaces are a necessary condition for increased toughness, with a sacrifice in the expected deterioration of the overall strength of the composite.[106,107] Contrary to the accepted materials design criteria in the role of interfacial strength in synthetic materials (as described in the previous section) in the structural design of biological materials such opposing effects are circumvented by the role of macromolecules due to their composite structures and resulting multifunctionality. Hence, there seems to be no need for a sacrifice in any of the properties, and therefore, both the toughness and the strength of the biocomposite increase, as seen in the laminated structure of nacre.

The unusual mechanical properties of nacre, absent in synthetic ceramics and composites, may, therefore, derive from: (i) the intrinsic properties of the constituent phases (brittle inorganic phase and soft organic matrix); (ii) the highly ordered organization of ceramic and biopolymer layers and their detailed structures, including the interface structures and properties; and (iii) the size of the ceramic and biopolymer layers which may be critical factors due to the intrinsic properties of biogenic aragonite and the organic matrix. Despite the fact that many of the structural features of abalone remain

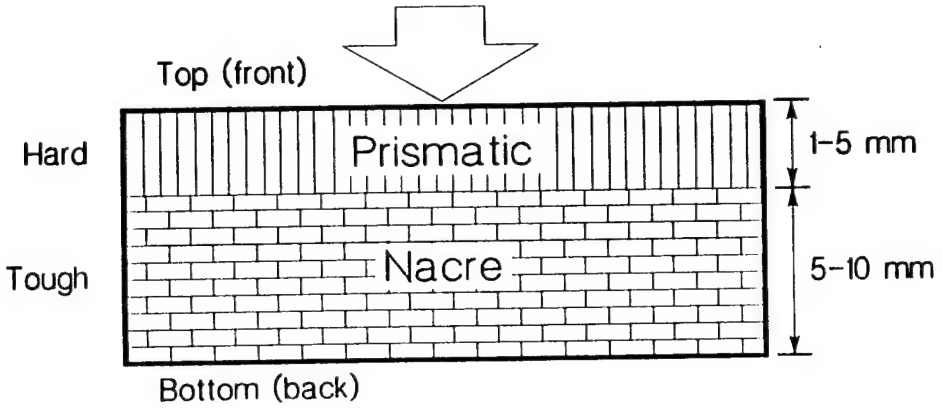

Figure 7. Schematic illustration of the cross-section of the abalone or pinctada shell, an ideal armor material with a hard front and a tough back.

a mystery (especially of the soft tissue), we can distinguish some guidelines using the knowledge of their excellent mechanical properties and structural architecture at the micro- and submicron levels to aid us in the processing of synthetic microstructures through biomimicking. Based on the previous studies of nacre,[30,85] the design of high-strength/high-toughness synthetic composites should incorporate the following:

(i) a laminate thickness of the hard and brittle component of less than 1 μm and a soft component of less than 100 nm, with an approximate ratio between 5:1 and 10:1

(ii) a highly plastic soft phase (deformability > 100 %)

(iii) strong interfaces between the soft and hard phases (so that the interface does not fail during crack propagation)

(iv) a soft phase able to bind to the surfaces of the hard component (strong interfacial bonding) and provide plasticity to the overall composite structure (for sliding and metal-like deformation behavior) or form ligaments to constrain crack opening (through crack bridging), depending on the state of resolved applied stress.

In actual processing of laminated composites, these guidelines may be difficult to apply. For example, there is currently no practical way to produce structural laminates with layer thicknesses thinner than about 10 μm[108,109] (except in *in-situ* laminates

formed through phase transformations in which overall architectural design is somewhat limited due to thermodynamics or kinetics limitations).[8] It is also difficult, if not impossible, to control the thickness ratio of the hard and soft components at these small dimensions. Nevertheless, the guidelines stated above, remain useful as they present the ultimate structural features. In the design of synthetic laminates, high hardness ceramics such as BN, B_4C, TiC, ZrO_2, and Al_2O_3 can be used as the brittle component. Highly plastic (superplastic) metals, such as Al and Cu (and their alloys), or organic polymers, such as polyethylene and polypropylene, may be good candidates for the soft phases. These constituent phases which give the best combination of properties, with emphasis on strong interfaces, could be used if they could be processed.

Some of the property requirements stated above have been met to a certain degree in the B_4C-Al[100,109] and B_4C-polymer[108] laminated systems designed for use as impact resistant materials. In one synthesis strategy for processing of B_4C-Al composites, porous B_4C layers with thicknesses below 100 μm, and as low as 15 μm, were tape-cast between thin sheets of Al. The stacks were heated to induce infiltration and to allow bonding between Al and B_4C without an excessive reaction. The resulting composite displays a structure in which both the Al-infiltrated B_4C and the alternating layers of pure Al form continuous films.[100,109] The overall architecture provides alternating layers of hard and soft components and strong interfaces. As a result, fracture toughness and fracture strength both show a 30 to 40 % increase over the isotropic B_4C-Al composite with the same phase ratios (Figure 6) in which Al and B_4C have a three-dimensional interpenetrating network.[100,109] The mechanical properties of B_4C-Al laminates, in terms of K_{IC} and specific fracture strength, are currently the best that can be achieved among the present cermet systems.

Despite the fact that improvements have been achieved in the mechanical properties of laminated composites based on biomimetic architecture, as in the example of B_4C-Al, these improvements have not yet come close to the superior properties of nacre over monolithic $CaCO_3$. This may be due primarily to insufficiently thin laminate layers. Thicknesses below 1 μm in the inorganic layers and below 100 nm in the organic layers (soft phase) are needed. Second, as will be clear from the discussion in the following section, both the inorganic and organic layers have complex structures, in terms of their crystallography, substructures, and morphology.

4.0 DETAILED STRUCTURE OF NACRE

In a layered composite design,[110] the most significant structural features are: (i) properties of the hard and soft components, (ii) interface structures and properties, (iii) thicknesses of the laminates and their ratio, and (iv) geometry of the lamellae. In the case of nacre, although many structural factors are known, some of the most significant questions are still unanswered. In nacre, for example, it is possible that the aragonite lattice may incorporate organic molecules.[90] If this is so, then the bulk properties (e.g., moduli) of the biogenic aragonite will differ significantly from those of geological aragonite.[30] As shown in Figure 8, biogenic aragonite contains a significant density of dislocations (in addition to other substructural features),[111] contrary to geological aragonite (an ionic crystal) in which dislocations could not be observed.[112] In nacre, the lamellae do not form simple continuous layers; instead the inorganic component, in the form of platelets (bricks), interrupts the continuity of a given layer with each platelet surrounded by a thin film of organic matrix. Even less is known about the composition and molecular and conformational structure of the organic matrix.[86,89,90,113-118]

Among all the features of nacre, the interface structure and properties are the least understood. Interfaces not only allow sliding of aragonite platelets and the formation of organic ligament under stress (both necessary conditions for the excellent properties), but they are also the sites of the nucleation and growth of the aragonite layers.[113-115,118,119] For these reasons, structural correlation of aragonite and the organic matrix deserve closer examination.

In the following sections we summarize the current understanding of morphological and crystallographic relationships among the structural components of nacre. First, we present an overview of these relationships between the inorganic building blocks. From this, we construct a model for the possible molecular conformation of the underlying organic matrix. We find that the model not only allows the crystallographic but also the morphological relationships among building units in nacre and forms a basis for shape formation and growth of the shell.

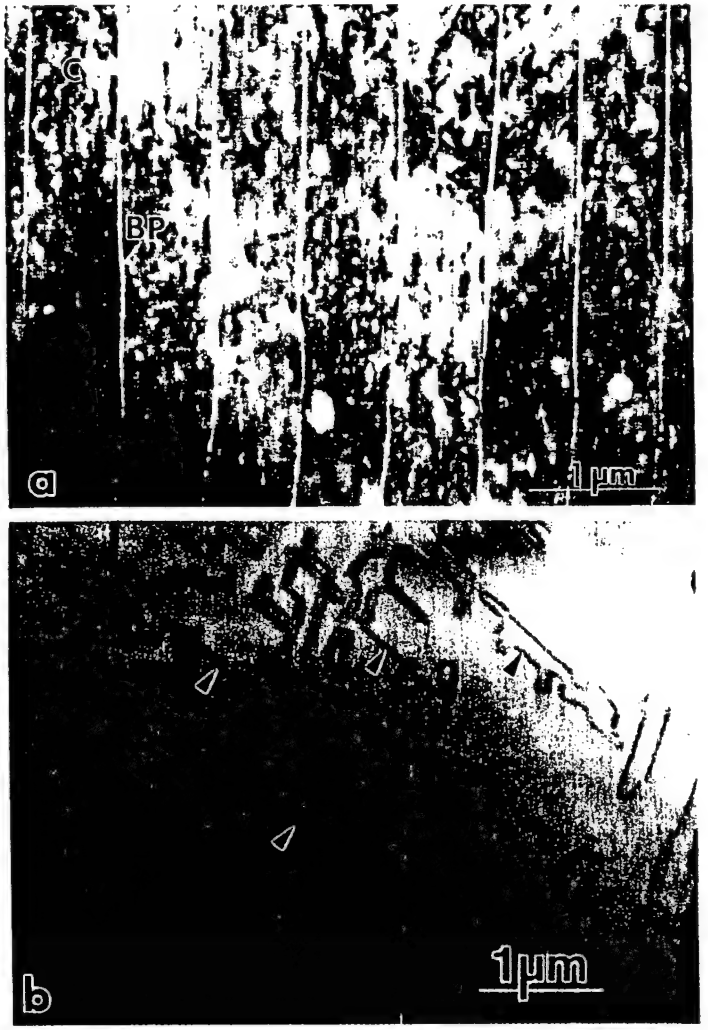

Figure 8. (a) Platelets of biological aragonite in an edge-on view of nacre of pinctada, and (b) geological aragonite (sample from Aragon, Spain) display substructural details. Note high dislocation density (in this orientation) in (a) but only antiphase boundaries in (b). [Twins in (a) are in face-on configuration and, hence, are not seen.]

4.1 STRUCTURE OF NACRE

Red abalone (*Haliotis rufescens*) belongs to the mollusk species in the family of gastropods. Gastropods first evolved about 500 million years ago, and, with little change, they have survived to the present time (abalone is, thus, considered a "living fossil").[21,91-94] The shell of the abalone is ear-shaped, with a large opening and a small spire (Figure 9). The shell has respiratory pores (about 20 in the adult) but only the last 4 to 5 are open at a given age. The organism has a large foot which, in the juvenile period, grabs onto a rock, allowing adult mollusk to forage for algae and plants on the bottom. Although other abalone species are much smaller, the shell of *H. rufescens* grows by about 2.5 cm per year and can reach 30 cm in diameter after which it only thickens (becoming more than a cm).

A longitudinal cross-section of the red abalone shell displays two types of microstructures: an outer prismatic layer and inner nacreous layer (see Figures 7, 9, and 10). Two forms of $CaCO_3$, calcite (rhombohedral, $R\bar{3}m$) and aragonite (orthorhombic, Pmnc), constitute the inorganic phase of the composite in the prismatic and nacreous layers, respectively. These architectures, especially the highly ordered inorganic component (aragonite platelets), are possible to study crystallographically with the aid of electron microscopy directly and in great detail. This is mainly because electron radiation damage poses less of a threat during the observation of the $CaCO_3$ crystals than does the organic matrix.

The structures of shells are seen in the SEM images in Figure 10, from the fractured surfaces of red-abalone and nautilus. The images display stacked platelets (aragonite) in nacre on the inner portion, and elongated crystallites (calcite) in the prismatic section on the outer portion. Platelets in nacre are typically arranged in either columns (abalone and nautilus) or sheets (pinctada). The stacking is not random and, in a fully grown specimen, resembles a brick and mortar architecture. The platelets vary in thickness; an average of 0.25, 0.4, and 0.5 μm in red abalone, nautilus, and pinctada, respectively, and edge length is 5-10 mm. Organic matrix is between 10 and 50 nm thick. The dimensions of the aragonite platelets and the organic matrix vary depending on the site of the shell from which the sample is extracted and the species of the mollusks.

Figure 9. Schematic drawing of (a) a top view and (b) an inside view of *Haliotis rufescens*.

4.2 STRUCTURE OF THE ORGANIC MATRIX

As described by other researchers,[90,119,120] the organic matrix is thought to be a composite of macromolecules stacked in a sandwich form. This is primarily based on indirect investigation of the characteristics of the biological macromolecules that are extracted from the shell through decalcification.[90,114,119,120] Macromolecules are divided into two groups: those soluble in weak acids, and those that are not.[90] In the former case, the proteins extracted were found to contain aspardic and glutamic acids (see references in Table-II). These amino acids are known to be major components of structural proteins that form sheet-like structures, such as in β-pleated sheets, that are found throughout the animal kingdom.[23] An extensive literature survey reveals the major amino acid compositions of the proteins in various species of mollusks given in Table-II. There is also speculation of the composition of the insoluble portion of the organic matrix, but it is probably much less accurate. It is possible, based on many investigations, that this portion of the matrix may constitute polysaccharides in addition to proteins (see Table-II).

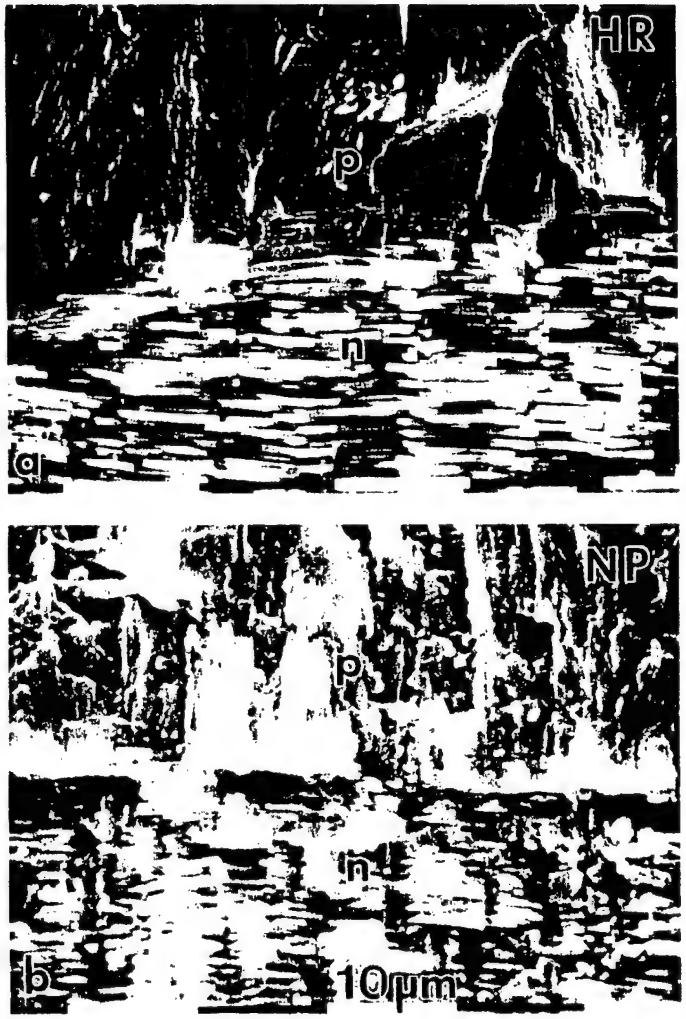

Figure 10. Images of fractured surfaces of abalone (a) and nautilus (b) exhibit both the prismatic (p) and the nacre (n) sections.

The major flaw in each of these studies has been that the macromolecules extracted from the shell have not been specific to a certain section in the shell. In fact, the shell is often pulverized, with both the calcitic (prismatic) and aragonitic (nacre) sections

intermixed before decalcification. The organic macromolecules are expected to have different stoichiometric compositions, and hence different conformations with respect to each other. These differences may, in turn, greatly affect the structure, crystallography, and the geometry of the inorganic crystals. The analysis which gives a mixture of all the biological macromolecules in a shell, therefore, has so far not been adequate in describing the true composition and the structure of the macromolecules that make up the nacre structure. (Several investigators - D. E. Morse,[121i] University of California, Santa Barbara, D. L. Kaplan,[121ii] Natick Research Center, ARO Lab, and C. E. Furlong, the University of Washington,[121iii] are working towards isolating macromolecules from different portions of the shell.)

Nevertheless, based on the findings so far, and limited direct analysis, the organic matrix may actually have a sandwich structure containing three organic sublayers, each with its own unique composition and molecular conformation.[114] According to this scheme, the central portion of the organic matrix is composed of chitin (polysaccharides), which is surrounded on both sides by β-pleated protein sheets. The layer next to the inorganic is then composed of acidic proteins. In this scheme, while the chitin provides the structural (mechanical) stability to the composite forming a backbone (framework macromolecules), the β-pleated sheets act as the substrate and provide the biomineralization sites (nucleator macromolecules). The acidic proteins are there to fill in the gaps between the organic matrix and the aragonite crystals. Neither the composition of these layers nor their structure has yet been clearly identified. The investigation of the structural relationship between the organic and the inorganic layers is, therefore, far from complete.[30]

Similarly, it may be possible to directly study the organic macromolecules in the TEM if proper molecular markers are developed.[122,123] For this, isolation of each of the major macromolecules from the organic matrix seems to be necessary. Once this is done development of antibodies and proper stains will follow. These stains can then be used in ultramicrotomed thin sections to identify locations and concentrations of each of the macromolecules. A preliminary work has been carried out to reveal the structures of the macromolecules in samples that are either ultramicrotomed or low temperature ion-beam milled.[124] Two such micrographs are displayed in Figure 11. Figure 11(a) reveals layered structure of the organic matrix in an ultramicrotomed section.[124]

Table-II. Amino acid compositions of the mollusk shells used in this study (table is made using the literature data)

		Asx	Thr	Ser	Glx	Pro	Gly	Ala	Val	Tyr	ref.
H. rufescens	W	25.0	?	10.2	8.2	?	48.5	4.52	?	?	i
	N	20.0	2.0	9.2	4.3	3.6	18.4	17.1	?	?	ii
	P	20.0	11.0	6.8	5.7	5.7	11.0	6.8	?	?	ii
N. pompilius	WI	7.1	1.3	9.8	4.5	0.5	35.3	25.0	1.4	0.6	iii/iv
	N	2.0	1.3	6.3	6.7	0.0	19.7	48.0	2.3	0.0	v
	NS	26.1	4.8	7.9	6.6	4.6	23.6	4.4	1.5	6.4	vi
P. margaritifera	P	9.4	2.9	3.9	2.2	5.6	22.3	3.2	?	5.5	vii

N: Nacre only; P: prismatic only; NS: nacre-soluble proteins; W: whole shell; WI: whole shell, insoluble only.

i. M. Cariolu and D. E. Morse, "Purification and Characterization of Calcium-binding Conchiolin Shell Peptides from the Mollusc, *Haliotis rufescens*, as a Function of Development," J. Comp. Biol. B, **157**, 717-729 (1988).
ii. N. Nakahara, G. Bevelander, and M. Kakei, "Electron Microscopic and Amino Acid Studies of the Outer and Inner Shell Layers of Haliotis rufescens," Venus, **41** [1] 34-46 (1982).
iii. M. F. Voss-Foucart, "Assais de solubilization et de fractionationnement d'une concioline (nacre mulare de *Nautilus pompelius*, mollusque cephalepode)," Comp. Biochem., **26**, 877-886 (1968).
iv. E. T. Degens, D. W. Spencer, and R. H. Parker, "Pleobiochemistry of Molluscan Shell Proteins," Comp. Biochem. Physiol., **20**, 553-579 (1967).
v. S. Weiner and L. Hood, "Soluble Protein of the Organic Matrix of Mollusk Shells: A Potential Template for Shell Formation," Science, **190**, 987-989 (1975).
vi. G. Goffinet and C. Jeuniaux, "Composition chimique de la function "nacrpine" de la conchioline de nacre de *Nautilus pompelius* Lamarck," Comp. Biochem. Physiol., **29**, 277-282 (1969).
vii. S. Tanaka, H. Hatano, and O. Itasaka, Biochemical Studies on Pearl. IX. Amino Acid Composition of Conchiolin in Pearl and Shell," Bull. Chem. Soc. Japan, 33, 543-545 (1960).
viii. H. Nakahara, M. Kakei, and G. Bevelander, "Fine Structure and Amino Acid Composition of the Organic Envelope in the Prismatic Layer of Some Bivalve Shells," Venus, **39** [3] 167-177 (1980).

The contrast difference is due to differential staining of the organic sub-layers by uranyl acetate due to their differences in composition and structure. A detailed structure of the interface between organic layer and aragonite is shown in Figure 11 (b). The image was taken from a sample that was low-temperature ion-milled and then slightly etched by gold citrate.[124] The preferential etching of the aragonite platelets gives them a saw-tooth appearance. The light acid used that causes this feature also dissolves away the acid soluble portion of the organic sublayers. As a result, central sublayers of the organic matrix are exposed. This is the part we think is made up of polysaccharides

since they are known to be resistant to such treatment. Further studies are underway to correlate these characteristic features related to the structures of aragonite and the organic matrix.

From the point of biomimetics it is essential to understand what the function of the organic matrix in nacre is in controlling nucleation of the inorganic crystals, their shape formation and growth. In future crystal engineering, in making nanostructures and laminated composites based on biological hierarchical composites using either synthetic or biological macromolecules, the first requirement is to understand the mechanism of inorganic-organic interactions in biological systems. Further detailed investigation, especially in a hard tissue like nacre having a relatively simple structure, appears to be well warranted. The following section attempts to address this issue.

4.3 CRYSTALLOGRAPHY OF ARAGONITE PLATELETS

Prior studies have postulated the crystallinity of the organic matrix that it contains chitin and silk fibroin-like proteins as the outer and middle sublayers of a sandwich structure and that these macromolecules are known to self-assemble in crystalline arrangements.[90,114-115,119,120] The outermost sublayer in the organic matrix, the one in contact with $CaCO_3$, consists mostly of soluble charged macromolecules (proteins) and presumably acts as the binder to the inorganic phase. This scheme suggests that active sites on the matrix align with those on the $CaCO_3$, i.e., either Ca^{2+} ions[90,114] or CO_3^- sites (ionotropy mechanism).[113,119]

It has been impossible to study both the organic and inorganic crystals simultaneously, and the structural relationships between the components of the nacre exist only as a conjecture.[90,113-115,119,120,125-128] Bulk studies, performed by X-ray diffraction, on the nacre revealed that the aragonite platelets are organized with their [001] axis perpendicular to the layers.[90,114,128] It has been postulated that the axes within the layer plane in each platelet are oriented randomly.[90,114] Furthermore, it was assumed from this scheme that each aragonite platelet grew on the crystallographically related organic template, which itself has a local random orientation.[90] From the composition of the insoluble fraction of the organic matrix, i.e., the inner crystalline sublayers which contain a high fraction of aspartic and glutamic acid, it might be possible to deduce a self-

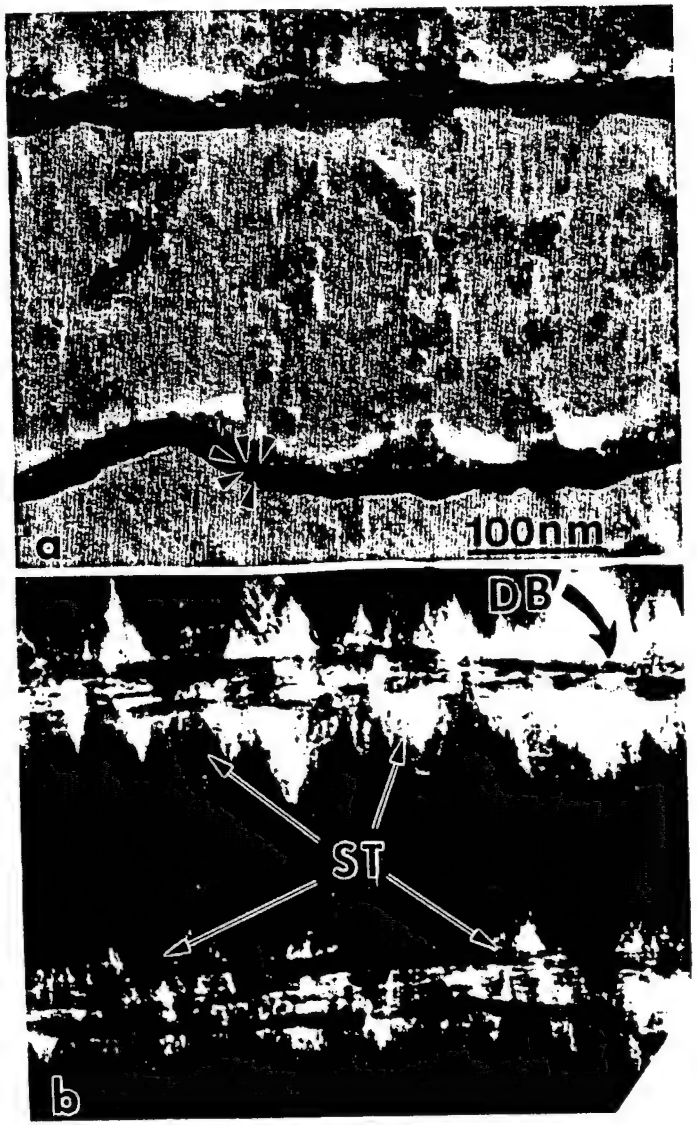

Figure 11. Structure of the organic matrix in nacre of abalone. The sample in (a) was ultramicrotomed, decalcified, fixed, and stained. Five sublayers (arrows) are exposed in the organic matrix, possibly due to their differential staining. The image in (b) was taken from an ion-beam milled sample that was slightly acid etched. It reveals insoluble (central) portion of the organic layer DB (dark bands) and the saw-tooth (ST) appearance of the etched aragonite/matrix interface.

assembled structure that would be related commensurately to the aragonite lattice along the [001] projection.[90,114,120,128]

In the present work, each aragonite crystallite was analyzed by electron diffraction separately and its crystallographic orientation relationship was established with respect to its neighbors, both on the same layer and across the thickness of the nacre, hence, enabling us to complete a three-dimensional picture.[30] First, we found that adjacent platelets on the same layer belong to the same [001] zone axis with a slight rotation among them. The question whether there is any crystallographic relationship between the a and b axes of platelets on the same layer was also answered; we found that they are twin-related with a twin plane of {110} type.[30] In this scheme, all of the platelets on the same layer are twin-related whether they share a boundary or not, constituting *first generation twins* since this twinning takes place at the highest spatial scale [Figure 12 (a-b)]. Further analysis indicated that each platelet consists of several domains which are crystallographically related (Figure 12 (c-f)). The diffraction patterns from all the domain boundaries show twin reflections with domains belonging to either (110) or (110) variant. Adjacent domains, therefore, are twin related and constitute the *second generation twins*.

The angle between each pair of domains in an ideal hexagonally-shaped platelet with six twin-related domains would be 60°. This is not possible, however, since the outer edges of the platelets are parallel to {110} planes. The angle between each pair of planes - for example, between (110) and (110) - is 63.5°; this leaves a 3.5° unaccounted for. This induces strain into the aragonite lattice and must be accommodated by some structural deformation, such as, by slip or twin formation. In the present case, nanometer-scale twins form on {110} planes, shown in Figure 12 (g), that are similar to the growth twins in geological minerals. Since they occur at the smallest scale, we refer to them as the *third generation twins*.[30] (A portion of the lattice stress created by the 3.5°-strain can also be accommodated by the misalignment of adjacent domains, as frequently observed. This misalignment, however, cannot account for all the strain accommodation, as the interfaces between the domains show a high degree of coherency.) These three twin structures cover a size scale of six orders of magnitude, from the nanometer to the submillimeter, and reveal, for the first time, a hierarchical structure in a biological hard tissue.

Figure 12 (a-g). TEM images reveal crystallographic relation between aragonite platelets and domains. Images in (a) and (b) reveal that A-C-E are twin related to B-D-F, as confirmed by electron diffraction (image recorded with a slight tilt about the [001] axis that is normal to the plane of the paper).

4.4 THE CONFORMATION OF ORGANIC MACROMOLECULES

The interaction between the species on an organic substrate and a crystalline organic phase must include geometrical, electrostatic, and stereochemical interactions.[113-115,119,120,127-131] Therefore, the nucleation and growth of the crystals will be influenced by both the nearest neighbor interactions and those higher on the scale. The aragonite crystal structure belongs to the space group Pmcn (No. 62) with lattice parameters a = 4.94 Å, b = 7.94 Å, and c = 5.72 Å.[132] The location of Ca^{2+} ions in [001] projection is shown in Figure 12(a) giving the crystal a pseudo-hexagonal symmetry. In the unit cell, CO_3^- groups would reduce the symmetry to an orthorhombic form.[132] This is an important physical characteristic in terms of the crystallographic relationships of the hierarchical twinned components of the nacre aragonite and the stereochemical relationship that might exist between the aragonite and the macromolecules in the organic matrix.

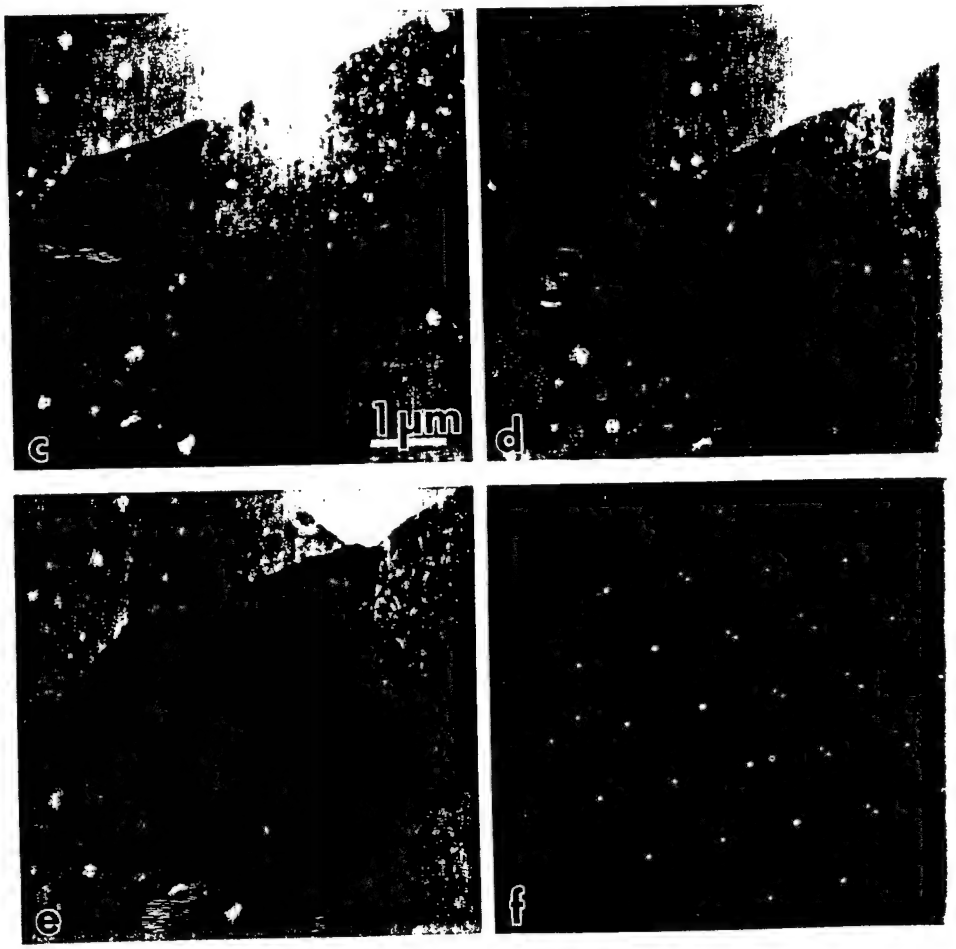

Figure 12 (cont.). Images in (c) and (d) are from a platelet in (e) containing four domains. [001] diffraction pattern (f) taken from a domain boundary in (e) reveals that the domains are twin related.

The nucleation and growth of the aragonite crystals may involve both Ca^{2+} and other ions, but for simplicity, only the arrangement of Ca^{2+} ions is illustrated in Figure 13. True hexagonal closed-packed formation would require an axial ratio of b/a = 1.63; however, the observed value is only 1.69. In the actual aragonite lattice, the Ca^{2+} ions are not in contact but are separated by O^{2-} ions, and the pseudo-hexagonal arrangement refers to the centers of Ca^{2+} ions rather than their actual packing. Since the same {110

twinning takes place at all length scales, superimposition of the lattices on all three possible twins with a 63.5° angle with respect to each other generates a new superlattice structure based on the coincidence lattice sites (CLS)[133] and is called *superstructure*[30,134] (Figure 13(c)). Taking the actual distance between the Ca^{2+} ions as 3.94 Å, the calculated distance between these lattice points would be about 30-40 Å. If the nucleation and growth of the aragonite platelets takes place on the underlying organic matrix, then the geometric configuration of the active sites for binding Ca^{2+} ions on the organic matrix must accommodate this superlattice and thus all twins in the nacre. To explain this phenomenon, we assume that the binding sites on the template form a single crystalline pseudo-hexagonal lattice, or integer multiples of it. Many two-dimensional membranes tend to form hexagonal lattices during self-assembly.[135] This hypothesis (that the organic matrix may be a single crystal) is an essential structural feature for the formation of the highly organized platelets in nacre.[30,134] The local crystalline organization of the matrix proposed earlier,[90,114] with no relationship between the neighboring areas and therefore no long-range order, would result in aragonite crystals with no definite crystallographic orientation relationships.

By tracing the possible twin boundaries, the superlattice allows the generation of the hierarchical twin structure and all the shapes, geometry, and crystallography-related features, including five-edged platelets with 90°-domains, sixfold symmetry of platelets, and six- and three-edged domains.[30,134] The fact that one can generate all the possible configurations in this way illustrates again that a pseudo-hexagonal template structure (and not the lattice of a single domain) might be a possible solution for the structure of an organic matrix that can accommodate all the twin relationships. The ultrastructure in the organic matrix would be single crystalline not only on the flat surface but also through the transverse direction of nacre as demonstrated from the twin orientation-relation of the crystals across the thickness direction as well.[30] The platelets do not leave space when packed on a given layer because of the crystallographic and geometrical requirements, hence called *space filling tiles*. The tiles (aragonite platelets) can have several different edges (3-, 4-, 5-, and 6-edged) but still have regular shapes. Based on a mathematical description,[136] we call them *multiple tiles*.[137] Since the tiles also have domains at lower dimensional scale, we can call the configuration of the tiles within the nacre in three-dimensional space as multiple tiling with hierarchical twins.[137]

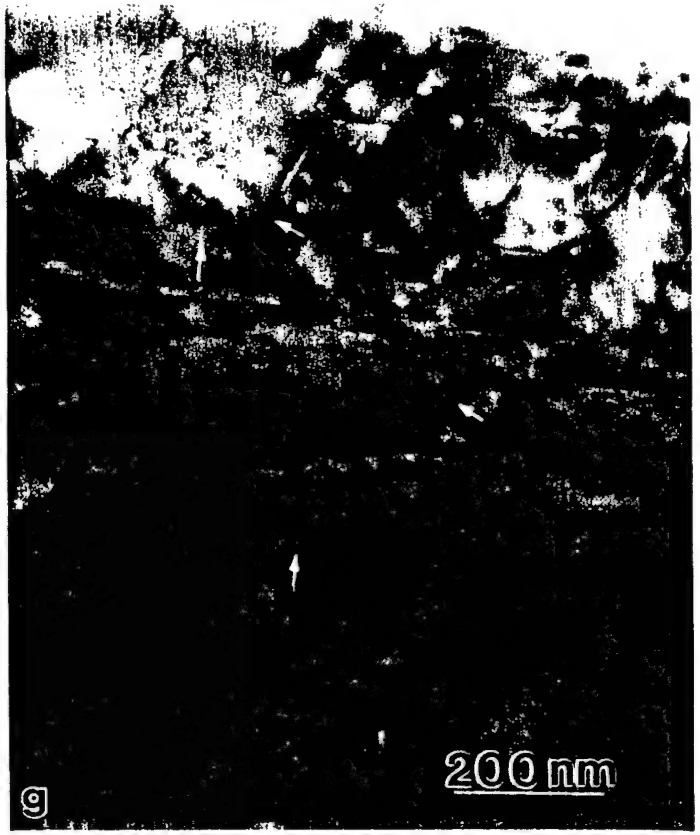

Figure 12 (cont.). (g) Bright Field image taken in [001] orientation shows the ultrafine twins on two {110} variants within a domain.

5.0 GROWTH AND SHAPE FORMATION OF THE SHELL: MORPHOGENESIS

Although six-fold twin structures also occur in geological aragonite,[111] the hierarchical arrangement in nacre is unique in that each platelet is separated from the others during the early stage of growth.[134,137] This is illustrated in Figure 14 which shows the layers of aragonite are separated on the growing edge of the shell by a thin film of organic matrix, and the new platelets grow on it independently. In geological aragonite, by contrast, the mimetic twin domains grow in contact, one after the other, and each is influenced by the presence of another.[111,112] In nacre, however, even after crystalliza-

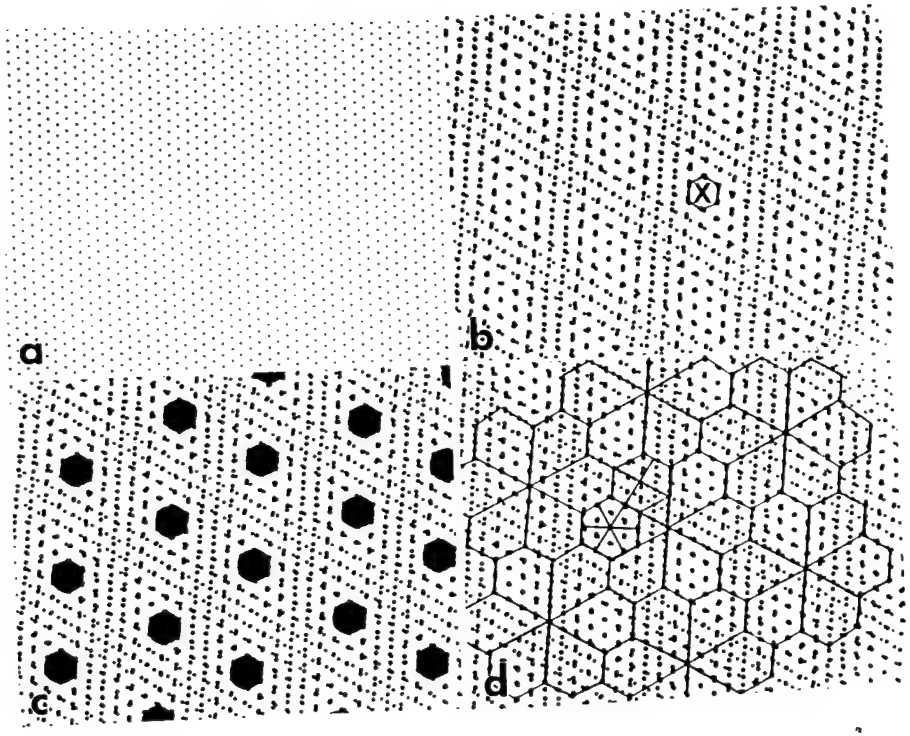

Figure 13. (a) The model of the aragonite lattice in [001] projection with only Ca^{2+} ions highlighted. (b) Superimposition of three lattices each with a successive rotation of 63.5° (angle between {110} planes) produces a Morié fringe pattern. (c) Highlighted coincidence lattice sites produce a pseudo-hexagonal pattern. (d) Platelets, which retain the crystallographic and morphological relations, can be drawn based on the CLS model.

tion is complete, the platelets remain separated from each other by an organic membrane.[132] The fact that separate platelets grow simultaneously and, yet, have a definite crystallographic orientation relationship suggests that the growth process might be mediated by the organic template beneath each of the individual crystals, as proposed earlier.[114,115,119,120]

As can be determined from Figure 14, which was recorded from the growth edge of a juvenile abalone, the organic membranes actually form layers of sheet with an empty

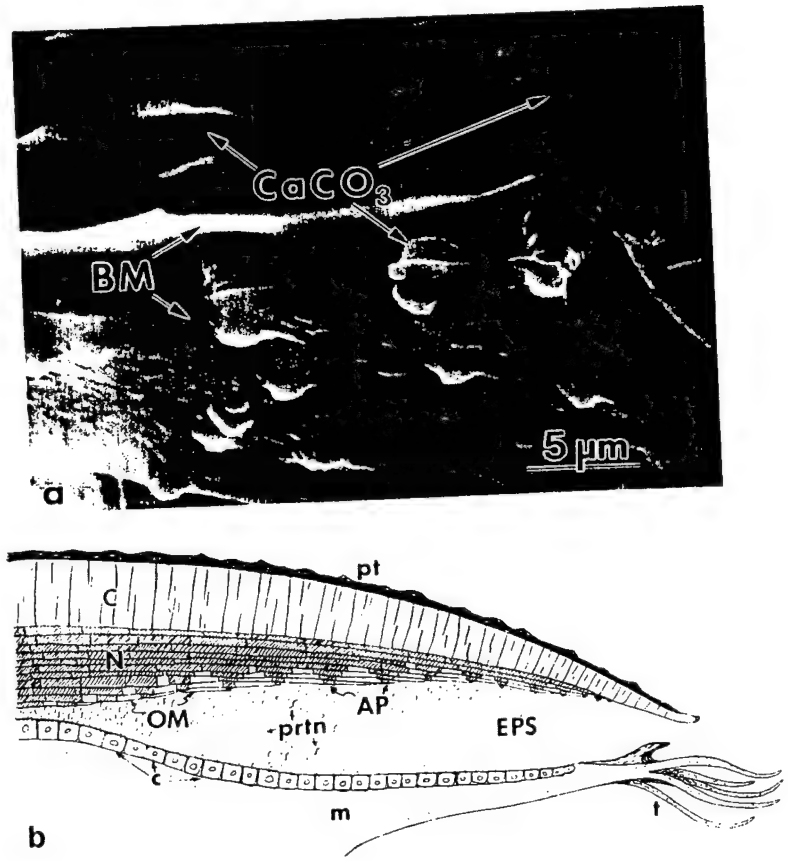

Figure 14. (a) Secondary electron image of the growing edge of a juvenile red abalone in an edge-on view shows organic matrix (BM) between the newly forming aragonite platelets ($CaCO_3$) in a columnar organization. Notice the bottommost organic layer with newly formed aragonite nuclei. (b) A schematic drawing illustrates the growing edge of the abalone shell. C: prismatic layer; N: nacreous layer; EPL: extrapallial space; pt: periostracum; c: cells; prtn: self assembling proteins and polysaccharides; m: muscle of the foot; t: tentacles, OP: organic matrix; and AP: aragonite platelets.

layer occasionally separates into several sublayers, and this is repeated for many layers, seemingly in a random fashion, throughout the thickness. This suggests a hierarchical organization of the organic membrane as well. The production of further organic layers originating from a single membrane also has significant implications in terms of the mechanism of self-assembly of the macromolecules that make up the framework of the organic matrix. Although attempts have been made,[119,126,135-137] a clear description

explaining how the successive single layers form in the nacre, or any other hard tissue has not been established. The best description so far has been the presence of compartments which would initially form as small boxes on top of the older and much larger ones. These would then eventually grow as the inorganic crystallites form within them. In this "compartmentalization" scheme, it is not clear how the layers actually come into being in the first place and how each compartment would form and be enlarged.

In contrast, we show that successive layers form from an original membrane as subsidiary layers, which would themselves act as originators of further subsidiary layers in a cascading fashion.[137] This mechanism is similar to the reproduction of cells in organisms in making new cells and subcellular features (such as organelles). If this scheme is correct, then the layers must be in closer scrutiny by the organism than what has been hitherto thought as merely being formed through self-assembly. In other words, the cell membrane formation is a further step up in the hierarchy of making cells than the self-assembly of macromolecules which is a quaternary step in the organization of macromolecules in organisms, such as protein clusters, or structural polysaccharides. It can also be noted, in this case, that both proteins and polysaccharides are thought to be present in the organic matrix structures, adding more evidence that the organic matrix might be a membrane in the sense of physiological terms. A membrane therefore, having proper proteins in their respective locations, both within the composite layers of the organic matrix and on certain locations of the membrane surfaces, would serve the function of being structural proteins, and of transport proteins regulating the passage of the inorganic ions in and out of the membrane for the formation of $CaCO_3$ on the surface. This description on the formation and the function of the organic matrix as, what we will call, a *pseudomembrane*,[137] is conjectural and requires further study. These studies would be essential to find the true nature of structures and growth of hard tissues.

The shapes of many mollusk shells can be described mathematically by a helicospiral.[138,139] This is demonstrated schematically in Figure 15(a) for abalone shell. In two-dimensions (x-y plane) the equation of the spiral is: $r = ae^{\phi}$ where r is the radius of the spiral at any position of the angle ϕ, a is a constant specific to a species of the mollusk. The depth is given to the shell by a variation in the third dimension, z. What

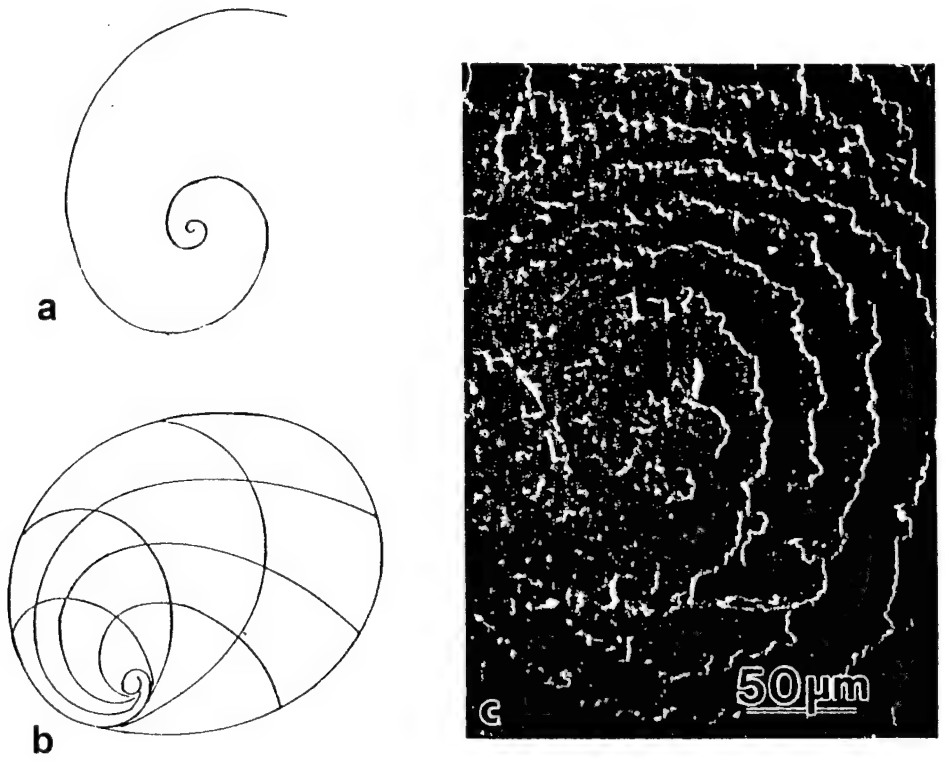

Figure 15. (a) Logarithmic spiral. (b) A schematic illustration of growth spirals of abalone shell. (c) Local spirals of aragonitic platelets in nacre (secondary electron image).

has not been recognized so far, neither by biologists nor by mathematicians, however, is the possibility of the design of the overall shape of the shell based on the underlying organic matrix within the hard tissue.[138,139] This design may be a result of the structural interrelationship between the crystallography of the aragonite lattice and the crystallographic conformation of the Ca^{2+}-binding (or CO_3^- -binding) matrix nucleator proteins. For instance, assuming that macromolecular conformation based on the proposed superstructural model above provides a template for the $CaCO_3$ formation, then the growth of an individual aragonite platelet follows a spiral [Figure 15(b)]. This growth scheme may allow adjacent platelets to grow in a spiral manner, as demonstrated in the SEM image in Figure 15(c). Spiral growth of platelets in local

regions along and behind the growing edge of the shell would lead to the growth of the shell at hierarchically higher scales, eventually leading to the final specific shape of each of the mollusk species. In this proposed growth scheme, the overall morphology of the shell is designed at the molecular scale by the organic matrix.[137] In terms of biomimetics, this hypothesis, if proven correct, may have implications in net-shape formation of technological ceramics, and, therefore, constitutes another important area of future investigation.

6.0 SUMMARY AND FUTURE DIRECTIONS

We have reviewed the results of some of the recent studies on mechanical properties and structure of the nacre section of mollusks. Nacre, which is about 95 vol. % aragonite and about 5 vol. % organic macromolecules, has fracture toughness and fracture strength properties that are orders of magnitude higher than those of monolithic aragonite. The inorganic and organic components in nacre have a high degree of organization not encountered in synthetic materials. From our analysis of toughening and strengthening mechanisms, we conclude that the unique structure of nacre is responsible for these superior properties. The current understanding of these toughening and strengthening mechanisms, and their relation to the sizes of the component phases, is far from complete.

Morphological and crystallographic analyses by electron microdiffraction of the inorganic phase biogenic aragonite indicate that the individual aragonite platelets in nacre form a multiple tiling system in which twins form hierarchical defect structures to control the overall structural order. Assuming that crystal-matrix recognition is applicable, a model is forwarded for the structural conformation of the active sites in the organic matrix which may then act as the template for the formation of nacre. This model, called the *superstructure*, explains all the experimentally observed crystallographic and morphological relationships in the aragonite phase. The geometric and crystallographic model of aragonite platelets proposed in this review is referred to as *multiple tiling*. It appears that nature utilizes this technique in nacre to form a highly ordered structure compatible with both the soft component and the crystalline and geometrical structural constraints of the hard component. Tiling may also play an important role in determining the overall shape formation of the nacre and its mechanical properties. Many mollusks species, such as gastropods, cephalopods,+ and bivalves have aragonite platelets as the fundamental building blocks in their nacre, but they also have grossly different overall shapes. In red abalone, for example, the shell is quite flat and thick; in nautilus, the shell is round and thin and forms an elegant chambered structure in which even the separation walls of the chambers are made of nacre. In all these nacre structures, the aragonite platelets have more or less the same dimensions, about 0.2 to 0.8 μm thick and 5 to 10 μm long on the edge. On the other hand, the multiple tiling of the platelets and the crystallographic relationship between the platelets may differ in these organisms due to slightly different structures and compositions in their underlying organic matrices. Further studies on various species of these organisms of both the crystallography of the mineral component and the structural and compositional analyses of the organic matrices, are warranted if we are to discern their structures and the unifying, underlying principles for the organization and formation of the various shapes of shell containing nacre structures. A fundamental understanding of these structures is essential for the possible formation of synthetic composites through biomimetics.

This new approach, in which the structure of an organic material is indirectly deduced from a detailed knowledge of the structural relationships among the subcomponents of the inorganic phase, may prove a viable approach for studying other biocomposites that also have a highly organized inorganic structure. This approach would serve as a new methodology, not only for studying the way the overall shape is determined in various species of mollusks, but also for understanding general biomineralization concepts in single and multicell organisms, including bone and teeth in higher organisms.

Despite considerable effort in the field, our understanding of the mechanisms that operate in nacre to create such a tough composite, and of the composition and structure of the organic matrix and its structural relationship with the inorganic phase are still limited. Some of the major issues, from which an agenda for future research may be drawn, are as follows:

(i) *On Mechanical Properties.* A quantitative understanding of the toughening and strengthening mechanisms in nacre is necessary because these mechanisms depend upon the structural relationships of the organic and inorganic phases. Mechanical property

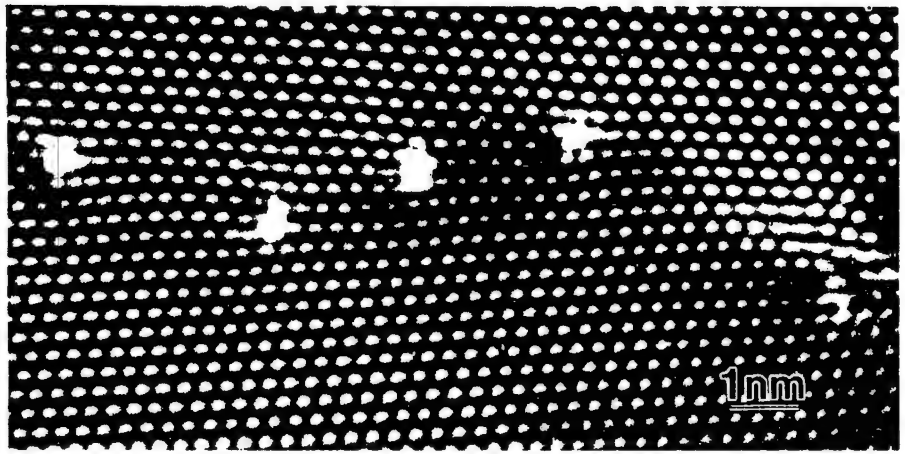

Figure 16. Atomic resolution transmission electron image of a low-angle boundary in biogenic aragonite in nacre of abalone displays dislocation core structures in the [001] electron beam direction (recorded at 400 kV). Although it is unusual for aragonitic lattice, as an ionic crystal, to have such defects, they are common substructural features in biogenic aragonite crystals.

evaluation of the overall shell, particularly under the dynamic conditions in which the organism lives and makes use of its multifunctional characteristics, is also essential for the design of multifunctional materials through biomimicking. Future research should include proper testing techniques for measurement including interfacial properties, analysis of paths for crack propagation, and their micromechanical analyses. For this, the knowledge of actual properties of the individual phases (organic matrix and biogenic aragonite) is essential, which, in turn, requires careful analysis of true structures [substructures and defects (Figure 16)] and compositions of the component phases. The coupling between the component phases and their size (size-effect) and conformation (crystallography) need to be studied to reveal sources of nanocomposite effects.

(ii) *On the Organic Matrix.* The protein and polysaccharide compositions in nacre, their conformations, identification as nucleator and framework macromolecules, and structural relationships of the organic matrix as well as its relationship to the inorganic aragonite phase are necessary parameters for consideration in the design of synthetic materials. The relationship between the organic matrix and calcite in the prismatic

layer should also be investigated.

(iii) *On the Mechanism of Growth and Morphogenesis.* An investigation of the nucleation of the inorganic phase in the presence of an organic matrix, beginning at the embryonic and juvenile stages of the mollusk and comprehension of the degree to which the organic matrix controls growth will assist the understanding the overall formation and shaping of the shell.

(iv) *On Biomimicking.* New synthetic strategies are necessary to process thinner ceramic, metal, and polymeric layers for ceramic-metal and ceramic-organic composites with controlled substructures and interfaces, controlled lamination to achieve novel layered composites with desired architecture.

(v) *On Bioduplication.* Fundamental studies involving *in vitro* isolation, purification, and self-assembly of various components of the shell organic matrices, separately and in combination, are essential as the ground work. These would be followed by biomineralization of $CaCO_3$ and other biogenic ceramics on biogenic or engineered organic matrices under controlled conditions leading to a fundamental understanding of how the synthesis and structural evolution of hard biological structures might be controlled. Finally, these studies would open up new avenues in biduplication of technologically more significant ceramics, such as Fe_3O_4 and $BaTiO_3$, in various morphological forms (particles, platelets, laminates, and thin films).

Both biomimicking and, eventually, bioduplication may prove invaluable tools for materials engineers. Using these methods to design and process novel materials similar to biogenic multifunctional, nanolaminated composites like nacre, however, will be deferred until we answer the crucial questions discussed regarding the structure and function of this and other similar biocomposite systems.

7.0 ACKNOWLEDGEMENTS

This work was performed under the sponsorship of Air Force Office of Scientific Research under Grant # AFOSR-91-0281, and Army Research Office, Grant # DAAL03-92-G-0241.

8.0 REFERENCES

1. See, for instance, i. P. Haasen, *Physical Metallurgy* (Cambridge University Press, London, 1978); *Ceramic Microstructures*, R. M. Fulrath and J. A. Pask (eds.) (John Wiley and Sons, New York, 1968); ii. *High Performance Polymers*, E. Baer and A. Moet (eds.) (Hanser, Munich, 1991).

2. i. Nippon-to no kagateki kenkyu, K. Tawara (Tokyo, 1953); ii. H. Tanimura, "Development of the Japanese Sword," *JOM*, 32 [2] 63-73 (1980); iii. *A Search for Structure*, C. S. Smith (MIT Press, Cambridge, 1981) pp. 66-72; iv. O. D. Sherby, T. Oyama, D. W. Kum, and J. Wadsworth, *JOM*, **37** [6] 50-56 (1985).

3. R. P. Anders et al., "Research Opportunities on Clusters and Cluster Assembled Materials," *J. Mater. Res.*, **4**, 704-496 (1989).

4. See, for instance, *Decomposition of Austenite by Diffusional Processes*, V. F. Zackay and H. I. Aaronson (ed.) (Interscience, New York, 1962).

5. *Phase Transformations in Metals and Alloys*, D. A. Porter and K. E. Easterling (Van Nostrand Reinhold, Berkshire, UK, 1981) Chap. 5.

6. i. G. S. Kreimer, *Strength of Hard Alloys* (Consultants Bureau, New York, 1968) pp. 1-30; ii. H. E. Exner and J. Gurland, "A Review of Parameters Influencing Some Mechanical Properties of Tungsten Carbide - Cobalt Alloys," *Powder Metallurgy*, **13**, 13-31 (1970); iii. H. C. Lee and J. Gurland, "Hardness and Deformation of Cemented Tungsten Carbide," *Mater. Sci. Eng.*, **33**, 125-133 (1978).

7. *Superalloys*, M. Gell, D. H. Duhl, and A. F. Giamei (ASM-International, Metals Park, OH, 1980).

8. i. D. Baral, J. B. Ketterson, and J. E. Hilliard, "Mechanical Properties of Compositionally Modulated Cu-Ni Foils," *J. Appl. Phys.*, **57** [4] 1076-1084 (1985); ii. Anomalous Increase in the Strength of In-Situ Formed Ultrafine Cu-Nb Multifilamentary Composites," *J. Appl. Phys.*, **49** [12] 6031-6038 (1979); iii. *Metallic Superlattices*, T. Shinjo and T. Takada (eds.) (Elsevier, Amsterdam, 1987).

9. See, for instance, *High Temperature Superconductors: Relationships Between Properties, Structure, and Solid-State Chemistry*, J. D. Jorgensen, K. Kitazawa, J. M. Tarascon, M. S. Thomson, and J. B. Torrance (eds.) Proc. MRS, Vol. 156 (Materials Research Society, Pittsburgh, 1989).

10. J. F. Scott and C. A. Paz de Araujo, "Ferroelectric Memories," *Science*, **246**,1400-1405 (1989).

11. i. R. Bringer, U. Herr, and H. Gleiter, "Nanocrystalline Materials - A First Report," *Trans. Jap. Inst. Metall.*, Suppl., **27**, 43-52 (1986); ii. *Microclusters*, S. Sugano, Y. Nishina, and S. Ohnishi (eds.) (Springer and Verlag, Amsterdam, 1987); iii. L. E. Brus, "Semiconductor Crystallites," *Acc. Chem. Res.*, **23**, 183-188 (1990).

12. See, for instance, *Layered Structures, Epitaxy, and Interfaces*, J. M. Gibson and L. R. Dawson (eds.) Proc. MRS ,Vol. 37 (Materials Research Society, Pittsburgh, 1984).

13. See, for instance, *Epitaxial Heterostructures*," D. W. Shaw, J. C. Bean, V. G. Keramidas, and P. S. Peercy (eds.) Proc. MRS, Vol. 198 (Materials Research Society, Pittsburgh, 1989).

14. See, for instance, i. R. T. Bate, "The Quantum Size Effect: Tomorrow's Transistors," *Scientific American*, **258** [3] 96-106 (1988); ii. *Clusters and Cluster-assembled Materials*, R. S. Averback, D. L. Nelson, and J. Bernhole (eds.) Proc. MRS, Vol. 206 (Materials Research Society, Pittsburgh, 1991); iii. *Microclusters*, S. Ugano, Y. Nishina, and S. Ohuishi (eds.) (Springer and Verlag, Heidelberg, 1987).

15. *Smart Structures and Materials*, 1993 North American Conference, Albuquerque, New Mexico, U.S.A., Jan. 31 - Feb. 4, 1993.

16. R. E. Newnham and G. R. Rushan, "Smart Electroceramics," *J. Am. Ceram. Soc.*, **74** [3] 463-480 (1991).

17. See for instance, i. *Materials Research Bulletin*, **12** [3] (1987); ii. R. E. Newnham, S. E. McKinstry, and H. Ikawa, "Multifunctional Ferroic Nanocomposites," in: *Multifunctional Materials*, A. J. Buckley, G. Gallagher-Daggitt, F. E. Karasz, and D. R. Ulrich (eds.) Proc. MRS, Vol. 175 (Materials Research Society, Pittsburgh, 1990) pp. 161-168.

18. E. Baer, A. Hiltner, and R. J. Morgan, "Biological and Synthetic Hierarchical Composites," *Physics Today*, October, 60-67 (1992).

19. *Mechanical Design in Organisms*, S. A: Wainwright, W. D. Briggs, J. D. Currey, and J. M. Gosline (eds.) (John Wiley & Sons, New York, 1976).

20. J. D. Currey, "Biological Composites," *J. Mater. Edu.* **9** [1-2] 118-296 (1987).

21. i. *Biomineralization*, K. Simkiss, and K. M. Wilbur (Academic Press, New York, 1989); ii. *On Biomineralization*, H. A. Lowenstam and S. Weiner (Oxford University Press, New York, 1989); iii. *Biomineralization: Chemical and Biochemical Perspectives*, S. Mann, J. Webb, and R. J. Williams (eds.) (VCH Publishers, Weinheim, 1989).

22. i. P. Calvert and S. Mann, "Synthetic and Biological Composites Formed by *in situ* Processing," *J. Mater. Sci.*, **23**, 3801-3815 (1988); ii. *Materials Synthesis Using Biological Processes*, P. C. Rieke, P. D. Calvert, and M. Alper (eds.), Proc. MRS, Vol. 174 (Materials Research Society, Pittsburgh, 1990); iii. *Materials Synthesis Based on Biological Process*, M. Alper, P. D. Calvert, R. Frankel, P. Rieke, and D. Tirrell (eds.) Proc. MRS, Vol. 218 (Materials Research Society, Pittsburgh, 1991); iv. *Hierarchically Structured Materials*, I. A. Aksay, E. Baer, M. Sarikaya, and D. A. Tirrell (eds.), Proc. MRS, Vol. 255 (Materials Research Society, Pittsburgh, 1992).

23. *Biochemistry*, C. K. Mathews and K. E. van Holde (The Benjamin/Cummings Publ. Co., Redwood City, CA, 1990).

24. H. A. Lowenstam, "Biological Minerals," *Science*, **211**, 1126-1128 (1981).

25. T. Degens, "Molecular Mechanisms on Carbonate, Phosphate, and Silica Deposition in the Living Cell," *Top. Curr. Chem.*, **64**, 1-112 (1976).

26. i. M. Paulsson, "Basement Membrane Proteins: Structure, Assembly, and Cellular Interactions," *Critic. Rev. in Biochem. and Molec. Bio.*, **27** [1/2] 93-120 (1992); ii. W. A. Cramer, D. M. Engleman, and G. von Heijne, "Forces Involved in the Assembly and Stabilization of Membrane Proteins," *FASEB J.*, **6** [15] 3397-3405 (1992); iii. T. Hashimoto, K. Kimishama, and H. Hasegawa, "Self-Assembly and Patterns in Binary Mixtures of SI Block Copolymers and PPO," *Macromol.*, **24** [20] 5604-5710 (1991).

27. L. Addadi and S. Weiner, "Interaction between Acidic Proteins and Crystals: Stereochemical Requirements in Biomineralization," *Proc. Natl. Acad. Sci., USA, Biophysics*, **82**, 4110-4114 (1985).

28. i. H. R. Crane, "Principles and Problems of Biological Growth," *Sci. Monthly*, **70**, 376-389 (1950); ii. S. Mann, "Mineralization in Biological Systems," *Structure and Bonding*, Vol. 54 (Springer-Verlag, Berlin, 1983) pp. 125-174.

29. K. M. Wilbur, "Shell Formation and Regeneration," in *Physiology of Mollusca*, K. M. Wilbur and C. M. Yonghe (eds.) Vol. 1 (Academic Press, New York, 1964) p. 243.

30. M. Sarikaya and I. A. Aksay, "Nacre of Abalone Shell: a Natural Multifunctional Nanolaminated Ceramic-Polymer Composite Material," in: *Results and Problems in Cell Differentiation in Biopolymers*, Steven Case (ed.) (Springer and Verlag, Amsterdam, 1992) pp. 1-25.

31. L. Addadi and S. Weiner, "Interactions between Acidic Macromolecules and Structured Surfaces; Stereochemistry and Biomineralization," *Mol. Cryt. Liq. Cryst.*, **134**, 305-322 (1986).

32. Y. Bouligand, "Sur une architecture torsadee repandue dans de nombreuses cuticules d'arthropodes," *C R Hebd. Sceances Acad. Sci.*, **261** [12] 3665-3668 (1965).

33. M. M. Giraud-Guille, "Fine Structure of the Chitin-Protein System in the Crab Cuticle," *Tissue Cell* **16**, 75-92 (1984).

34. *Iron Biominerals*, B. Frankel and R. P. Blakemore (eds.) (Plenum, New York, 1991).

35. M. Gosline, M. E. DuMont, and M. W. Denny, "Structure and Properties of Spider Silk," *Endeavour* **10** [1] 37-43 (1986).

36. M. Denny and J. M. Gosline, "The Physical Properties of the Terrestrial Slug," *J. Exp. Biol.*, **88**, 375-393 (1980).

37. A. I. Caplan, "Cartilage," *Sci. Amer.*, **251** [4] 84-94 (1984).

38. i. *Biochemistry of Collagen*, G. N. Ramachandran and R. H. Reddi (eds.) (Plenum Press, New York, 1976); ii. Y. Bouligand and M. M. Giraud-Guille, "Spatial Organization of Collagen Fibrils in Skeletal Tissues: Analogies with Liquid Crystals," in: *Biology of Invertebrate Collagens*, A. Bairati and R. Garrone (eds.) (Plenum, New York, 1985) pp. 115-134; iii. E. Baer, J. J. Cassidy, and A. Hiltner, "Hierarchical Structure of Collagen and Its Relationship to the Physical Properties of Tendon," Chap. 9, in: *Collagen: Biochemistry and Biomechanics*, M. E. Nimi (ed.) (CRC Press, Inc., New York, 1988) pp. 177-199; iv. P. Borstein and W. Traub, "The Chemistry and Biology of Collagen," in *The Proteins*, H. Neurath and R. L. Hill (eds.) 3rd Ed. (Academic Press, New York, 1979) pp. 412-632.

39. W. M. Kier and K. K. Smith, "Tangues, Tentacles, and Trunks: Biomechanics of Movement in Muscular Hydrostats," *Zool. J. Linn. Soc.*, **83**, 307-324 (1985).

40. *Introduction to Plant Biochemistry*, T. W. Goodwin and E. I. Mercer (Pergamon, Oxford, 1983).

41. See, for instance, References 20, 21, 25, and 30.

42. See, for instance, A. Boyde, "Comparative Histology of Mammalian Teeth," in *Dental Morphology and Evolution*, A. A. Dahlberg (ed.) (Chicago University Press, Chicago, 1971) pp. 81-94. Also, see Reference 43.

43. *Chemistry and Biology of Mineralized Tissues*, H. C. Slavkin and P. Price (eds.) (Excerpta Medica, Elsevier, Amsterdam, 1992).

44. K. Markel and P. Gorny, Zur Funktionellen Anatomie der Seeigelzahne (Echinodermata and Echinoidea), *Z. Morphol. Tiere*, **75**, 223-242 (1973).

45. K. M. Towe, "Echinoderm Calcite: Single Crystal or Polycrystalline Aggregate, "*Science*, **157**, 1048-1050 (1967).

46. i. R. P. Blakemore, "Magnetotactic Bacteria," *Science* **190**, 377-379 (1975); ii. R. P. Blakemore, "Magnetotactic Bacteria," *Ann. Rev. of Microbiology*, **36**, 217-238 (1982).

47. C. T. Dameron, R. N. Reese, R. K. Mehra, A. R. Kortan, P. J. Carrol, M. L. Steigerwald, L. E. Brus, and D. R. Winge, "Biosynthesis of Cadmium Sulfide Quantum Semiconductor Crystallites," *Nature*, **338**, 596-597 (1989).

48. i. *Enzyme Structure and Mechanism*, A Fersht, 2nd Ed. Chaps. I and II (Freeman, New York, 1985); ii. M. Alper, "Enzymatic Synthesis of Materials - An Overview," in *Materials Synthesis Based on Biological Processes*, M. Alper, P. Calvert, R. B. Frankel, P. Rieke, and D. A. Tirrell (eds.) Proc. MRS, Vol. 218 (Materials Research Society, Pittsburgh, 1991) pp. 3-6.

49. S. F. Mathews, "The Structure, Function, and Evolution of Proteins," *Prog. Biophys. Mol. Sci.*, **45**, 1-56 (1985).

50. M. Fournier, H. S. Creel, K. P. McGrath, M. T. Krejchi, E. D. T. Atkins, T. L. Mason, and D. A. Tirrell, "Genetic Synthesis of Periodic Protein Materials," J. *Bioct. Compat. Polymers*, **6**, 326-338 (1991).

51. *Research Opportunities for Materials with Ultrafine Microstructures*, National Research Council (National Academy Press, Washington, DC, 1989).

52. P. M. Harrison, P. J. Artymiuk, G. C. Ford, D. M. Lawson, J. M. A. Smith, A. Treffry, and J. L. White, "Ferritin: Function and Structural Design of an Iron-Storage Protein," in *Biomineralization: Chemical and Biochemical Perspectives*, edited by S. Mann, J. Webb, and R. J. P. Williams (eds.) (VCH, Weinheim, 1989) pp. 257-294.

53. i. B. Frankel, R. P. Blakemore, and R. S. Wolfe, "Magnetite in Freshwater Magnetotactic Bacteria," *Science*, **203**, 1355-1356 (1979); ii. R. P. Blakemore, "Magnetotactic Bacteria," *CRC Critical Rev. in Biochem.*, **20** [4] 365-380 (1986).

54. D. A. Bazylinski, R. B. Frankel, A. Garrat-Reed, and S. Mann, "Biomineralization of Iron Sulfides in Magnetotactic Bacteria from Sulfidic Environments," in *Iron Biominerals*, R. B. Frankel and R. P. Blakemore (eds.) (Plenum Press, New York, 1991) pp. 239-256.

55. i. B. M. Moskowitz, R. B. Frankel, P. J. Flanders, R. P. Blakemore, and B. B. Schwartz, "Magnetic Properties of Magnetotactic Bacteria," *J. Magnetism and Mag. Maters.*, **73**, 273-280 (1988); ii. S. Krieger, G. J. Olson, J. J. Rhyne, R. P. Blakemore, Y. A. Gorby, and N. Blakemore, "Small Angle Neutron and X-Ray Scattering from Magnetic Crystals in Magnetotactic Bacteria," *J. Magnetism and Mag. Maters.*, **82**, 17-28 (1989); iii. K. M. Towe and T. T. Moench, "Electron-Optical Characterization of Bacterial Magnetite," *Earth and Planetary Sci. Lett.*, **52**, 213-220 (1981).

56. i. S. Mann, R. B. Frankel, and R. P. Blakemore, "Structure, Morphology, and Crystal Growth of Bacterial Magnetite," *Nature*, **310**, 405-407 (1984); ii. S. Mann, N. H. C. Sparks, and V. J. Wade, "Crystallochemical Control of Iron Oxide Biomineralization," in *Iron Biominerals*, R. B. Frankel and R. P. Blakemore (eds.) (Plenum Press, New York, 1990).

57. M. Sarikaya, N. Pellerin, J. T. Staley, and I. A. Aksay, unpublished results (1992).

58. J. F. Stolz, S-B R. Chang, and J. L. Kirschvink, "Magnetotactic Bacteria and Single-Domain Magnetite in Hemipelagic Sediments," *Nature*, **321**, 849-851 (1986).

59. W-H. Shih, M. Sarikaya, W. Y. Shih, and I. A. Aksay, "Geometrical Arrangement of Magnetosomes in Magnetotactic Bacteria," in *Materials Synthesis Based on Biological Processes*, M. Alper, P. Calvert, R. B. Frankel, P. Rieke, and D. A. Tirrell (eds.) Proc. of MRS, Vol. 218 (Materials Research Society, Pittsburgh, 1991) pp. 109-114.

60. i. See paper by D. A. Bazylinski and R. B. Frankel, "Biomineralization of Iron Sulfides in Magnetotactic Bacteria in Sulfidic Environments," in ref. 34., pp. 239-255, and also D. A. Bazylinski, A. J. Garratt-Reed, and R. B. Frankel, "Electron Microscopic Studies in Magntetotactic Bacteria, in: *Microscopy of Self-Assembled*

Materials and Biomimetics, M. Sarikaya (ed.) *J. Microsc. Res. Tech* (1993); ii. M. Farina, D. M. S. Esquivel, and H. G. P. Lins de Barros, "Magnetic Iron-Sulphur Crystals from Magnetotactic Microorganisms," *Nature*, **343**, 256-258.

61. i. *Membranemimetic Chemistry*, J. H. Fendler (Wiley-Interscience, New York, 1982); ii. J. H. Fendler, "Atomic and Molecular Clusters in Membrane Mimetic Chemistry," *Chem. Rev.*, **87**, 887-899 (1987).

62. i. H. Liu, G. L. Graff, M. Hyde, M. Sarikaya, and I. A. Aksay, "Synthesis of Ultrafine Multicomponent Particles Using Phospolipid Vesicles," in *Materials Synthesis Based on Biological Processes*, M. Alper, P. Calvert, R. B. Frankel, P. Rieke, and D. A. Tirrell (eds.) Proc. MRS, Vol. 218 (Materials Research Society, Pittsburgh, PA, 1991) pp. 115-121; ii. Sung Pak, "Potential Application of Microemulsions in Ceramic Processing," M.S. Thesis (University of Washington, Seattle, 1979).

63. I. A. Aksay, W. Y. Shih, and M. Sarikaya, "Colloidal Processing of Ceramics with Ultrafine Particles," in *Ultrastructure Processing of Advanced Ceramics, Glasses, and Composites*, J. D. MacKenzie and D. R. Ulrich (eds.) (Wiley, New York, 1988) pp. 393-406.

64. Y. A. Gorby, T. J. Beveridge, and R. P. Blakemore, "Characterization of the Bacterial Magnetosome Membrane," *J. Bacteriology*, **170** [2] 834-841 (1988).

65. R. B. Frankel and D. A. Bazylinski, "Structure and Function of Magnetosomes in Magnetotactic Bacteria," this book, pp. 199-216.

66. E. Kniprath, "Ultrastructure and Formation of Sea Urchin Tooth," *Calcif. Tiss. Res.*, **14**, 211-228 (1974).

67. i. S. Weiner, "Organic Matrixlike Macromolecules Associated with the Mineral Phase of Sea Urchin Skeletal Plates and Teeth" *J. Exp. Zool.*, **234**, 7-15 (1985); ii. D. J. Veis, T. M. Albinger, J. Clohisy, M. Rahima, B. Sabsay and A. Veis, "Matrix Proteins of Sea Urchin *Lytechinus variegatus*," *J. Exp. Zool.*, **240**, 35-46 (1986); iii. A. Berman, L. Addadi, L. Leiserowitz, S. Weiner, M. Nelson, and A. Kvik, "A Synchrotron X-ray Study of a Unique Protein-Calcite Composite Material," *Science*, **250**, 664-667 (1990).

68. M. Sarikaya, J. Liu, and I. A. Aksay, "Ultrastructure of the Mineral Phase in Sea-Urchin Teeth," unpublished research.

69. K. Brear and J. D. Curry, "Structure of the Sea-Urchin Tooth," *J. Mater. Sci.*, **11**, 1977-1978 (1976).

70. I. A. Aksay and M. Sarikaya, "Bioinspired Processing of Composite Materials" in *Ceramics: Toward the 21st Century, Centennial International Symposium*, S. Soga and A. Kato (eds.), (Ceramic Society Japanese, Tokyo, 1991) pp. 136-149.

71. *Fundamental Principles of Fiber Reinforced Composites*, K. H. G. Ashbee (Technomic Publishing, Lanchester, PA, 1989).

72. J. Kastelic, I. Palley, and E. Baer, "A Structural Mechanical Model for Tendon Crimping," *J. Biomechanics*, **13**, 887-893 (1980); ii. E. Baer, J. J. Cassidy, and A. Hiltner, "Hierarchical structure of Collagen Composite Systems: Lessons from Biology," this book, pp. 13-34.

73. i. D. L. Kaplan, S. J. Lombardi, W. S. Muller, and S. A. Fossey, "Silks," in *Biomaterials*, D. Byrom (ed.) (Stockton Press, New York, 1991) pp. 1-53; ii. J. Gosline, C. Nichols, P. Guerette, A. Cheng, and S. Katz, "The Macromolecular Design of Spiders' Silks," this book, pp. 237-262.

74. *The Biology of Anthropod Cuticle*, A. Neville (Springer, Berlin, 1975).

75. M. M. Giraud-Guille, "Liquid Crystalline Order of Biopolymers in Cuticles and Bones," in *Microscopy of Self-Assembled Materials and Biomimetics*, M. Sarikaya (ed.) Special Issue of *J. Microsc. Res. Tech.* (1994) pp. 420-428.

76. i. S. L. Gunderson and R. C. Schiavone, "The Insect Exoskeleton: A Natural Structural Material," *JOM*, **41** [11] 80-82 (1989); ii. S. L. Gunderson and R. C. Schiavone, "Microstructure of an Insect Cuticle and Applications to Advanced Composites," this book, pp. 163-198.

77. H. Ghiradella, D. Aneshansley, T. Eisner, R. E. Silberglied, and H. E. Hinton, "Ultraviolet Reflection of Male Butterfly: Interference Color Caused by Thin-Layer Elaboration of Wing Scales, *Science*, **178**, 1214-1217 (1972).

78. i. J. Samseth, R. J. Spontak, and K. Mortensen, "The Response of Microstructure to Processing in a Series of Poly (siloxaneimide) Copolymers," *J. Poly. Sci.*, Part B, **31** [4] 467-475 (1993); ii. R. J. Spontak, S. D. Smith, and A. Ashraf, "Morphological Studies of Linear $(AB)_n$ Multiblock Copolymers and Their Blends," in *Microscopy of Self-Assembled Materials and Biomimetics*, M. Sarikaya (ed.) Special Issue of *J. Microsc. Res. Tech.* (1994) pp. 412-419.

79. E. Baer, "Advanced Polymers," *Scientific American*, **255** [4] 178-190 (1986).

80. J. Glimcher, "On the Form and Function of Bone: from Molecules to Organs" in *The Chemistry and Biology of Mineralized Biological Tissues: Wolff's Law Revisited*, A. Veis (ed.) (Elsevier, New York and Amsterdam, 1981) pp. 617-673.

81. *Studies in the Development, Function, and Evolution of Teeth*, P. M. Butler and K. A. Joysey (eds.) (Academic, London, 1973).

82. C. Grégoire, "Structure of the Molluscan Shell," in: *Chem. Zoology*, M. Florkin and M. Scheer (eds.) (Academic Press, New York, 1972) pp. 45-102.

83. i. J. D. Currey, "The Mechanical Properties of Some Molluscan Hard Tissues," *J. Zool. London*, **173**, 39-406 (1974); ii. J. D. Currey, "Further Studies on the Mechanical Properties of Mollusc Shell Material," *J. Zool. London*, **180**, 445-453 (1976).

84. A. P. Jackson, J. F. V. Vincent, and R. M. Tunner, "The Mechanical Design of Nacre," *Proc. Roy. Soc. London*, **B234**, 415-440 (1988)

85. M. Sarikaya, K. E. Gunnison, M. Yasrebi, and I. A. Aksay, "Mechanical Property-Microstructural Relationships in Abalone Shell," *Materials Synthesis Using Biological Processes*, P. C. Rieke, P. D. Calvert, and M. Alper (eds.) Proc. MRS, Vol. 174 (Materials Research Society, Pittsburgh, 1990) pp. 109-116.

86. W. Schober, "Precipitated Calcium Carbonate: A Quite Market Expects Excellence," *Industrial Minerals*, No. 265, October Issue, 69-81 (1989).

87. i. H. Nakahara, G. Bevelander, and M. Kakei, "Electron Microscopic and Amino Acid Studies on the Outer and Inner Shell Layers of *Haliotis rufescens*," *VENUS (Japn. Jour. Malac.)* **41** [1] 33-46 (1982); ii. G. Bevelander and H. Nakahara, "An Electron Microscopy Study of the Formation of the Nacreous Layers in the Shells of Certain Bivalve Molluscs," *Calc. Tiss. Res.*, **3**, 84-92 (1968).

88. i. K. Bandel, "Ubergange von der Perlmutter-Schicht zu Prismatischen Schichttypen bei Mollusken," Biomineralization, **2**, 28-47 (1970); ii. K. M. Wilbur and K. Simkiss, "Calcified Shells," *Comprehensive Biochemistry*, **26A**, 229-295 (1968).

89. N. Watabe, "Studies on Shell Formation: XI. Crystal-Matrix Relationship in the Inner Layers of Mollusk Shells," *Ultrastr. Res.*, **12**, 351-370 (1965).

90. i. S. Weiner, W. Traub, and H. A. Lowenstam, "Organic Matrix in Calcified Exoskeletons," in *Biomineralization and Biological Metal Accumulation*, P. Westbroek and E. W. de Jong (eds.) (Dordrecht: Reidel, 1983) pp. 205-224; ii. S. Weiner, Y. Talmon, and W. Traub, "Electron Diffraction Studies of Molluscan Shell Organic Matrices and Their Relationship to the Mineral Phase," *Int. J. Biol. Macromol.* **5**, 325-328 (1983); iii. S. Weiner and W. Traub, "Macromolecules in Mollusc Shells and Their Functions in Biomineralization," *Phil. Trans. R. Soc. Lond.*, B **304**, 425-434 (1984); iv. D. Worms and S. Weiner, "Mollusk Shell Organic Matrix: Fourier Transform Infrared Study of the Acidic Macromolecules," *J. Exp. Zool.*, **237**, 11-20 (1986);

91. *The Biology of Marine Animals*, A. Nicol (Interscience, New York, 1960).

92. *Molluscs*, E. Morton, 5th Edition (Hutchinson, London, 1979).

93. i. H. Mutvei, "Ultrastructure of the Mineral and Organic Components of Molluscan Nacreous Layers," *Biomineralization* **2**, 48-72 (1970); ii. H. Mutvei, "Ultrastructural Characteristics of the Nacre in Some Gastropods," *Zool. Scripta*, **7**, 287-296 (1978).

94. *Physiology of Mollusca*, K. Wilbur and C. M. Yonge (eds.) (Academic Press, New York, 1964).

95. i. W. F. Brown, Jr. and J. E. Srawley, "Plain Strain Fracture Toughness Testing of High Strength Metallic Materials," *ASTM Technical Publ. No 410* (American Society for Testing and Materials, Philadelphia, 1966); ii. *Plane Strain Fracture Toughness Testing*, ASTM E599 (American Society for Testing and Materials, Philadelphia, 1983).

96. J. D. Currey, "Mechanical Properties of Mother of Pearl in Tension," *Proc. Roy. Soc. London*, B**196**, 443-463 (1977).

97. *Deformation of Ceramic Materials II*, R. E. Tressler and R. C. Bradt (eds.) *Materials Science Research*, Vol. 18 (Plenum Press, New York, 1984).

98. *Science and Technology of Zirconia*, N. Claussen, M. Ruhle, and A. Heuer (eds.) (American Ceramic Society, Inc., Columbus, Ohio, 1984); ii. S. M. Wiederhorn, "Brittle Fracture and Toughening Mechanisms in Ceramics," *Ann. Rev. Mater. Sci.*, **14**, 373-403 (1984).

99. See, for instance, W. Davidge, *Mechanical Behaviour of Ceramics* (Cambridge University Press, Cambridge, 1979).

100. See, for instance, i. References 30 and 85, and also, ii. M. Yasrebi, G. H. Kim, D. L. Milius, M. Sarikaya, and I. A. Aksay, "Biomimetic Processing of Ceramics and Ceramic-Based Composites," in: *Better Ceramics Through Chemistry-IV*, B. J. J.

Zelinski, C. J. Brinker, D. E. Clark, and D. R. Ulrich (eds.) Proc. MRS, Vol. 180 (Materials Research Society, Pittsburgh, 1990) pp. 625-635.

101. See, for instance, *The Plastic Deformation of Metals*, W. K. Honeycombe (St. Martin's Press, New York, 1968).

102. A. A. Griffith "The Phenomena of Rupture and Flow in Solids," *Phil. Trans. CCXXI* **A**, 163-198 (1920).

103. *An Introduction to Composite Materials*, D. Hull (Cambridge University Press Cambridge, 1981) pp. 81-85.

104. i *British and Continental Arms and Armor*, C. H. Ashdown (Dover Publications, New York, 1975); ii. *Arrows Against Steel: The History of the Bow*, (Mason/Charter, New York, 1975); iii. V. Hurley, M. L. Wilkins, C. F. Cline, and C. A. Honodel, *Light Armor*, Report UCRL-7-1817, Lawrence Livermore National Laboratory, Livermore, CA, USA (1969).

105. H. Silyn-Robertson and R. M. Sharp, "Crystal Growth and the Role of the Organic Network in Eggshell Biomineralization," *Proc. Roy. Soc. Lond.*, **B 227**, 303-324 (1986).

106. R. W. Rice, "Microstructure Dependence of Mechanical Behavior," in *Treatise on Materials Science and Technology*, Vol. II, *Properties and Microstructure*, R. K. McCrone (ed.) (Academic Press, New York, 1977) pp. 199-381.

107. i. A. G. Evans and R. M. MacMeeking, "On the Toughening of Ceramics by Strong Reinforcements," *Acta. Metall.*, **34** [12] 2435-2441 (1986); ii. A. G. Evans, "High Toughness Ceramics," *J. Mater. Sci. Eng.*, **A105/106**, 65-75 (1988); iii. A. G. Evans and D. A. Marshall, "The Mechanical Behavior of Ceramic Matrix Composites," *Acta. Metall.* **37** [10] 2567-2583 (1989).

108. S. Khanuja, "Processing and Structure-Property Relationships of Laminated B_4C-Polymer Composites," *M.Sc. Thesis* (University of Washington, Seattle, 1991).

109. G. H. Kim, "The Effect of Metallic Phase and Microstructure on the Strengthening Behavior of B_4C-Al Cermets, *Ph.D. Thesis* (University of Washington, Seattle, 1993).

110. See, for instance, i. P. Boch, T. Chartier, and M. Huttepain, "Tape Casting of Al_2O_3/ZrO_2 Laminated Composites," *J. Am. Ceram. Soc.*, **69** [8] C191-C192 (1986); ii. H. Takeba and K. Morinaga, "Fabrication and Mechanical Properties of Lamellar Al_2O_3 Ceramics," *J. Ceram. Soc. Jap. Int'l. Ed.*, **96**, 1122-1128 (1988);

iii. D. B. Marshall, J. J. Ratto, and F. F. Lange, "Enhanced Fracture Toughness in Layered Nanocomposites of Ce-ZrO_2 and Al_2O_3," *J. Am. Ceram. Soc.*, **74** [12] 2979-2987 (1991).

111. i. K. M. Towe and G. H. Hamilton, "Ultrastructure and Inferred Calcification of the Mature and Developing Nacre of Bivalve Mollusks," *Calc. Tiss. Res.*, **1**, 306-318 (1968); ii. K. M. Towe and G. R. Hamilton, "The Structure of Some Bivalve Shell Carbonates Prepared by Ion-Beam Thinning," *Calc. Tiss. Res.*, **10**, 38-48 (1972).

112. i. Bragg, "The Structures of Aragonite," *Proc. Roy. Soc. London, Ser. A*, **17** (1928); ii R. Wenk, D. J. Barber, and R. J. Reeder, "Microstructures in Carbonates" in *Reviews in Mineralogy*, Vol. 11, R. J. Reeder (ed.) (Miner. Soc. Amer., Washington D.C., 1983) p. 301.

113. M. A. Crenshaw and H. Ristedt, "Histochemical and Structural Study of Nautiloid Septal Nacre," *Bomineralization*, **8**, 1-8 (1975).

114. i. S. Weiner, "Organization of Extracellularly Mineralized Tissues: A Comparative Study of Biological Crystal Growth," *CRC Crit. Rev. in Biochem.*, **20** [4] 365-380 (1986); ii. L. Addadi and S. Weiner, "Interactions between Acidic Macromolecules and Structured Crystal Surfaces: Stereochemistry and Biomineralization," *Mol. Cryst. Liq. Cryst.* **134**, 305-322 (1986); L. Addadi and S. Weiner, "Control and Design Principles in Biological Mineralization," *Angew. Chem. Intl. Ed. Engl.*, **31**, 153-169 (1992).

115. S. Mann, "Molecular Recognition in Biomineralization," *Nature*, **33**, 119-123 (1988).

116. J. A. Keith, S. A. Stockwell, D. H. Ball, W. S. Muller, D. L. Kaplan, T. W. Thannhauser, and R. W. Sherwood, "Characterization of the Complex Matrix of the Mytilus Edulis Shall and the Implications for Biomimetic Ceramics," in *Hierarchically Structured Materials*, I. A. Aksay, E. Baer, M. Sarikaya, and D. A. Tirrell (eds.), Proc. MRS, Vol. 255 (Materials Research Society, Pittsburgh, 1992) pp. 3-8.

117. M. A. Cariolou and D. E. Morse, "Purification and Characterization of Calcium-binding Conchiolin Shell Peptides from the Mollusc, *Haliotis rufescens*, as a Function of Development," *J. Comp. Physiol B.*, **157**, 717-729 (1988).

118. i. N. Watabe, "Crystal Growth of Calcium Carbonate in the Invertabrates," *Prog. Crystal Growth Charact.*, Vol. 4 (Pergamon Press, London, 1981) pp. 99-147; ii. C. Grégoire, "Structure of the Molluscan Shell," *Chem. Zool.*, **45**, 102-130 (1972);

S. W. Wise, "Microarchitecture and Mode of Formation of Nacre (mother-of-pearl) in Pelecypods, Gastrapods, and Cephalopods," *Eclogae geal Helv.*, **63** [3] 775-797 (1970).

119. i. M. Greenfield, D. C. Wilson, and M. A. Crenshaw, "Ionotropic Nucleation of Calcium Carbonate by Molluscan Matrix," *Amer. Zool.*, **24**, 925-932 (1984); ii. A. Crenshaw, "Mechanism of Normal Biological Mineralization of Calcium Carbonates" in *Biological Mineralization and Demineralization*, G. H. Nancollas (ed.) (Springer, Berlin and New York, 1972) pp. 243-257.

120. i. S. Weiner and W. Traub, "X-ray Diffraction Study of the Insoluble Organic Matrix of Mollusc Shells," *FEEBS Letters*, **111** [2] 311-316 (1980); ii. S. Weiner and W. Traub, "Organic Matrix-Mineral Relationships in Mollusc Shell Nacreous Layers" in *Structural Aspects of Recognition and Assembly in Biological Macromolecules*, M. Balaban, J. L. Sussman, W. Traub, and A. Yonath, (eds.) (Balaban ISS, Yehevot Philadelphia, 1981) pp. 462-487; iii. S. Weiner and W. Traub, "Macromolecules in Mollusc Shells and Their Functions in Biomineralization," *Phil. Trans. R. Soc. London* **B304,** 425-434 (1984).

121. i. D. E. Morse, University of California, Santa Barbara, CA - private communication (1992); ii. D. L. Kaplan, Army Research Center, Nattick, MA, private communication (1992); iii. C. E. Furlong, University of Washington, private communication (1993).

122. C. E. Furlong and R. Humbert, "Design of Protein Producing Bioreactors for Self-Assembling Systems," in *Hierarchically Structured Materials*, I. A. Aksay, E. Baer, M. Sarikaya, and D. A. Tirrell (eds.), Proc. MRS, Vol. 255 (Materials Research Society, Pittsburgh, 1992) pp. 435-442.

123. C. E. Furlong, R. Humbert, M. Sarikaya, and I. A. Aksay, unpublished research (1993).

124. K. Gunnison, M. Sarikaya, J. Liu, and I. A. Aksay, "Structure-Mechanical Property Relationships in a Biological Ceramic-Polymer Composite: Nacre," in *Hierarchically Structured Materials*, I. A. Aksay, E. Baer, M. Sarikaya, and D. A. Tirrell (eds.), Proc. MRS, Vol. 255 (MRS, Pittsburgh, 1992) pp. 171-183.

125. N. Watabe and K. M. Wilbur, "Influence of the Organic Matrix on Crystal type in Molluscs," *Nature*, **188,** 334-336 (1960).

126. R. Meenakshi, G. Donnay, P. L. Blackwelder, and K. M. Wilbur, "The Influence of Substrata on Calcification Patterns in Molluscan Shell," *Calc. Tiss. Res.*, **15**, 31-44 (1974).

127. A. Crenshaw, "Mechanism of Normal Biological Mineralization of Calcium Carbonates" in *Biological Mineralization and Demineralization*, G. H. Nancollas (ed.) (Springer, Berlin and New York, 1972) pp. 243-257.

128. S. Weiner, "Organization of Extracellularly Mineralized Tissues: a Comparative Study of Biological Crystal Growth," *CRC Crit. Rev. in Biochem*, **20** [4] 365-380 (1986).

129. S. Mann, "Biogenic Inorganic Materials," in *Inorganic Materials*, D. W. Bruce and D. O'Hare (eds.) (John Wiley & Sons, New York, 1992) pp. 237-294.

130. i. L. Addadi, Z. Berkovitch-Yellin, I. Weissbuch, M. Lahav, and L. Leiserowitz, "A Link between Macroscopic Phenomena and Molecular Chirality: Crystals as Probes for the Direct Assignment of Absolute Configuration of Chiral Molecules," in *Topics in Stereochemistry*, Vol. 16 (Wiley, New York, 1986) pp. 1-85; ii. I. Weisbuch, L. Addadi, M. Lahav, and L. Leiserowitz, "Molecular Recognition at Crystal Interfaces," *Science*, **253**, 637-645 (1991).

131. i. S. Mann, B. R. Heywood, S. Rajam, and D. Birchall, "Controlled Crystallization of $CaCO_3$ under Stearic Acid Monolayer," *Science*, **334,** 692-695 (1988); ii. S. Mann, B. R. Heywood, S. Rajam, and J. D. Birchall, "Interfacial Control of Calcium Carbonate Under Organized Stearic Acid Monolayers," *Proc. R. Soc. Lond.*, A, **423**, 457-471 (1989); iii. S. Mann, B. R. Heywood, S. Rajam, and J. B. A. Walker, "Structural and Stereochemical Relationships between Langmuir Monolayers and Calcium Carbonate Nucleation," *J. Phys. D: Appl. Phys.*, **24**, 154-164 (1991).

132. *Crystal Structures*, R. W. G. Wyckoff (Interscience Publ., New York, 1960).

133. See, for instance, D. Romeu, "Decagonal Phase Model with Multiple Periods and Quasiperiodic Coincidence Lattice," *J. Non-Cryst. Solids*, **153/154**, 232-240 (1993).

134. J. Liu, M. Sarikaya, and I. A. Aksay, "A Hierarchically Structured Model Composite: A TEM Study of the Hard Tissue of Red Abalone," in *Hierarchically Structured Materials*, I. A. Aksay, E. Baer, M. Sarikaya, and D. A. Tirrell (eds.), Proc. of MRS Symp., Vol. 258: (Materials Research Society, Pittsburgh, 1992) pp. 9-17.

135. N. Unwig and R. Henderson, "The Structure of Proteins in Biological Membranes," *Scientific American*, February, 78-94 (1985).

136. i. *Pattern and Tiling*, B. Grünbaum (Plenum, New York, 1987); ii. *Tilings and Patterns*, B. Grünbaum and G. C. Shephard (W. H. Freeman and Company, New York, 1987).

137. M. Sarikaya, J. Liu, and I. A. Aksay, unpublished research (1993).

138. *On the Growth and Form*, d'Arcy Thompson (University Press, Cambridge, 1952) Chap. XI.

139. D. R. Fowler, H. Meinhardt, and P. Prusinkiewicz, "Modelling Seashells," *Computer Graphics*, **26** [2] 379-387 (1992).

BIOMINERALIZATION, THE INORGANIC-ORGANIC INTERFACE, AND CRYSTAL ENGINEERING

Stephen Mann

School of Chemistry, University of Bath
Bath BA2 7AY, United Kingdom

The study of biomineralization and related model systems has advanced to a level where major insights in materials science can be expected in the near future. The application of principles such as molecular recognition and self-assembly in the regulation of nucleation and growth is pivotal to a new perspective in the fabrication of advanced inorganic materials. Nanophase and composite materials are immediate candidates for biomimickry. This paper summarizes the main features of biomineralization placing particular emphasis on the importance of specific molecular interactions at interfaces comprising inorganic and organic surfaces. Adaptation of these ideas to synthetic systems involving the integration of supramolecular chemistry (vesicles, micelles, Langmuir monolayers) into materials science is described. Geometric, electrostatic and stereochemical factors are responsible for crystal chemical specificity in these model systems.

1.0 INTRODUCTION

The successful fabrication and utilization of advanced inorganic materials depend on the integration of two key objectives. First, developments are required in the synthetic capabilities of generating new structures tuned to electronic, optical, and magnetic properties. This is the realm of synthetic chemistry and while much progress has been made in organic (polymer) chemistry, achievements in the rational preparation of inorganic materials remain limited. The use of organometallic compounds as tailored precursors to controlled synthesis is gaining momentum and appears promising. Related to the need to produce novel materials is a requirement for more advanced molecular engineering of currently technologically useful products. In principle, the functional use of many materials depends on ultrastructural properties such as crystal size, shape, tex-